COMPUTATIONAL PREDICTION AND EXPERIMENTAL MEASUREMENT OF TIME RESOLVED FLUORESCENCE PROPERTIES OF TRYPTOPHAN AND 5-FLUORO-TRYPTOPHAN DIPEPTIDES

by

Carl Ashley Fahlstrom

A dissertation submitted in partial fulfillment
of the requirements for the degree

of

Doctor of Philosophy

in

Chemistry

MONTANA STATE UNIVERSITY
Bozeman, Montana

April, 2016

ACKNOWLEDGEMENTS

I would like to acknowledge Professors Lee Spangler and Patrik Callis, and all their group members, for their mentoring and support. The experimental results presented here would not have been possible without the assistance of Gregory Gillispie at Fluorescence Innovations. Access to a prototype direct waveform recording instrument was provided. Dr. Gillispie also provided considerable assistance in the analysis of time resolved fluorescence data. I would also like to acknowledge the members of my committee for taking the time to review this thesis.

TABLE OF CONTENTS

TABLE OF CONTENTS - CONTINUED

TABLE OF CONTENTS - CONTINUED

LIST OF TABLES

LIST OF TABLES - CONTINUED

LIST OF FIGURES

LIST OF FIGURES - CONTINUED

LIST OF FIGURES - CONTINUED

LIST OF FIGURES - CONTINUED

LIST OF FIGURES - CONTINUED

LIST OF FIGURES - CONTINUED

LIST OF FIGURES - CONTINUED

LIST OF FIGURES - CONTINUED

LIST OF FIGURES - CONTINUED

ABSTRACT

The widely exploited high sensitivity of the amino acid tryptophan (Trp) fluorescence wavelength and quantum yield on local environment in proteins results in multiexponential decay from two mechanisms: quenching rate heterogeneity and/or spectral relaxation. 5-fluorotryptophan (5FTrp) reduces quenching rate heterogeneity by suppression of electron transfer quenching. A comparison of fluorescence properties of Trp and 5FTrp provides a means of differentiating between relaxation and heterogeneity. Four observations concerning the fluorescence of Trp dipeptides required further explanation: decay components of approximately 20 ps, a sub 300 fs 10% loss of quantum yield, the quantum yield for Gly-Trp being significantly lower than Trp-Gly, and the fluorescence wavelength of Trp-X being 10 nm shorter than X-Trp at pH 5. With the goal of distinguishing between electron and proton transfer quenching mechanisms, the time resolved fluorescence—with time resolution of 0.5 ns—for dipeptides was measured in the X-Trp and Trp-X configurations(where X=Leu, Gly, Asp, Arg, Met), with 5FTrp substitution, at pH 5 and pH 10, and in water and D_2O solvent—resulting in 84 distinct species. Molecular dynamics simulations were performed on Gly-Trp and Trp-Gly dipeptides with ground and excited state charges employing multiple force fields. The methods developed by Callis and coworkers were used to calculate the instantaneous rates of electron transfer rates, quantum yield, and fluorescence wavelength. Experimentally three types of multiexponential decay were observed: quenching rate heterogeneity with no relaxation, relaxation only, and combinations thereof. The substitution of 5FTrp for Trp reduced quenching rate heterogeneity, resulting in reduction of short lifetime components, allowing for the observation of relaxation components that were most likely masked in the Trp case. Calculated electron transfer rates support lifetimes of approximately 20 ps, but not those less than 300 fs, and predict a lower quantum yield for Trp-Gly than Gly-Trp. Calculated fluorescence wavelengths reproduce the observed shorter fluorescence wavelength of Trp-X zwitterions. Failure to predict quantum yields may be caused by the inability of the molecular dynamics force fields to reproduce the conformational populations. Results support both relaxation and heterogeneity in Trp dipeptides. 5FTrp is a useful tool in distinguishing between heterogeneity and relaxation.

1

INTRODUCTION

Three naturally occurring amino acids display significant fluorescence properties in the near ultraviolet: tryptophan (Trp), tyrosine (Tyr), and phenylalanine (Phe) [82]. Tryptophan displays the highest molar absorptivity and highest intensity fluorescence emission of these amino acids. Trp is also found to have the greatest variation in fluorescence properties with environment. The fluorescence of Trp in proteins has shown a strong dependence on its local environment in both wavelength and quantum yield. The quantum yield of Trp in proteins ranges from almost 0 to about 0.30, which is the quantum yield of 3-methylindole, independent of solvent polarity (representing no fluorescence quenching). The peak fluorescence wavelength (λ_{max}) can vary from about 308 nm to approximately 360 nm. Figure 1.1 shows this wide ranging variability for 20 single Trp proteins. Proteins with multiple naturally occurring Trp residues are frequently converted to single Trp by site directed mutagenesis (Trp is most frequently replaced by Phe).

While the variability of Trp fluorescence has proven a significant challenge for quantitative explanation, it has also become an important tool in the study of protein dynamics. Due to the strong dependence on local structure, the changes in fluorescence quantum yield and wavelength as a function of some system perturbation have been used to study protein folding, protein hydration, protein conformation and dynamics, and protein-protein and protein-ligand interactions [46] [45] [87] [76]. Protein folding can frequently be modeled as a two state model with respect to the fluorescence intensity of the Trp fluorescence. Tryptophan is an intrinsic fluorophore to many proteins. Therefore, in many cases the protein can be studied in its native

Figure 1.1: Graph of fluorescence quantum yield normalized fluorescence spectra of single Trp containing proteins. This figure displays the wide variation in both fluorescence wavelength and quantum yield of Trp in proteins. The height of the fluorescence emission plots is proportional to quantum yield. The highest of these corresponds to a quantum yield of 0.34, which is equivalent to unquenched fluorescence from 3-methylindole. This figure taken from P. Callis Collection [9]

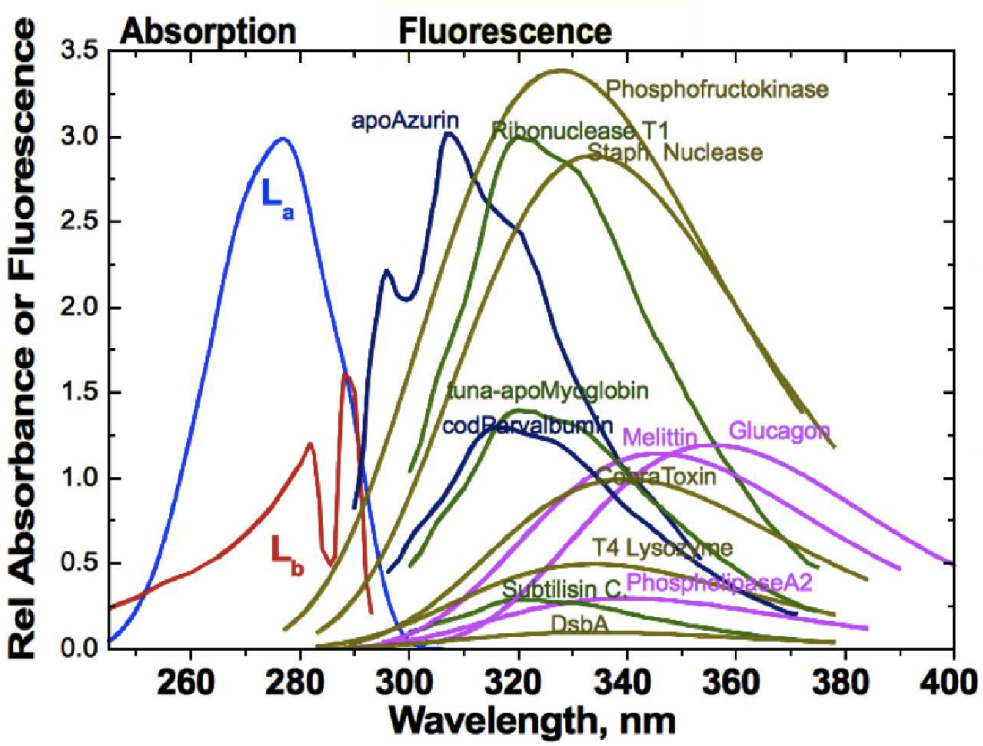

state. Tryptophan can be mutated into different positions in the primary sequence of a protein, often with little or no change in structure or dynamics, to study conformational changes in different locations along the peptide chain.

Understanding the fluorescence properties of Trp in proteins has been a subject of investigation for over 50 years. The work of Callis and Vivian in 2003 and Callis and Liu in 2004 provided the first semi-quantitative prediction of fluorescence quantum yield based on the local structure of the Trp in a protein [13] [15]. This group has also provided an understanding of the fluorescence wavelength shifts in proteins

based on electrostatic (de)stabilization of the change in electron density between the ground and fluorescing states [12] [91]. Figure 1 shows the results of fluorescence wavelength prediction for a selection of proteins with widely varying fluorescence emission wavelengths. Before this work there was no way to predict whether a Trp in a protein would have a high or low fluorescence quantum yield. The fluorescence quantum yield is defined as the ratio of absorbed photons to emitted photons and can be calculated by the following formula:

$$\Phi = \frac{k_r}{k_r + k_{nr} + k_{et} + k_{pt}} \tag{1.1}$$

Where Φ is the quantum yield, k_r is the radiative rate constant, k_{nr} is the non-radiative rate constant (inclusive of intersystem crossing and internal conversion), k_{et} is the electron transfer rate constant, k_{pt} is the proton transfer rate constant. The electron and proton transfer quenching rates provide an explanation as to the high variability of Trp fluorescence quantum yield with environment while that of 3-methylindole is independent of solvent polarity at approximately 0.30 [61].

Trp in proteins and in its zwitterionic state displays significant non-exponential (multi-exponential) decay, leading to difficultly in the interpretation of time resolved data. There are two explanations for multi-exponential decay: (1) multiple ground state subpopulations with different lifetimes (quenching rate heterogeneity) and (2) conformational relaxation during the excited state lifetime (solvent relaxation and/or a transition between rotamer conformations). Contributions from multiple rotamer conformations in the ground state have been implicated by several investigators [69] [18]. Ground state conformational subpopulations of Trp in proteins are evidenced by X-Ray crystal structures, fluorescence lifetime measurements, and molecular dynamics simulations. Relaxation-produced multi-exponential decay results from a single

species whose wavelength shifts in time. This relaxation results from a combination of solvent relaxation and excited state rotamer transitions. Multiexponential decay is frequently interpreted as multiple species with different lifetimes even in cases where the mechanism is relaxation. Non-exponential decay is described in terms of multiple species each with their own spectrum [55] [44]. Decay associated spectra (DAS) are used to display multiple wavelength space spectra each with a different fluorescence lifetime. In the case of multiexponential decay produced by relaxation would lead to one DAS similar to the steady state fluorescence spectrum and another with sinusoidal shape (positive coefficients for short wavelength and negative coefficients for long wavelength) [44] [18]. This is caused by removal of population from the ensemble of molecules with higher fluorescing state energies and addition of population to the ensemble of molecules with lower fluorescing state energy.

The next 3 sections discuss background on Trp photophysics and the two quenching pathways present, electron transfer and proton transfer quenching. We will discuss results in the literature concerning solvation dynamics around Trp and how those relate to this study. The following sections will discuss how the substitution of 5FTrp in place of a Trp residue results in the reduction of multiexponential fluorescence decay via a reduction of ET-heterogeneity, background on the dipeptides that we will use as our model system, and an overall description of the experimental and computational studies presented herein.

Tryptophan: A Tool For Biophysical Protein Characterization

The understanding of protein structure and dynamics is critical to the understanding of many processes in biology. There have been a wide variety of techniques developed to study this on a wide variety of time scales, from minutes to femtoseconds. The intrinsic fluorescence lifetime of tryptophan in proteins has been employed at a

variety of time scales. Equilibrium protein-protein and protein ligand binding are studied by investigating the change in the decay kinetics of tryptophan in the protein over longer time scales.

Molecular dynamics simulations have the capability to probe protein motions on the sub-femtosecond time scale. It is however computationally prohibitive to investigate the dynamics on a time scale required to probe mechanisms of protein folding and protein-protein interactions. These molecular dynamics simulations are dependent on empirically calibrated force fields. These force fields are mainly calibrated by high frequency bandwidth methods of IR and Raman vibrational spectroscopy, which are much faster than the elementary configurational dynamics of proteins.

The work presented here provides insight into measurements on a time scale intermediate between the microseconds and longer provided by NMR measurements and the 100 fs - 200 ps time scale provided by ultrafast laser spectroscopic methods. In terms of protein motion, these time scales represent the dynamics of large conformational fluctuations and the elementary configurational changes that lead to them. The more elementary configurational changes in protein and solvent dynamics have been monitored by methods such as fluorescence up-conversion [99] [68] and 2D-IR methods [37]. Fluorescence up-conversion of Trp fluorescence has been applied to the study of solvent dynamics. Methods have also been developed to analyze these results in terms of separate protein and solvent contributions with the aid of molecular dynamics simulations [64].

Tryptophan Photophysics

The fluorescing excited state of Trp in polar solvents is the L_a state, nominally an excitation from the HOMO to LUMO of the indole ring. Upon excitation there

is a shift in the electron density from the 5-membered ring to the 6-membered ring portion of the indole. This can be stabilized by high dielectric constant solvent or by localized charges of protein or peptide. The orientation of the shift in electron density upon excitation from the ground state to the L_a state is shown in figure 1.3.

The water solvent molecules around a solvent exposed Trp residue reorient their dipoles about this change in charge distribution. The energy of the L_a state lowers as the reorientation occurs, resulting in a time dependent shift to longer fluorescence wavelength. The reorientation of water about the change in dipole occurs on an ultrafast time scale (50 fs to 2 ps in the case of Trp zwitterion in water) [56] [101]. The change in dipole can also create a torsion force about the dihedral angles defining the rotamer state (term used to express combination of Chi 1, Chi 2 (see figure 1.2), Phi and Psi (protein backbone dihedrals)), leading to a time dependent shift likely to operate on a time scale longer than solvent reorganization. These two processes, water reorganization and conformational change, lead to multiexponential decay through relaxation.

The large change in dipole moment leads to a high degree of sensitivity to the local electrostatic environment, therefore multiple rotamer conformations have different fluorescence spectra, leading to ET-heterogeneity in fluorescence wavelength, and if these rotamers have different lifetimes (and quantum yields), which will frequently be the case, the results will display two or more DAS with positive amplitudes.

The indole ring of Trp in the ground state has a small dipole moment. Trp has two nearly degenerate singlet excited states, L_a and L_b. The change in dipole is greater for the L_a state as opposed to the L_b state. The L_a state is primarily the result of transition from the HOMO to LUMO. The relaxation of polar solvent molecules around the larger dipole of the L_a state leads to this state's energy being lower than

Figure 1.2: The orientation of the indole ring with respect to the peptide backbone is changed by rotation about χ 1 and χ 2.

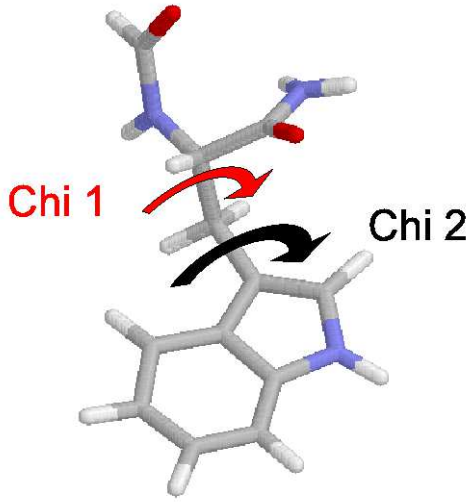

L_b in polar solvents, whereas L_b is the lowest energy state in perfluoro-carbon solvents and in the gas phase [42] [38] [58] [81].

The large dipole of the L_a state can be stabilized by a high dielectric constant solvent or by localized charges of protein or peptide. In this thesis all samples will have similar solvent exposure, but the effect of local charge is investigated and compared with similar work in the literature. The orientation of the dipole is shown in figure 1.3.

The variability of quantum yield of Trp in proteins has been explained in terms of fluorescence quenching by the amide group of the protein backbone. Several mechanisms of quenching were considered: a dipole-dipole resonance energy transfer to the amide, enhancement of non-radiative decay through vibrational coupling between amide and aromatic ring [22], or proton transfer from the excited aromatic

Figure 1.3: The electron density in the six member ring of the indole fused ring is higher in the L_a state than in the ground state. This figure shows the approximate direction of the electron density shift from the ground state to the L_a state. This shift results in a dipole change that can range in magnitude from 6 to 12 Debye.

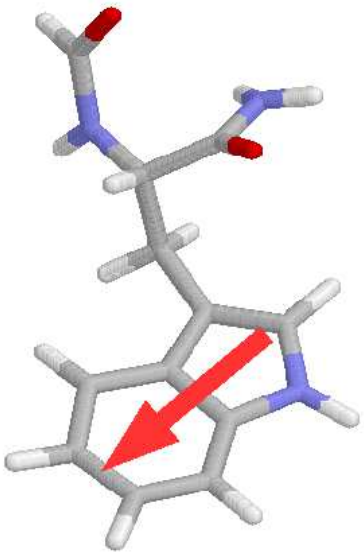

ring to the carbonyl group [94]. More recently this has been understood to be an electron transfer reaction [19] [15] [13], and this will be described in greater detail in the subsequent section. Quenching by a proton transfer mechanism has also described in the cases of simple indoles and the Trp zwitterion [24] and is discussed in greater detail in section 3 of this chapter. However this mechanism has yet to be shown in protein fluorescence quenching.

Hybrid quantum mechanical/molecular mechanical (QM/MM) methods have been used to explain the shift in fluorescence wavelength and variance in quantum yield [13] [15] [12].

The fluorescence lifetime for a single conformation is the inverse of the sum of all rate constants: the radiative rate of the indole, the non-radiative rates of the indole (internal conversion and intersystem crossing), the electron transfer rate, and the proton transfer rate. The quantum yield is the ratio of the radiative rate to the sum of all rates. For the compounds used in this study the radiative, internal conversion and intersystem crossing rates of the indole will be approximately constant. There are a number of theoretical models for the determination of the radiative rate based on the absorbance and fluorescence spectra of the electronic excited state. These models will not be applied in this study as they require mirror image absorbance and emission spectra. In the case of indole compounds the overlap of the ^1L_a and ^1L_b states complicates this analysis. It is found that the absorbance and emission spectra are symmetric when the ^1L_a is resolved independently.

The observation that methylated indole derivatives, and hence Trp, have an unusually large Stokes shift in polar solvents has long been a subject of investigation. The work of Meech, et al. described the fluorescence of methyl indole derivatives in solvents of varying polarities [61]. While the fluorescence emission wavelength maximum is highly dependent on the medium polarity the absorbance and quantum yield are relatively unaffected.

Isotope Effects of Tryptophan Fluorescence

The fluorescence intensity of Trp and indole derivatives have been shown to have a strong dependence on deuterium substitution [63]. The work of Nakanishi, et al. found that fluorescence intensity of indole compounds in a 1:1 mixture of water and deuterium oxide increased by 9 to 37 % over that in water. The substitution of the indole ring at several ring positions has been shown to strongly effect the extent of the isotope effect [63].

Electron Transfer Quenching of Tryptophan

The variation in fluorescence quantum yield as a function of local environment can be explained in terms of a photoinduced electron transfer reaction to the amide group of the protein backbone, shown to be capable of fluorescence quenching by Barkley, et al. [20]. This has been utilized to quantitatively predict the fluorescence quantum yields of a variety of single tryptophan proteins [13]. Briefly this work involved molecular dynamics simulations of the protein in question with explicit solvent (water). At periodic time steps in the MD simulation, the energies of the L_a and CT states are calculated in the ZINDO method (INDO/S2 cis) including all non QM atoms as point charges. The electron transfer rate constant is calculated via Fermi's golden rule.

$$k_{et}\left(\Delta E_{00}\right) = \frac{2\pi}{\hbar} V^2 \rho_{FC}\left(\Delta E_{00}\right) \tag{1.2}$$

Where ΔE_{00} is the difference in zero point energies between the CT state and the L_a state. V^2 is the electron transfer matrix element (or electronic coupling). This is essentially the method employed in this study and it will be described in more detail in the methods section.

In the case of bimolecular quenching of the indole chromophore (in the form of indole or 3-methylindole) the quencher requires 2 amide groups. This is the case of backbone amide quenching of tryptophan in proteins; the dipeptides in this study however only contain a single amide group. Our results will clearly show strong electron transfer in the dipeptides.

The charge transfer state is nominally an excitation from the indole HOMO to the amide LUMO. It has been found that the energy of the CT state is far more

sensitive to the local electrostatic environment than is the La state, due to the larger charge separation produced.

In addition to providing a mechanism for the variation in quantum yield, electron transfer quenching can also provide an explanation for non-exponential decay produced from ET-heterogeneity. Electron transfer quenching can be strongly influenced by the rotamer state of the tryptophan ring.

Proton Transfer Quenching of Tryptophan

The other quenching mechanism of interest in this study is proton transfer quenching form the protonated amine in the zwitterion form.

Proton transfer quenching is strongly evidenced in Trp by fluorescence titration experiments. This quenching mechanism has a strong kinetic isotope effect, with values in the literature typically ranging from 2-4, which can be utilized to partially distinguish it from electron transfer quenching. A recent study reported a KIE of 8 for quenching from an ornithine residue by a proton transfer mechanism. [60] This study by the Parson group further supports proton transfer quenching from a protonated amine.

Based on fluorescence titration and H/D exchange measurements it has been shown that the fluorescence quantum yield of Tryptophan is quenched by the proton transfer from the protonated amine, Lysine, Tyrosine or hydronium ion [19]. Photochemical H/D exchange has indicated that the fluorescence of simple indoles are quenched by proton transfer to multiple locations on the indole ring. In the work of Yu, et al., the proton transfer quenching of simple indoles was studied [100]. Exchange is detected at carbons 2, 4, and 7 of the indole ring in 3-methylindole. The numbering convention used for the indole ring is shown in the following figure.

The proton transfer quenching of Trp by the protonated amine at low pH (below 7) has been extensively characterized [49] [74] [73]. Photochemical H/D exchange in Trp has been found to occur primarily at C-4 of the indole ring, with up to 96% of D incorporation at this location [74] [73]. Incorporation of D at C-2 and C-7 are observed as minor products. The fluorescence quenching of tryptamine (no carboxylate to participate in quenching) is quenched only by proton transfer from the amine [78]. This quenching mechanism was confirmed to be an intramolecular proton transfer from the protonated amine of Trp [79]. The proton transfer quenching mechanism is inhibited if the protonated amine is complexed with a 18-crown-6 ether [79] [78].

High level quantum chemical calculations (CASSCF) in the gas phase have suggested that the proton transfer reaction can occur through a conical intersection [7]. This work suggests that a proton coupled electron transfer rather than simple proton transfer is a requirement for the quenching of Trp [7].

Fluorescence of Monellin and 5FTrp-Monellin

The fluorescence decay of the single Trp protein Monellin has been extensively studied by two research groups utilizing ultrafast fluorescence upconversion spectroscopy [68] [99]. This is the only example in which two research groups performed the same upconversion experiment on the same protein. These groups have obtained very similar data; however, they have arrived at very different interpretations. A time dependent spectral shift, termed in the literature as a time dependent fluorescence Stokes shift (TDFSS), is observed on the 1.2 and 16 ps time scales. Both groups find two sub-nanosecond decay components, 1.2 ps and 16 ps. Both groups assign the 1.2 ps component to bulk solvent reorganization in response to the excited state electron density. This explains the 1.2 ps spectral shift unambiguously in terms of relaxation of water solvent.

Zewail, et al. interpret the 16 ps component to the relaxation of a layer of constrained water around the protein, the "biological water" description. This would be the result of a population whose energy lowers over the 16 ps time scale. The other group, Xu, et al., produced decay associated spectra from their time resolved fluorescence emission data and found only positive amplitudes in the 16 ps component. This 16 ps component was blue-shifted (higher energy) in wavelength with respect to the other components observed. This lead them to conclude that this component was the result of a highly quenched subpopulation of conformations. A blue-shifted population with a decay rate faster than an accompanying red-shifted population with a slower decay rate will result in an observed spectral shift in the fluorescence wavelength as a function of time.

Subsequently, 5FTrp was substituted for Trp in the Monellin protein and the fluorescence decay was measured by fluorescence upconversion. [97] Replacement of Trp by 5FTrp converted the 16 ps all positive DAS to a 20 ps DAS with nearly equal positive (short wavelength) and negative (long wavelength) amplitudes. This observation confirms that the 16 ps component in the Trp-Monellin is the result of electron transfer rate heterogeneity and that this is suppressed in 5FTrp-Monellin. The observation of the relaxation component in 5FTrp-Monellin suggests that a similar relaxation component is present in the Trp-Monellin, but is masked by the faster decay in that case. This relaxation is likely the result of constrained water relaxation.

This type of spectral shift is the result of ET-heterogeneity and has been termed a pseudo-TDFSS by Callis and coworkers. [97] These pseudo-TDFSS effects can be especially difficult to differentiate from TDFSS in Tryptophan due to the observation that shorter lifetime components are almost universally shifted to shorter wavelength in comparison to longer lifetime components. The measurement of the time resolved

fluorescence emission of cyclic hexapeptides provided a large number of DAS in which the shorter lifetime components were always associated with the shorter wavelength DAS. [66] An explanation for this affect was provided by Pan, et al. using QM/MM methods developed by Callis and coworkers to correlate calculated wavelength and electron transfer rate of single tryptophan containing cyclic hexapeptides. [67] This leads to a red shifting pseudo-TDFSS that is difficult to distinguish from a TDFSS. Very strong evidence for pseudo-TDFSS is provided in the case of the synthetic amino acid Aladan incorporated into the B1 domain of streptococcal protein G. [1] Here the time resolved emission spectra display a shift to higher energy in the longer time scale of the experiment (1-10 ns). A shift to higher energy cannot be the result of solvent or protein reorganization in response to the charge difference between the ground and excited states of the chromophore. In the study by Boxer, et. al., the Aladan residue was incorporated into multiple sites in the protein chain. Longer fluorescence lifetimes were associated with the substitutions that had shorter fluorescence wavelength maxima. Therefore decay from two populations which have different fluorescence lifetimes and wavelength maxima, will lead to a blue shifting pseudo-TDFSS that cannot be mistaken for reorganization of the environment.

Tryptophan containing dipeptides have also been shown to exhibit fluorescence decay components on the order of tens of picoseconds [98]. Providing a definitive determination of the source of these tens of picosecond components, through the incorporation of 5FTrp in dipeptides, represented an initial motivation for the work presented here. A hypothesis of this work is that 5FTrp suppresses pseudo-TDFSS caused by electron transfer quenching, but not TDFSS caused by relaxation.

Fluorescence Properties of Tryptophan Dipeptides

Early studies on the fluorescence properties of Trp and Trp dipeptides were conducted in solutions at pH 7, leading to complication in the analysis of fluorescence data form the similarity of the population of anion and zwitterion forms. The work of Chen, et al. [18] correlated the fluorescence properties of Trp-X and X-Trp, where X is any other amino acid, dipeptides to the rotamer model of multiexponential decay. The rotamer model was first described to explain the multi-exponential fluorescence decay kinetics of tyrosyl derivatives [27]. This model describes conformations created through rotation about the C_α-C_β bond (The Chi1 dihedral), where each conformation can have a different fluorescence lifetime. This model has been applied to Trp fluorescence by a number of investigators, in terms of chi1 dihedral alone (giving 3 canonical rotamers) [18] as well as the chi1 and chi2 dihedral (C_β-C_γ bond), to produce 6 canonical rotamers.

Further evidence of the interaction between the Trp-X and NH3 groups are provided by the fluorescence properties of Trp-Trp. The fluorescence lifetimes of the Trp-Trp dipeptide are more consistent with X-Trp than Trp-X dipeptides. The wavelength of the emission is also consistent with the X-Trp dipeptides.

These dipeptides have a wavelength of maximum fluorescence (λ_{max}) that is about 10 nm shorter wavelength for Trp-X dipeptides as compared to X-Trp dipeptides. This is found to be universal with respect to the identity of the other amino acid. In addition the absorbance spectra of the Trp-X zwitterion is slightly shifted to lower wavelength with respect to the X-Trp zwitterion. The absorbance of two configurations of the anion are not different to a significant level [18].

Photochemical H-D exchange has been observed for Trp and Trp-X dipeptides, but not for X-Trp dipeptides, indicating a configuration dependence on proton transfer quenching [18].

The fluorescence decay kinetics of X-Trp dipeptides are found to be significantly more multi-exponential than that of Trp-X. The average lifetimes of the anions are longer than that of the zwitterions and the Trp-X configurations have longer lifetimes than the X-Trp for both anions and zwitterions. The authors report that these data suggest that the population of the Trp-X dipeptide consists primarily of a single rotamer conformation [18].

Osysko and Muino reported on the fluorescence properties of Trp, Trp-Asp and Trp-Arg in aqueous solutions of varying pH as well as alcohols with a range of polarities (Methanol, 1-Butanol, 1-Hexanol and 1-Octanol) [65] [62]. Two charged X residues were evaluated in the Trp-X peptides that were not studied in the work of Chen, et al. The spread of the quantum yield data were considerable in the cases of Trp and Trp-Asp.

The Quantum Yield and Initial Brightness Defects

Two studies describing rapid quenching of Trp dipeptides have been published. The first, published in 1991 by Chen, et al., showed a quantum yield defect in which the relative quantum yield measured by steady-state fluorescence methods was lower than that predicted by the observed average lifetime [18]. Based on the assumption that radiative and non-radiative rates of the indole moiety (k_r and k_{nr} in equation 1.1) are invariant between NATA and dipeptides, it was inferred that a quenching rate (k_{et} or k_{pt} in equation 1.1) occurred with a lifetime faster than the instrument response function, 50 ps for these experiments. The authors described this proposed mechanism as quasi-static self-quenching (QSSQ). Other studies had reported on the

possibility of static self quenching in indole derivatives, but the work of Chen, et al. provided more robust evidence for this.

QSSQ was further verified by a more recent study, with vastly greater time resolution, from the same research group published by Xu, et al., in which not only were components faster than the instrument response function of the work by Chen, et al., but also observed a lower initial brightness in an ultrafast fluorescence upconversion experiment, when compared to the initial brightness of NATA [98]. The authors suggested a very rapid quenching processes faster than the instrument response functions, with a width of 300 fs, of the time resolved fluorescence measurements [98]. That study also described 20-30 ps decay components which provided evidence for the QSSQ arguments put forward in the 1991 paper by Chen, et al. [18] In this previous work this was described in terms of static quenching in which a subpopulation of the ground state was in a conformation leading to fast quenching, faster than instrument response function. The level of static quenching was quantified by the ratio of the weighted average lifetime to the relative quantum yield. In their work Chen, et al. propose the term quasi-static self-quenching (QSSQ) to distinguish short lifetime components with low amplitudes that are undetected by instrumentation from classical static quenching from the formation of a dark complex in the ground state. This QSSQ is also supported by a fluorescence up-conversion study by the same group. Based on these observations, the authors conclude that interconversion of conformations is slow on the fluorescence time scale.

5-Fluorotryptophan Background

It is of interest to differentiate between ET-heterogeneity and relaxation in the multiexponential decay of Trp in proteins and peptides. A way to approach this is to suppress one of the two mechanisms. The use of 5-fluorotryptophan (5FTrp), is

used to reduce the effect of ET-heterogeneity, but not relaxation. Relaxation effects in multiexponential decay may even be enhanced for 5FTrp fluorescence compared to Trp, due to a larger dipole change upon excitation.

5FTrp has recently been used in place of the intrinsic fluorophore Trp for the study of protein biophysics; this leads to nearly single exponential fluorescence decay in single tryptophan (Trp) mutants of the dimeric mannitol transporter of *Escherichia coli*, EII^{mtl}. [8] [92] In this case the fluorescence lifetime of the 5FTrp is not quenched with respect to the 5-Fluoro-3-methylindole (5F3MI).

5FTrp exhibits a higher ionization potential compared to Trp of 0.19 eV in the gas phase as well as a lower L_a state energy of about 0.1 eV. [53] These effects combine to increase the energy of electron transfer quenching by 0.29 eV. This energy change was shown to reduce electron transfer quenching rates to nearly unresolvable levels for interactions up to 70 cm^{-1}. A combination of CASPT2 calculations, fluorescence anisotropy measurements and absorbance and emission spectra indicate that the fluorescing state is L_a as for Trp. This work showed that fluorination at any of the available positions on the indole ring lead to an increase in ionization potential, with the 5 position leading to the largest magnitude effect. For example, in the EII^{mtl} protein the Trp mutants all display 3 exponential fluorescence decay and 5FTrp mutants decay single exponentially; 6-fluorotryptophan (6FTrp) mutants were all best fit with 2 exponential decay, showing a reduction in ET-heterogeneity but to a lower degree compared to 5FTrp. The suppression of electron transfer quenching in this protein is further evidenced by a high degree of correlation between the fluorescence wavelength and lifetime. While 5FTrp significantly suppresses the electron transfer quenching mechanism, the similar increase in dipole moment upon excitation causes a similar dependence of fluorescence wavelength on environment.

Therefore multiexponential decay due to relaxation should not be eliminated by 5FTrp substitution.

The quantum yields of 5F3MI and 5-fluoro-N-acetyl-tryptophanamide (5FNATA) have been measured to be 0.25 and 0.21 respectively, with lifetimes of 6.8 and 4.4 ns. [8]

In a few studies the fluorescence lifetime of 5FTrp in protein is shown to be significantly quenched. [75] [96] While quenching is observed in these cases, the ET-heterogeneity of fluorescence decay is vastly reduced when compared to the corresponding Trp. In the case of the protein barstar, 5FTrp was engineered into the protein at position 53 in the peptide chain. [75] The fluorescence decay kinetics were measured for Trp and 5FTrp variants of the protein in the folded and unfolded state. Upon investigation of the NMR structure (PDB 1AB7 model 1) it is observed that this Trp is located in the hydrophobic core surrounded primarily by LEU, ALA, PHE, and ILE. Another study involved studies of the protein α-synuclein, which being a highly disordered protein will have 5FTrp residues that are highly solvent exposed. In this study a quantum yield of 0.2 and lifetimes of 3.4 ns were measured.

5FTrp has been investigated in FRET experiments, and it has been found that the rate of energy transfer from one 5FTrp residue to another is increased with respect to Trp due to an increase in the overlap of absorbance and fluorescence spectra in the case of 5FTrp. [75] [90]

The studies described here in addition to results presented later in this work will point to a pattern of 5FTrp fluorescence lifetime quenching in cases of high solvent exposure.

The fluorination of amino acids has an effect on the water dynamics of the solvent. Kwon, et al. describe the effect for replacing a leucine adjacent to a Trp residue with a tri-fluoridated analog. They find that this substitution leads to a

slowing of the hydration dynamics on the 10s of ps and faster time scales [47]. The increase in size of a fluoridated residue with respect to it hydrogenated counterpart by itself leads to faster dynamics of the water layer surrounding the residues. The longer time scale seems to be the result of a dipolar interaction between the C-F bond and nearby water molecules.

Conformation of Tryptophan Dipeptides

The ground state and excited state conformational populations of dipeptides have a significant effect on their fluorescence properties. These populations affect the propensity for ET-heterogeneity in fluorescence decay. The energy barriers between the conformational local minima, and thus the rate of conformational transitions, affect the level of spectral relaxation in fluorescence properties. Molecular dynamics is used to determine these populations and the rate of transitions between these conformations in this study.

Much attention has been paid to the conformational populations of dipeptides and other small peptides, with the ultimate goal of adding to our understanding of protein folding and the development of better force field models for molecular dynamics simulations. [54] [34] [30]. Three major backbone conformations have been identified or suggested, polyproline II (P_{II}), β-sheet (β), and right handed α-helix (α_R). Understanding the relative populations of each has been approached via a number of experimental and theoretical methods.

The majority of molecular dynamics force field in common use (CHARMM27, AMBER94(03), OPLSAA(/L)) are parametrized based on a combination of experimental and computational methods to reproduce the structures of the majority of folded protein structures. A recent study produced free energy surfaces (FESs) via the DFT ab initio method and also by metadynamics simulation with a variety of force

fields. [54] A comparison between the ab initio and force field FESs shows that the force fields differ significantly in their ability to reproduce the ab initio FES. None of the force fields reproduced the DFT FES more accurately in all conformational regions. Another recent study has shown that the addition of dispersion correcting atom centered potentials to the DFT method leads to more accurate structural characterization of peptides more complicated than the alanine dipeptide. [51] Other methods to include weak interactions important in peptides and other systems of biological importance are DFT-D [31] [32] [33] and newer functionals, such as M06 and M06-2X [102]. Weak interactions relevant to tryptophan residues, and other aromatic residues, are cation-pi, CH-π [39], $\pi - \pi$, and edge-pi interactions.

Most of the effort documented in the literature has been focused on short peptides of alanine, being one of the simplest amino acid side chains. [54] The vast majority of the literature to date is focused on the peptides with acetylated n-termini and amidated c-termini, as these are more relevant to amino acids in a protein. Our work will study the conformations of zwitterionic and anionic amino acid dipeptides. A large portion of the work associated with the alanine dipeptide has been in the mapping of the 2D energy landscape of ϕ and ψ angles. In the case of uncapped dipeptides, as in this study, only one of these angles will be defined for each peptide in the dipeptide, ψ of the n-terminal residue and ϕ for the c-terminal residue.

There are two configurations of peptides of interest in this study, X-Trp and Trp-X. In the X-Trp configuration the Trp is the c-terminal residue. Trp is the n-terminal residue in Trp-X. The structures of Gly-Trp and Trp-Gly are shown in figure 1.7 as examples.

Project Overview and Objectives

This section will present an outline of materials presented in the remainder of this document. Here the goals, motivations, and overall methods of this work are presented in broad general terms.

Significance

To advance the ability for the use of tryptophan fluorescence in biophysical studies, a method is needed to deconvolve the various effects on fluorescence decay from one another. If multiexponential decay caused by multiple populations of conformations in the ground state can be separated from those caused by conformational change during the excited state lifetime, a better understanding of peptide conformation and dynamics may be possible.

Motivations

An original motivation of this project was the definitive explanation of the nature of the short time scale (10-50 ps) components in tryptophan fluorescence decay that have been observed in Monellin. In order to evaluate the relative proportion of relaxation or ET-heterogeneity, substitution of Trp by 5FTrp was proposed in order to suppress possible ET-heterogeneity. If the 5FTrp substituted protein also displayed the tens of picoseconds decay component, it would suggest that this component is the result of relaxation. Unfortunately, attempts to incorporate 5FTrp into Monellin by a collaborator were unsuccessful. Therefore, tryptophan dipeptides, which were easily obtained in both Trp and 5FTrp variants were used in this thesis work. This work presented in this thesis was motivated by the experimental observation of a 20-30 ps decay component, with only positive amplitudes, in tryptophan dipeptides. [98]

An additional motivation is presented by the observed loss of initial brightness, suggesting possible electron transfer quenching with a rate high enough to produce a lifetime less than 300 fs, provides a compelling test of the QM/MM methods developed by Callis and co-workers. The origin of fluorescence decay components with rate constants of 20-30 ps or 300 fs for tryptophan is a continuing debate in the literature. This thesis work evaluated the potential contribution of electron transfer quenching to decay rates of 20-30 ps and 300 fs.

Experimental Fluorescence Overview

The steady state and time resolved fluorescence of Trp and 5FTrp dipeptides were measured in buffers of pH 5 or 10, and in water or D_2O solvent.

Goals. In this work the fluorescence properties of Trp and 5FTrp dipeptides were compared to distinguish between multiexponential decay from the following sources:

1. Electron transfer quenching.
2. Proton transfer quenching.
3. Relaxation processes based on a shift in dihedral angles defining the orientation of the indole ring.

To this end we determine the fluorescence decay kinetics of tryptophan and 5FTrp dipeptides in the zwitterion (low pH) and anion (high pH) forms in water and deuterium oxide solutions over a range of wavelengths.

Experimental Rationale. The suppression of electron transfer, and lack of proton transfer suppression, by substitution of tryptophan by 5FTrp, as well as the kinetic isotope effect of proton transfer quenching, facilitates the distinction between these quenching mechanisms. Conformational relaxation mechanisms are distinguished

Table 1.1: Table showing quenching mechanisms expected for each permutation or experimental conditions. (KIE) indicates that a kinetic isotope effect is expected in the quenching rate.

	Trp	**5FTrp**
pH 5	proton, electron	proton
pH 10	electron	none
pD 5	proton (KIE), electron	proton (KIE)
pD 10	electron	none

from ET-heterogeneity as these are not suppressed. The fluorescence decay of dipeptides at high pH provides a set of measurements only affected by electron transfer quenching. Measurements in D_2O allows for the determination of kinetic isotope effects on the rate of fluorescence quenching, allowing for an estimation of the proportion of electron transfer compared to proton transfer, as it is expected that such an isotope effect would be primarily the result of proton transfer quenching. The determination of quenching rates in both the zwitterionic and anion forms also illustrates the affect of changes in the local electrostatic environment on the electron transfer rate.

Steady state optical absorbance spectra and fluorescence excitation and emission spectra were compared to similar work presented in the work of Chen, et al. [18], which show shifts in these spectra between Trp-X and X-Trp peptide configurations, to determine if these were affected by the substitution of 5FTrp for tryptophan or the inclusion of charged X residues (Asp, Arg), which are new to this study. Decay associated spectra were produced from the collected time resolved waveforms of dipeptide fluorescence, to determine the propensity for dipeptides to display relaxation or ET-heterogeneity in their multiexponential decay as a function of configuration, pH, and 5FTrp substitution.

Computational Prediction Overview

The QM/MM method developed over the last decade by the Callis group was employed toward the following goals:

1. To determine the ground and excited state conformational populations and the rate of interconversion between conformations through microsecond molecular dynamics simulations. The populations of individual rotamers relate to quenching rate heterogeneity based non exponential decay and pseudo-TDFSS. Interconversion rates provide insight into the contribution of peptide conformational changes to the relaxation components of fluorescence decay, relating to TDFSS. Interconversion between rotamers of the protein is the only mechanism that could lead to relaxation components on the order of nanoseconds; bulk solvent relaxation occurs in about 1-2 ps and postulated protein-constrained water relaxation occurs in the range 10 - 200ps. [68] The interconversion rates between rotamer state were compared to the fluorescence lifetimes. Chen, et al. suggested that interconversion of rotamer states is slow on the time scale of the fluorescence lifetime and that Trp-X dipeptides are dominated by a single conformation. [18]

2. To calculate instantaneous electron transfer rates throughout molecular dynamics simulations. The fluorescence quantum yields and lifetimes of Trp-Gly and Gly-Trp were calculated, with the goal of understanding the long observed phenomenon that Gly-Trp has a significantly lower quantum yield than Trp-Gly. A subpopulation of conformations with instantaneous electron transfer rates high enough to produce lifetimes of 10-30 ps explains QSSQ in terms of fast electron transfer quenching. Instantaneous electron transfer rates were

compared with the experimental results suggesting that there are conformers quenched in less than 300 fs.

3. To calculate the fluorescence wavelength maxima and investigate the source of the universal blue shift in fluorescence wavelength of Trp-X dipeptides compared to X-Trp dipeptides; the contribution to the wavelength shift from solvent, and from zwitterionic charges (NH3+ and COO-) were calculated.

The results of these three goals analyzed together allow for the prediction of the relative amounts of TDFSS and psuedo-TDFSS in fluorescence results.

Figure 1.4: Calculated vs measured fluorescence wavelength. Calculated wavelengths determined by QM/MM method described in Callis and Vivian (2001) [91]. Figure is adapted from Callis and Vivian (2001) [91]. Figure from P. Callis Collection [9]

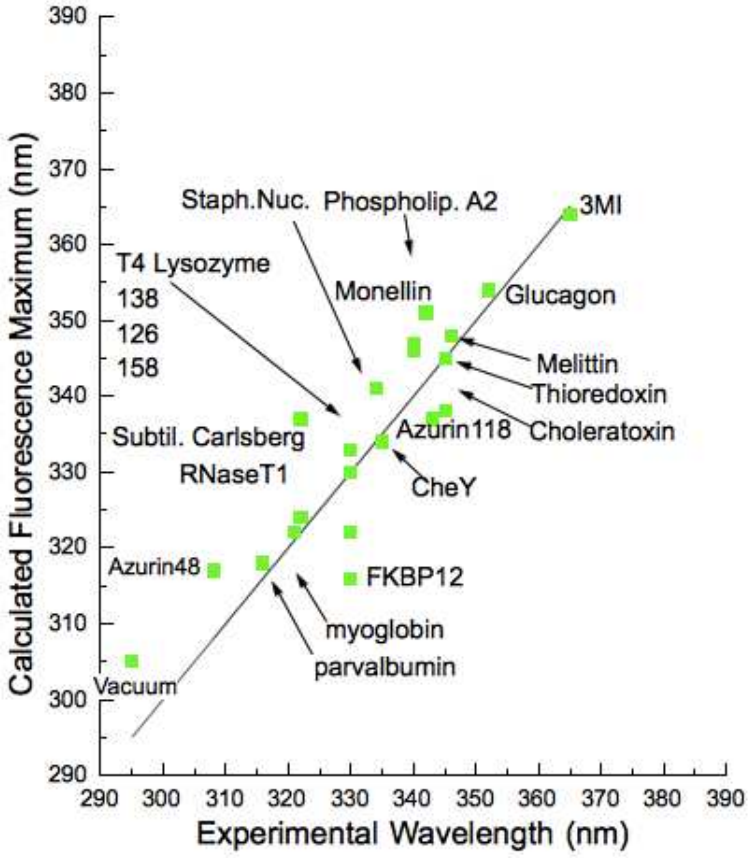

Figure 1.5: Calculated vs measured fluorescence quantum yield. The line is Calculated = Experimental. The quantum yields were calculated via the QM/MM method described in Callis and Liu (2004) (This figure adapted from Callis and Liu (2004)) [13].

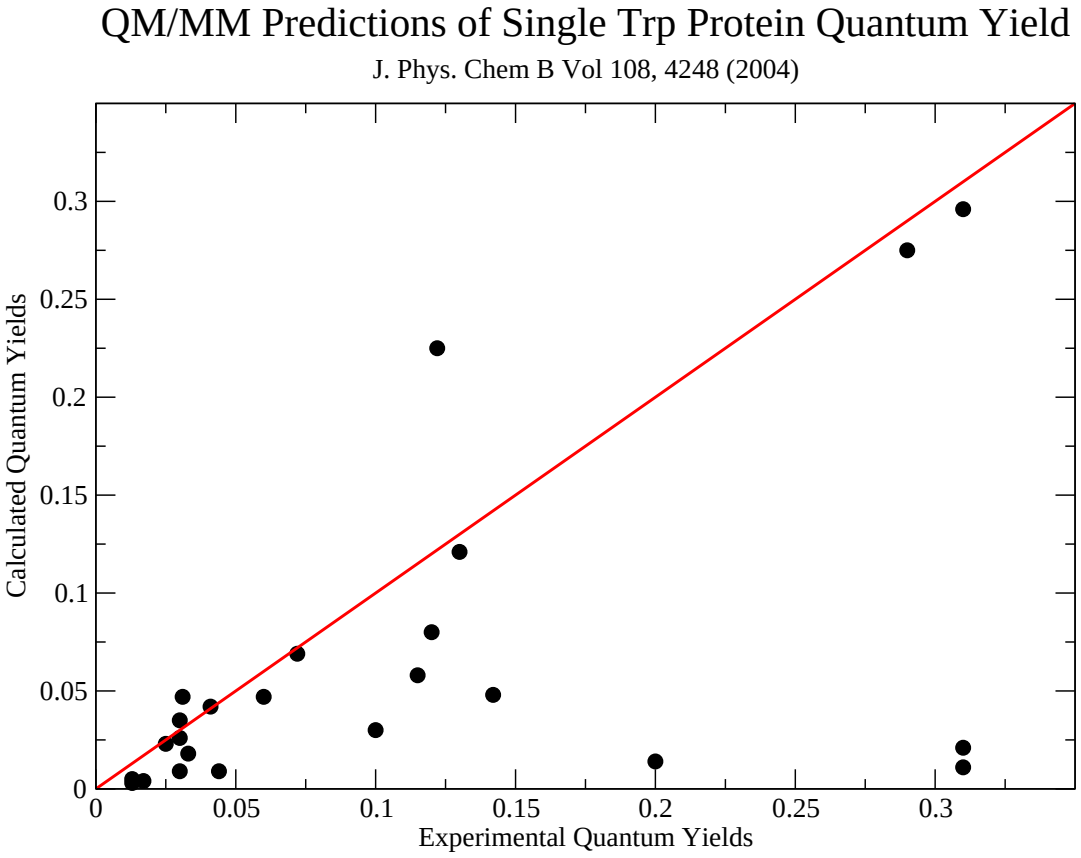

Figure 1.6: Structure of the indole ring with numbering.

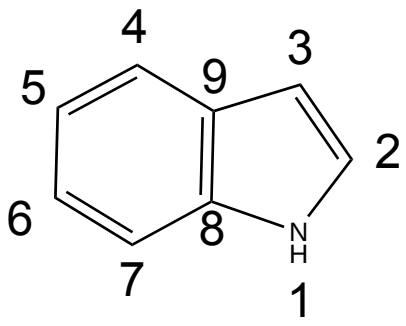

Figure 1.7: Representative structures of the X-Trp (left) and Trp-X (right) conformations. X=Gly in these figures.

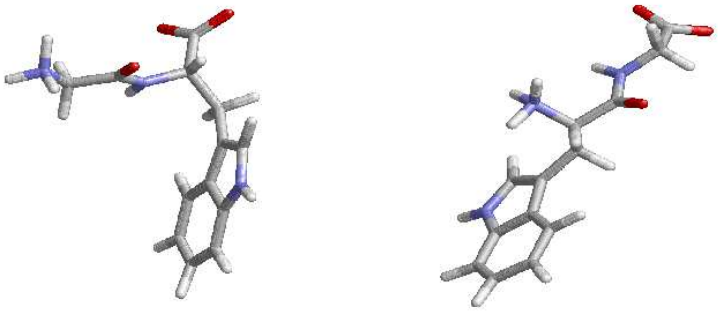

METHODS

This chapter describes the experimental and computational methods used in this thesis work. Nanosecond time scale laser induced fluorescence was measured by a direct waveform recording instrument developed by Fluorescence Innovations Inc. This method was used to determine the decay associated spectra and lifetimes of the decay components of tryptophan in the dipeptides studied. The average fluorescence lifetime and quenching rates over the majority of the fluorescence wavelength range was determined from these DAS. These results allowed the evaluation of the relative contributions of electron transfer to amide, proton transfer quenching, and relaxation to the multiexponential decay from tryptophan in these dipeptides. QM/MM methods developed by Callis and co-workers were used to calculate fluorescence wavelength and electron transfer rates.

Steady State Measurements

Fluorescence emission and excitation measurements were collected with a Jobin Yvon Horbia FluoroLog. A Perkin Elmer Lambda 25 UV/VIS was used to collect absorbance measurements. Fluorescence measurements were collected without excitation or emission polarizers. The excitation and emission slits were set to 1 nm and 5 nm bandpass respectively.

The absorbance and emission spectra of a fresh sample of NATA at pH 7 was used as a reference for each data collection.

Direct Waveform Recording Instrument

Fluorescence data were collected at Fluorescence Innovations, Inc. on a prototype ultraviolet fluorescence lifetime spectrometer. The data were collected

in the form of wavelength-time matrices, i.e., fluorescence decay curves at a series of emission wavelengths. Standard 10-mm internal pathlength fused silica cuvettes were used in these experiments. The excitation source in the instrument is a very compact frequency-doubled dye laser (pyrromethene 597 in ethanol solvent (Exciton)) pumped by a pulsed 532 nm microchip laser (Teem Photonics PowerChip), which was operated at 294 nm for these experiments. Relevant parameters include 0.3 μJ pulse energy, 1000 Hz pulse repetition frequency, and 0.5 ns pulse duration. The fluorescence detection module is a Varian Cary Eclipse spectrofluorimeter, which has been modified by replacing the standard photomultiplier tube (PMT) with a Hamamatsu R-7400 PMT. Time-domain fluorescence data were recorded with a proprietary transient digitizer that generates a complete fluorescence decay curve on every laser shot. The digitizer, which employs an analog memory, samples at 1 gigasample/sec (i.e., 1 ns spacing in the time domain). The effective sampling rate is increased to a time point every 200 ps via 5X interleaving. Each fluorescence decay waveform is averaged over 500 laser shots, corresponding to 0.5 second acquisition time per waveform. Fluorescence data were recorded every 5 nm from 300 to 400 nm at 20°C. The emission bandpass was set at 5 nm. Emission was collected through an emission polarizer set to the magic angle (54°). The PMT voltage was 320-560 V for these experiments. A freshly produced solution of N-acetyltryptophanamide (NATA) in water (DI or 18 MΩ Millipore) was used as a reference emitter at the same PMT voltage as sample collection.

Table 2.1 shows correction factors for the wavelength dependence of the instrument response.

Table 2.1: Correction factors as a function of wavelength provided by Fluorescence Innovations, Inc.

Wavelength (nm)	correction factor	λ	corr. fact.	λ	corr. fact.
310	1.60	360	0.981	410	0.473
315	1.33	365	0.946	415	0.458
320	1.13	370	0.894	420	0.446
325	1.00	375	0.830	425	0.443
330	0.959	380	0.765	430	0.444
335	0.918	385	0.699	435	0.442
340	0.942	390	0.636	440	0.443
345	0.965	395	0.583	445	0.444
350	1.00	400	0.534	450	0.447
355	1.01	405	0.503		

Analysis of Time Resolved Data

The instrument response function (IRF) of a time resolved fluorescence instrument is the time resolved waveform which would result from a sample with delta function emission. This can be estimated by the data collected from the scatter of the excitation source (laser scatter). The waveform measured from a sample is the convolution of the IRF and the exponential function of the actual fluorescence decay. In order to determine the mathematical form of the fluorescence decay (exponential function), the effect of the IRF must be removed from the data.

The instrument response function was deconvolved from the time resolved fluorescence spectrum via the iterative reconvolution method. The convolution of the instrument response function with the exponential function of the fluorescence decay (for a single exponential decay) is shown in the following equation [16].

$$F_{calc}(t) = \sum_{i=1}^{1,2or3} A_i \int_0^t IRF(t-t')exp^{-t'/\tau_i}dt' \tag{2.1}$$

$F_{calc}(t)$ is then compared with the measured fluorescence waveform by difference, resulting in the residuals. The sum of the residuals are minimized with respect to the preexponential amplitude (A) and the decay time constant (τ). The minimized residuals are analyzed statistically to determine goodness of fit. The data in this study is analyzed with one, two and three exponential fits.

In this study, the reference emitter method was used to remove the effects of the IRF. At 355 nm the fluorescence of NATA is single exponential with a lifetime of 3.1 ns.

The calculated waveform determined by the reference emitter method is given by the following equation. Derived by Greg Gillispie from Demas, et al. [16] [28]:

$$F_{calc}(t) = \sum \frac{A_i}{A_{ref}} \left[F_{ref}(t) + \left(\frac{1}{\tau_{ref}} - \frac{1}{\tau_i} \right) \int_0^t F_{ref}(t)\, e^{-(t-t')/\tau_i} dt' \right] \tag{2.2}$$

Evaluation of Fit Quality

Our data is fit to one, two and three exponential models. The quality of fit of fluorescence data collected by time correlated single photon counting (TCSPC) is typically evaluated based on the χ^2 goodness of fit parameter. This method does not strictly work for the direct waveform recording method because data from this method does not follow Possion statistics. For this reason, we minimize the numerator of the χ^2 expression and evaluate the autocorrelation of the residuals (the fit waveform subtracted from the measured waveform).

$$\chi^2 = \sum_{k=1}^{n} \frac{|N(t_k) - N_c(t_k)|^2}{N(t_k)} \tag{2.3}$$

Decay Associated Spectra

Non-exponential decay is described in terms of multiple species each with their own spectrum [55] [44].

$$F_m(t) = \sum_{i=1}^{N} A_i exp^{-t/\tau_i} \tag{2.4}$$

$$F_m(\lambda, t) = \sum_{i=1}^{N} A_i(\lambda)\, exp^{-t/\tau_i} \tag{2.5}$$

We convert the average lifetimes to the quenching rate constant by:

$$k_q = \tau_f^{-1} - \tau_{f_0}^{-1} = k_{et} + k_{pt} \tag{2.6}$$

Where τ_f is the lifetime measured and τ_{f_0} is the lifetime of the unquenched fluorophore (e.g. 3MI or 5F3MI). As the carboxylate group is unable to act as a quencher [19] and the amine only quenches in the protonated form by proton transfer, we use the lifetime of the anion of tryptophan or 5-fluorotryptophan in the appropriate solvent as the unquenched lifetime.

The proportion of the steady state fluorescence represented by a decay component is represented by the amplitude of the fit multiplied by the decay lifetime ($A_i\tau_i$) [48]. The steady state intensity is also represented by the integral of the time resolved waveform over all time $\sum_{i=1}^{\#comps.} \left(\int_0^\infty e^{-t/\tau_i} dt\right)$. As a test of our data quality and data analysis, the fractional fluorescence sums for each fit were plotted against the integrated waveforms and the steady state fluorescence spectrum.

Chemicals and Materials Used

Trp-X dipeptides have marginally lower pK_a values for the deprotonation of the primary amine compared to X-Trp dipeptides, and has been seen as further evidence that the indole ring or Trp interacts with the amine. In this work, samples are produced at pH values at least two units from the reported pK_a values, therefore is is unlikely that the difference between Trp-X and X-Trp will influence results to a significant degree. Zwitterion and anion samples were measured at pH 5.5 and 9.3 respectively by Chen, et al. (pH 5 and 10 in this work).

3-Methylindole, 5-fluoro-tryptophan, Trp-Gly and Leu-Trp were obtained from Sigma. Gly-Trp was obtained from TCI America. Trp-Leu, Arg-Trp, Asp-Trp, Met-Trp, Trp-Arg, Trp-Asp, Trp-Met were purchased from Bachem. 5-fluorotryptophan dipeptides were custom synthesized by Celtek Peptides (Celtek Bioscience LLC). D_2O (99 Atom%) was obtained from Cambridge Isotope Labs.

The amino acids of the tryptophan dipeptides were all of the L enantiomeric form. The 5-fluorotryptophan was a racemic mixture of D and L forms while the X residue was purely in the form of the L enantiomer.

Peptide samples were used as acquired from the vendor without further purification. Buffer solutions of pH 5 were produced with approximate 10 mM sodium acetate solutions pH adjusted with acetic acid.

Buffers for the determination of deuterium isotope effects were 10 mM carbonate or 10 mM acetate in 99.9% D_2O and pH adjusted to pH 10 or 5 respectively, with DCl (35 % w/w 99 atom % D) or KOD (40 % w/w 98+ atom % D) in D_2O (99 atom % D).

An Okton pHTester 30 was used to measure the pH of the buffers. For D_2O buffers pD was determined from the pH meter reading by $pD = pH + 0.4$ [29].

Computational Methods

Dynamics calculations were performed using GROMACS version 4.5.4 [36] [89] [52] [5] molecular dynamics software package. Starting form the unminimized rotamers produced in charmm, minimization by a steepest descent algorithm was performed in Gromacs until the maximum force was 200.0 kJ mol^{-}1 nm^{-}1 or 50000 steps of 0.001 nm were performed. This was followed by 100 ps of NVT dynamics with the peptide subjected to position restraints (heavy atoms only) for the purpose of equilibrating the explicit water solvent. The resulting structures were subjected to multiple microseconds of NPT dynamics, at a temperature of 300 K and pressure of 1 bar, in Gromacs with structures saved every 100 ps. Both NVT and NPT MD simulations were performed with 2 fs time steps. The P-LINCS algorithm [35] was used to constrain all atom bonds. All molecular dynamics simulations were conducted with 3 dimensional periodic boundary conditions with a cubic unit cell. The cutoff distance for short range electrostatic and van der Walls force calculations was 1.0 nm. Long range electrostatics were calculated via the particle mesh Ewald method [25]. Molecular dynamics simulations were performed with either OPLS-AA [70] [41] [93] [59] [40], CHARMM, or AMBER force fields. A sodium cation was added to dipeptide anion systems to neutralize the total charge.

The rate of conversion between rotamer populations was determined by the method described by Toptygin and Brand. [86] [85]

$$k_{nm} = \frac{\#\ of\ n \rightarrow m\ transitions}{Total\ time\ in\ rotamer\ n} \tag{2.7}$$

The quantum yields and fluorescence wavelengths of dipeptides were modeled by a QM/MM method [13]. The energies of the La and CT states are calculated by

the INDO/S2-CIS (Zindo) method, the code for which was provided to Prof. Patrik Callis in 1980 by the original developer, Prof. Michael Zerner [72] [83] [21]. This code was extended with the capability of reading input of electric fields and potentials calculated from the molecular dynamics environment.

The INDO/1 one-electron integrals, Mataga-Nishimoto electron repulsion parameters and interaction scaling factors of fσ = 1.267 and fπ = 0.585 are used in this method as well as improved parameters for Oxygen developed by Li, et al. [50] (implied by S2 in the method string).

The energies of the L_a and CT states and their response to electric fields are reproduced with sufficient accuracy [12], as shown by comparison to CASPT2 [4] [3] calculations of formamide-indole pairs as a function of electrostatic environment [53]. A fundamental quantum chemical study on indole [23] also indicates an accurate response of the Zindo method to fluctuations in the electric field.

The fluorescence quantum yield is described by the following equation:

$$\Phi_f = \frac{k_r}{k_r + k_{nr} + k_{et} + k_{pt}} \tag{2.8}$$

Where k_r, k_{nr}, k_{et}, and k_{pt} are the radiative, non-radiative, electron transfer and proton transfer rate constants respectively.

Electron transfer rate constants were calculated by the Fermi Golden Rule:

$$k_{et}\left(\Delta E_{00}\right) = \frac{2\pi}{h} V^2 \rho_{FC}\left(\Delta E_{00}\right) \tag{2.9}$$

ΔE_{00} is the difference in zero point energies between the CT state and the L_a state.

There are two potential methods for predicting the observed steady state quantum yield from the calculated electron transfer rates. Calculation of the instantaneous quantum yield at each frame of the MD trajectory and averaging is

represented by equation 2.10. Equation 2.11 shows calculation of the instantaneous electron transfer rate at each frame and averaging. The average electron transfer rate is used to calculate the average quantum yield.

$$\langle \Phi_f \rangle = \left\langle \frac{k_r}{k_r + k_{nr} + k_{et}} \right\rangle \tag{2.10}$$

$$\langle \Phi_f \rangle = \frac{k_r}{k_r + k_{nr} + \langle k_{et} \rangle} \tag{2.11}$$

A number of methods have been developed for the calculation of electron transfer matrix elements (V_{12}) including generalized Mulliken-Hush method [17], method of Corresponding Orbital Transformation [43] and the CIS method used here [14]. In short, V_{12} is taken from the CIS Hamiltonian elements coupling the HOMO-LUMO(ring) and the HOMO-ring amide π^* transitions.

Geometry optimization of neutral species and radical cation were performed at the DFT/B3LYP level of theory with the 6-31G* basis. Solvation in water was treated by PCM. [84] Frequency calculations at the same level were used to determine zero point energy corrections. Single point energy calculations used the DFT/B3LYP 6-311G+(2df,2p) PCM level of theory. All calculations utilized Gaussian 03. [26]. This procedure is similar to the procedure in Liu et al. [53], which compare very well with experiment, with the addition of the solvent model.

Atomic charges for molecular dynamics simulations were produced by the Merz-Singh-Kollman electrostatic potential fitting procedure implemented in Gaussian 03 (Pop=MK keyword) [80] [6]. This method has been shown to provide values with less variation based on the choice of basis set and theory level. [57]

Geometry optimization calculations at the DFT level of theory with the B3LYP hybrid functional have been shown to be effective at the accurate representation of relative energies of rotamer subpopulations. [54]

EXPERIMENTAL FLUORESCENCE RESULTS

The next two sections will describe the results of steady state and time resolved fluorescence measurements and how these results relate to partitioning between relaxation and ET-heterogeneity in tryptophan fluorescence decay.

Steady State Absorbance and Fluorescence Results

This section presents the results of state absorbance and fluorescence measurements. Shifts in fluorescence wavelengths are shown between Trp-X and X-Trp dipeptides.

Absorbance Shift of X-Trp vs Trp-X

The absorbance difference spectra between X-Trp and Trp-X are shown in figures 3.1 - 3.5. The difference spectra are computed by subtraction of the Trp-X(5FTrp-X) peak normalized absorbance spectra from that of the X-Trp(X-5FTrp). The peak normalized fluorescence excitation spectra of each of the dipeptides are shown in figures 3.6 - 3.9. Absorbance and excitation spectra show that in the zwitterionic form the absorbance of Gly-Trp is lower energy than Trp-Gly. The excitation spectra indicate that this shift is smaller for Gly-5FTrp vs 5FTrp-Gly. In the anionic form there is no apparent shift for Trp of 5FTrp dipeptides.

Fluorescence Excitation Spectra

Figures 3.6 - 3.9 display the fluorescence excitation spectra for X-Trp, Trp-X, X-5FTrp, and 5FTrp-X dipeptides at pH 5 and 10. These are shown for X=Gly and Leu.

Figure 3.1: The plot on the left shows the absorbance difference between Gly-Trp and Trp-Gly at pH 5. On the right the same is shown for Gly-5fw and 5fw-Gly at pH 5.

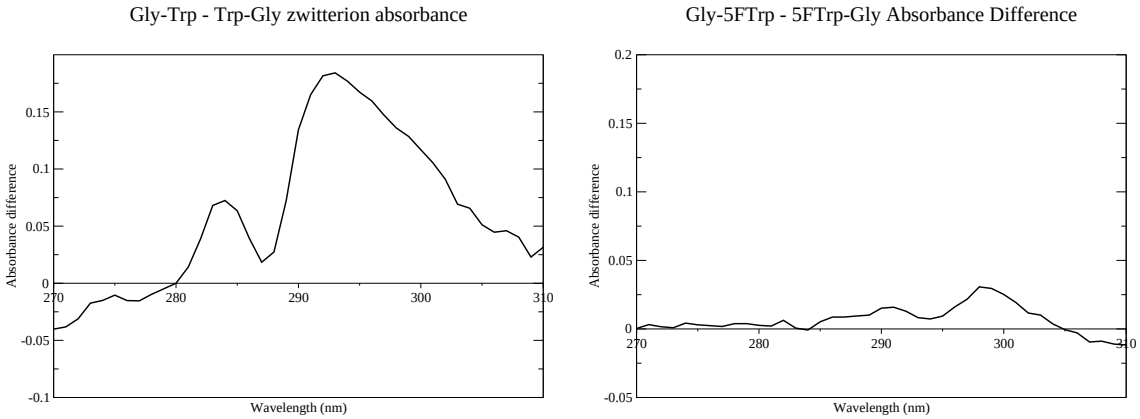

Fluorescence Emission Spectra

The steady state absorbance and fluorescence spectra of the various dipeptides are shown in figures 3.10 - 3.14. In several of the spectra shown, a peak is seen at approximately 330 nm, this corresponds to the water raman peak for excitation at 295 nm. We observe that absorbance spectra for 5FTrp dipeptides are shifted to lower energy as compared to the corresponding Trp dipeptide.

Nanosecond Results

In this section the results of direct waveform recording measurements will be presented. The DAS resulting from the global analysis of time resolved emission waveforms, and the average fluorescence decay parameters obtained from these are shown.

DAS of Tryptophan and 5-Fluorotryptophan

The DAS obtained for Trp and 5FTrp zwitterions are shown in figures 3.16 and 3.17. It is observed that both decay bi-exponentially with the short lifetime

Figure 3.2: The plot on the left shows the absorbance difference between Leu-Trp and Trp-Leu at pH 5. On the right the same is shown for Leu-5fw and 5fw-Leu at pH 5.

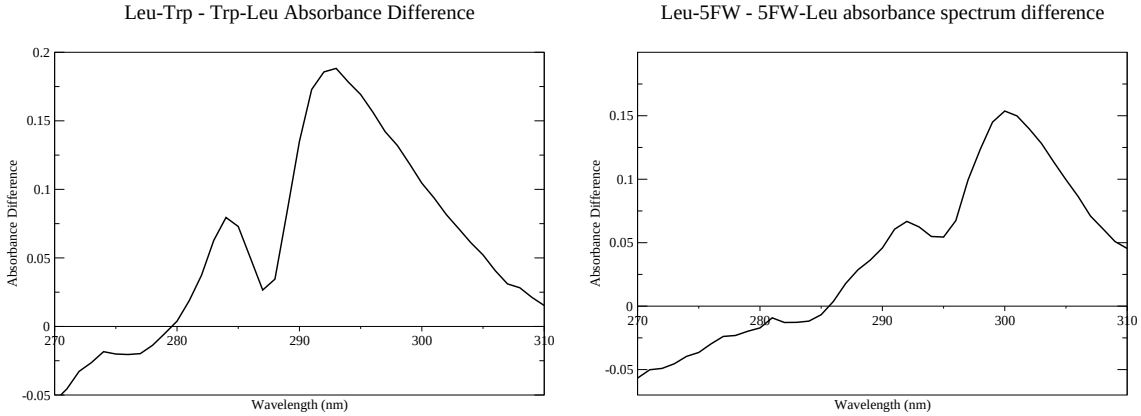

component having positive amplitudes at short wavelength and negative amplitudes at long wavelength.

In D_2O the proportion of negative amplitude of the short component of the Trp zwitterion fluorescence decay increases in agreement with the results of previous studies [95]. The decay constant for this component increases by a factor of 2 in D_2O. We find that 5FTrp has almost identical amplitudes and lifetimes of the short component. For both Trp and 5FTrp the lifetime of the long component increases by approximately a factor of 2.

The DAS of Trp and 5FTrp anions (pH(D) 10 and 11) are shown in figures 3.18 - 3.21. The significant difference between results at pH 10 and 11 should be noted.

DAS of Tryptophan and 5-Fluorotryptophan Dipeptides

The average decay associated spectra with standard deviations shown as error bars for the 2 exponential fits of Trp-Gly and Gly-Trp, 5FTrp-Gly, and Gly-5FTrp at pH(D) 5 and 10 are presented in figures 3.22 - 3.29. Figures for all other dipeptides are shown in appendix A.

Figure 3.3: The plot on the left shows the absorbance difference between Asp-Trp and Trp-Asp at pH 5. On the right the same is shown for Asp-5fw and 5fw-Asp at pH 5.

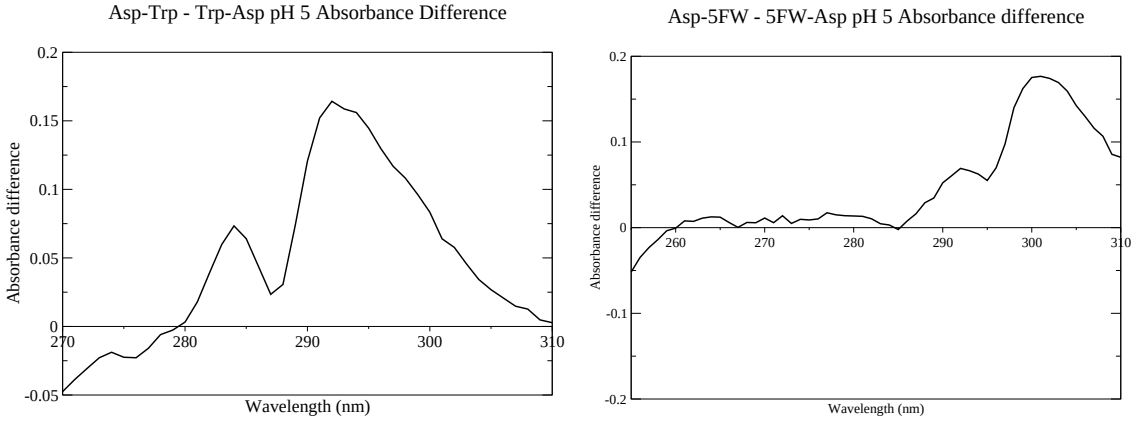

Figures 3.22 and 3.23 show the results for Gly-Trp and Gly-5FW zwitterions showing much smaller amplitudes of the shorter component in Gly-5FW compared to Gly-Trp. The anion results are shown in figures 3.24 and 3.25. The profiles of these components are similar to those of the zwitterion only with different lifetimes. The time resolved fluorescence results for Trp-Gly and 5FW-Gly zwitterion are shown in figures 3.26 and 3.27 with the anions in figures 3.28 and 3.29. The Trp-Gly zwitterion displays lower amplitude components compared to Gly-Trp and 5FW-Gly shows almost no second component. In the anion form both have nearly no second component.

A comparison of the DAS of the Gly-5FTrp anion with the other X-5FTrp anions, shown in Appendix A, shows that here is some variation in the level of ET-heterogeneity of the fluorescence decay of these samples. The short component DAS of Gly-5FTrp displays significant positive amplitudes and no negative amplitudes; that of Asp-5FTrp has small positive amplitudes and no negative amplitudes; Met-5FTrp has both positive and negative amplitude with slightly larger positive amplitudes; All 5FTrp-X anions display only a relaxation type short lifetime component. 5FTrp-X

Figure 3.4: The plot on the left shows the absorbance difference between Met-Trp and Trp-Met at pH 5. On the right the same is shown for Met-5fw and 5fw-Met at pH 5.

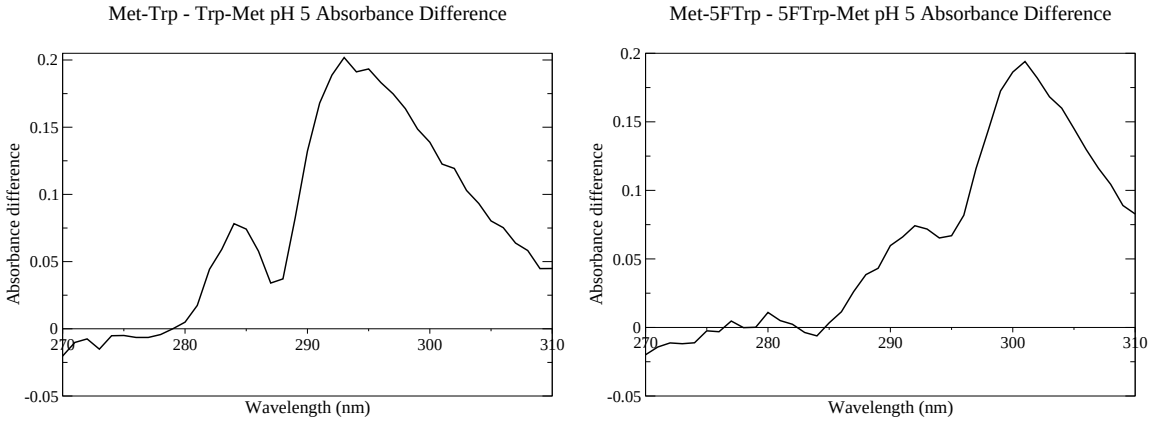

zwitterions all show significant quenching of their fluorescence in terms of the average quenching rate calculated. However, all 5FTrp-X zwitterions show little to no ET-heterogeneity in the DAS. All of the DAS for 5FTrp-X at low pH have a short lifetime component that is nearly equal positive and negative amplitude.

Time Resolved Emission Spectra

In this section Nanosecond fluorescence emission results are presented as time resolved emission spectra. The figures for a selection of examples are shown in this section. Figures 3.30 - 3.33 show the time dependent shift of the fluorescence spectrum for Gly-Trp, Gly-5FTrp, Trp-Gly, and 5FTrp-Gly. These figures show the peak normalized spectra averaged over 4 ns intervals. Data is plotted at intervals of 10 nm. All show significant shift in wavelength of maximum fluorescence over time. It is noted that the shift is largely smaller for Trp-Gly and 5FW-Gly. zwitterions.

The anion forms of all Gly containing dipeptides show noticeable time dependent shifts in their fluorescence wavelength. The Gly-Trp and Gly-5FTrp have larger shifts

Figure 3.5: Plot of absorbance difference between Arg-Trp and Trp-Arg at pH 5.

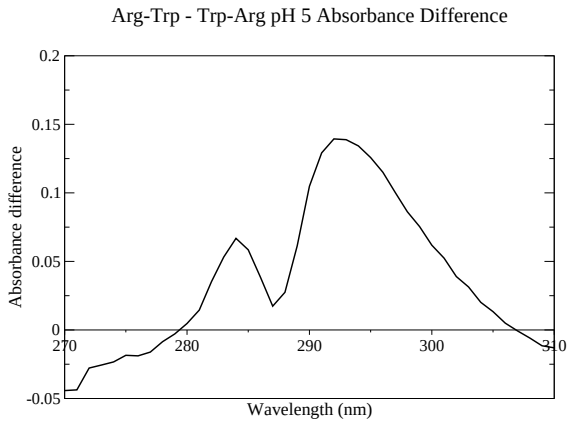

than the Trp-Gly and 5FTrp-Gly dipeptides. The zwitterion form of Trp-Gly has very little apparent shift in fluorescence wavelength.

From the decay associated spectra, we are able to determine the average fluorescence decay rate constant. Figures 3.34 and 3.35 shows charts that summarize the data averaged over the 8 analyzed wavelengths of all the dipeptides at pH(D) 5 and 10. The charts are organized with all pH 5 data on the left side and pH 10 to the right. Each set of 4 bars are arranged left to right, Trp-X, 5FTrp-X, X-Trp, X-5FTrp, where X is arranged in the order Gly, Leu, Asp, Arg, Met. The first chart shows the average fluorescence decay time constants determined from all wavelengths in the decay associated spectra as follows:

$$\langle \tau \rangle = \left(\frac{1}{\#comps.} \right) \sum_{i=1}^{\#comps.} \frac{\sum_{wavelengths} A_{wavelength}}{N_{wavelengths}} \tag{3.1}$$

In this equation $A_{wavelength}$ is the DAS amplitude at the specified wavelength for the current component.

Figure 3.6: The plot on the left shows the peak normalized fluorescence excitation spectra of Gly-Trp and Trp-Gly at pH 5. On the right the same is shown for Gly-5fw and 5fw-Gly at pH 5. Emission wavelength: 330 nm. The peak at 330 nm is scattering of excitation source.

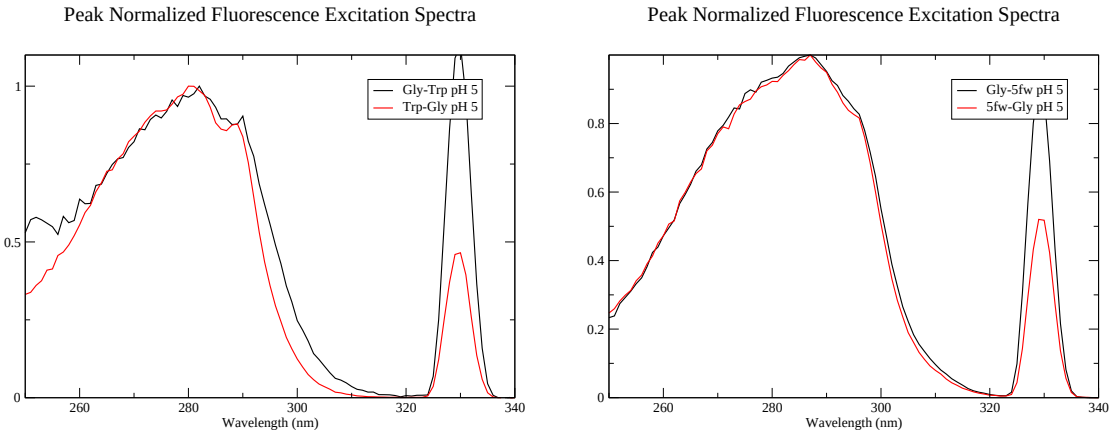

The second charts shows the data converted to quenching rates constants. In the determination of these, the sum of radiative and non-radiative rate constants (other than those for electron and proton transfer) is taken to be the decay rate constant of tryptophan or 5-fluorotryptophan at pH 11. These are unquenched at this pH. This pH is used for these samples whereas pH 10 is used for the dipeptide due to the higher pKa of tryptophan compared to dipeptides. This is due to the closer proximity of the carboxylate to the amine; the negative carboxylate is more stabilizing of the protonated amine.

Among the most notable observations is that there is a complete lack of fluorescence quenching at high pH in the cases of Trp-X, 5FTrp-X and X-5FTrp. The obvious exception to this for all X residues is the X-Trp configuration, where there is significant quenching that must be due to electron transfer to amide. At low pH the quenching rates of the 5FTrp dipeptides are significantly suppressed compared to the corresponding tryptophan dipeptide. At low pH the X-Trp dipeptide is quenched to a significantly greater level than the corresponding Trp-X dipeptide.

Figure 3.7: The plot on the left shows the peak normalized fluorescence excitation spectra of Gly-Trp and Trp-Gly at pH 10. On the right the same is shown for Gly-5fw and 5fw-Gly at pH 10. Emission wavelength: 330 nm. The peak at 330 nm is scattering of excitation source.

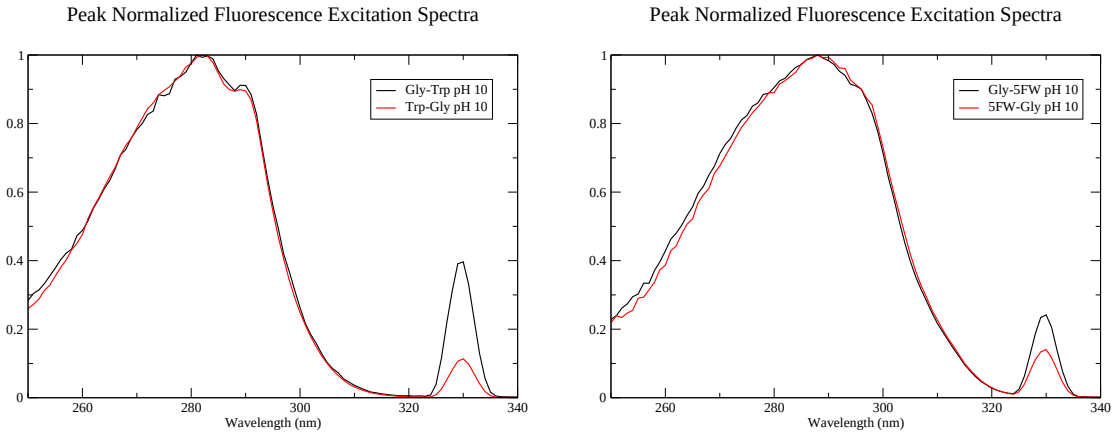

Both configurations of 5FTrp dipeptides, 5FTrp-X and X-5FTrp, are quenched to a similar extent for a given X residue. The kinetic isotope effects of the quenching rates are shown in figure 3.35.

The measured kinetic isotope effects of X-Trp dipeptides are universally close to 1 for both pH 5 and 10. This suggests that the approximate doubling in the rate of fluorescence quenching is due to electrostatic stabilization of the electron transfer mechanism by the positive charge of the protonated amine, rather than the addition of proton transfer mechanism.

If the kinetic isotope effect for electron transfer is 1, as is usually assumed, the isotope effects in our systems can be expressed as in the following equation.

$$KIE = \frac{k_{et_{H_2O}} + k_{pt_{H_2O}}}{k_{et_{D_2O}} + k_{pt_{D_2O}}} = \frac{k_{et} + k_{pt}}{k_{et} + \frac{k_{pt}}{2}} \tag{3.2}$$

Based on this result the rate of proton transfer quenching in Trp-Gly at pH 5 is about twice that of electron transfer quenching. The ratios of proton to electron transfer quenching for all peptides are shown in table 3.2. In general it can be seen that the

Figure 3.8: The plot on the left shows the peak normalized fluorescence excitation spectra of Leu-Trp and Trp-Leu at pH 5. On the right the same is shown for Leu-5fw and 5fw-Leu at pH 5. Emission wavelength: 330 nm. The peak at 330 nm is scattering of excitation source.

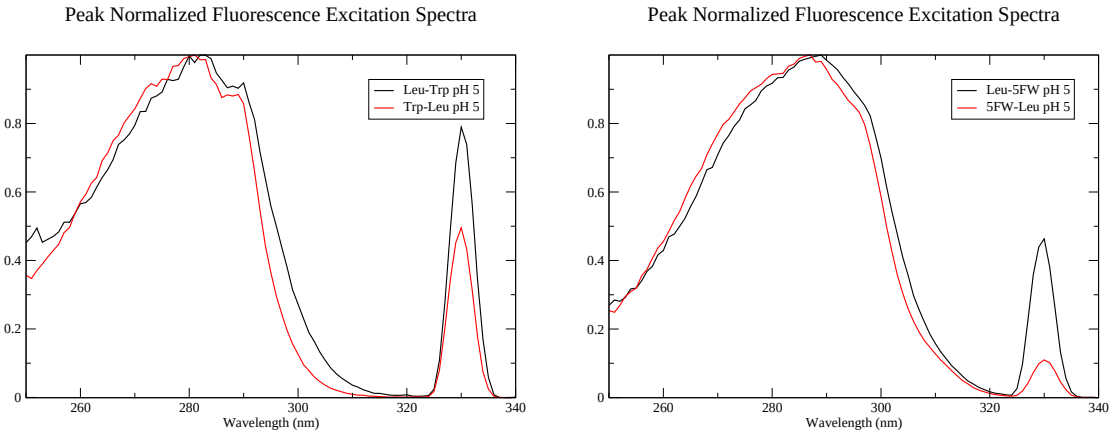

5-fluoro substitution leads to a decrease in proton transfer quenching rate in addition to the decrease in electron transfer rate. Also striking is the fact that all peptides of Met seem to not show significant proton transfer quenching.

In this work we are able to compare our results directly to those of Chen, et al. for a subset of the peptides studied. The following table shows the data collected for the dipeptides studied by both groups. The results from the work of Chen, et al. are determined from a single emission wavelength of 350 nm.

For the decay kinetics of the tryptophan and 5FTrp anion forms it is observed that the KIE in D_2O is of greater extent in the case of tryptophan compared to 5FTrp.

Figure 3.9: The plot on the left shows the peak normalized fluorescence excitation spectra of Leu-Trp and Trp-Leu at pH 10. On the right the same is shown for Leu-5fw and 5fw-Leu at pH 10. Emission wavelength: 330 nm. The peak at 330 nm is scattering of excitation source.

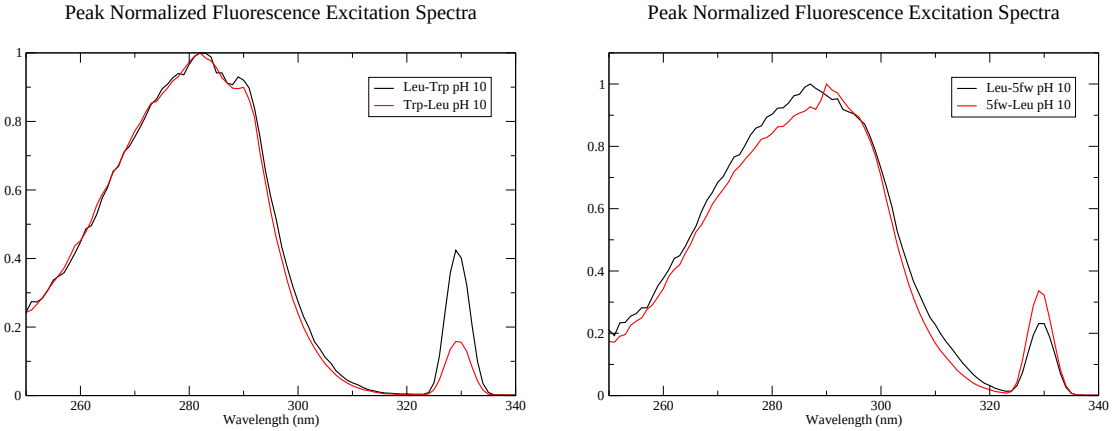

Table 3.1: Peak wavelength of Steady State Fluorescence Data. Wavelengths in nm. The number of sample replicates with steady state emission spectra are shown with the number of sample replicates for absorbance spectra shown in parenthesis.

Sample Name	Peak λ	# of samples	Sample Name	Peak λ	# of samples
Arg-Trp pH 10	361	2 (2)	Arg-Trp pH 5	363	3 (2)
Trp-Arg pH 10	361	3 (2)	Trp-Arg pH 5	352.5	2 (2)
5fw-Arg pH 10	363.5	2 (2)	5fw-Arg pH 5	354	2 (2)
Asp-Trp pH 10	362.5	2 (2)	Asp-Trp pH 5	362.5	3 (2)
Asp-5FTrp pH 10	368.5	2 (2)	Asp-5FTrp pH 5	366	2 (2)
Trp-Asp pH 10	362	2 (3)	Trp-Asp pH 5	353	2 (2)
5FTrp-Asp pH 10	366	3 (2)	5fw-Asp pH 5	357	2 (2)
Gly-Trp pH 10	363	2 (2)	Gly-Trp pH 5	360	3 (2)
Gly-5FTrp pH 10	369.5	2 (2)	Gly-5FTrp pH 5	361.5	2 (2)
Trp-Gly pH 10	361	2 (2)	Trp-Gly pH 5	351	2 (2)
5FTrp-Gly pH 10	365	2 (2)	5fw-Gly pH 5	356	3 (2)
Leu-Trp pH 10	362	4 (2)	Leu-Trp pH 5	361	3 (2)
Leu-5fw pH 10	364.5	2 (2)	Leu-5fw pH 5	361.5	2 (2)
Trp-Leu pH 10	361	2 (2)	Trp-Leu pH 5	353	2 (2)
5fw-Leu pH 10	363	2 (2)	5fw-Leu pH 5	355	2 (2)
Met-Trp pH 10	362	3 (2)	Met-Trp pH 5	361	3 (2)
Met-5fw pH 10	366	2 (2)	Met-5fw pH 5	365	2 (2)
Trp-Met pH 10	361	4 (2)	Trp-Met pH 5	351	2 (2)
5fw-Met pH 10	365	3 (2)	5fw-Met pH 5	354	2 (2)

Table 3.2: k_{pt}/k_{et} ratio for peptides at pH 5.

Trp-Gly	1.80	5FTrp-Gly	2.70	Gly-Trp	0.39	Gly-5FTrp	–
Trp-Leu	1.80	5FTrp-Leu	0.64	Leu-Trp	0.71	Leu-5FTrp	0.30
Trp-Asp	1.17	5FTrp-Asp	0.89	Asp-Trp	0.12	Asp-5FTrp	0.20
Trp-Arg	0.90	5FTrp-Arg	0.23	Arg-Trp	0.03	Arg-5FTrp	NA
Trp-Met	0.09	5FTrp-Met	0.25	Met-Trp	0.00	Met-5FTrp	0.04

Table 3.3: A comparison of the data presented here with the work of Chen, et al. The third component in Chen, et al. is often excessively long, longer than unquenched indoles. No evidence to support these are seen in this work. Quantum yields from this work are calculated as $0.04ns^{-1}(\tau(ns))$. This implies a radiative rate of $0.04ns^{-1}$

	Chen, et al.					
Dipeptide	$\langle\tau\rangle$	τ_1	τ_2	τ_3	% τ_1	% τ_2
Gly-Trp pH 5	0.81	1.15	0.41	3.36	75.6	23.0
Gly-Trp pH 10	1.50	1.89	0.61	10.72	80.7	18.5
Trp-Gly pH 5	1.38	1.63	0.39	6.18	82.6	7.8
Trp-Gly pH 10	5.60	6.63	0.24	16.73	95.6	0.08
Leu-Trp pH 5	1.88	2.51	0.92	19.93	66.5	32.3
Leu-Trp pH 10	4.26	4.09	1.21	8.46	85.7	5.4
Trp-Leu pH 5	2.26	2.12	0.61	5.85	62.6	5.7
Trp-Leu pH 10	6.28	7.74	5.49	1.28	64.2	33.9
	This work					
Dipeptide	$\langle\tau\rangle$	τ_1	τ_2	τ_3	% τ_1	QY
Gly-Trp pH 5	0.97	1.30	0.47	–	59	0.04
Gly-Trp pH 10	2.13	3.11	1.08	–	56	0.09
Trp-Gly pH 5	1.73	2.06	0.68	–	76	0.07
Trp-Gly pH 10	7.71	8.12	0.97	–	94	0.31
Leu-Trp pH 5	1.42	2.47	0.66	–	45	0.06
Leu-Trp pH 10	4.05	4.41	1.56	–	87	0.16
Trp-Leu pH 5	1.69	2.41	0.73	–	70	0.07
Trp-Leu pH 10	8.0	8.12	1.10	–	98	0.32

Table 3.4: Average τ and standard deviation. This average fluorescence lifetime is averaged over the 8 fluorescence wavelengths analyzed in the global analysis (in the wavelength range 335-400 nm). The % τ_1 is the global analysis.

Sample	$\langle\tau\rangle$	$\sigma_{\langle\tau\rangle}$	$\langle\tau_1\rangle$	$\sigma_{\langle\tau_1\rangle}$	$\langle\tau_2\rangle$	$\sigma_{\langle\tau_2\rangle}$	% τ_1	λ_{max_1}	λ_{max_2}
Trp pD 11	10.99	0.02	11.26	0.03	1.98	0.11	97	355	340
Trp pH 11	8.48	0.41	8.68	0.27	1.09	0.08	97	360	340
Trp pD 10	8.09	0.02	9.99	0.01	4.03	0.07	68	355	345
Trp pH 10	6.73	0.75	8.57	0.44	2.36	0.15	70	355	345
Trp pD 5	5.53	0.20	5.97	0.03	0.81	0.21	91	350	335
Trp pH 5	2.64	0.109	3.17	0.03	0.60	0.02	90	350	335
5FTrp pD 11	5.98	0.01	6.07	0.02	1.22	0.33	97	360	340
5FTrp pH 11	5.77	0.21	5.83	0.15	0.91	0.12	97	360	340
5FTrp pD 10	4.77	0.01	5.20	0.02	1.83	0.01	87	360	340
5FTrp pH 10	4.84	0.48	5.79	0.15	1.92	0.05	75	360	350
5FTrp pD 5	3.79	0.07	4.13	0.03	0.70	0.06	90	355	335
5FTrp pH 5	2.74	0.15	2.87	0.03	0.60	0.01	94	355	335

Figure 3.10: Steady state absorbance and fluorescence spectra of Arg-Trp and Trp-Arg and 5FTrp-Arg (Arg-5FTrp was not available). Black line is Trp dipeptide absorbance spectrum, red line is 5FTrp dipeptide absorbance spectrum, green line is Trp dipeptide emission spectrum, blue line is 5FTrp emission spectrum.

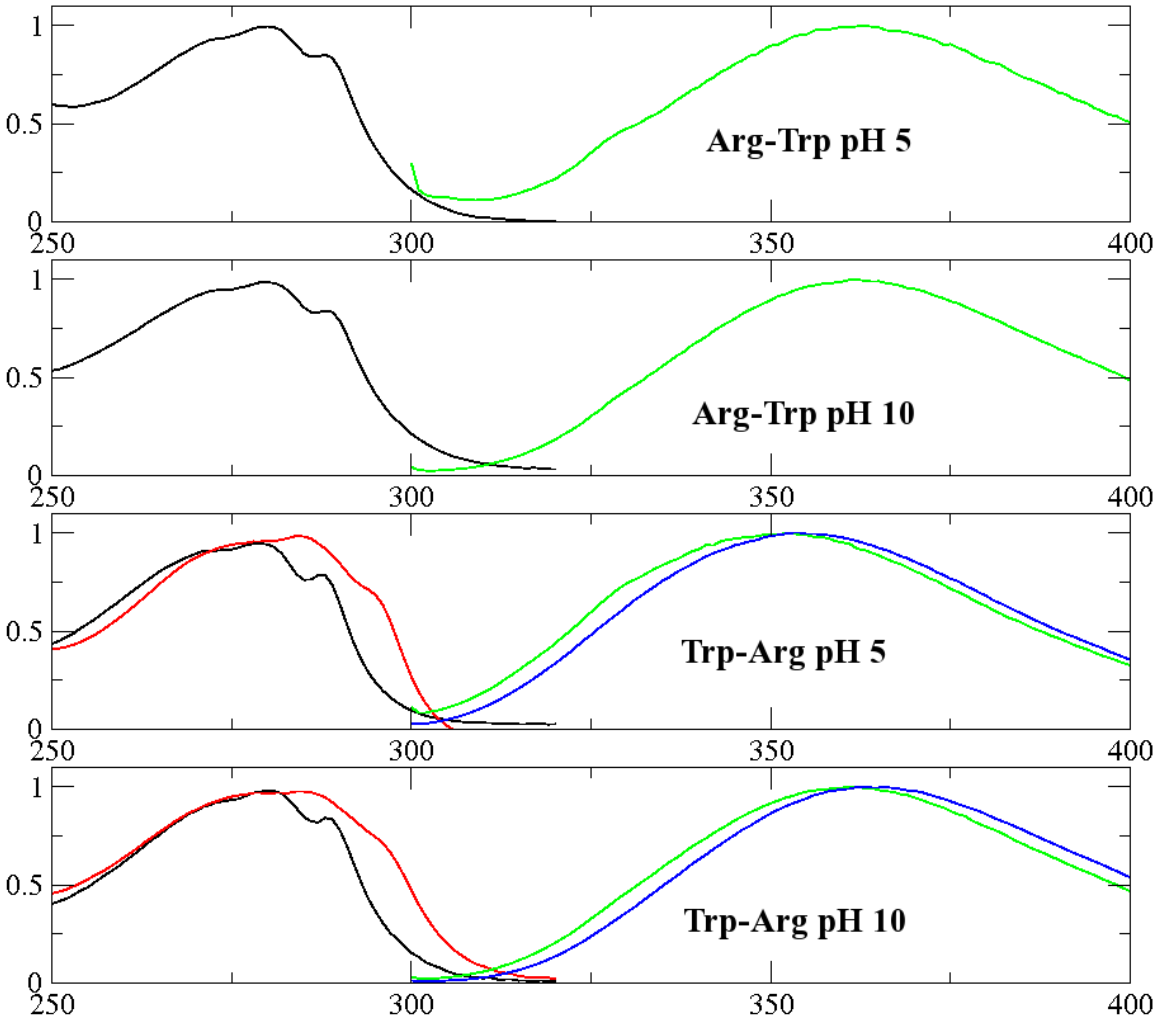

Figure 3.11: Steady state absorbance and fluorescence spectra of Asp-Trp, Trp-Asp, Asp-5FTrp and 5FTrp-Asp. Black line is Trp dipeptide absorbance spectrum, red line is 5FTrp dipeptide absorbance spectrum, green line is Trp dipeptide emission spectrum, blue line is 5FTrp emission spectrum.

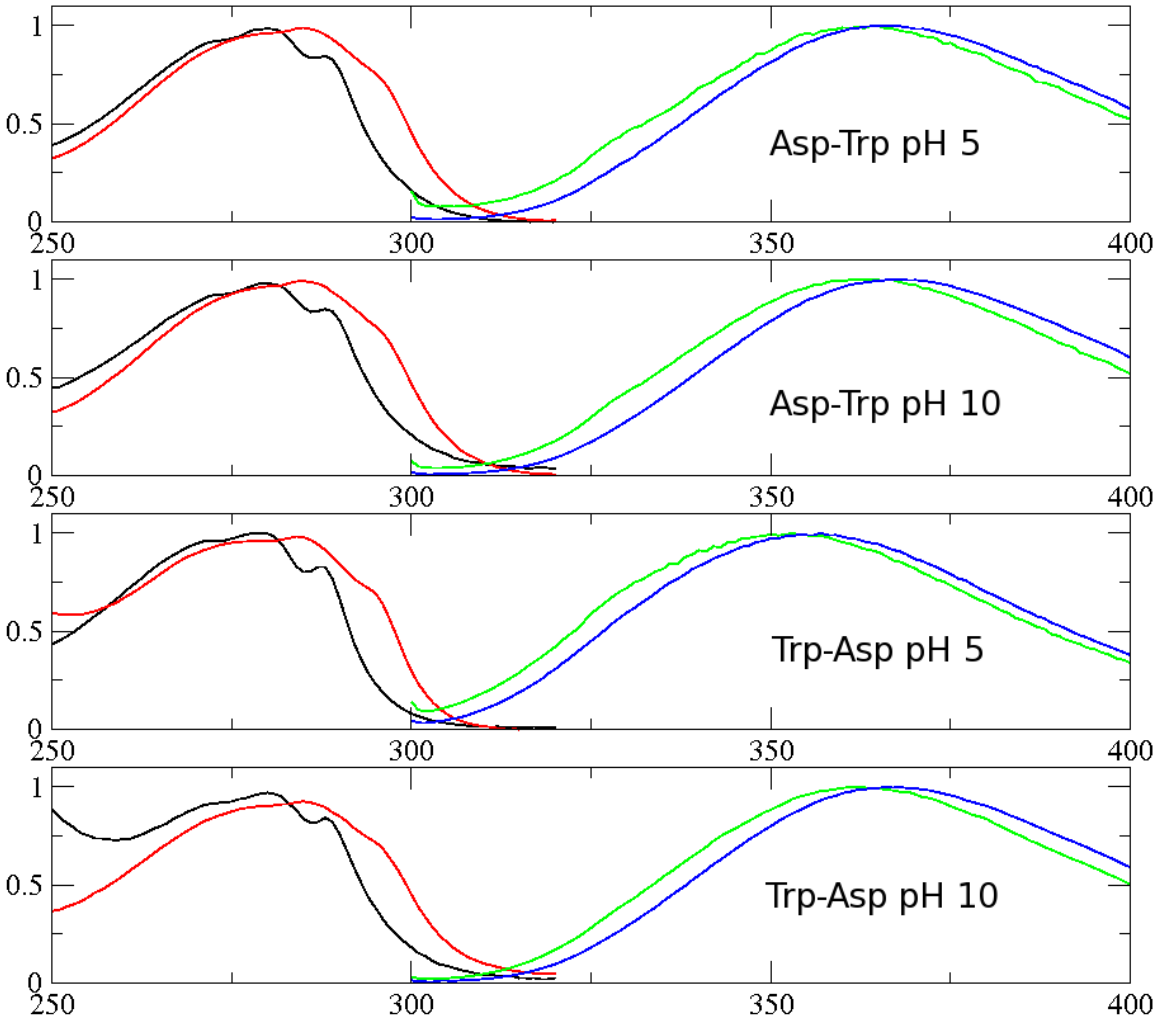

Figure 3.12: Steady state absorbance and fluorescence spectra of Gly-Trp, Trp-Gly, Gly-5FTrp and 5FTrp-Gly. Black line is Trp dipeptide absorbance spectrum, red line is 5FTrp dipeptide absorbance spectrum, green line is Trp dipeptide emission spectrum, blue line is 5FTrp emission spectrum.

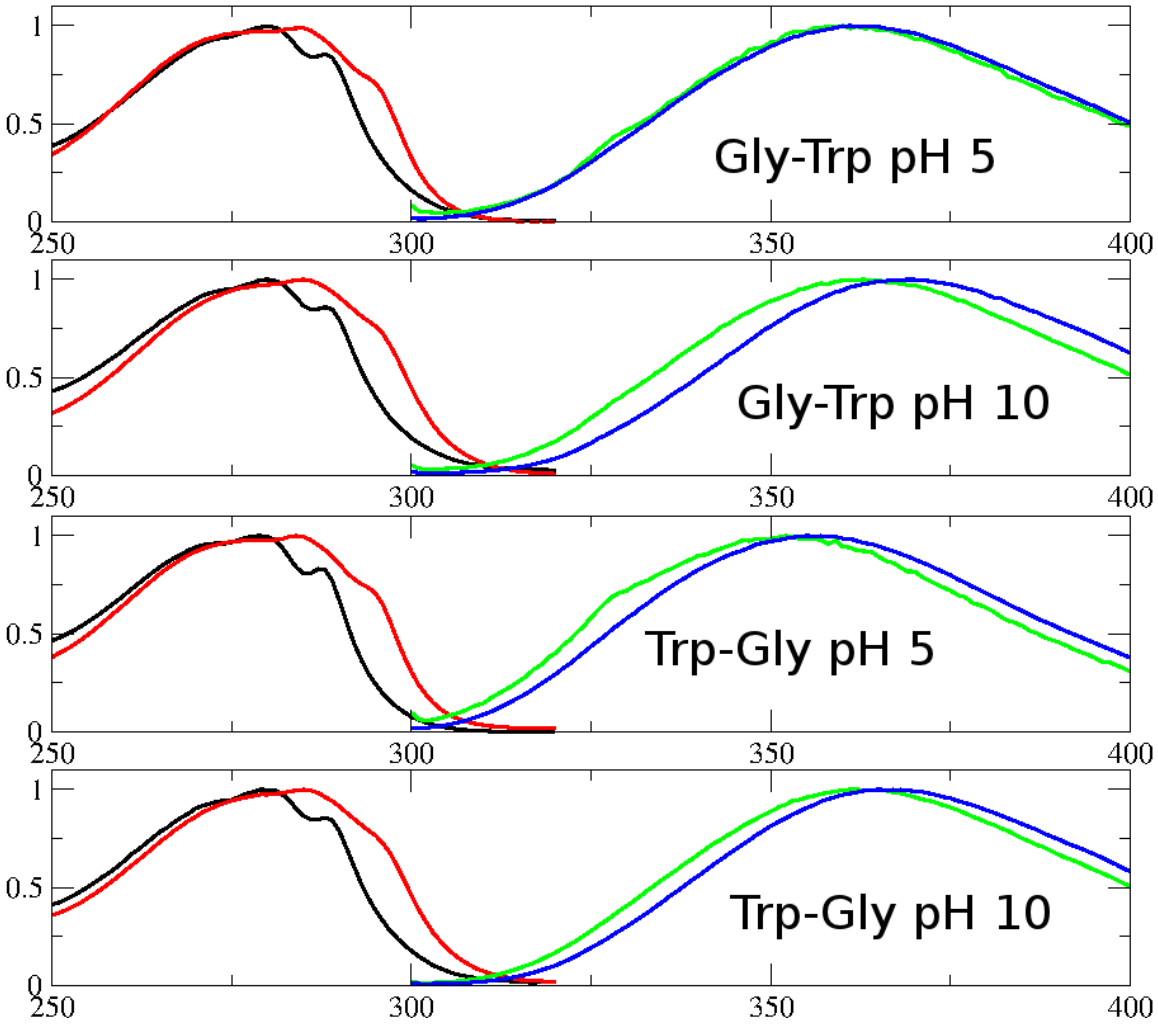

Figure 3.13: Steady state absorbance and fluorescence spectra of Leu-Trp, Trp-Leu, Leu-5FTrp and 5FTrp-Leu. Black line is Trp dipeptide absorbance spectrum, red line is 5FTrp dipeptide absorbance spectrum, green line is Trp dipeptide emission spectrum, blue line is 5FTrp emission spectrum.

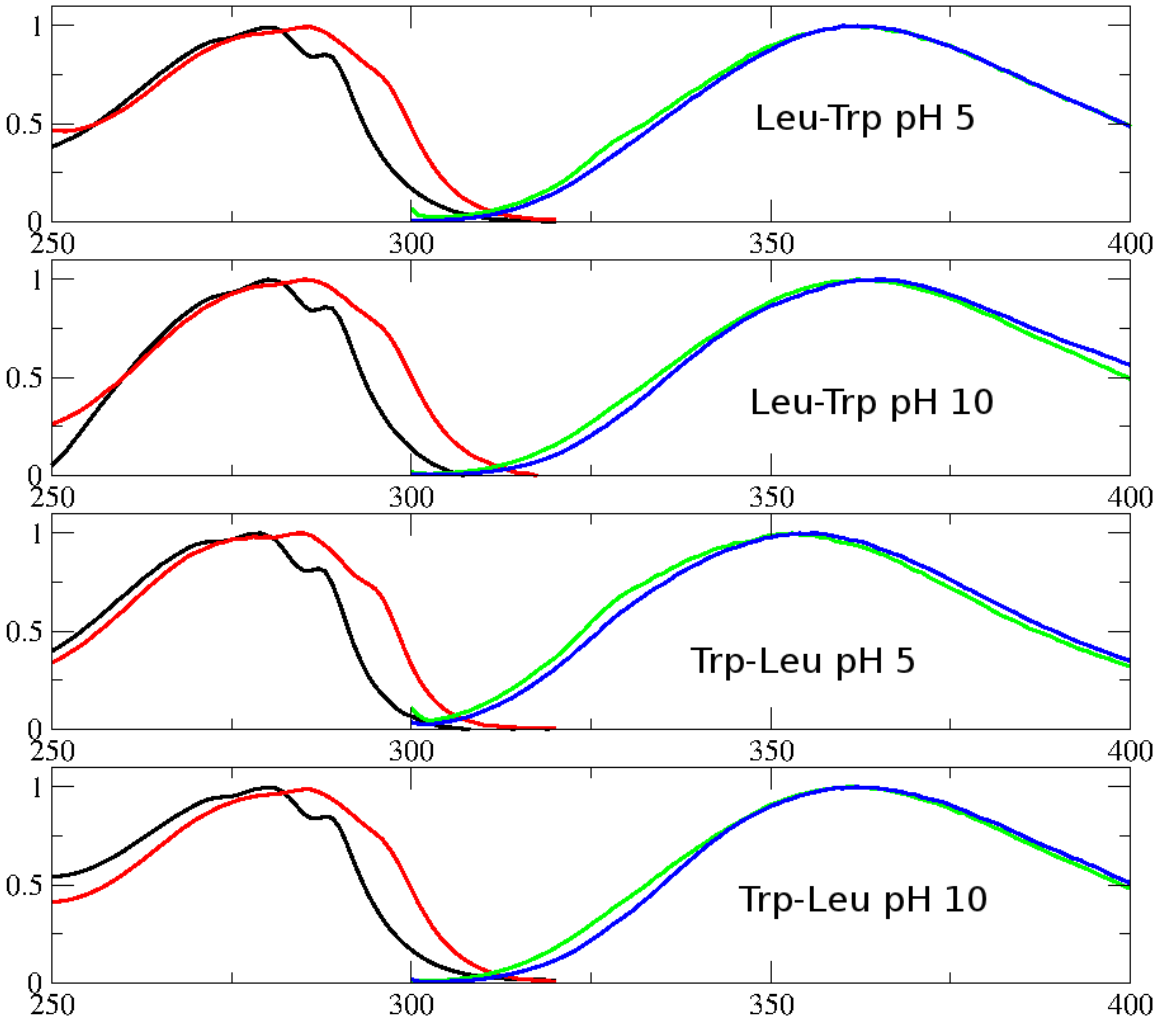

Figure 3.14: Steady state absorbance and fluorescence spectra of Met-Trp, Trp-Met, Met-5FTrp and 5FTrp-Met. Black line is Trp dipeptide absorbance spectrum, red line is 5FTrp dipeptide absorbance spectrum, green line is Trp dipeptide emission spectrum, blue line is 5FTrp emission spectrum.

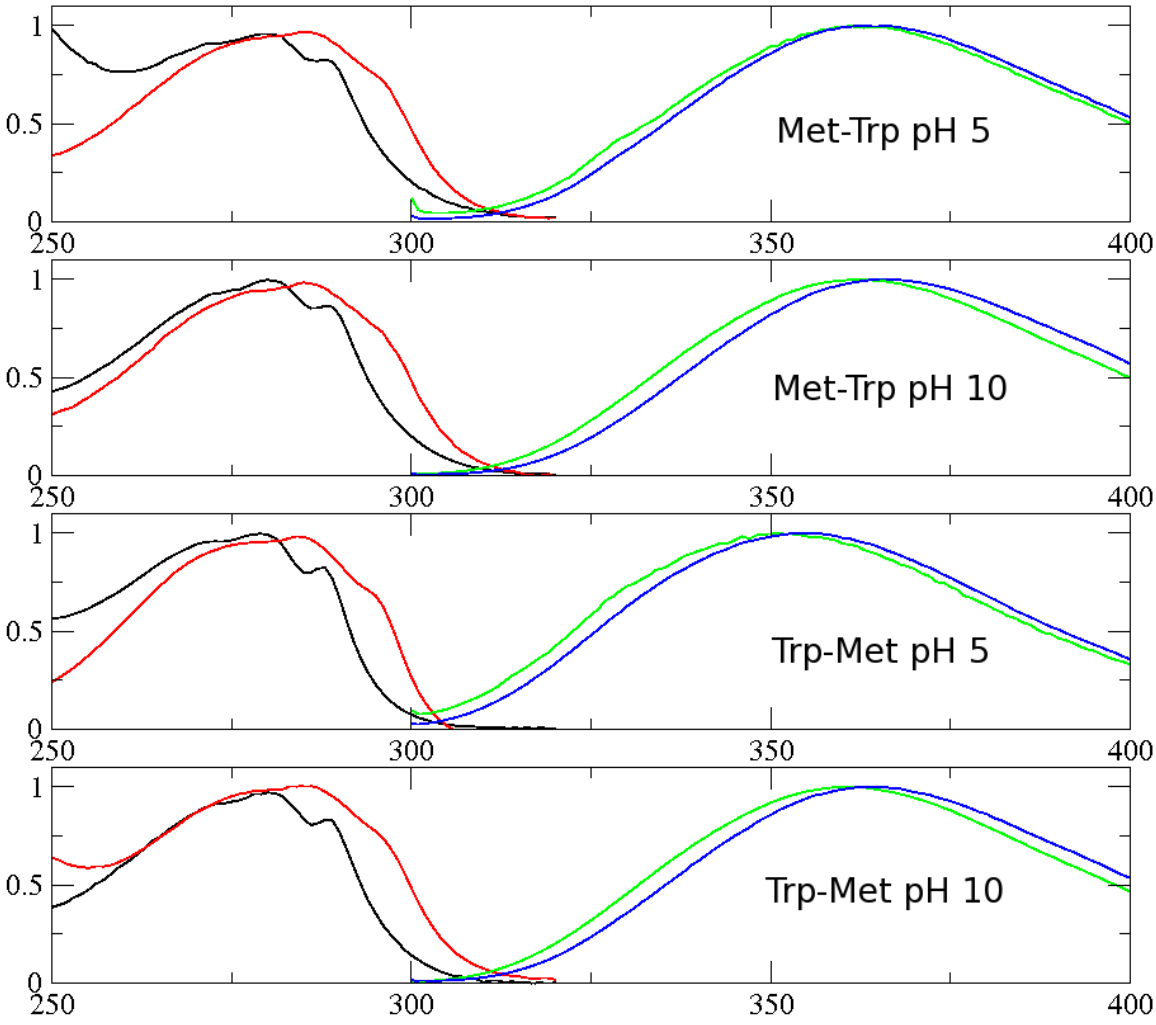

Figure 3.15: Graph showing experimental wavelength results for Trp-X and X-Trp dipeptides at pH 5 and 10.

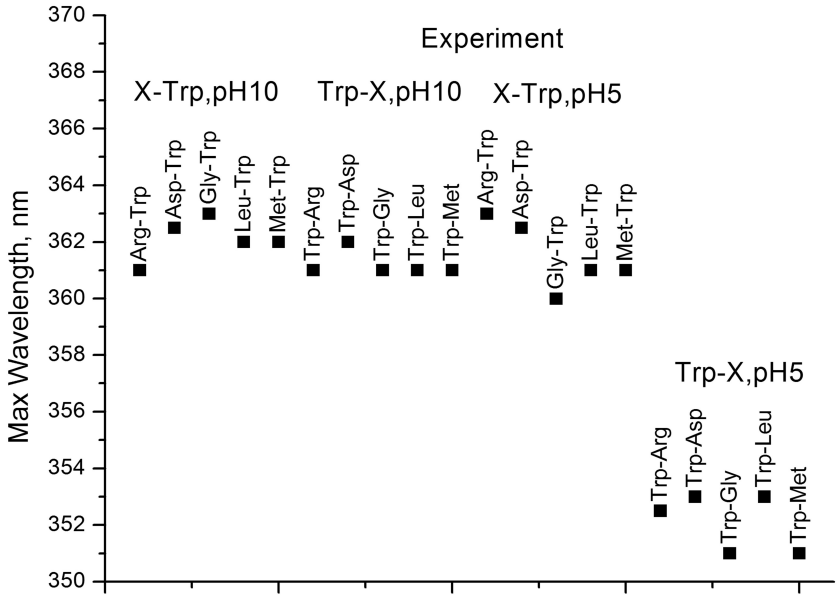

Figure 3.16: Decay Associated Spectra of Tryptophan at pH(D) 5. Left is pH 5, right is pD 5. Error bars are +/- one standard deviation.

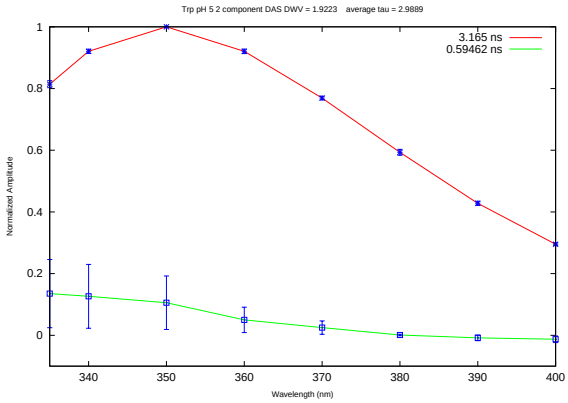

(a) Trp pH 5 DAS

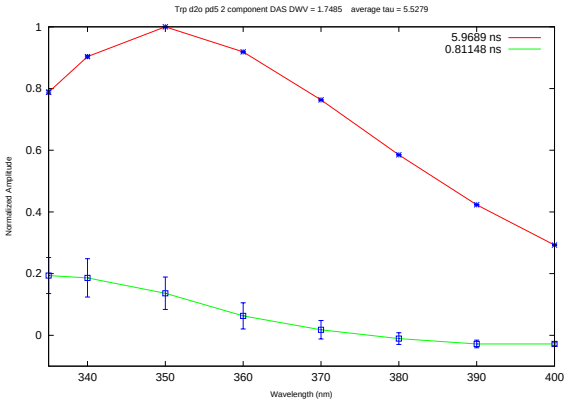

(b) Trp pD 5 DAS

Figure 3.17: Decay Associated Spectra of 5-Fluoro-Tryptophan at pH(D) 5. Left is pH 5, right is pD 5. Error bars are +/- one standard deviation.

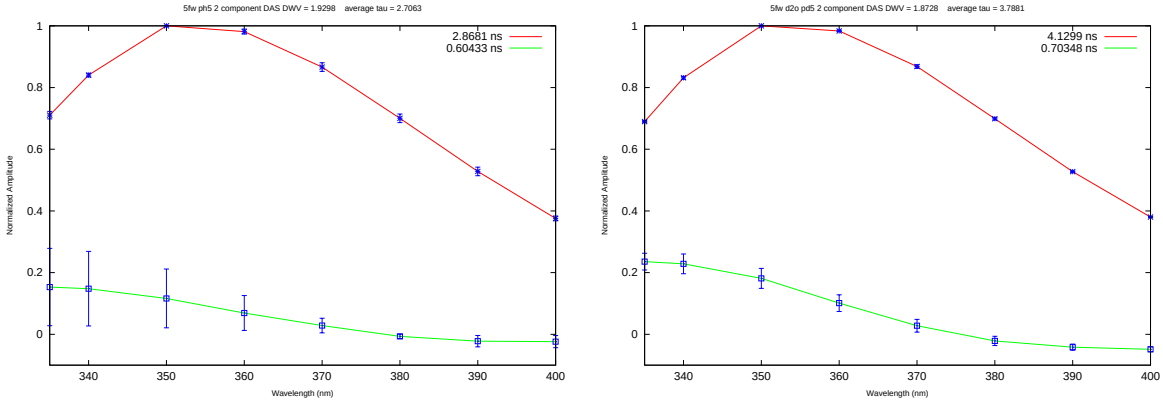

(a) 5FTrp pH 5 DAS

(b) 5FTrp pD 5 DAS

Figure 3.18: Average Decay Associated Spectra of Tryptophan at pH(D) 10. Error bars are +/- one standard deviation.

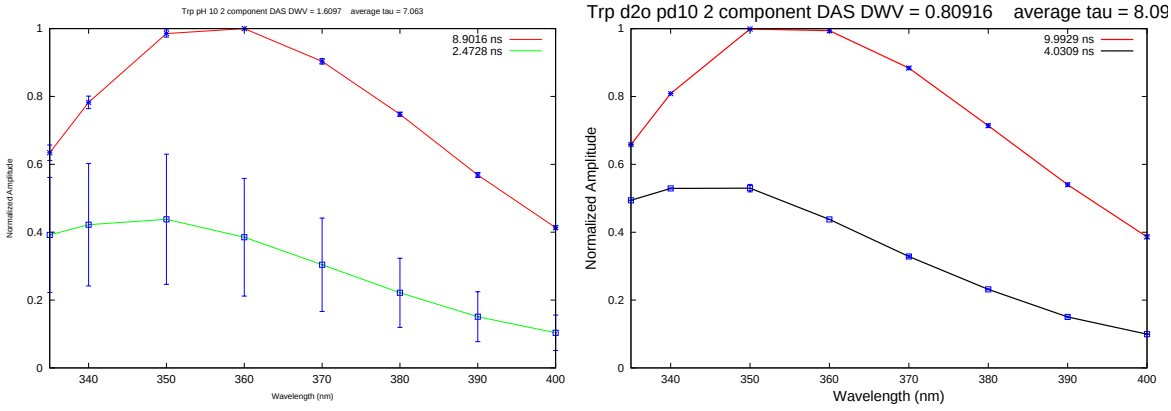

(a) Trp pH 10 DAS

(b) Trp pD 10 DAS

Figure 3.19: Average Decay Associated Spectra of 5-Fluoro-Tryptophan at pH(D) 10. Error bars are +/- one standard deviation.

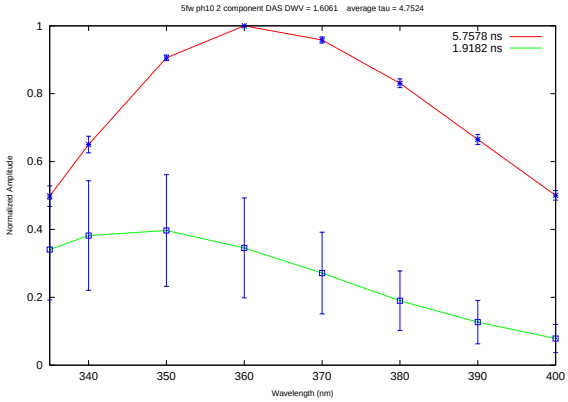

(a) 5FTrp pH 10 DAS

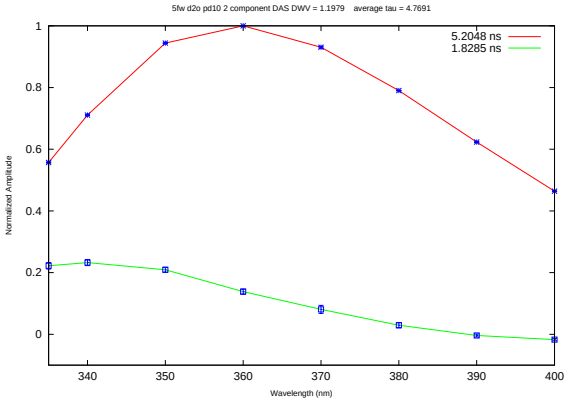

(b) 5FTrp pD 10 DAS

Figure 3.20: Average Decay Associated Spectra Tryptophan at pH(D) 11. Error bars are +/- one standard deviation.

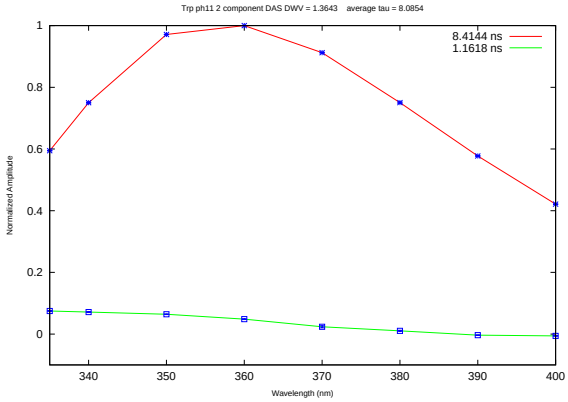

(a) Trp pH 11 DAS

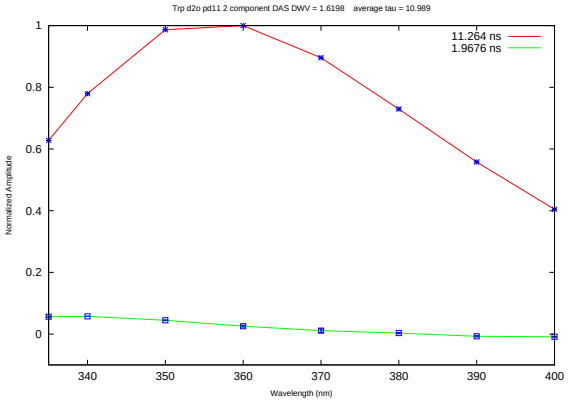

(b) Trp pD 11 DAS

Figure 3.21: Decay Associated Spectra of 5-Fluoro-Tryptophan at pH(D) 11. Error bars are +/- one standard deviation.

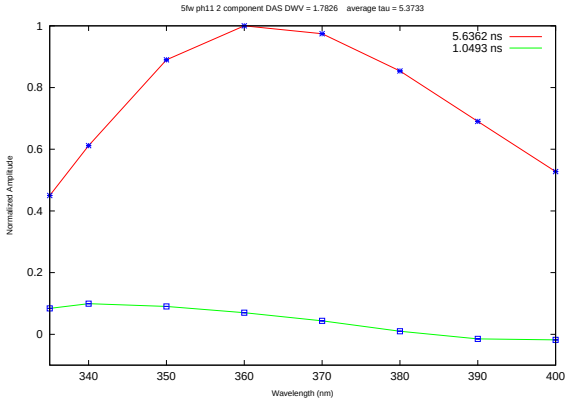

(a) 5FTrp pH 11 DAS

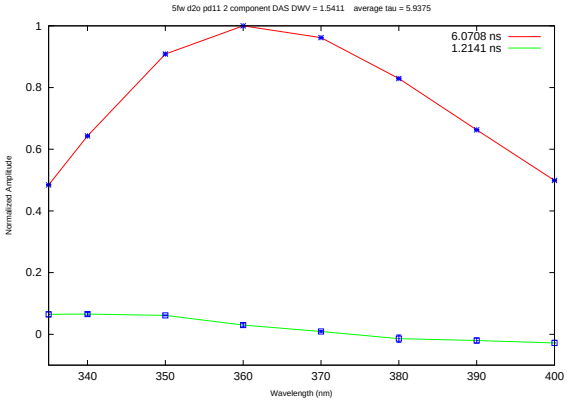

(b) 5FTrp pD 11 DAS

Figure 3.22: Average Decay Associated Spectra of Gly-Trp at pH(D) 5. Error bars are +/- one standard deviation.

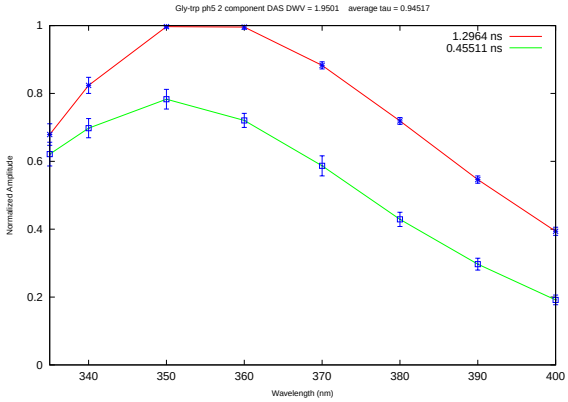

(a) Gly-Trp pH 5 DAS

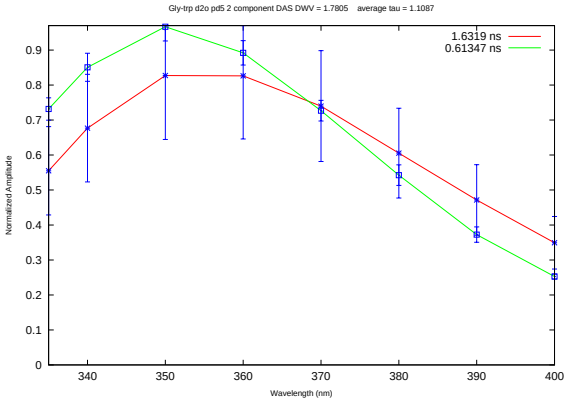

(b) Gly-Trp pD 5 DAS

Figure 3.23: Average Decay Associated Spectra of Gly-5FTrp at pH(D) 5. Error bars are +/- one standard deviation.

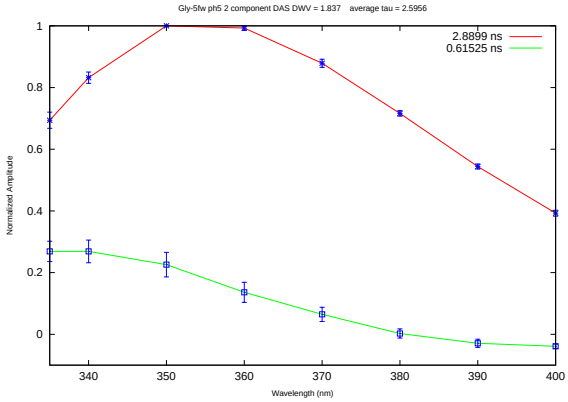

(a) Gly-5FTrp pH 5 DAS

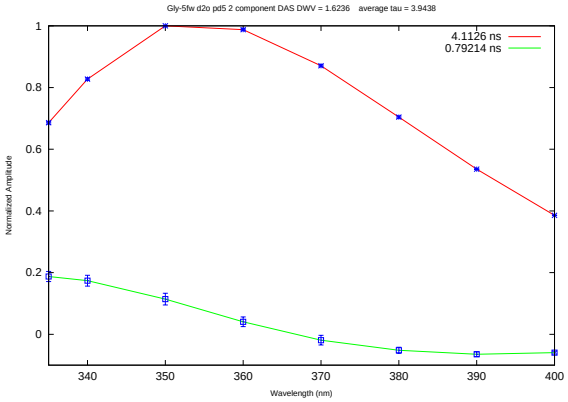

(b) Gly-5FTrp pD 5 DAS

Figure 3.24: Average Decay Associated Spectra of Gly-Trp at pH(D) 10. Error bars are +/- one standard deviation.

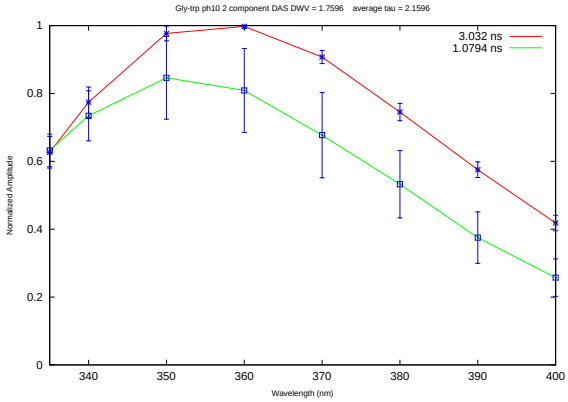

(a) Gly-Trp pH 10 DAS

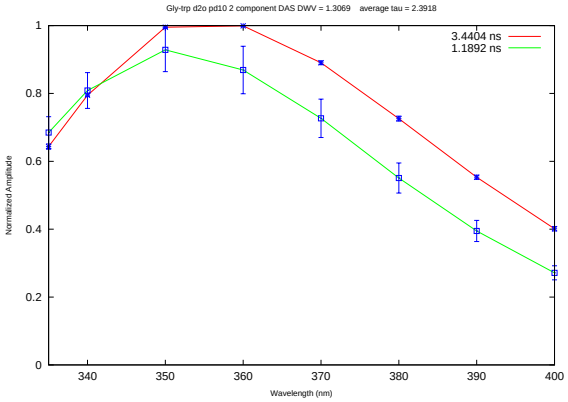

(b) Gly-Trp pD 10 DAS

Figure 3.25: Average Decay Associated Spectra of Gly-5FTrp at pH(D) 10. Error bars are +/- one standard deviation.

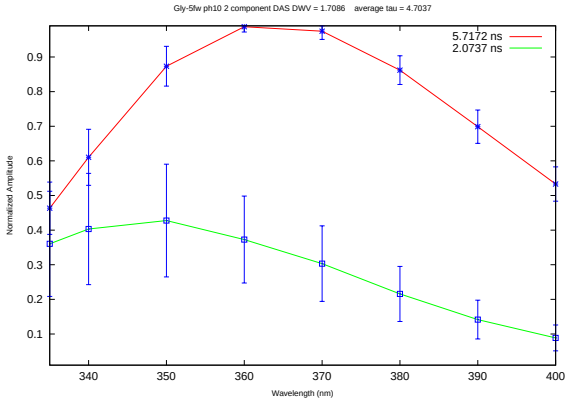

(a) Gly-5FTrp pH 10 DAS

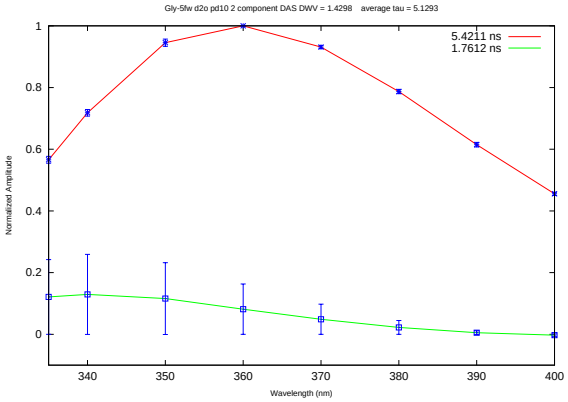

(b) Gly-5FTrp pD 10 DAS

Figure 3.26: Average Decay Associated Spectra of Trp-Gly at pH(D) 5. Error bars are +/- one standard deviation.

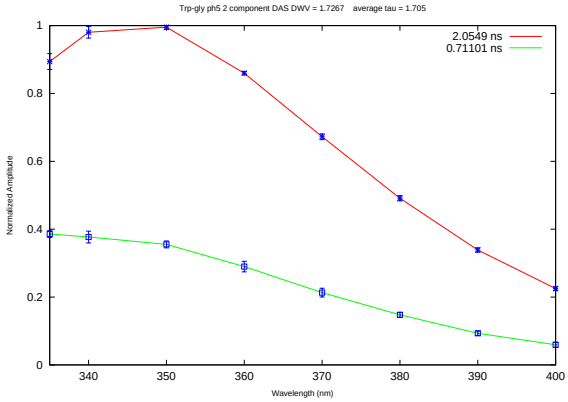

(a) Trp-Gly pH 5 DAS

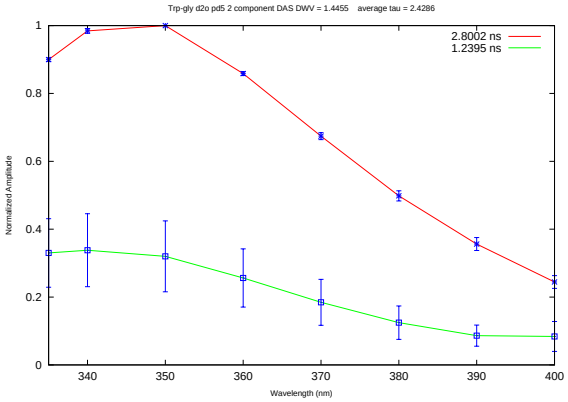

(b) Trp-Gly pD 5 DAS

Figure 3.27: Average Decay Associated Spectra of 5FTrp-Gly at pH(D) 5. Error bars are +/- one standard deviation.

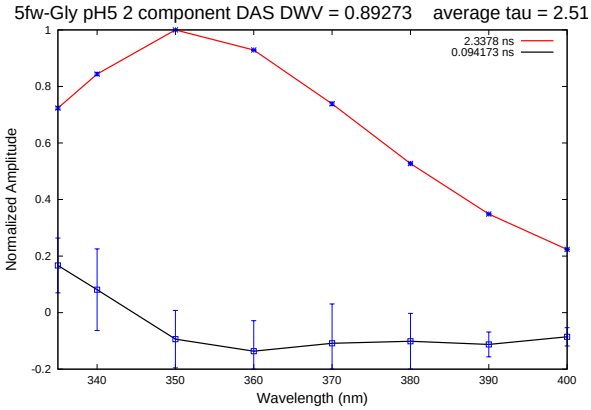

(a) 5FTrp-Gly pH 5 DAS

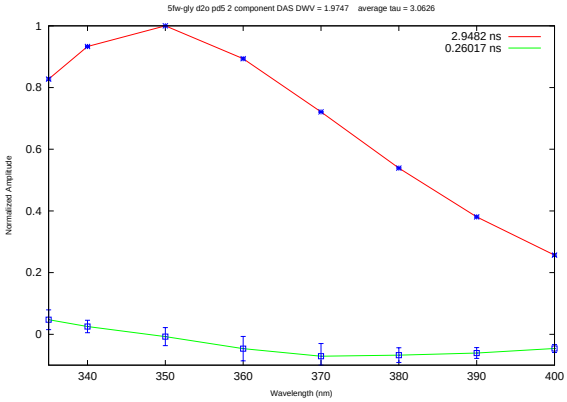

(b) 5FTrp-Gly pD 5 DAS

Figure 3.28: Average Decay Associated Spectra of Trp-Gly at pH(D) 10. Error bars are +/- one standard deviation.

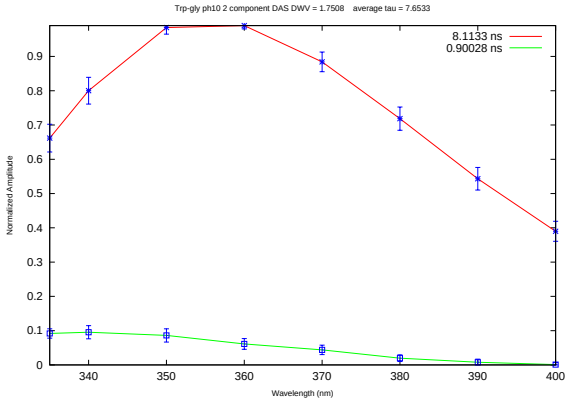

(a) Trp-Gly pH 10 DAS

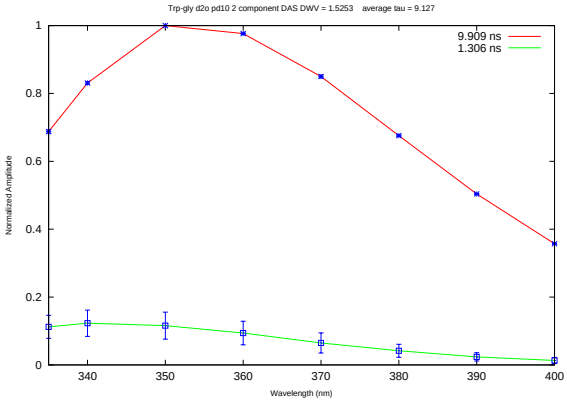

(b) Trp-Gly pD 10 DAS

Figure 3.29: Average Decay Associated Spectra of 5FTrp-Gly at pH(D) 10. Error bars are +/- one standard deviation.

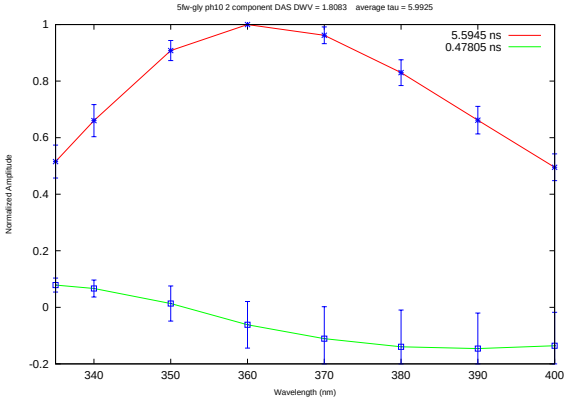

(a) 5FTrp-Gly pH 10 DAS

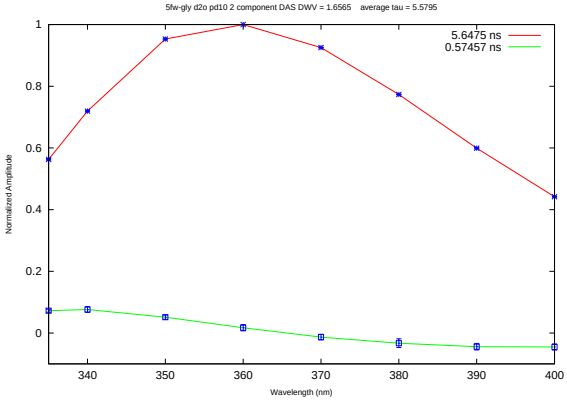

(b) 5FTrp-Gly pD 10 DAS

Figure 3.30: Time slices of nanosecond time resolved data for Gly-Trp (left) and Gly-5FTrp (right) at pH 10. Each curve is the average of 4 ns. Each sequential curve is the next block of 4 ns. The Raman scatter of the excitation wavelength (295 nm) from water is evident in the Gly-Trp pH 10 spectrum.

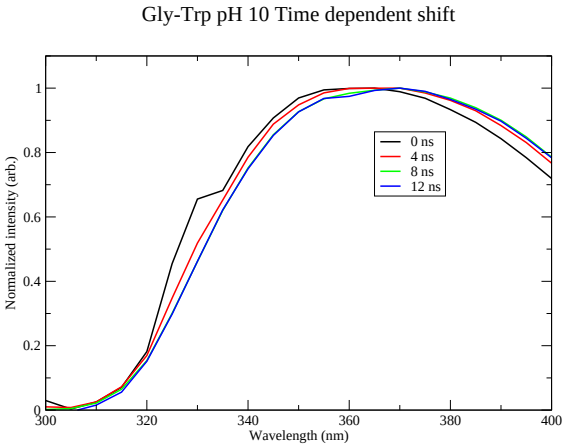

(a) Gly-Trp pH 10

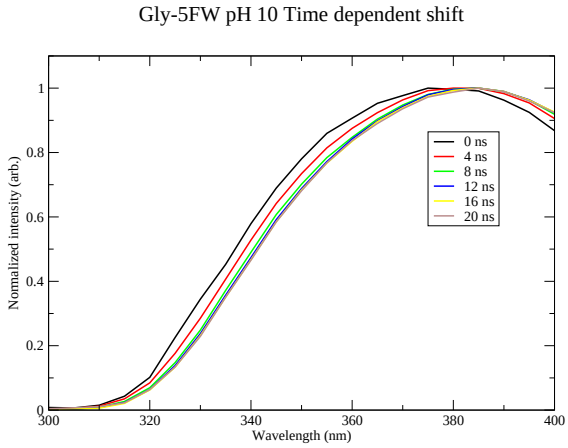

(b) Gly-5FTrp pH 10

Figure 3.31: Time slices of nanosecond time resolved data. Each curve is the average of 4 ns. Each sequential curve is the next block of 4 ns. The Raman scatter of the excitation wavelength (295 nm) from water is evident in the Trp-Gly pH 10 spectrum.

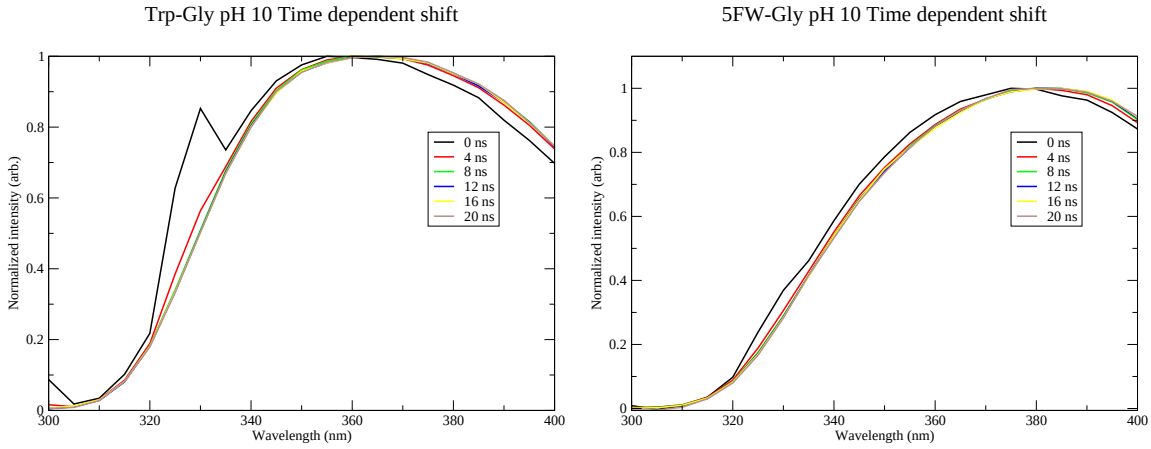

(a) Trp-Gly pH 10

(b) 5FTrp-Gly pH 10

Figure 3.32: Time slices of nanosecond time resolved data. Each curve is the average of 4 ns. Each sequential curve is the next block of 4 ns.

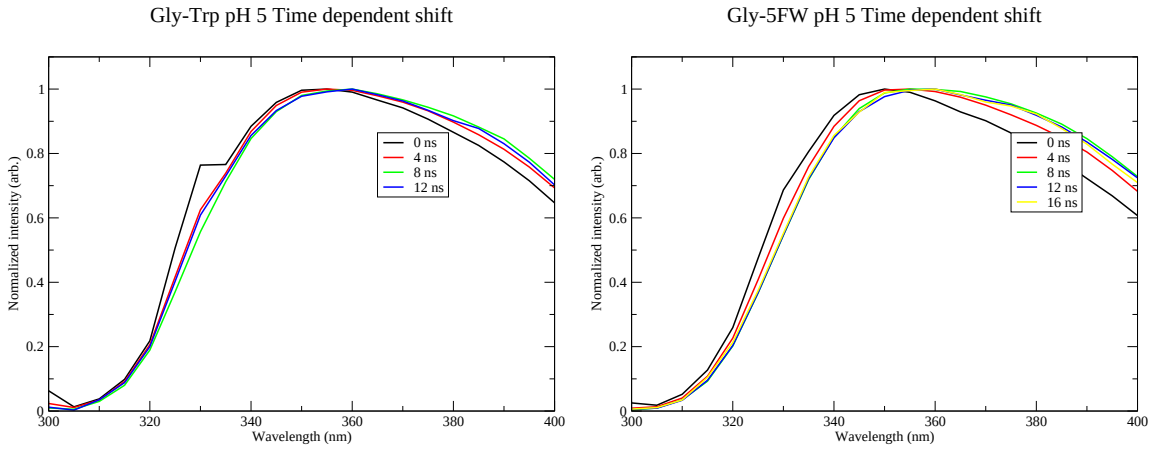

(a) Gly-Trp pH 5

(b) Gly-5FTrp pH 5

Figure 3.33: Time slices of nanosecond time resolved data. Each curve is the average of 4 ns. Each sequential curve is the next block of 4 ns.

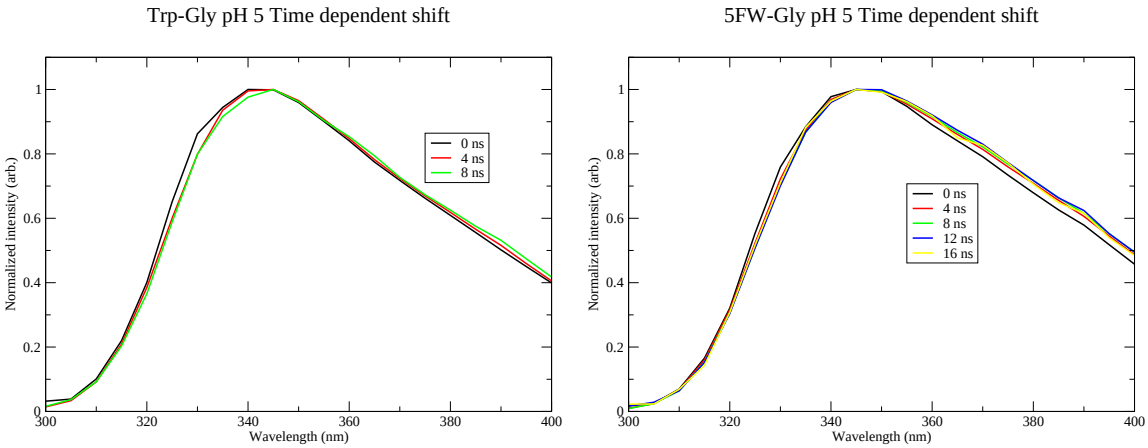

(a) Trp-Gly pH 5

(b) 5FTrp-Gly pH 5

Table 3.5: Fluorescence parameters for X-Trp and X-5FTrp at pH(D) 5.

Sample	$\langle\tau\rangle$	$\langle\tau_1\rangle$	$\sigma_{\langle\tau_1\rangle}$	$\langle\tau_2\rangle$	$\sigma_{\langle\tau_1\rangle}$	% τ_1	λ_{max_1}	λ_{max_2}
Gly-Trp pH 5	0.97	1.30	0.023	0.47	0.032	59	360	350
Gly-5FTrp pH 5	2.75	2.87	0.038	0.58	0.021	88	360	340
Gly-Trp pD 5	1.11	1.62	0.075	0.61	0.019	49	365	350
Gly-5FTrp pD 5	4.00	4.11	0.031	0.79	0.025	97	355	NA
Leu-Trp pH 5	1.42	2.47	0.036	0.66	0.034	45	355	350
Leu-5FTrp pH 5	3.17	3.17	0.027	1.02	0.088	100	355	NA
Leu-Trp pD 5	1.75	2.96	0.005	0.84	0.025	45	360	350
Leu-5FTrp pD 5	3.32	3.32	0.028	1.10	0.141	100	355	NA
Met-Trp pH 5	1.46	2.41	0.429	1.03	0.355	53	360	350
Met-5FTrp pH 5	2.29	2.69	0.034	1.10	0.056	75	365	350
Met-Trp pD 5	1.44	2.27	0.064	0.74	0.097	49	360	350
Met-5FTrp pD 5	2.51	2.92	0.043	1.39	0.119	73	360	350
Arg-Trp pH 5	1.42	2.58	0.500	0.94	0.097	37	360	350
Arg-Trp pD 5	2.20	2.25	0.068	0.69	0.162	52	360	350
Asp-Trp pH 5	1.21	2.13	0.165	0.71	0.071	36	360	350
Asp-5FTrp pH 5	1.92	2.27	0.012	1.07	0.037	71	370	350
Asp-Trp pD 5	1.43	2.31	0.056	0.87	0.037	41	360	350
Asp-5FTrp pD 5	2.20	2.78	0.467	1.29	0.073	71	370	350

Figure 3.34: Average decay constants for tryptophan and 5FTrp dipeptides, tryptophan and 5FTrp. Results shown for water and D_2O buffers at pH 5 and 10.

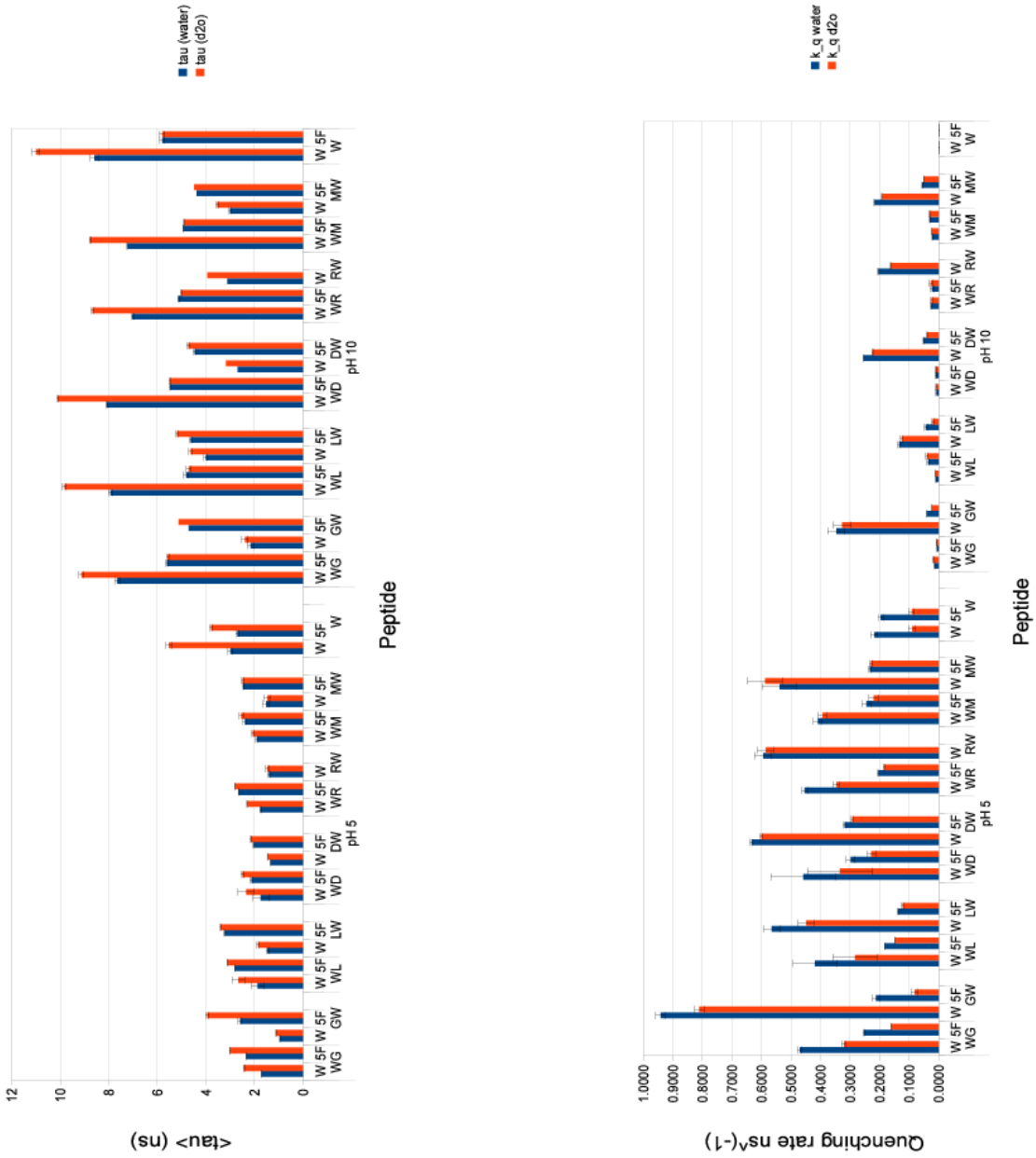

(a) Average Tau

(b) Quenching rate constants

Figure 3.35: Chart of kinetic isotope effects on quenching rates.

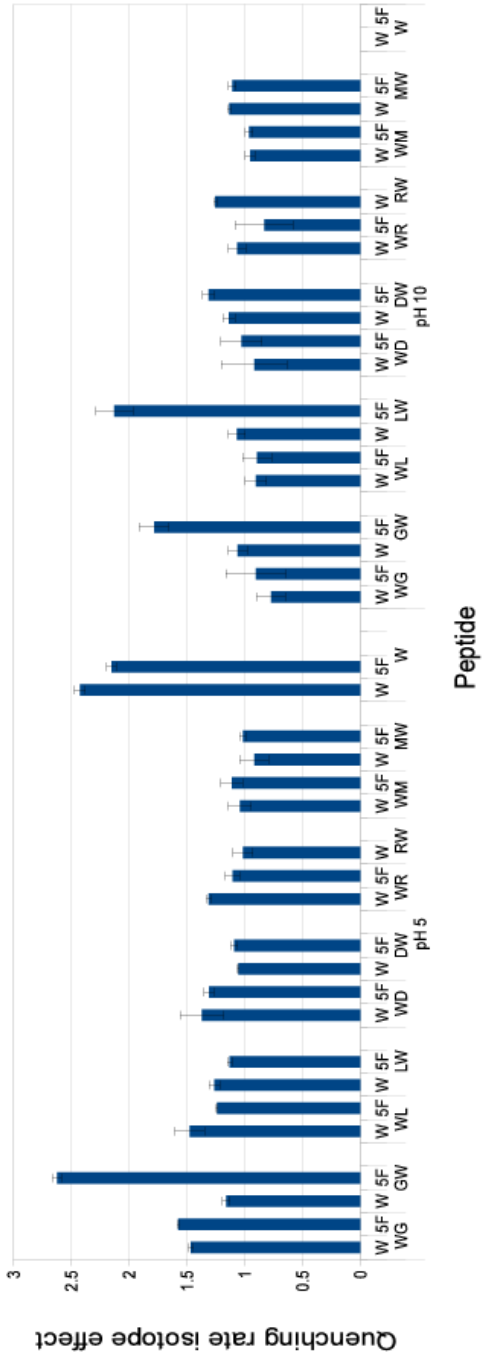

Table 3.6: Fluorescence parameters for X-Trp and X-5FTrp at pH(D) 10.

Sample	$\langle\tau\rangle$	$\sigma_{\langle\tau\rangle}$	$\langle\tau_1\rangle$	$\sigma_{\langle\tau_1\rangle}$	$\langle\tau_2\rangle$	$\sigma_{\langle\tau_1\rangle}$	% τ_1	λ_{max_1}	λ_{max_2}
Gly-Trp pH 10	2.13	0.137	3.11	0.098	1.08	0.024	56	370	350
Gly-5FTrp pH 10	4.66	0.078	5.71	0.086	2.05	0.149	71	380	340
Gly-Trp pD 10	2.37	0.092	3.52	0.053	1.24	0.132	54	360	350
Gly-5FTrp pD 10	5.03	0.400	5.42	0.318	1.76	0.089	89	370	340
Leu-Trp pH 10	4.05	0.075	4.41	0.037	1.58	0.106	87	360	345
Leu-5FTrp pH 10	4.64	0.113	4.77	0.024	1.40	0.304	93	375	NA
Leu-Trp pD 10	4.10	0.339	5.45	0.044	1.30	0.392	80	355	345
Leu-5FTrp pD 10	5.55	0.323	5.24	0.342	1.27	0.154	99	365	NA
Met-Trp pH 10	2.98	0.022	4.38	0.093	2.04	0.147	61	370	NA
Met-5FTrp pH 10	4.42	0.033	4.55	0.029	1.42	0.069	96	365	355
Met-Trp pD 10	3.51	0.046	4.38	0.093	2.04	0.147	65	360	350
Met-5FTrp pD 10	4.49	0.063	4.72	0.029	1.49	0.069	94	370	335
Arg-Trp pH 10	3.14	0.019	3.40	0.086	1.18	0.046	88	360	340
Arg-Trp pD 10	3.83	0.041	4.28	0.183	1.77	0.154	82	355	340
Asp-Trp pH 10	2.68	0.013	3.40	0.058	1.16	0.070	68	360	350
Asp-5FTrp pH 10	4.50	0.036	4.79	0.031	1.47	0.104	91	375	NA
Asp-Trp pD 10	3.11	0.168	4.25	0.189	1.38	0.229	64	360	350
Asp-5FTrp pD 10	4.88	0.151	5.00	0.030	1.68	0.138	90	375	345

Table 3.7: Fluorescence parameters for Trp-X and 5FTrp-X at pH(D) 5.

Sample	$\langle\tau\rangle$	$\sigma_{\langle\tau\rangle}$	$\langle\tau_1\rangle$	$\sigma_{\langle\tau_1\rangle}$	$\langle\tau_2\rangle$	$\sigma_{\langle\tau_1\rangle}$	% τ_1	λ_{max_1}	λ_{max_2}
Trp-Gly pH 5	1.73	0.021	2.06	0.043	0.68	0.078	76	340	330
5FTrp-Gly pH 5	2.36	0.010	2.32	0.044	0.25	0.230	99	350	NA
Trp-Gly pD 5	2.42	0.039	2.77	0.054	1.11	0.271	83	340	337
5FTrp-Gly pD 5	2.95	0.010	2.95	0.010	0.26	0.070	100	345	NA
Trp-Leu pH 5	1.69	0.261	2.41	0.089	0.73	0.226	70	340	330
5FTrp-Leu pH 5	2.83	0.008	2.83	0.008	0.09	0.055	97	345	NA
Trp-Leu pD 5	2.70	0.070	3.03	0.077	1.20	0.420	81	340	337
5FTrp-Leu pD 5	3.10	0.021	3.10	0.021	0.09	0.042	100	340	NA
Trp-Met pH 5	1.76	0.050	3.01	0.711	1.23	0.201	35	340	340
5FTrp-Met pH 5	2.37	0.088	2.46	0.049	0.70	0.246	95	345	NA
Trp-Met pD 5	2.11	0.209	2.72	0.200	1.23	0.538	64	340	340
5FTrp-Met pD 5	2.59	0.181	2.67	0.119	0.75	0.265	93	345	NA
Trp-Arg pH 5	1.74	0.033	2.50	0.158	0.96	0.064	52	340	337
5FTrp-Arg pH 5	2.61	0.018	2.75	0.011	0.97	0.061	91	345	330
Trp-Arg pD 5	2.29	0.026	2.76	0.005	1.12	0.050	71	340	337
5FTrp-Arg pD 5	2.82	0.166	2.95	0.070	0.71	0.067	94	345	NA
Trp-Asp pH 5	2.00	0.332	2.22	0.142	0.83	0.827	67	340	340
5FTrp-Asp pH 5	2.07	0.066	2.26	0.042	0.93	0.082	87	345	330
Trp-Asp pD 5	2.36	0.141	2.84	0.111	1.18	0.359	71	355	330
5FTrp-Asp pD 5	2.51	0.029	2.59	0.024	0.48	0.106	96	345	330

Table 3.8: Fluorescence parameters for Trp-X and 5FTrp-X at pH(D) 10. An entry of "NA" for λ_{max_2} indicates that the component was equal positive and negative amplitudes.

Sample	$\langle\tau\rangle$	$\sigma_{\langle\tau\rangle}$	$\langle\tau_1\rangle$	$\sigma_{\langle\tau_1\rangle}$	$\langle\tau_2\rangle$	$\sigma_{\langle\tau_1\rangle}$	% τ_1	λ_{max_1}	λ_{max_2}
Trp-Gly pH 10	7.71	0.109	8.12	0.096	0.97	0.140	94	365	330
5FTrp-Gly pH 10	5.54	0.050	5.61	0.021	0.50	0.353	99	380	330
Trp-Gly pD 10	8.63	0.849	9.91	0.071	1.31	0.377	91	355	340
5FTrp-Gly pD 10	5.64	0.060	5.65	0.023	0.58	0.093	81	370	NA
Trp-Leu pH 10	7.995	0.070	8.12	0.024	1.10	0.065	98	360	330
5FTrp-Leu pH 10	4.65	0.102	4.75	0.025	1.08	0.806	97	370	330
Trp-Leu pD 10	9.72	0.114	9.99	0.071	1.31	0.377	98	355	NA
5FTrp-Leu pD 10	4.71	0.026	4.79	0.167	1.52	0.899	97	360	340
Trp-Met pH 10	7.30	0.055	7.60	0.077	1.14	0.069	95	355	337
5FTrp-Met pH 10	4.97	0.025	5.03	0.075	1.31	0.084	98	365	NA
Trp-Met pD 10	8.86	0.164	9.28	0.057	1.31	0.209	95	360	NA
5FTrp-Met pD 10	4.90	0.019	5.01	0.029	1.31	0.211	98	355	NA
Trp-Arg pH 10	7.16	0.122	7.51	0.124	1.55	0.181	94	355	330
5FTrp-Arg pH 10	5.14	0.143	5.15	0.148	1.19	0.183	99	365	NA
Trp-Arg pD 10	8.67	0.055	9.19	0.163	1.69	0.095	94	350	337
5FTrp-Arg pD 10	4.88	0.193	5.25	0.013	1.07	0.112	96	360	340
Trp-Asp pH 10	8.15	0.171	8.43	0.116	1.06	0.030	96	360	330
5FTrp-Asp pH 10	5.53	0.054	5.61	0.025	0.90	0.150	98	370	NA
Trp-Asp pD 10	10.09	0.172	10.51	0.053	1.47	0.413	95	355	NA
5FTrp-Asp pD 10	5.44	0.026	5.59	0.022	1.42	0.068	97	370	340

COMPUTATIONAL PREDICTION OF FLUORESCENCE PROPERTIES

This chapter will present the results obtained via a QM/MM method [13] [12] [14] and how they related to the observed blue shift of Trp-X vs X-Trp dipeptides, and experimentally determined quenching rates and quantum yields [18]. We will also use this QM/MM method to access the postulated quasi-static self quenching mechanism described by Chen, et al. [18] The same research group later described a lack of initial brightness in ultrafast fluorescence upconversion measurements and presented this as further evidence of QSSQ in a paper by Xu, et al. [98] The results of instantaneous electron transfer rate calculations presented in this section will be use to evaluated the likelihood that there are conformations with high enough electron transfer rates to explain a sub 300 fs lifetime.

In this section, the results of molecular dynamics simulations and QM/MM calculations are presented. The pursuit of these results was motivated by a desire to further our understanding of the relative contributions of subpopulations of rotamers vs relaxation during the excited state lifetime. Reports in the literature and our own work have shown a time dependent shift in the fluorescence emission maximum. This shift could be explained by a shift in wavelength during the excited state lifetime, a pseudo-shift resulting from two populations of rotamers each with different lifetimes and different fluorescence wavelength maxima, or a combination of these mechanisms. In the experimental results section we showed that the DAS fell into three general categories: ET-heterogeneity, relaxation, and a combination of the two. Molecular dynamics simulations were conducted with either ground or excited state (L_a) charges on the indole ring. The distribution of peptide conformation are displayed in histograms of molecular dynamics simulation results. The populations of each of the canonical rotamer configurations are determined from these histograms.

The rate of transition between canonical rotamers is shown and related to relaxation rates in fluorescence data. An analysis of contributions from the various subgroups (amide, -NH_3^+, -COO^-) to the wavelength shift of Trp-X vs X-Trp, revealed a more complicated picture than what has been described previously in the literature.

Rotamer Populations and Dynamics

In this section the populations of and rate of transition between rotamer populations are presented. Results are shown for force fields from three classes: CHARMM, OPLS, and AMBER. In this section the conformational distributions of dipeptide dihedral angles and the transition rates between those angles will be presented. These results are shown for indole ring charges in both the ground and excited (L_a) states.

Figures 4.1 and 4.2 show the labeling convention for the dihedral angles used to define the various rotamer conformations of the peptides. We have followed convention of assigning dihedrals from N to C terminus.

Dipeptide Conformational Distributions

This section displays the dihedral angle populations for simulations performed in ground state or L_a state charges. In the case of dipeptides, the relative populations of the cis and trans peptide bond are not definitively known. Therefore, it is necessary to conduct molecular dynamics simulations in the cis peptide bond configuration as well (omega = 0). The results of these simulation are also shown with figure captions that state the omega dihedral. The difference in dihedral angle populations between cis and trans are minimal.

Figures 4.3 - 4.10 display the populations of conformations of dihedral angles of Gly-Trp in the zwitterionic form. The Chi1 angles are distributed among the three

Figure 4.1: Gly-Trp zwitterion dipeptide with key atom labels for the definition of dihedral angles. Dihedral angles: $\chi 1$ is torsion about 5-6 with numbering 4-7; $\chi 2$ is torsion about 6-7 with numbering 5-8; ψ is torsion about 2-3 with numbering 1-4; ϕ is torsion about 4-5 with numbering 3-5,9; ω is torsion about 3-4 with numbering 2-5.

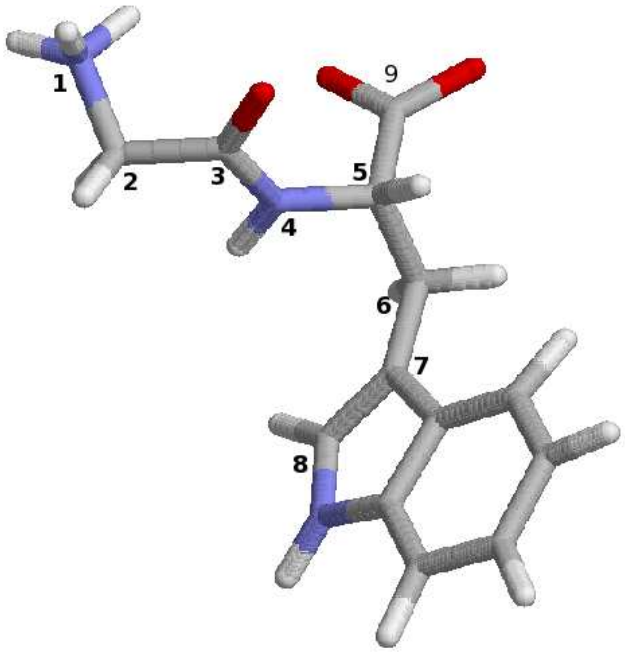

typical canonical values of -60, 60, and 180 degrees. The relative abundance of each of these rotamer state is dependent on the charges of the indole ring (ground or La) and the force field employed in the simulation. Use of the OPLS force field results in distributions of chi1 angles 60:-60:180 of 60:15:25 for ground charges and 60:5:35 for La charges. The chi2 angle primarily adopts two conformations, 90 and -90. However, there is significant population in the region between these two rotamers. The relative populations in the rotamer states of Chi2 are less dependent on the indole charges; they are however significantly shifted in angle. The Psi angle of Gly-Trp zwitterions adopt a single canonical conformation of approximately 180 degrees. The widths

Figure 4.2: Trp-Gly zwitterion dipeptide with key atom labels for the definition of dihedral angles. Dihedral angles: $\chi 1$ is torsion about 2-7 with numbering 1,2,7,8; $\chi 2$ is torsion about 7-8 with numbering 2,7,8,9; ψ is torsion about 2-3 with numbering 1-4; ϕ is torsion about 4-5 with numbering 3-6; ω is torsion about 3-4 with numbering 2-5.

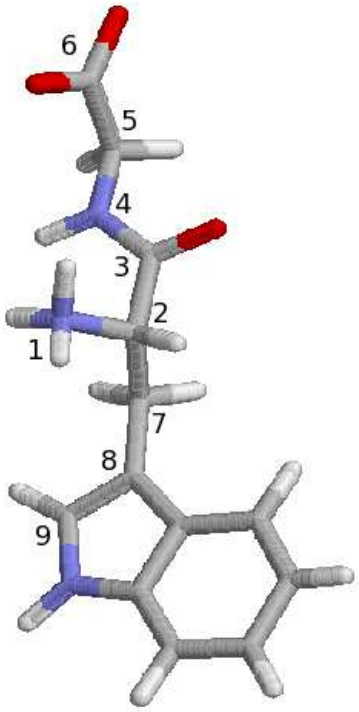

of the distributions of Psi are drastically increased with the use of CHARMM or AMBER force fields. The Phi angles are distributed between a dominate population at -150 and a minor at -90 degrees. When using La state charges, a very small population develops at 90 degrees, the -90 conformation losses population and the -150 conformation gains a small amount of population. The relative populations of these two conformations are strongly dependent on force field. The difference in dihedral angle populations are minimal when comparing cis/trans peptide bond for the simulations with the OPLS force field. There are 3, 2, 2 and 1 conformations

for chi1, chi1, phi, and psi respectively for Gly-Trp zwitterion, leading to 12 distant rotamer conformations. The populations of these rotamers are shown in table 4.1.

Figures 4.15 - 4.26 show the dihedral angle distributions for Trp-Gly zwitterion when simulated with OPLS, CHARMM, and AMBER type force fields. The chi1 dihedral is distributed to three populations at -60, 60, and 180 degrees. Similarity to Gly-Trp the distribution of chi1 is highly dependent on the indole ring charges and the force field employed in the simulation. Two populations at -90 and 90 degree make up the distribution of chi2 angles. The Trp-Gly zwitterion chi2 distribution contained less conformations with angles intermediate between the two major populations. The Psi angle of Trp-Gly was distributed primarily between to populations, at 150 and -60 degrees.

The dihedral angle populations of the Gly-Trp anion are shown in figure 4.11 - 4.14. Two populations of the Psi angle were present in the case of the Gly-Trp anion with trans omega dihedral, at approximately 0 and 180 degrees. The relative abundance of these was unaffected by change from ground to La charges. All other angle distributions have very little difference in comparison with the zwitterion results.

Figures 4.27 - 4.30 display the results for the Trp-Gly anion. The chi1 angle is dominated by the population at 180 degrees in the ground state and to a lesser extent in the La state. The rotamers at 60 and -60 increase in population between ground and La state simulations. All other dihedral angles show very little difference in population in comparison of ground and La state. Similarity to the Gly-Trp anion, the Trp-Gly anion with trans omega dihedral angle has a population with a Psi angle of approximately zero degrees.

Figure 4.3: On the left the histogram of Chi1 dihedral angle of the Gly-Trp zwitterion during an approximately 1.5 microsecond molecular dynamics simulation with OPLS force field parameters. On the right the histogram for Chi2 dihedral during the same simulation. The Omega dihedral was nominally 180 degrees (trans) for this simulation.

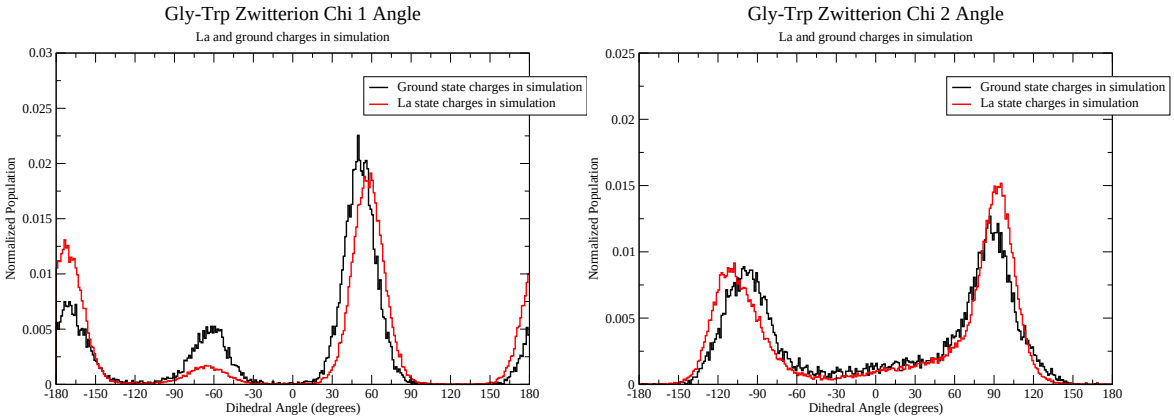

Figure 4.4: On the left the histogram of Psi dihedral angle of the Gly-Trp zwitterion during an approximately 1.5 microsecond molecular dynamics simulation with OPLS force field parameters. On the right the histogram for Phi dihedral during the same simulation. The Omega dihedral was nominally 180 degrees (trans) for this simulation.

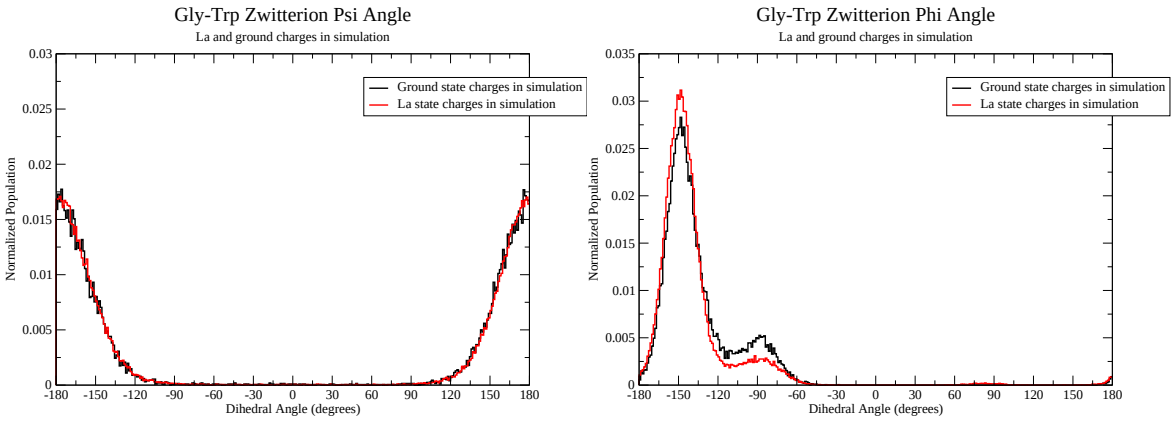

Figure 4.5: On the left the histogram of Chi1 dihedral angle of the Gly-Trp zwitterion during a 1.7 microsecond molecular dynamics simulation with CHARMM27 force field parameters. On the right the histogram for Chi2 dihedral during the same simulation. The Omega dihedral was nominally 180 degrees (trans) for this simulation.

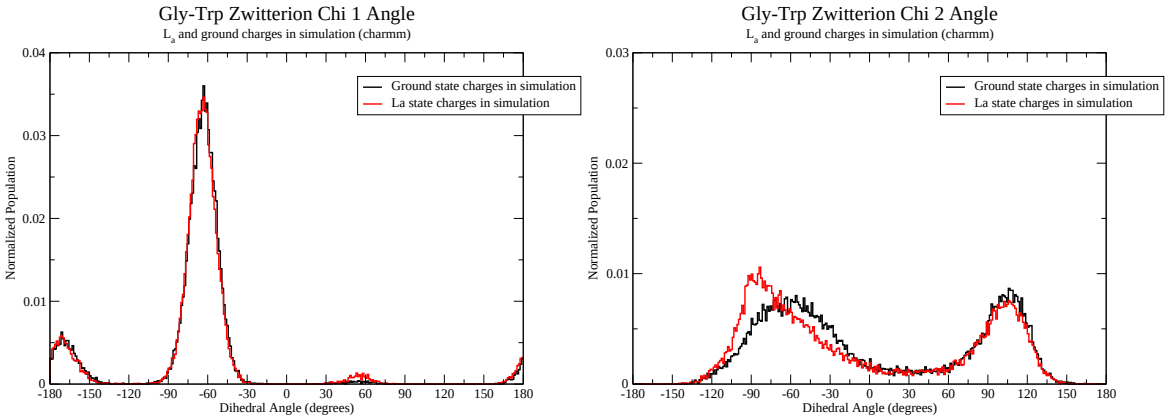

Figure 4.6: On the left the histogram of Psi dihedral angle of the Gly-Trp zwitterion during a 1.7 microsecond molecular dynamics simulation with CHARMM27 force field parameters. On the right the histogram for Phi dihedral during the same simulation. The Omega dihedral was nominally 180 degrees (trans) for this simulation.

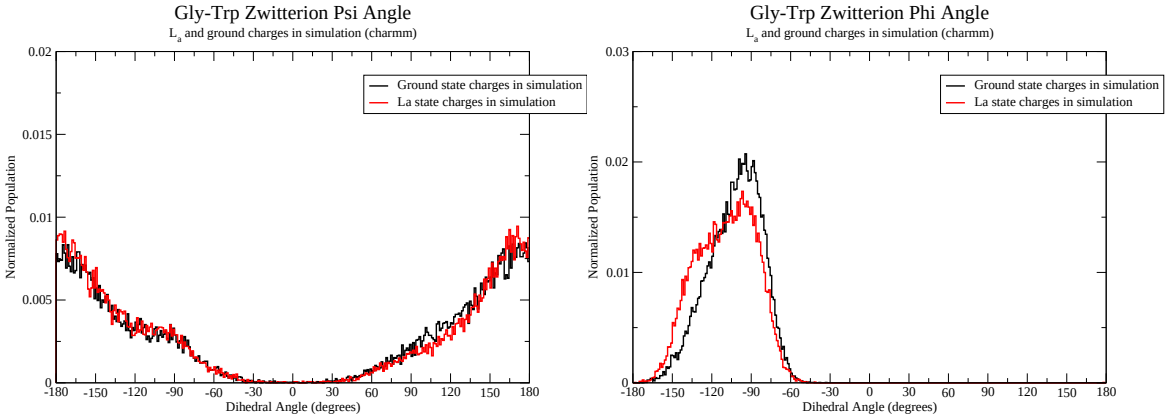

Figure 4.7: On the left the histogram of Chi1 dihedral angle of the Gly-Trp zwitterion during a 1.7 microsecond molecular dynamics simulation with AMBER99SB-ILDN force field parameters. On the right the histogram for Chi2 dihedral during the same simulation. The Omega dihedral was nominally 180 degrees (trans) for this simulation.

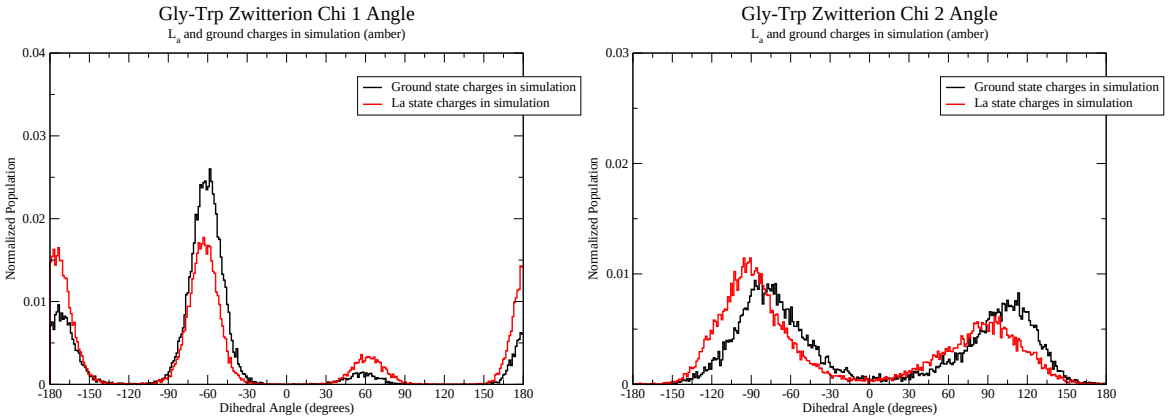

Figure 4.8: On the left the histogram of Psi dihedral angle of the Gly-Trp zwitterion during a 1.7 microsecond molecular dynamics simulation with AMBER99SB-ILDN force field parameters. On the right the histogram for Phi dihedral during the same simulation. The Omega dihedral was nominally 180 degrees (trans) for this simulation.

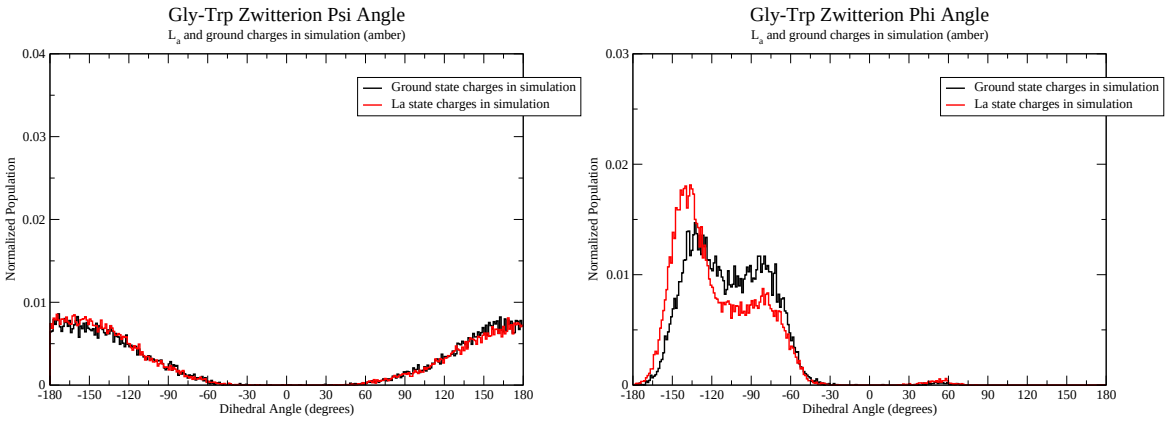

Figure 4.9: On the left the histogram of Chi1 dihedral angle of the Gly-Trp zwitterion during a 1.7 microsecond molecular dynamics simulation with OPLS force field parameters. On the right the histogram for Chi2 dihedral during the same simulation. The Omega dihedral was nominally 0 degrees (cis) for this simulation.

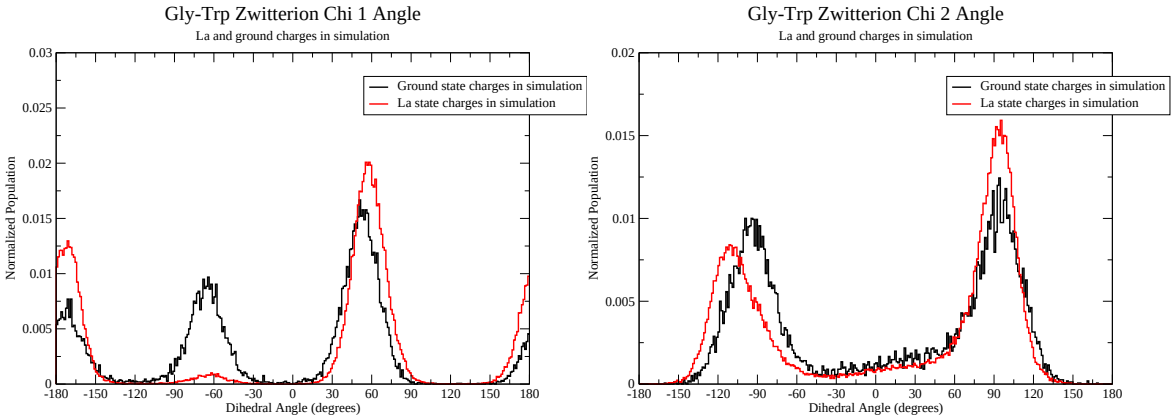

Figure 4.10: On the left the histogram of Psi dihedral angle of the Gly-Trp zwitterion during a 1.7 microsecond molecular dynamics simulation with OPLS force field parameters. On the right the histogram for Phi dihedral during the same simulation. The Omega dihedral was nominally 0 degrees (cis) for this simulation.

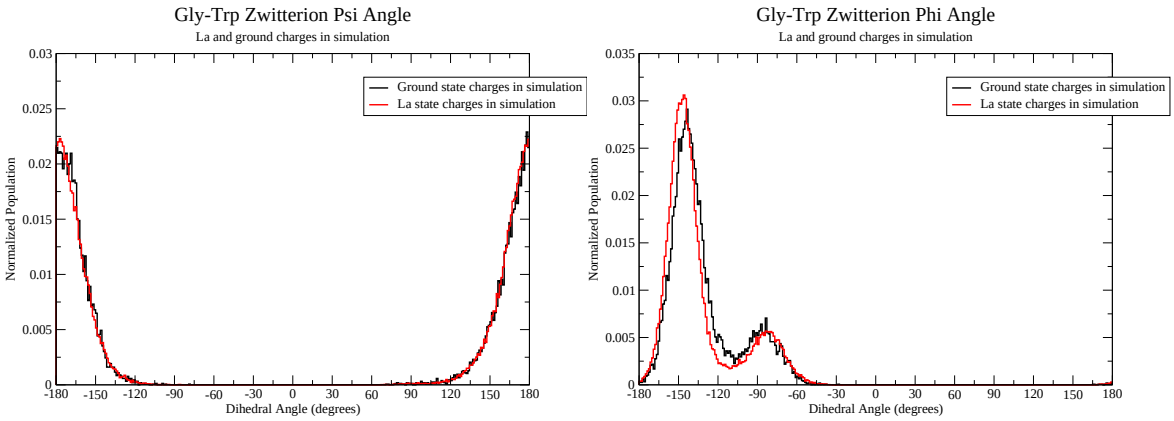

Figure 4.11: On the left the histogram of Chi 1 dihedral angle of the Gly-Trp anion during a 1.7 microsecond molecular dynamics simulation with OPLS force field parameters. On the right the histogram for Chi 2 dihedral during the same simulation. The Omega dihedral was nominally 180 degrees (trans) for this simulation.

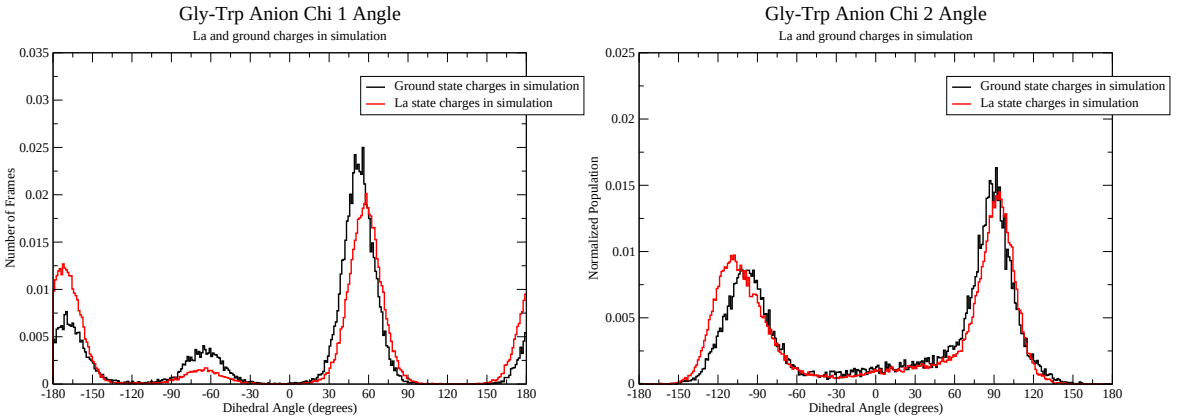

Figure 4.12: On the left the histogram of Psi dihedral angle of the Gly-Trp anion during a 1.7 microsecond molecular dynamics simulation with OPLS force field parameters. On the right the histogram for Phi dihedral during the same simulation. The Omega dihedral was nominally 180 degrees (trans) for this simulation.

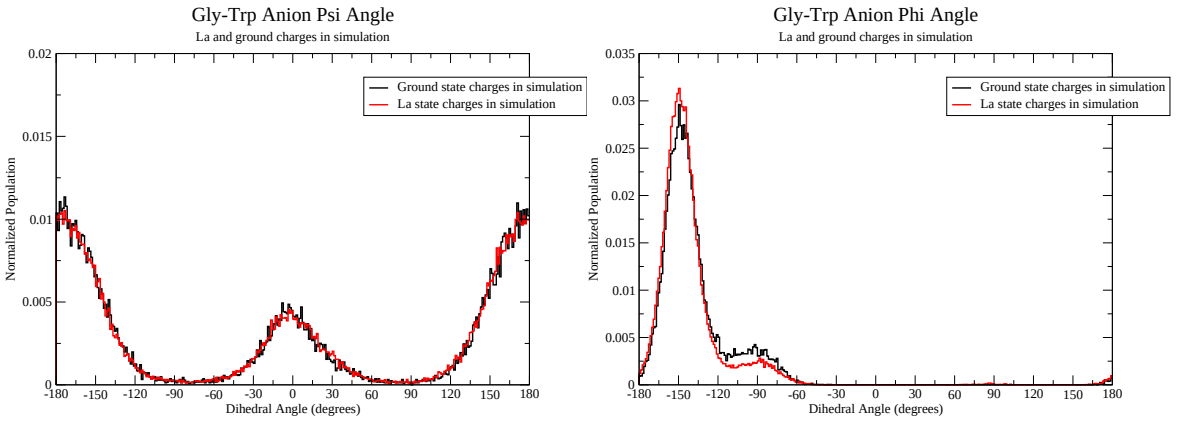

Figure 4.13: On the left the histogram of Chi 1 dihedral angle of the Gly-Trp anion during a 1.7 microsecond molecular dynamics simulation with OPLS force field parameters. On the right the histogram for Chi 2 dihedral during the same simulation. The Omega dihedral was nominally 0 degrees (cis) for this simulation.

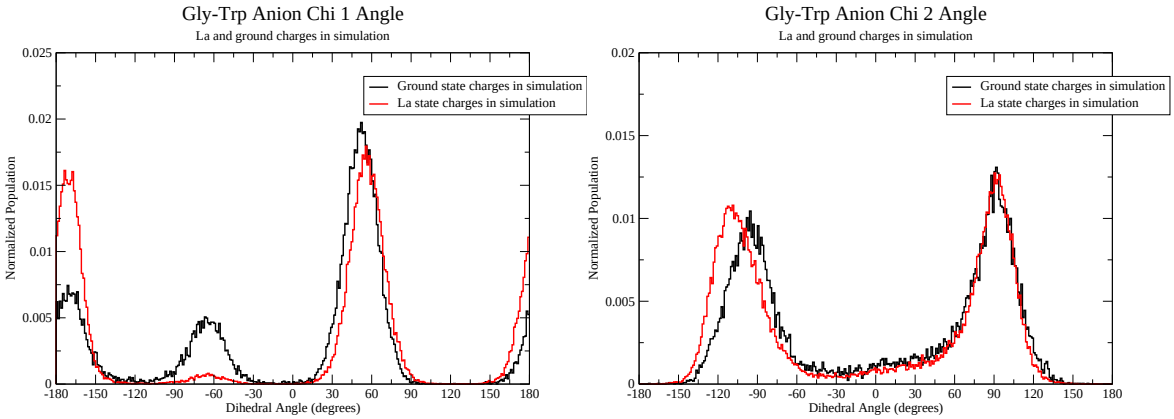

Figure 4.14: On the left the histogram of Psi dihedral angle of the Gly-Trp anion during a 1.7 microsecond molecular dynamics simulation with OPLS force field parameters. On the right the histogram for Phi dihedral during the same simulation. The Omega dihedral was nominally 0 degrees (cis) for this simulation.

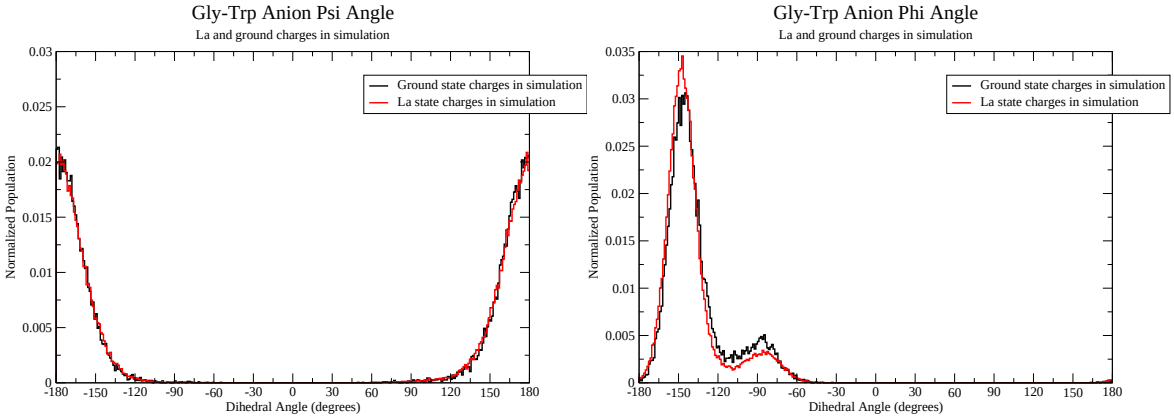

Figure 4.15: On the left the histogram of Chi1 dihedral angle of the Trp-Gly zwitterion during a 1.7 microsecond molecular dynamics simulation with OPLS force field parameters. On the right the histogram for Chi2 dihedral during the same simulation. The Omega dihedral was nominally 180 degrees (trans) for this simulation.

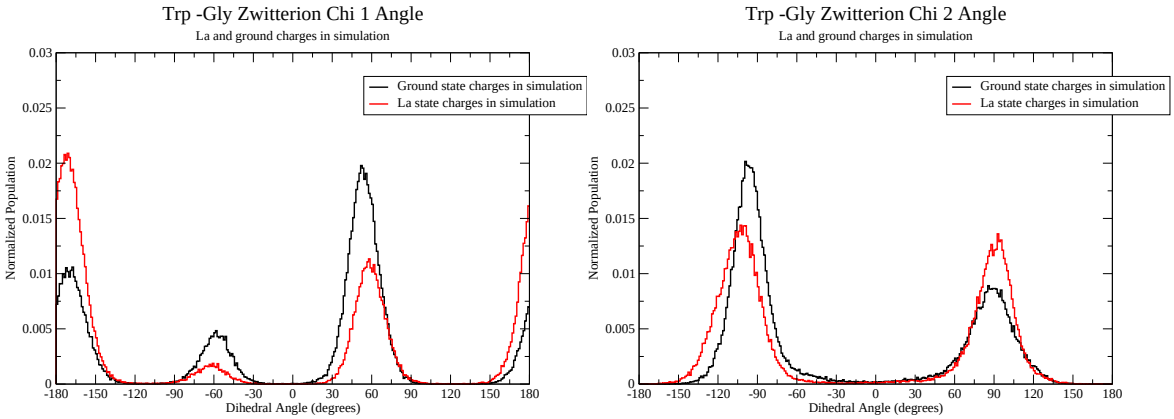

Figure 4.16: On the left the histogram of Psi dihedral angle of the Trp-Gly zwitterion during a 1.7 microsecond molecular dynamics simulation with OPLS force field parameters. On the right the histogram for Phi dihedral during the same simulation. The Omega dihedral was nominally 180 degrees (trans) for this simulation.

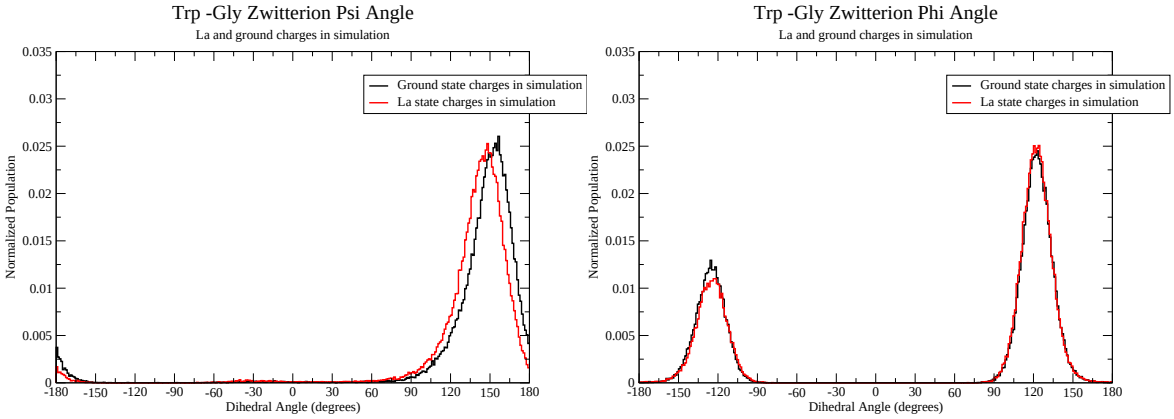

Figure 4.17: On the left the histogram of Chi1 dihedral angle of the Trp-Gly zwitterion during a 1.7 microsecond molecular dynamics simulation with CHARMM27 force field parameters. On the right the histogram for Chi2 dihedral during the same simulation. The Omega dihedral was nominally 180 degrees (trans) for this simulation.

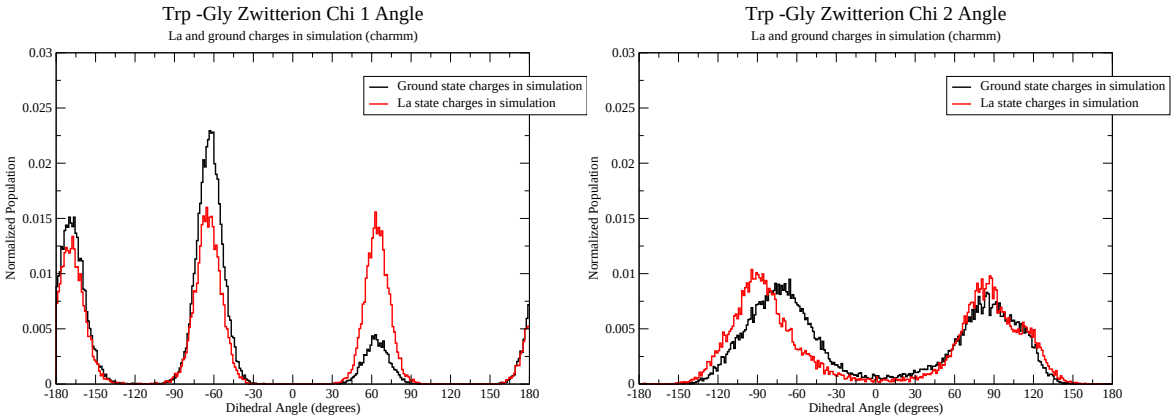

Figure 4.18: On the left the histogram of Psi dihedral angle of the Trp-Gly zwitterion during a 1.7 microsecond molecular dynamics simulation with CHARMM27 force field parameters. On the right the histogram for Phi dihedral during the same simulation. The Omega dihedral was nominally 180 degrees (trans) for this simulation.

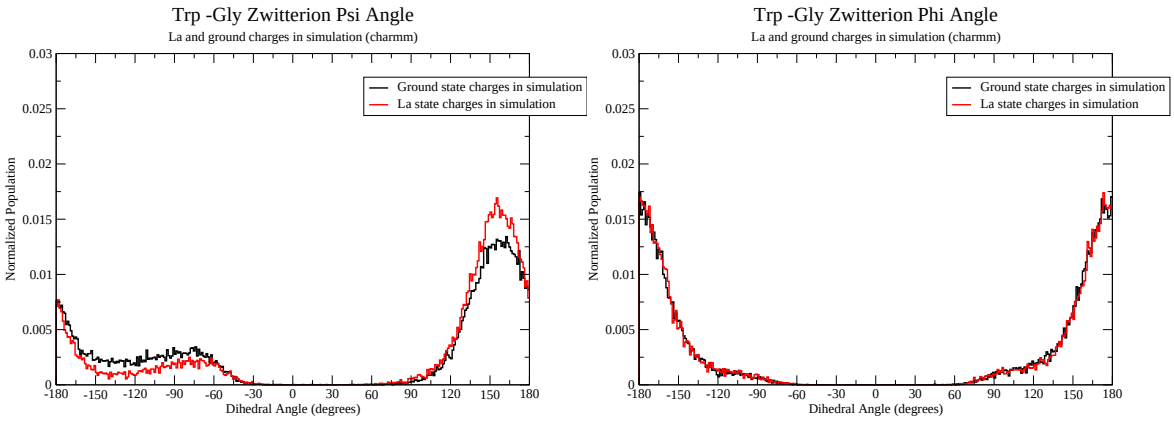

Figure 4.19: On the left the histogram of Chi1 dihedral angle of the Trp-Gly zwitterion during a 1.7 microsecond molecular dynamics simulation with AMBER99SB-ILDN force field parameters. On the right the histogram for Chi2 dihedral during the same simulation. The Omega dihedral was nominally 180 degrees (trans) for this simulation.

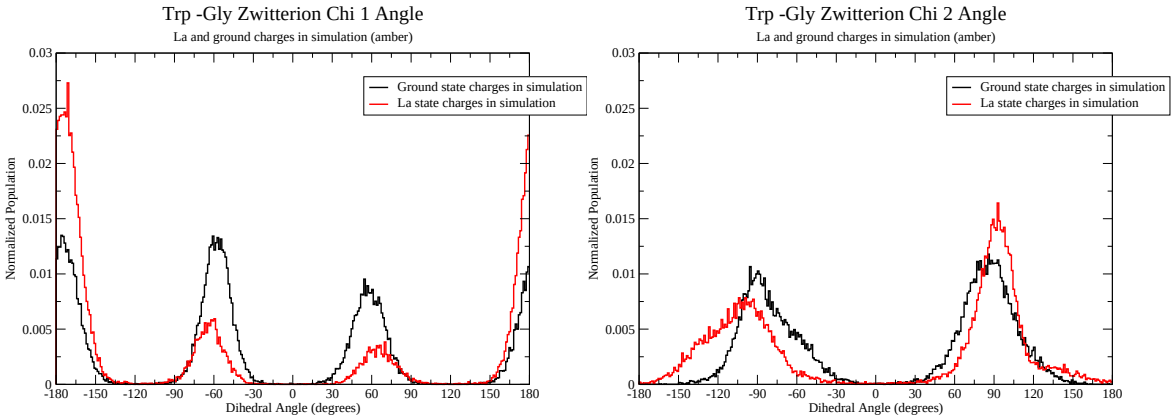

Figure 4.20: On the left the histogram of Psi dihedral angle of the Trp-Gly zwitterion during a 1.7 microsecond molecular dynamics simulation with AMBER99SB-ILDN force field parameters. On the right the histogram for Phi dihedral during the same simulation. The Omega dihedral was nominally 180 degrees (trans) for this simulation.

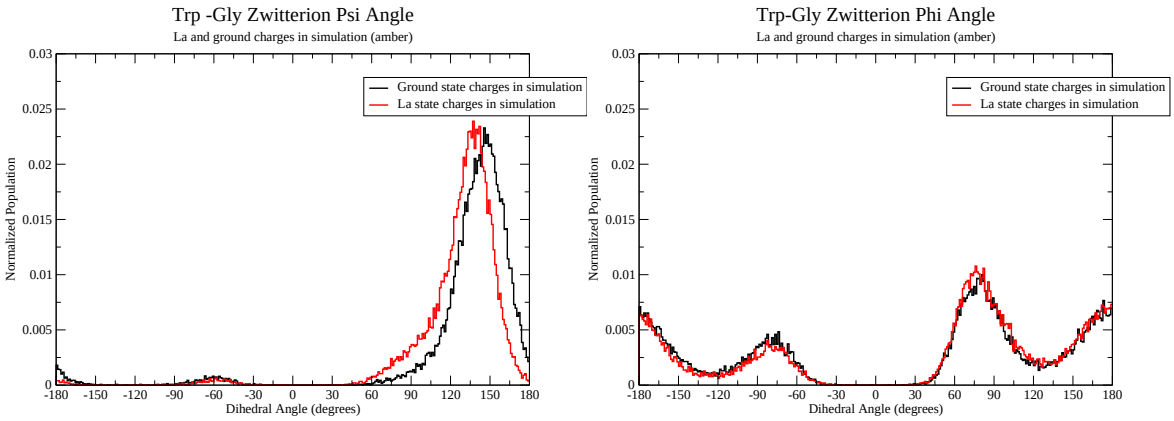

Figure 4.21: On the left the histogram of Chi1 dihedral angle of the Trp-Gly zwitterion during a 1.7 microsecond molecular dynamics simulation with OPLS force field parameters. On the right the histogram for Chi2 dihedral during the same simulation. The Omega dihedral was nominally 0 degrees (cis) for this simulation.

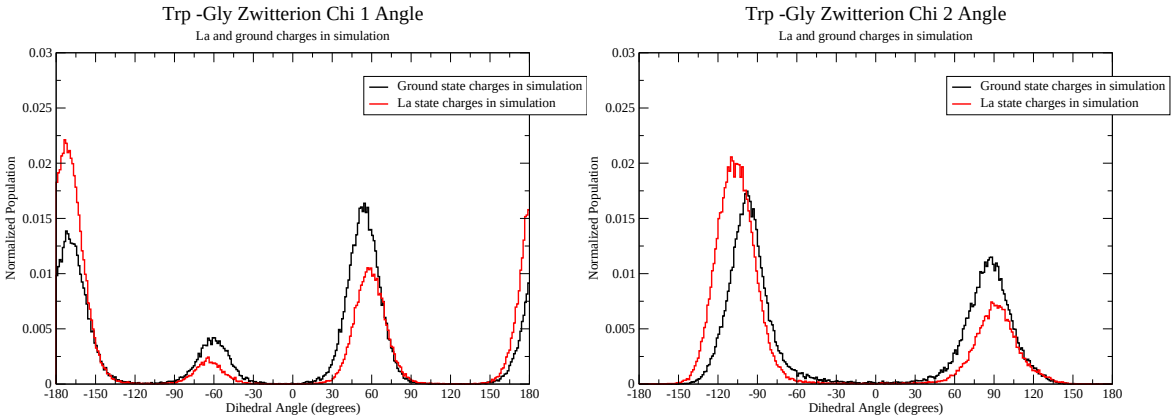

Figure 4.22: On the left the histogram of Psi dihedral angle of the Trp-Gly zwitterion during a 1.7 microsecond molecular dynamics simulation with OPLS force field parameters. On the right the histogram for Phi dihedral during the same simulation. The Omega dihedral was nominally 0 degrees (cis) for this simulation.

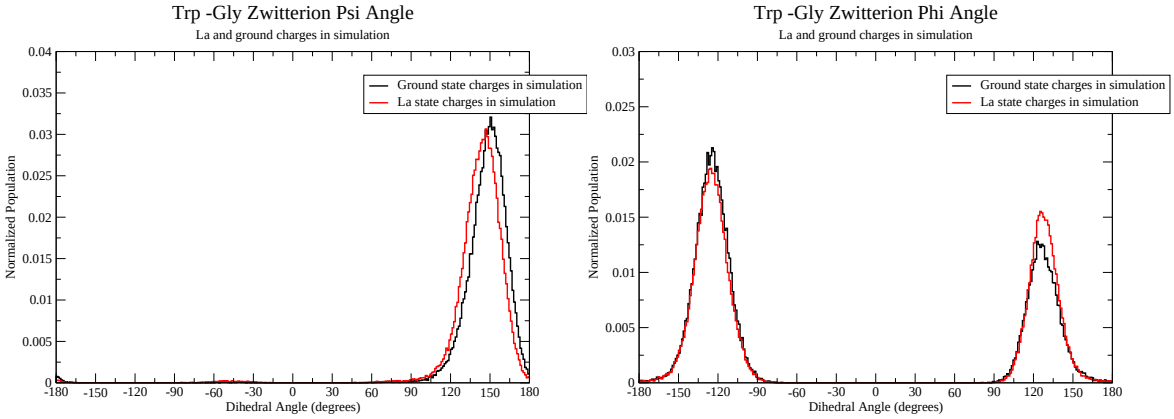

Figure 4.23: On the left the histogram of Chi1 dihedral angle of the Trp-Gly zwitterion during a 1.7 microsecond molecular dynamics simulation with CHARMM27 force field parameters. On the right the histogram for Chi2 dihedral during the same simulation. The Omega dihedral was nominally 0 degrees (cis) for this simulation.

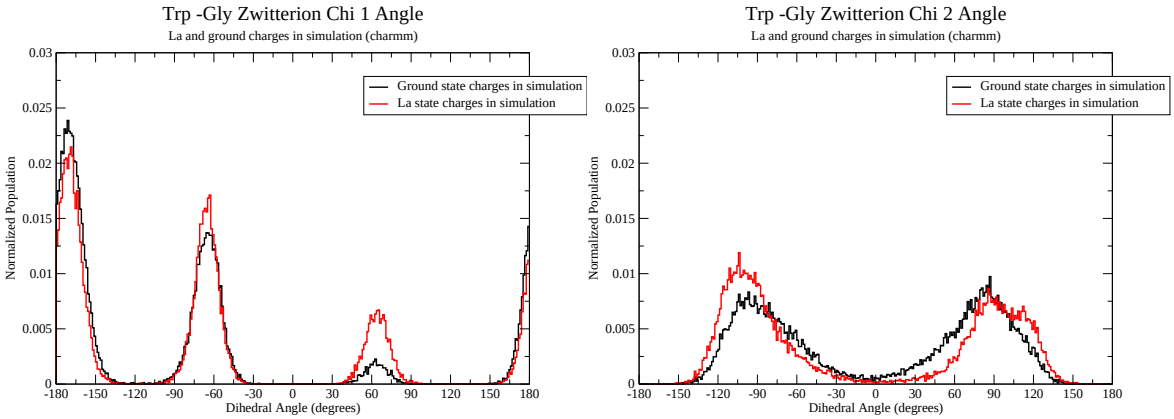

Figure 4.24: On the left the histogram of Psi dihedral angle of the Trp-Gly zwitterion during a 1.7 microsecond molecular dynamics simulation with CHARMM27 force field parameters. On the right the histogram for Phi dihedral during the same simulation. The Omega dihedral was nominally 0 degrees (cis) for this simulation.

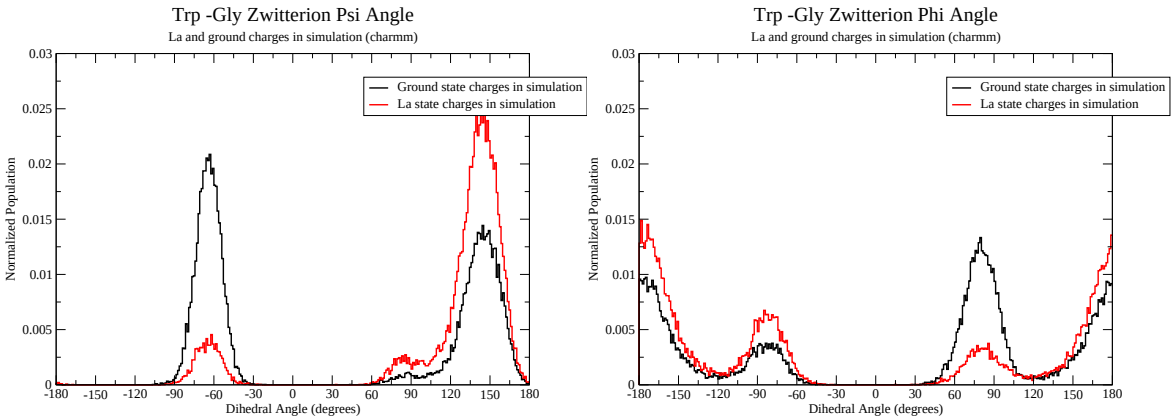

Figure 4.25: On the left the histogram of Chi1 dihedral angle of the Trp-Gly zwitterion during a 1.7 microsecond molecular dynamics simulation with AMBER99SB-ILDN force field parameters. On the right the histogram for Chi2 dihedral during the same simulation. The Omega dihedral was nominally 0 degrees (cis) for this simulation.

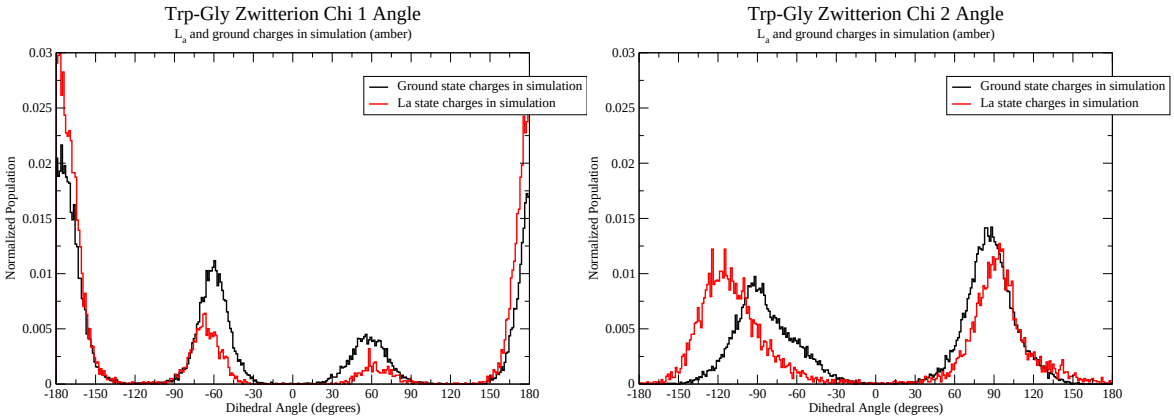

Figure 4.26: On the left the histogram of Psi dihedral angle of the Trp-Gly zwitterion during a 1.7 microsecond molecular dynamics simulation with AMBER99SB-ILDN force field parameters. On the right the histogram for Phi dihedral during the same simulation. The Omega dihedral was nominally 0 degrees (cis) for this simulation.

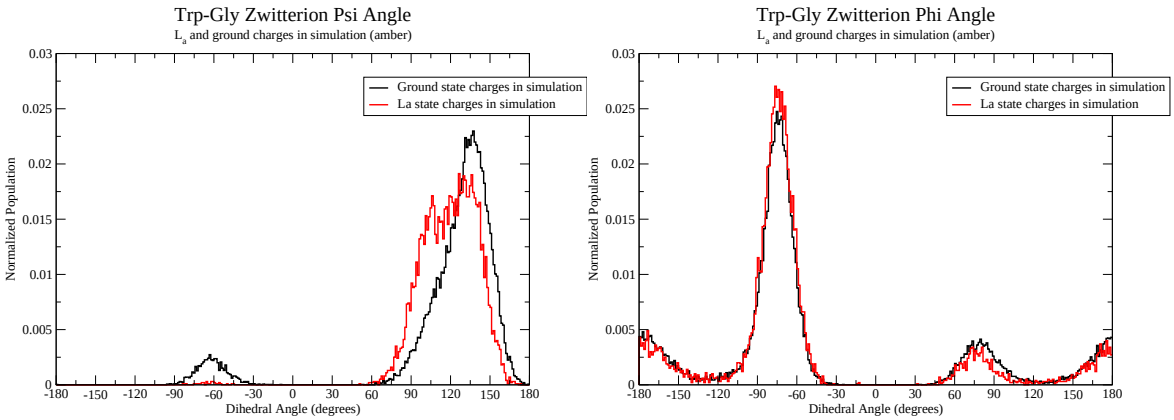

Figure 4.27: On the left the histogram of Chi1 dihedral angle of the Trp-Gly anion during a 1.7 microsecond molecular dynamics simulation with OPLS force field parameters. On the right the histogram for Chi2 dihedral during the same simulation. The Omega dihedral was nominally 180 degrees (trans) for this simulation.

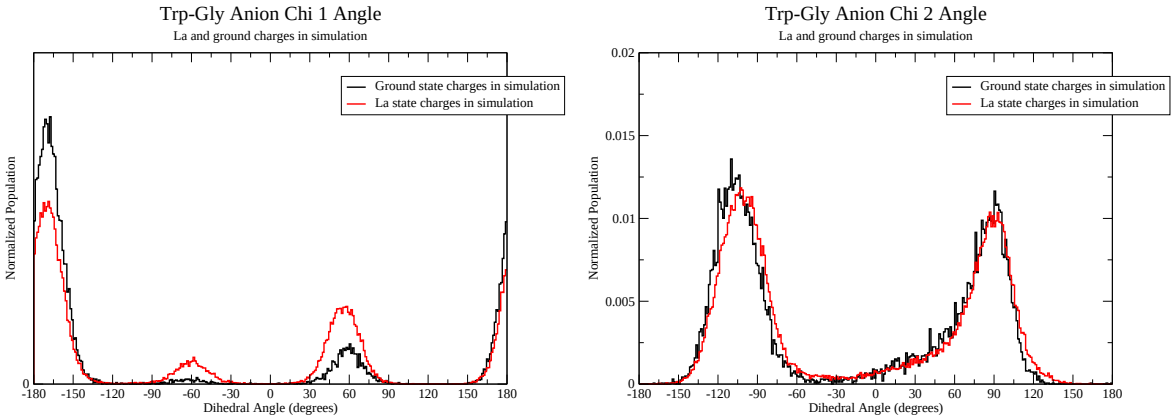

Figure 4.28: On the left the histogram of Psi dihedral angle of the Trp-Gly anion during a 1.7 microsecond molecular dynamics simulation with OPLS force field parameters. On the right the histogram for Phi dihedral during the same simulation. The Omega dihedral was nominally 180 degrees (trans) for this simulation.

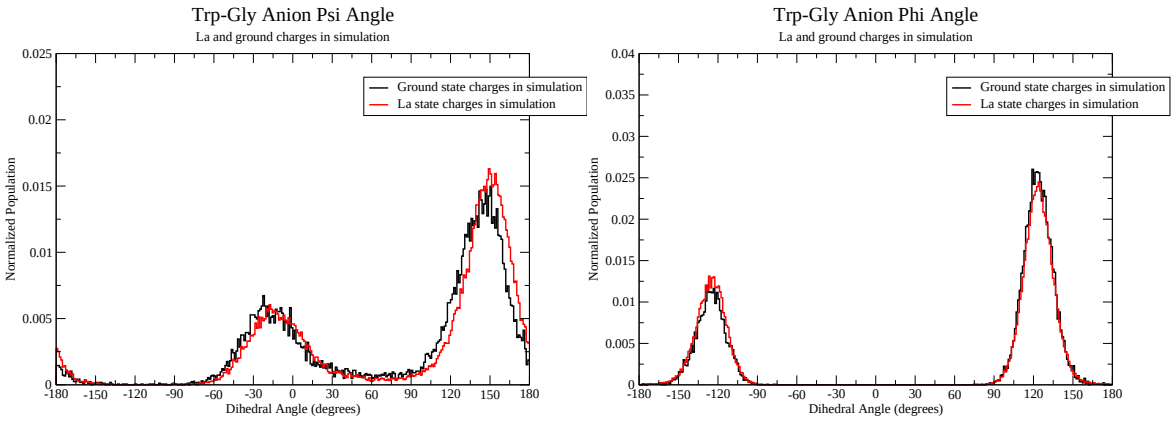

Figure 4.29: On the left the histogram of Chi1 dihedral angle of the Trp-Gly anion during a 1.7 microsecond molecular dynamics simulation with OPLS force field parameters. On the right the histogram for Chi2 dihedral during the same simulation. The Omega dihedral was nominally 0 degrees (cis) for this simulation.

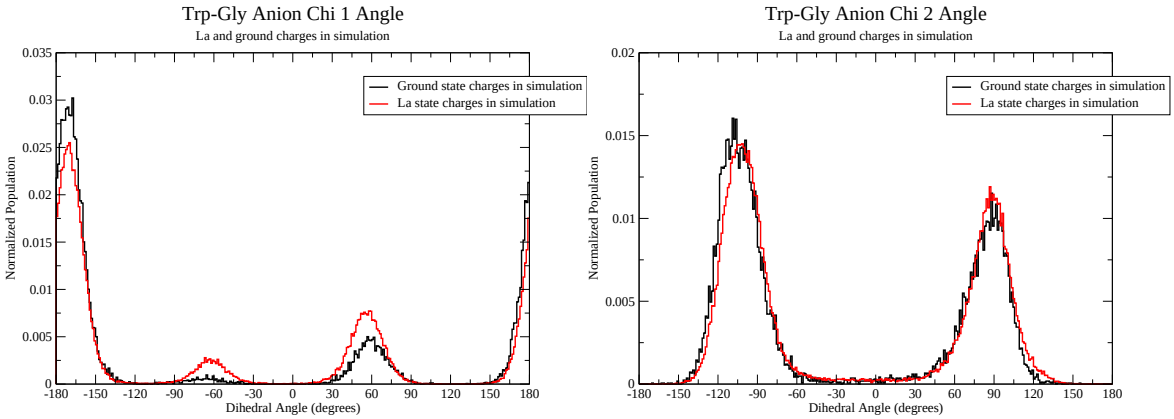

Figure 4.30: On the left the histogram of Psi dihedral angle of the Trp-Gly anion during a 1.7 microsecond molecular dynamics simulation with OPLS force field parameters. On the right the histogram for Phi dihedral during the same simulation. The Omega dihedral was nominally 0 degrees (cis) for this simulation.

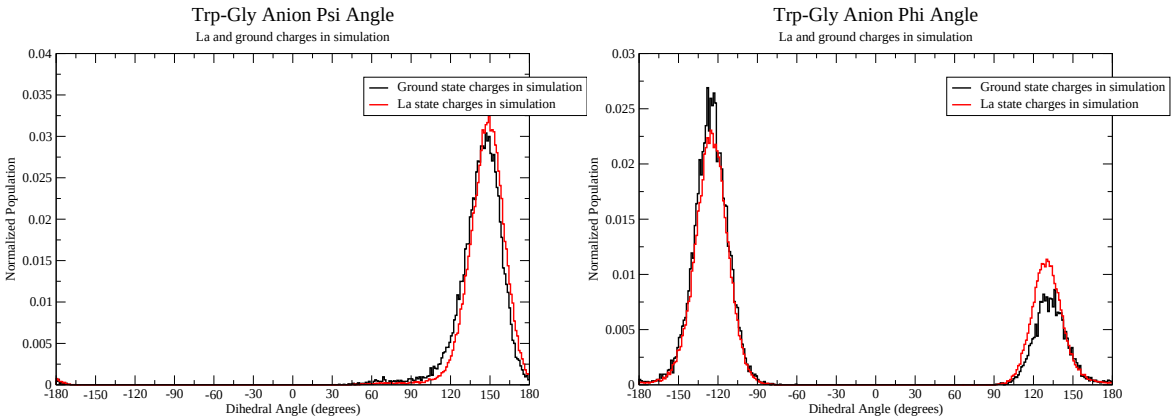

Rotamer Transition Dynamics

This section will show the transitions between dipeptide rotamer conformations over the course of molecular dynamics simulations. These results relate to the rate of re-equilibration between rotamer populations. The contribution of relaxation to multi-exponential fluorescence decay will relate to the re-equilibration between rotamer populations. Figures 4.31 - 4.40 present the dihedral angles of the dipeptides over the course of the MD simulation. The full trajectories as well as 200 ns windows to show the rates of transition between rotamer states more easily. These figures show a fairly rapid rate of transition between rotamer populations. In these examples approximately 30 transitions are observed in 200 ns. Transitions are distributed relatively evenly throughout the simulation. There are not long periods in which the conformation is trapped in a given state.

Figures 4.31 - 4.33 show the dihedral angles as a function of time of the Gly-Trp zwitterion with trans omega dihedral angle during a nearly 1.5 microsecond molecular dynamics simulation. In addition to the expected single rotamer conformation of the omega dihedral, the Psi and Phi dihedral maintain a single canonical configuration over the course of this simulation. On the other hand, the Chi1 and Chi2 dihedrals undergo transitions between canonical states at a very high rate. Very similar results are found for Gly-Trp with cis omega angle and Trp-Gly with cis or trans peptide bond as shown by figures 4.34 - 4.40.

Rotamer Redistribution Rates

Tables 4.2 and 4.3 shows the rate constants for the re-equilibration between rotamer populations. These results were calculated using equation 2.7.

Figure 4.31: On the left the Chi1 dihedral angle of the Gly-Trp zwitterion during a nearly 1.5 microsecond molecular dynamics simulation with OPLS force field. On the right the Chi2 dihedral during the same simulation. The Omega dihedral was nominally 180 degrees (trans) for this simulation. Charges on the indole ring were those of the L_a state. Points are plotted every 2 ns.

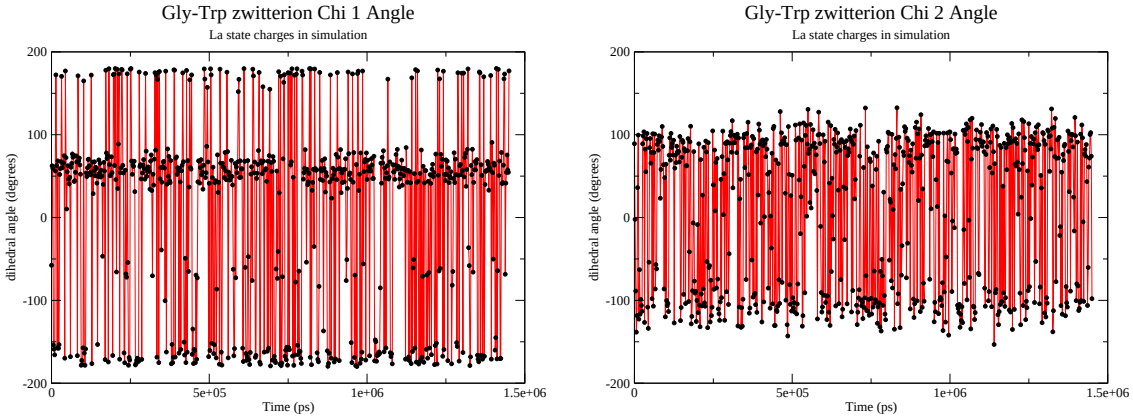

Figure 4.32: On the left the Chi1 dihedral angle of the Gly-Trp zwitterion during 200 ns of a nearly 1.5 microsecond molecular dynamics simulation (OPLS). On the right the Chi2 dihedral during the same simulation. Here a subset of simulation time is shown to allow for clear observation of the rate of transition between the canonical populations. The Omega dihedral was nominally 180 degrees (trans) for this simulation. Charges on the indole ring were those of the La state. Points are plotted every 2 ns.

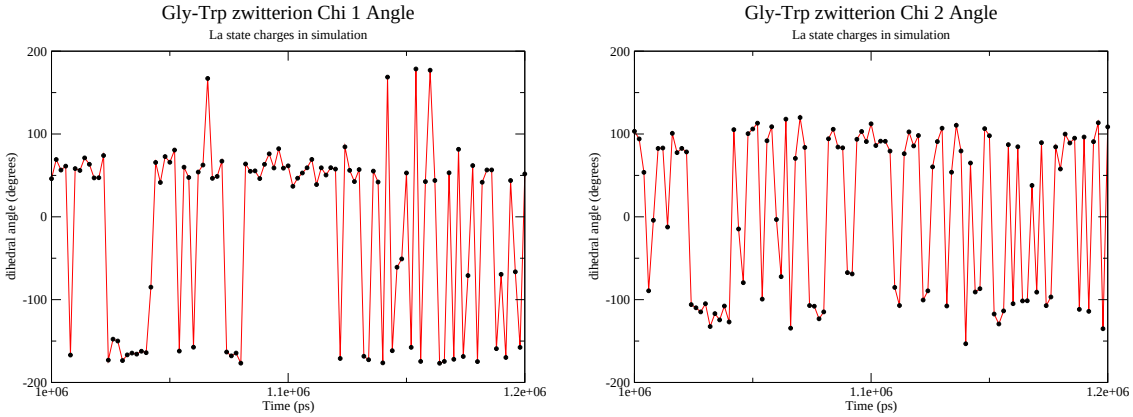

Figure 4.33: On the left the Psi dihedral angle of the Gly-Trp zwitterion during a nearly 1.5 microsecond molecular dynamics simulation (OPLS). On the right the Phi dihedral during the same simulation. The Omega dihedral was nominally 180 degrees (trans) for this simulation. Charges on the indole ring were those of the La state. Points are plotted every 2 ns.

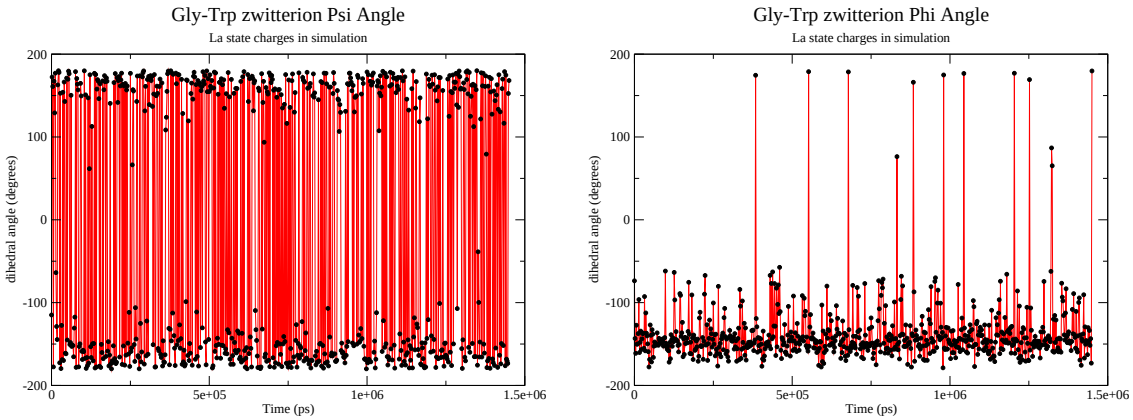

Figure 4.34: On the left the Chi1 dihedral angle of the Gly-Trp zwitterion in the cis peptide bond conformation during a nearly 1.5 microsecond molecular dynamics simulation (OPLS). On the right the Chi2 dihedral during the same simulation. The Omega dihedral was nominally 0 degrees (cis) for this simulation. Charges on the indole ring were those of the La state. Points are plotted every 2 ns.

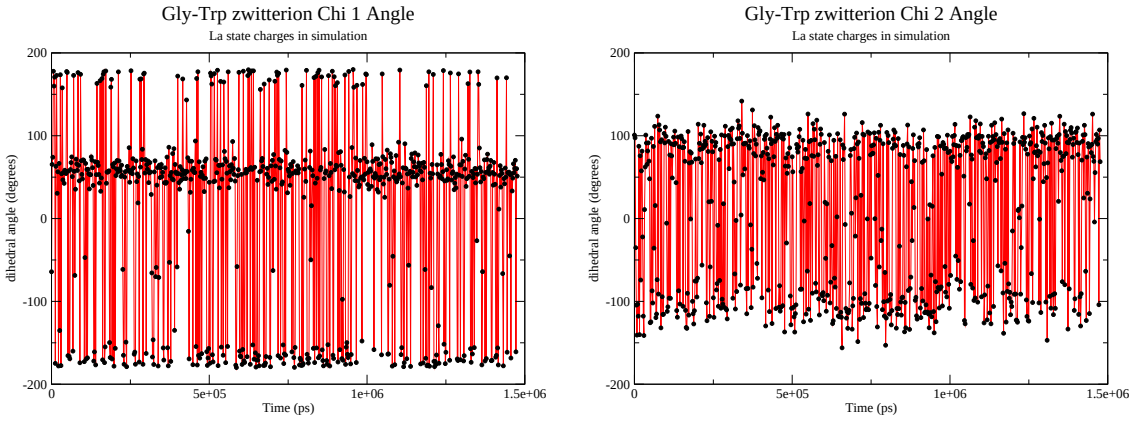

Figure 4.35: On the left the Chi1 dihedral angle of the Gly-Trp zwitterion during 200 ns of a nearly 1.5 microsecond molecular dynamics simulation (OPLS). On the right the Chi2 dihedral during the same simulation. Here a subset of simulation time is shown to allow for clear observation of the rate of transition between the canonical populations. The Omega dihedral was nominally 0 degrees (cis) for this simulation. Charges on the indole ring were those of the La state. Points are plotted every 2 ns.

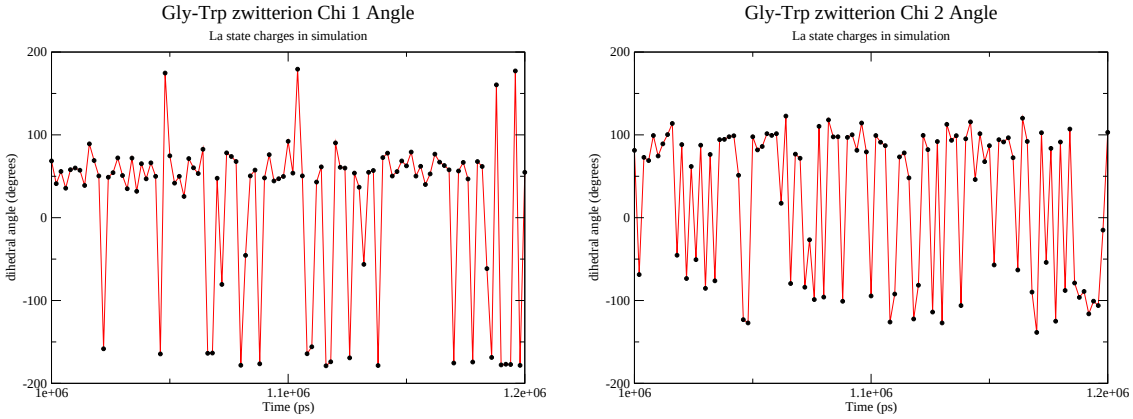

Figure 4.36: On the left the Psi dihedral angle of the Gly-Trp zwitterion in the cis peptide bond conformation during a nearly 1.5 microsecond molecular dynamics simulation (OPLS). On the right the Phi dihedral during the same simulation. The Omega dihedral was nominally 0 degrees (cis) for this simulation. Charges on the indole ring were those of the La state. Points are plotted every 2 ns.

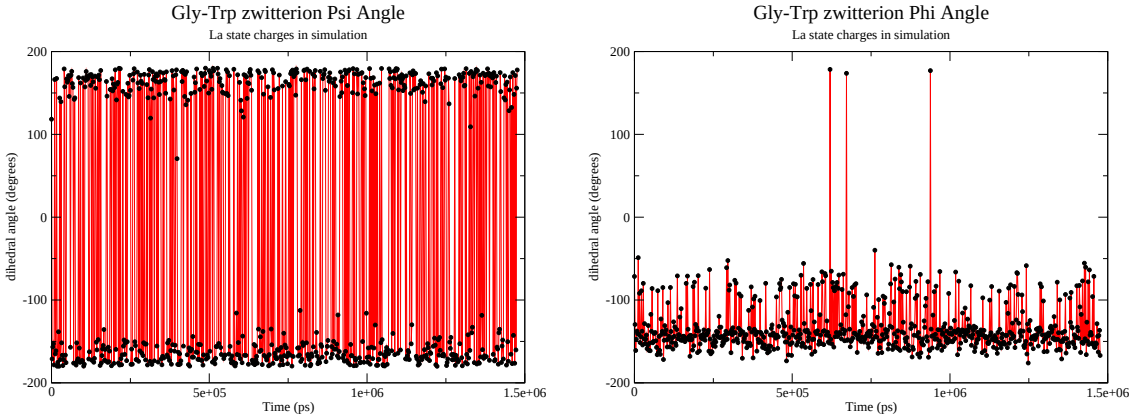

Figure 4.37: On the left the Chi1 dihedral angle of the Trp-Gly zwitterion during a 1.7 microsecond molecular dynamics simulation (OPLS). On the right the Chi2 dihedral during the same simulation. The Omega dihedral was nominally 180 degrees (trans) for this simulation. Charges on the indole ring were those of the La state. Points are plotted every 2 ns.

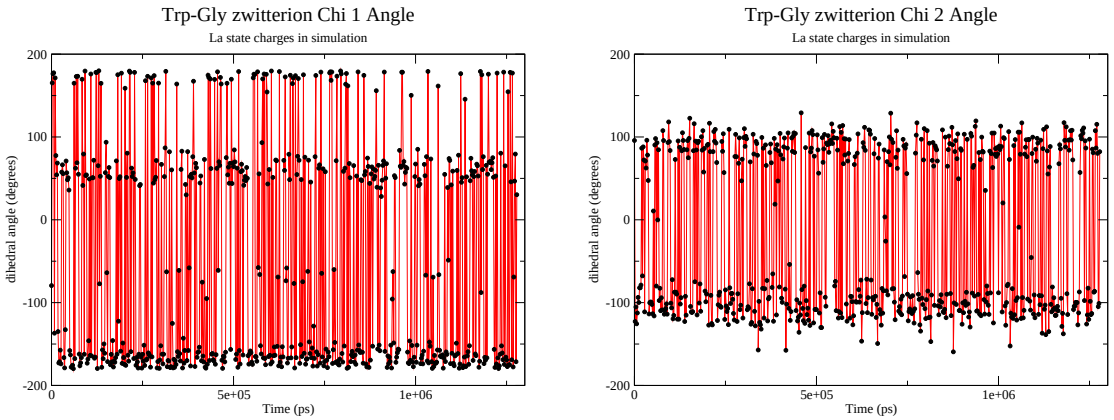

Figure 4.38: On the left the Psi dihedral angle of the Trp-Gly zwitterion during a 1.7 microsecond molecular dynamics simulation (OPLS). On the right the Phi dihedral during the same simulation. The Omega dihedral was nominally 180 degrees (trans) for this simulation. Charges on the indole ring were those of the L_a state. Points are plotted every 2 ns.

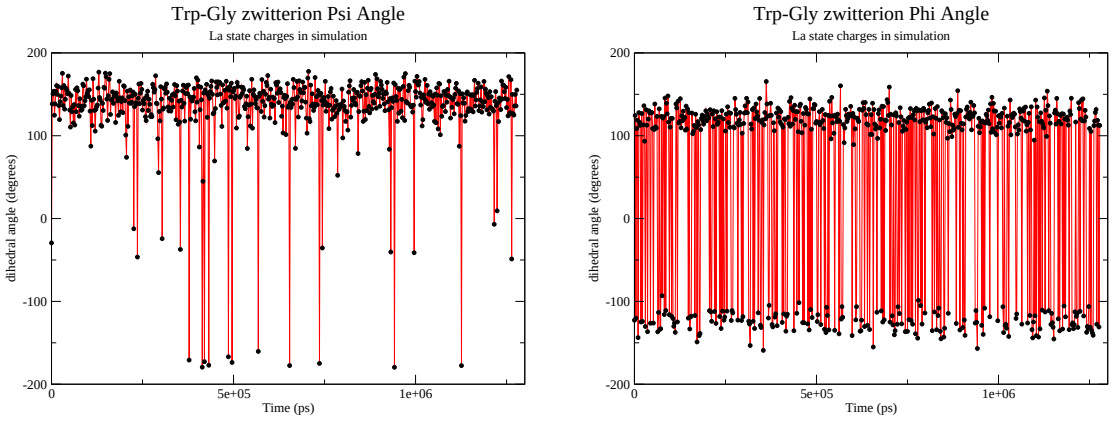

Figure 4.39: On the left the Chi1 dihedral angle of the Trp-Gly zwitterion during a 1.7 microsecond molecular dynamics simulation (OPLS). On the right the Chi2 dihedral during the same simulation. The Omega dihedral was nominally 0 degrees (cis) for this simulation. Charges on the indole ring were those of the La state. Points are plotted every 2 ns.

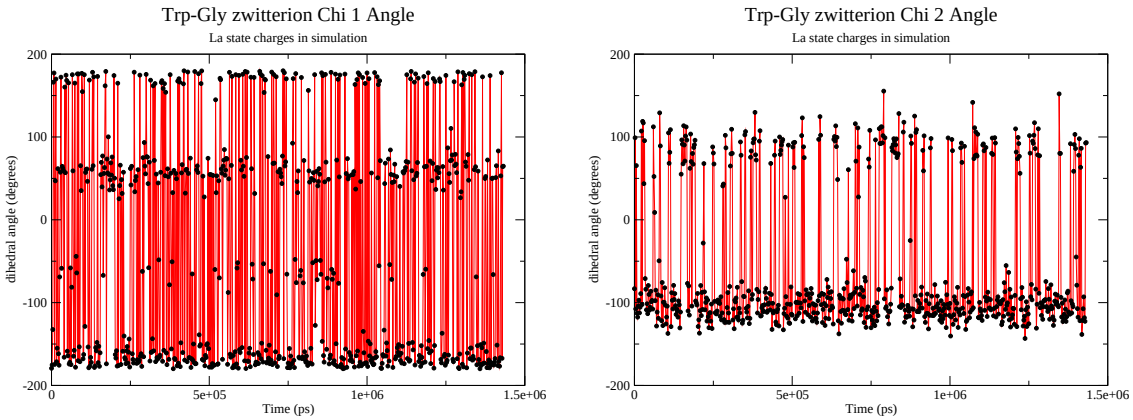

Figure 4.40: On the left the Psi dihedral angle of the Trp-Gly zwitterion during a 1.7 microsecond molecular dynamics simulation (OPLS). On the right the Phi dihedral during the same simulation. The Omega dihedral was nominally 0 degrees (cis) for this simulation. Charges on the indole ring were those of the L_a state. Points are plotted every 2 ns.

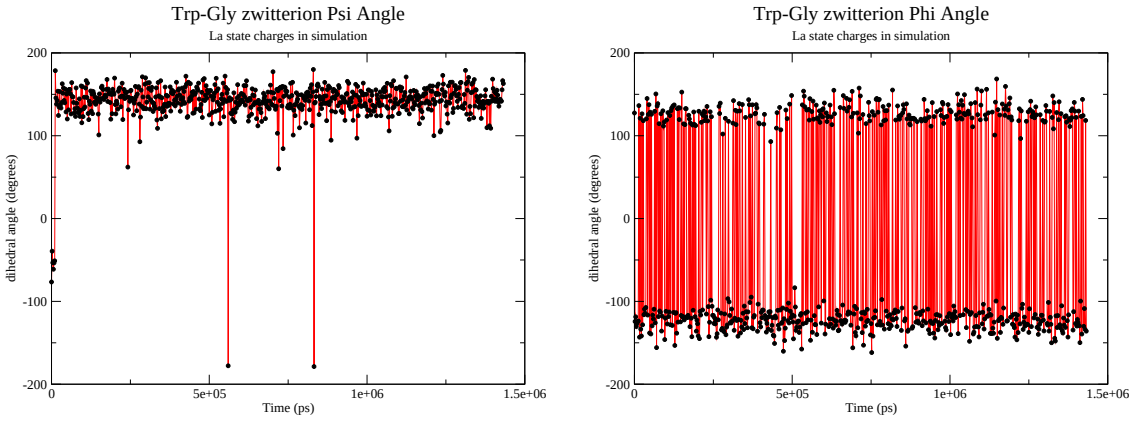

Calculated Electron Transfer Rates and Fluorescence Quantum Yields

This section presents the calculated energy gap between L_a and CT states of frames in a molecular dynamics simulation. The results of electronic coupling calculations are also shown. The electron transfer rate was calculated, using these results in Fermi Golden Rule, for individual frames over the course the molecular dynamics simulations. Quantum yields were calculated from the electron transfer rates for comparison with experiment.

Energy Gap and Electronic Interaction Contributions

Referencing equation 2.9 in the methods chapter, the term V^2 and ΔE_{00} are the electronic coupling and CT-La energy gap. The values of these are displayed in the figures that follow. An increase in the electronic coupling increases the electron transfer rate. As the CT-La energy gap decreases the density of states in the Fermi Golden Rule relation increases, raising the electron transfer rate. These values are then used to calculate the instantaneous rates and fluorescence quantum yields shown in the next section. There appears to be no general correlation between energy gap and electronic interaction contributions.

Figures 4.41 - 4.44 display the energy gap between the La and CT states (left plot) and the electronic coupling between these states (right plot) over the course of the molecular dynamics simulations for Gly-Trp and Trp-Gly zwitterions with trans and cis peptide bond geometries. For comparison the figure 4.45 displays the same type of data for a simulation of NATA. Both energy gap and electronic iteration vary widely over the course of the simulation. The energy gaps calculated here are generally higher than those of tryptophan in proteins with similar reported quantum yields.

An empirical offset is applied to the CT-La energy gaps when calculating the instantaneous rates and quantum yields. This is done to match experimental quantum yields more closely. The offset applied in this work was larger than those used in other studies by this group. The calculated energy gap is smaller in the case of NATA compared to the Gly-Trp zwitterion, predicting a lower quantum yield for NATA than Gly-Trp, in disagreement with the experimental results. The electronic couplings are of similar magnitude with the exception of the few extraordinarily high frames in the dipeptide zwitterion cases. The calculated electronic couplings over the course of a molecular dynamics simulation display a very large variation. The majority of values are on the low end of the distribution.

Figure 4.41: On the left the CT-La energy gap of the Gly-Trp zwitterion during a nearly 1.5 microsecond molecular dynamics simulation with OPLS force field. On the right the electronic coupling during the same simulation. The Omega dihedral was nominally 180 degrees (trans) for this simulation. Charges on the indole ring were those of the La state. Points are plotted every 2 ns.

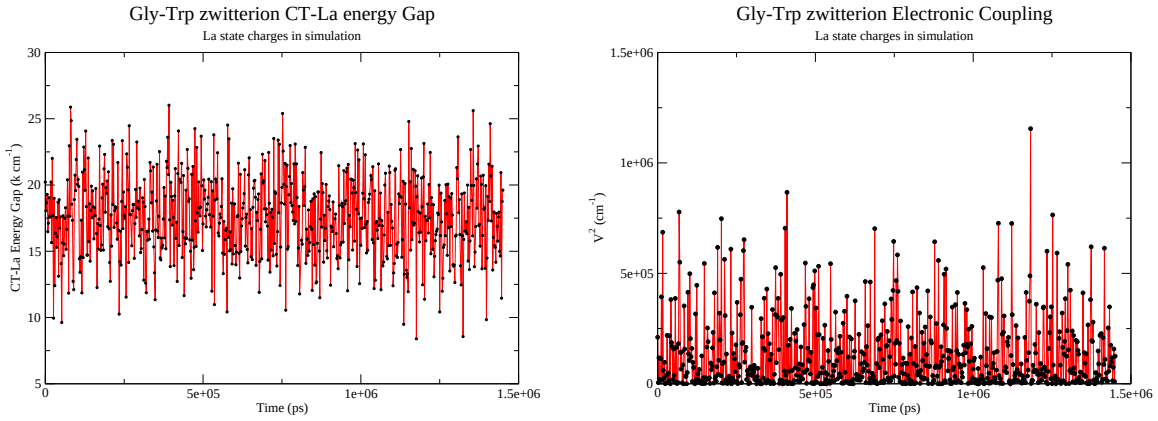

Instantaneous ET Rates

This section presents the instantaneous electron transfer rates over the course of MD trajectories calculated from the energy gaps and electronic interactions presented

Figure 4.42: On the left the CT-La energy gap of the Gly-Trp zwitterion during a nearly 1.5 microsecond molecular dynamics simulation (OPLS). On the right the electronic coupling during the same simulation. The Omega dihedral was nominally 0 degrees (cis) for this simulation. Charges on the indole ring were those of the La state. Points are plotted every 2 ns.

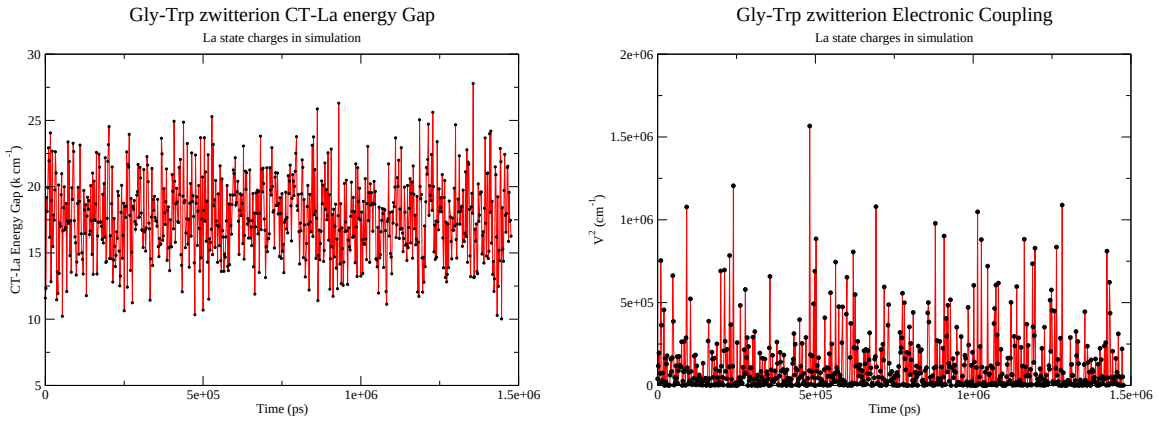

Figure 4.43: On the left the CT-La energy gap of the Trp-Gly zwitterion during a nearly 1.5 microsecond molecular dynamics simulation (OPLS). On the right the electronic coupling during the same simulation. The Omega dihedral was nominally 180 degrees (trans) for this simulation. Charges on the indole ring were those of the La state. Points are plotted every 2 ns.

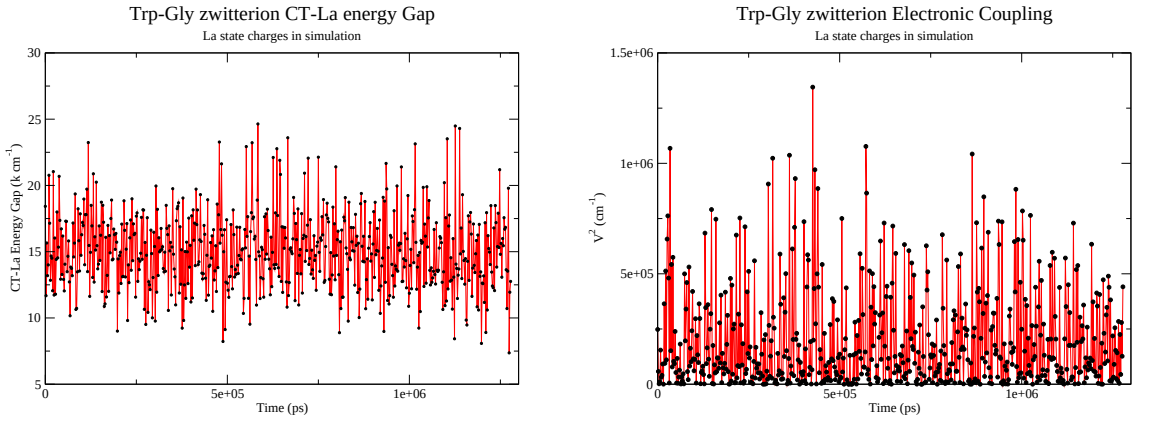

Figure 4.44: On the left the CT-La energy gap of the Trp-Gly zwitterion during a nearly 1.5 microsecond molecular dynamics simulation (OPLS). On the right the electronic coupling during the same simulation. The Omega dihedral was nominally 0 degrees (cis) for this simulation. Charges on the indole ring were those of the La state. Points are plotted every 2 ns.

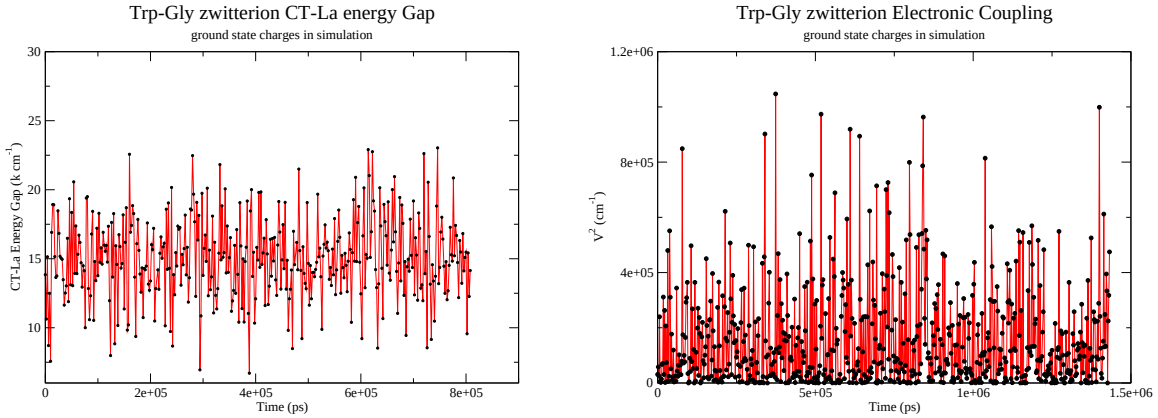

above. Rates were calculated for every tenth frame of the molecular dynamics trajectories. Here rates are presented for both ground and L_a state charges on the indole ring. Instantaneous rates for trajectories with ground state charges relate to loss of initial brightness experimental results in the literature. Before the environment has reorganized to the charge difference of the L_a state compared to the ground state, the energy of the L_a state will be higher leading to greater electron transfer quenching. The results shown here confirm higher electron transfer rates in the ground state reaction field. While there are some frames with rates that are several orders of magnitude above the mean, there are no calculated instantaneous rates that are high enough to explain a loss of initial brightness. These observations were made on instruments with response functions on the order of a few hundred femtoseconds. The fastest rates calculated for the zwitterions, with an offset of -1000 cm^{-}1, are about 100 ns^{-}1, corresponding to a lifetime of 10 ps. If offsets of -5500 and -12000

Figure 4.45: On the left the CT-La energy gap of the NATA over the course of a molecular dynamics simulation. On the right the electronic coupling between CT and La states during the same simulation.

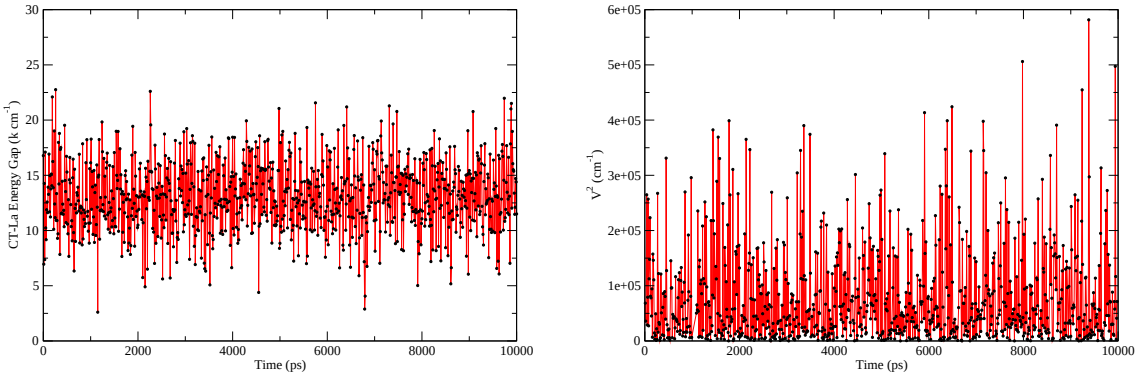

cm^{-}1 are used, then configurations with lifetimes as short as 200-1000 fs and 30-50 fs respectively.

Table 4.4 summarizes the QM/MM results showing the electronic coupling, energy gap and average quantum yield. Figures 4.46 - 4.53 display the calculated instantaneous electron transfer rates of Gly-Trp and Trp-Gly for both zwitterion and anion. Rates are calculated a each MD frame for which a CT-La gap and electronic coupling were calculated. An offset of -1000 wavenumbers was applied to the calculation of these rates. This offset was selected to get an average quantum yield to match experimental results. This match was in the single molecule interpretation which lead to an offset that is more physically reasonable than the offset in the individual molecules interpretation of -12000 wavenumbers. Figure 4.56 shows an example of rates calculated with the 12000 cm^{-}1 offset. In the case of NATA offsets of -5500 (individual molecules) and -1000 (single molecule) wavenumbers leads to agreement with experiment. Figure 4.54 shows the rates calculated for NATA with the -5500 wavenumber offset. Application of an offset of -5500 wavenumbers to the

calculation of rates for Gly-Trp zwitterion (figure 4.55) leads to a predicted quantum yield of 0.24.

There are two interpretations of a molecular dynamics simulation that may be used to predict a macroscopic observation of quantum yield from experiment. One is to calculate the quantum yield from the average of the instantaneous rates from each frame of the simulation. This is the single molecule interpretation. The other is to calculate an instantaneous quantum yield at each step in the simulation. The reported macroscopic quantum yield is the average of the instantaneous values. This interpretation treats each frame as individual molecules.

Figure 4.46: The electron transfer rates are shown for the Gly-Trp zwitterion during a nearly 1.5 microsecond molecular dynamics simulation. The plot on the left is the result for ground state charges on the indole ring. On the right the charges on the indole ring were those of the L_a state. The omega dihedral angle during this simulation was 180 (trans). Points are plotted every 2 ns.

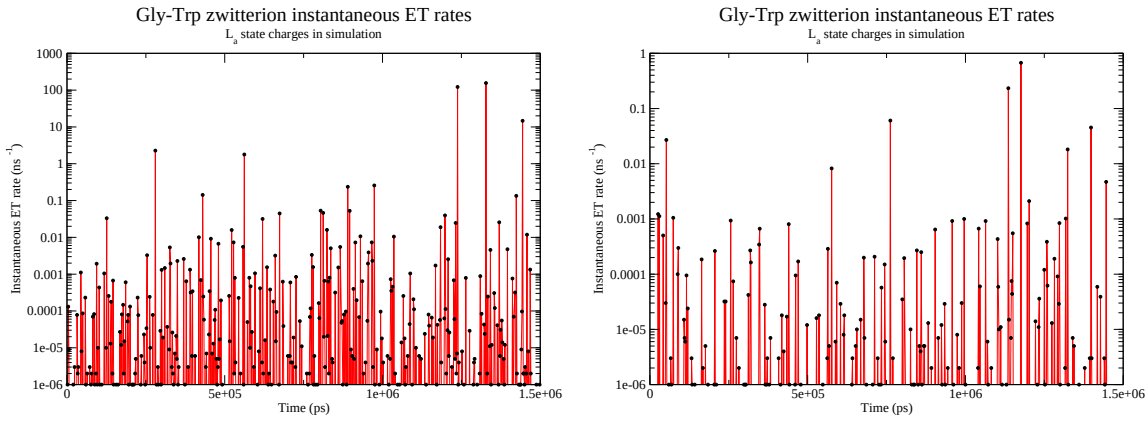

Contribution to CT-La Energy Gaps from Subgroups

Figures 4.57 - **??** display the affect of each of the major charge groups (ammonium, carboxylate, and water molecules) on the energy of the charge transfer state energy. Results are shown for Gly-Trp with either la or ground state charges;

Figure 4.47: The electron transfer rates are shown for the Gly-Trp zwitterion during a nearly 1.5 microsecond molecular dynamics simulation. The plot on the left is the result for ground state charges on the indole ring. On the right the charges on the indole ring were those of the L_a state. The omega dihedral angle during this simulation was 0 (cis). Points are plotted every 2 ns.

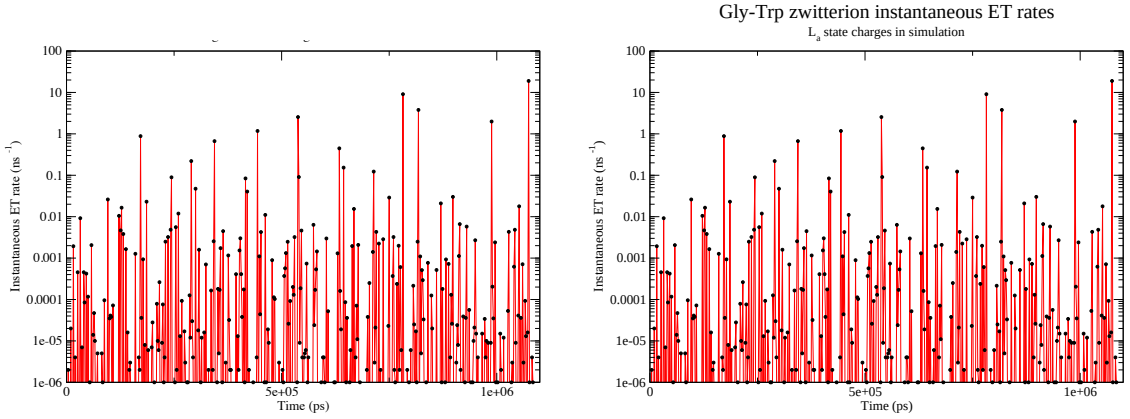

Figure 4.48: The electron transfer rates are shown for the Trp-Gly zwitterion during a nearly 1.5 microsecond molecular dynamics simulation. The plot on the left is the result for ground state charges on the indole ring. On the right the charges on the indole ring were those of the L_a state. The omega dihedral angle during this simulation was 180 (trans). Points are plotted every 2 ns.

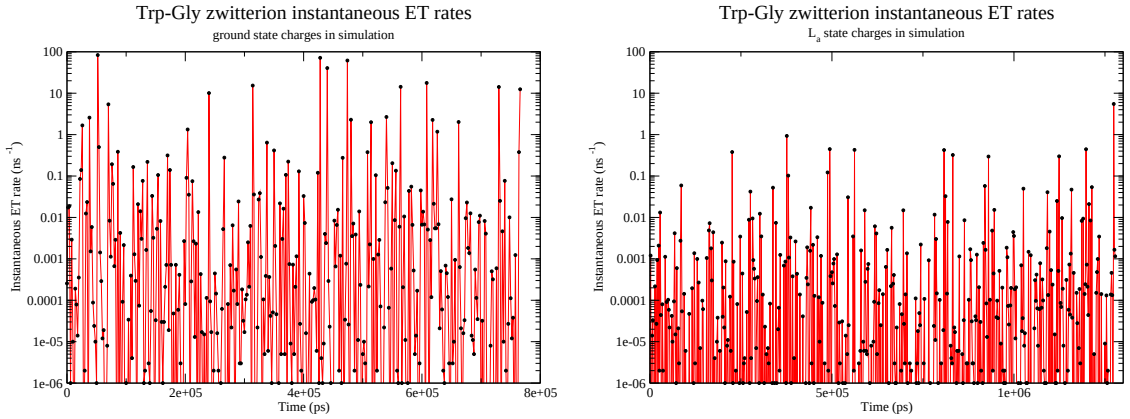

Figure 4.49: The electron transfer rates are shown for the Trp-Gly zwitterion during a nearly 1.5 microsecond molecular dynamics simulation. The plot on the left is the result for ground state charges on the indole ring. On the right the charges on the indole ring were those of the L_a state. The omega dihedral angle during this simulation was 0 (cis). Points are plotted every 2 ns.

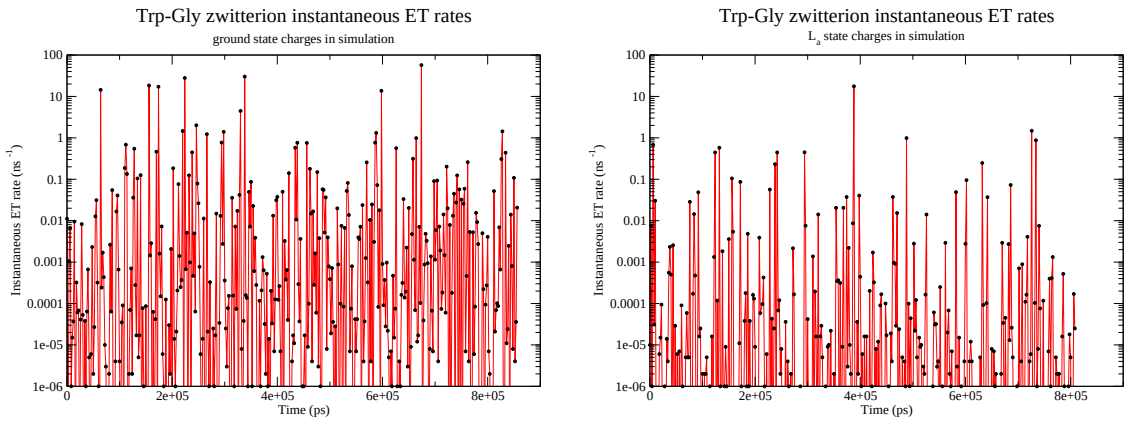

Figure 4.50: The electron transfer rates are shown for the Gly-Trp anion during a nearly 1.5 microsecond molecular dynamics simulation. The plot on the left is the result for ground state charges on the indole ring. On the right the charges on the indole ring were those of the L_a state. The omega dihedral angle during this simulation was 180 (trans). Points are plotted every 2 ns.

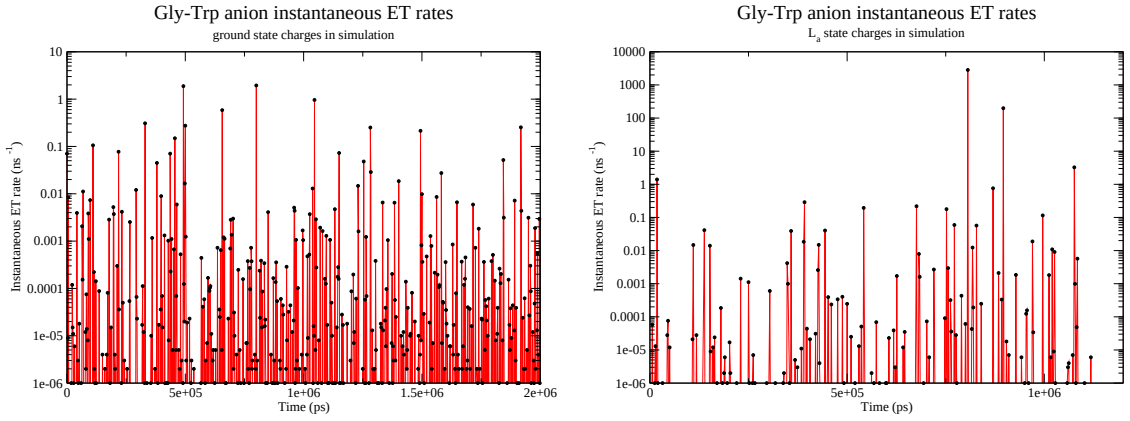

Figure 4.51: The electron transfer rates are shown for the Gly-Trp anion during a nearly 1.5 microsecond molecular dynamics simulation. The plot on the left is the result for ground state charges on the indole ring. On the right the charges on the indole ring were those of the L_a state. The omega dihedral angle during this simulation was 0 (cis). Points are plotted every 2 ns.

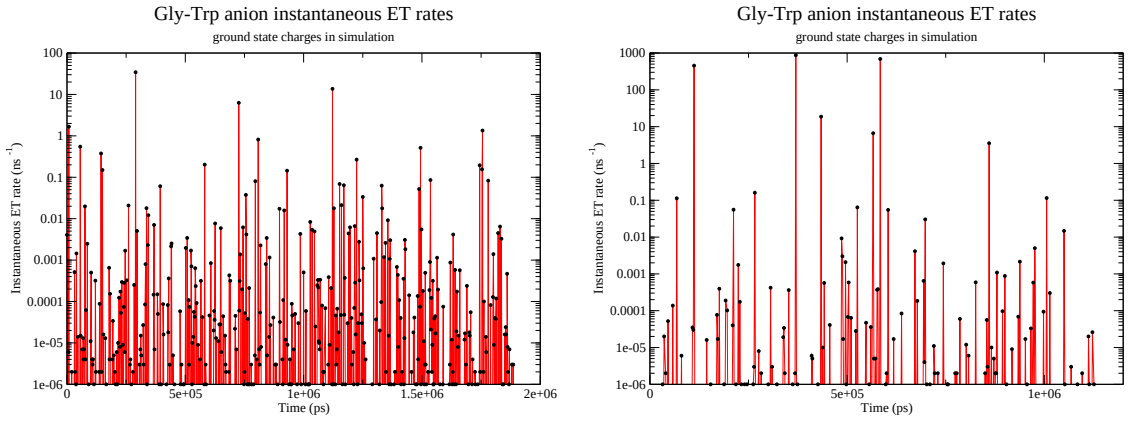

Figure 4.52: The electron transfer rates are shown for the Trp-Gly anion during a nearly 1.5 microsecond molecular dynamics simulation. The plot on the left is the result for ground state charges on the indole ring. On the right the charges on the indole ring were those of the L_a state. The omega dihedral angle during this simulation was 180 (trans). Points are plotted every 2 ns.

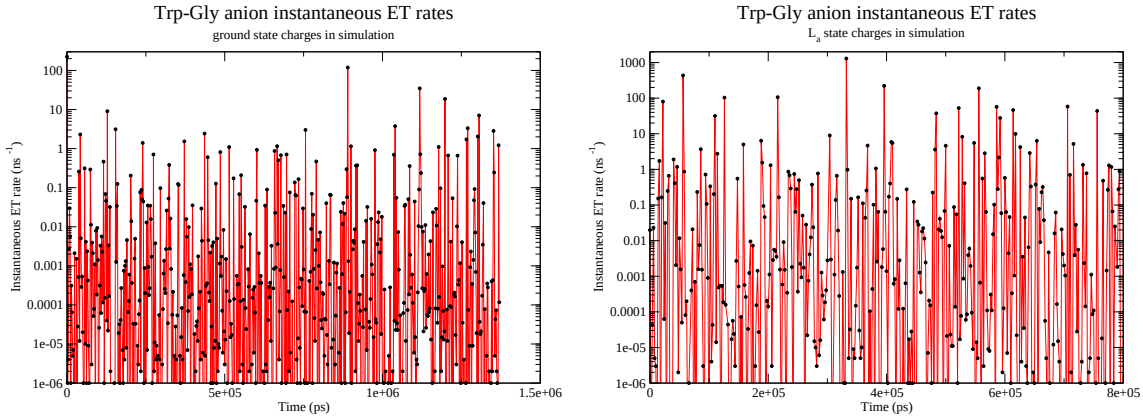

Figure 4.53: The electron transfer rates are shown for the Trp-Gly anion during a nearly 1.5 microsecond molecular dynamics simulation. The plot on the left is the result for ground state charges on the indole ring. On the right the charges on the indole ring were those of the L_a state. The omega dihedral angle during this simulation was 0 (cis). Points are plotted every 2 ns.

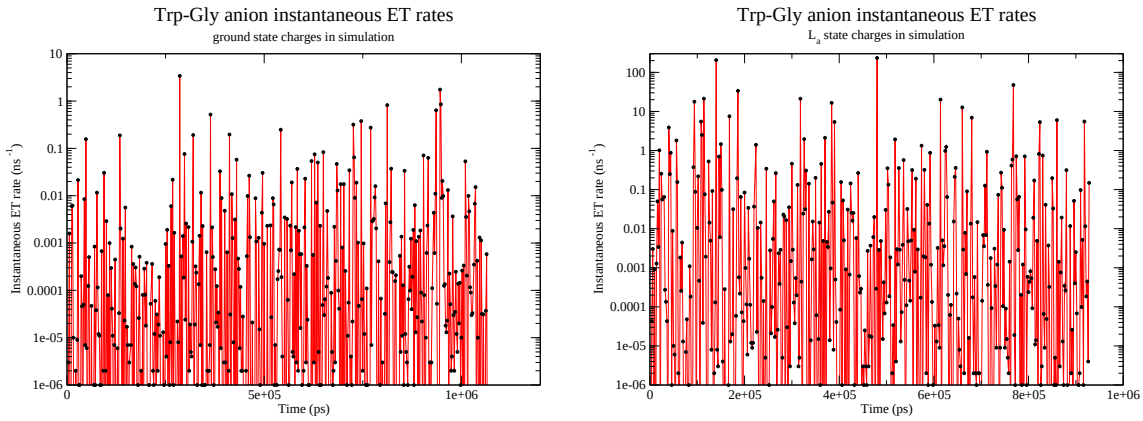

Figure 4.54: The electron transfer rates are shown for NATA during a molecular dynamics simulation. The applied shift to the CT-La gap was -5500 wavenumbers in the calculation of rates. This offset was empirically selected to match the quantum yield of NATA of 0.15. On the left data is plotted on a linear scale. The right plot is the same data plotted in a semilog plot.

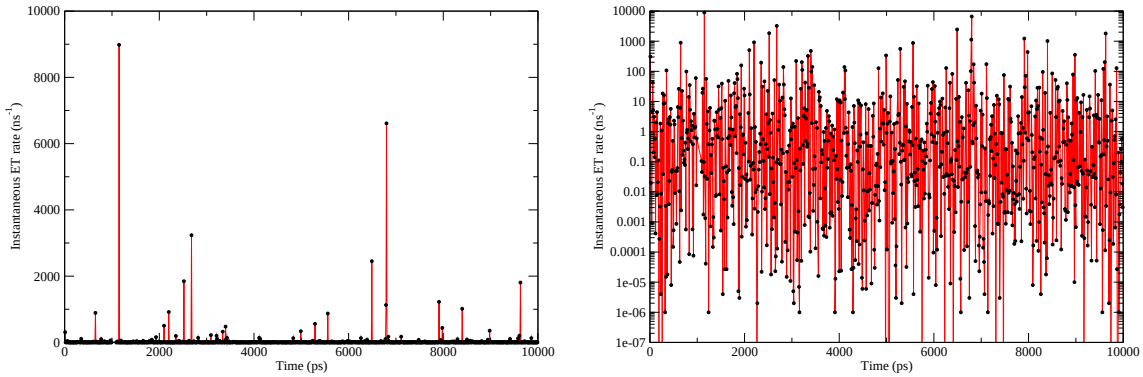

Figure 4.55: The electron transfer rates are shown for Gly-Trp zwitterion during a molecular dynamics simulation. The applied shift to the CT-La gap was -5500 wavenumbers in the calculation of rates. On the left data is plotted on a linear scale. The right plot is the same data plotted in a semilog plot.

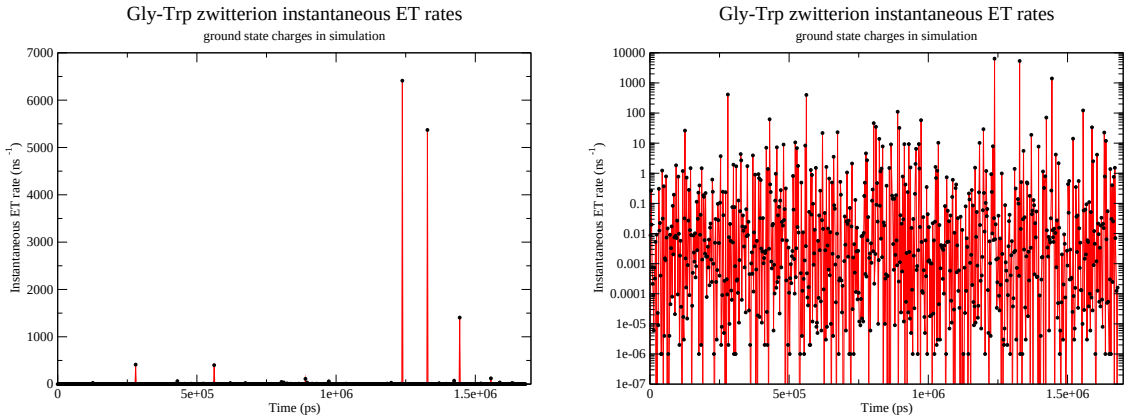

Figure 4.56: The electron transfer rates are shown for the Gly-Trp zwitterion during a nearly 1.5 microsecond molecular dynamics simulation. The plot on the left is the result for ground state charges on the indole ring. On the right the charges on the indole ring were those of the L_a state. The omega dihedral angle during this simulation was 180 (trans). Points are plotted every 2 ns.

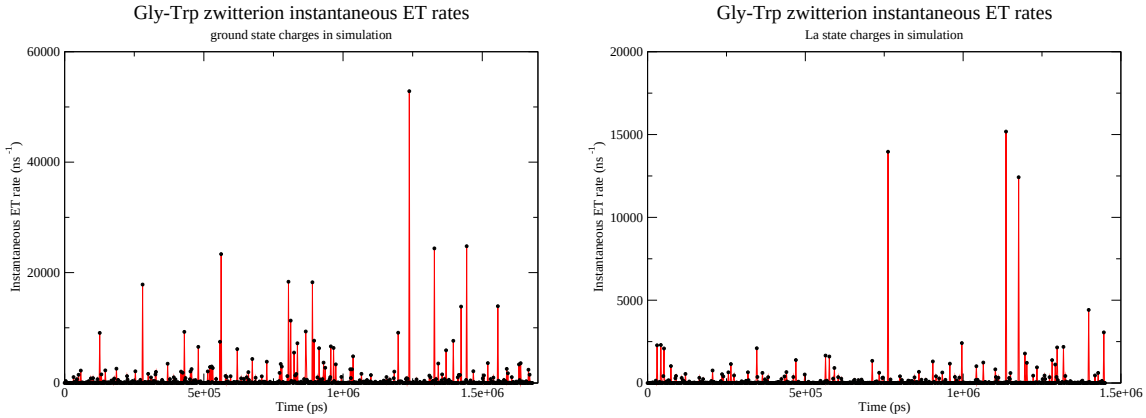

also, cis or trans peptide omega dihedral angle; then, OPLS, CHARMM27 or AMBER99 force field. The overall distributions of each contribution are relatively independent of the force field used in simulation. The geometry of the peptide bond (cis or trans) has very little effect on the distributions of energy contributions. The only visible effect is seen in the case of simulation with the AMBER force field. Here the cis peptide has a bimodal distribution compared to the monodisperse distribution in the trans dipeptide. Water configurations have a more heterogeneous distribution in energy contribution by about two times compared to those of the two zwitterion charges. This is easily seen in the height of the curves as they are area normalized. The distribution of the total energy contributions of zwitterion charges and water molecules does not display the sharp structures and multi-nodal shape that frequently characterizes the contributions from the zwitterion charges.

In all zwitterion calculations, for both Trp-Gly and Gly-Trp, the electrostatic contribution of the NH_3 group is to lower the energy of the CT state. The carboxylate group almost universally leads to a destabilizing electrostatic energy contribution to the CT state. Both Trp-Gly and Gly-Trp zwitterions have a small fraction of MD frames in which the carboxylate group stabilizes the CT state. The contribution of the positive charge of the NH_3 group is large enough in magnitude to override the combined effects of water and carboxylate destabilization of the CT state in Gly-Trp zwitterion.

Figures 5.1 - 5.3 display the structures of water solvent molecules near the dipeptides at various time points in the molecular dynamics trajectory. The contribution of the combined solvent water molecules is an increase in the energy of the CT state. The effect of solvation by water is usually to lower the energy of the CT state, with respect to vacuum, primarily through hydrogen bonding to the amide oxygen. The molecular dynamics frames shown in figures 5.1 - 5.3 display three

frames, one near the minimum, one near the maximum, and one near mean of the distribution of electrostatic energy contributions throughout the MD trajectory. The variability in the water contribution is focused upon as the contributions of the NH3 and COO are more narrowly distributed within a molecular dynamics trajectory.

The average magnitude of the different contributions are widely separated in Gly-Trp. The difference in average CT-La energy gap contribution between each of the groups is much smaller in the case of Trp-Gly, regardless of the force field employed. In Try-Gly the zwitterionic charges have effects that are on average equal in magnitude and opposite in sign. The contribution from waters lowers the energy of the CT state in Trp-Gly simulations.

In the anion form the effects of peptide groups (COO- and NH2) are very narrowly distributed. The contribution from water solvent groups are distributed with a variance about 3 times that of the water contributions in zwitterion MD simulations.

Figure 4.57: The contribution to the (de)stabilization of the CT energy of the Gly-Trp zwitterion in wavenumbers from the -NH_3, -COO, and water solvent molecules and the total wavelength shift. Molecular dynamics conducted with the OPLS force field and L_a state charges on the indole ring. On the left the plot shown is for the peptide with trans peptide bond, on the right the results are shown for the cis peptide bond.

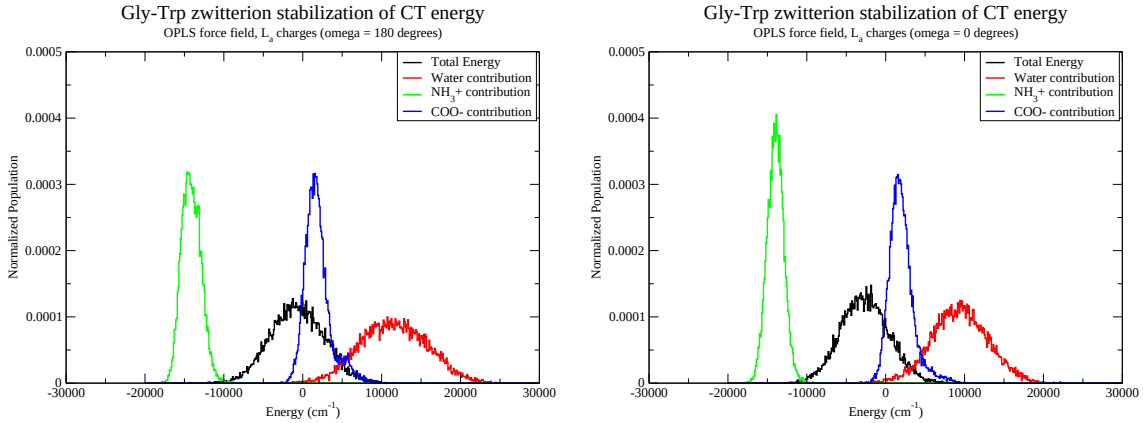

Figure 4.58: The contribution to the (de)stabilization of the CT energy of the Gly-Trp zwitterion in wavenumbers from the -NH_3, -COO, and water solvent molecules and the total wavelength shift. Molecular dynamics conducted with the OPLS force field and ground state charges on the indole ring. On the left the plot shown is for the peptide with trans peptide bond, on the right the results are shown for the cis peptide bond.

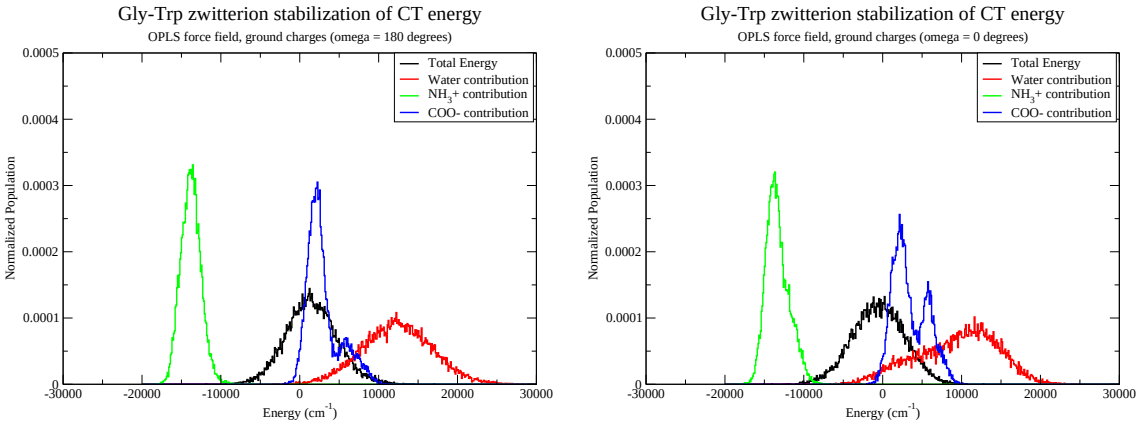

Figure 4.59: The contribution to the (de)stabilization of the CT energy of the Gly-Trp zwitterion in wavenumbers from the -NH_3, -COO, and water solvent molecules and the total wavelength shift. Molecular dynamics conducted with the CHARMM27 force field and L_a state charges on the indole ring. On the left the plot shown is for the peptide with trans peptide bond, on the right the results are shown for the cis peptide bond.

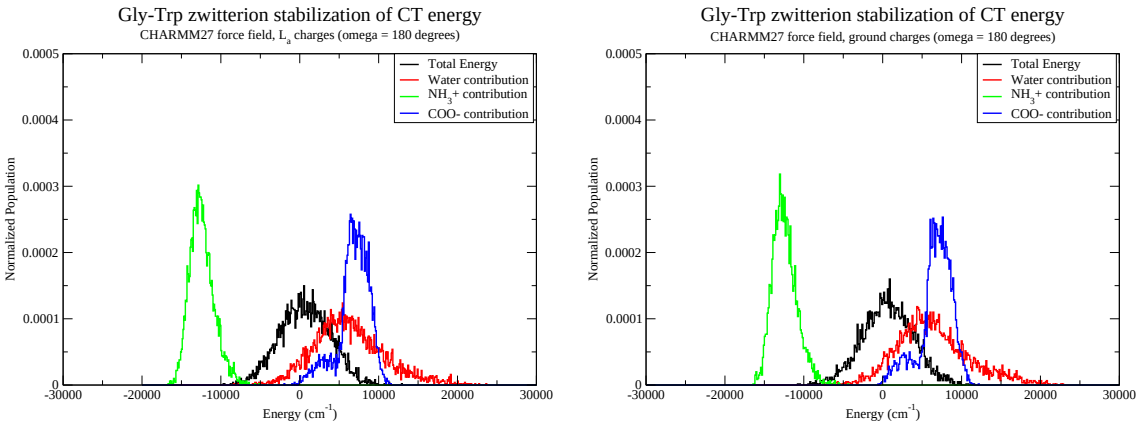

Figure 4.60: The contribution to the (de)stabilization of the CT energy of the Gly-Trp zwitterion in wavenumbers from the -NH_3, -COO, and water solvent molecules and the total wavelength shift. Molecular dynamics conducted with the CHARMM27 force field and ground state charges on the indole ring. On the left the plot shown is for the peptide with trans peptide bond, on the right the results are shown for the cis peptide bond.

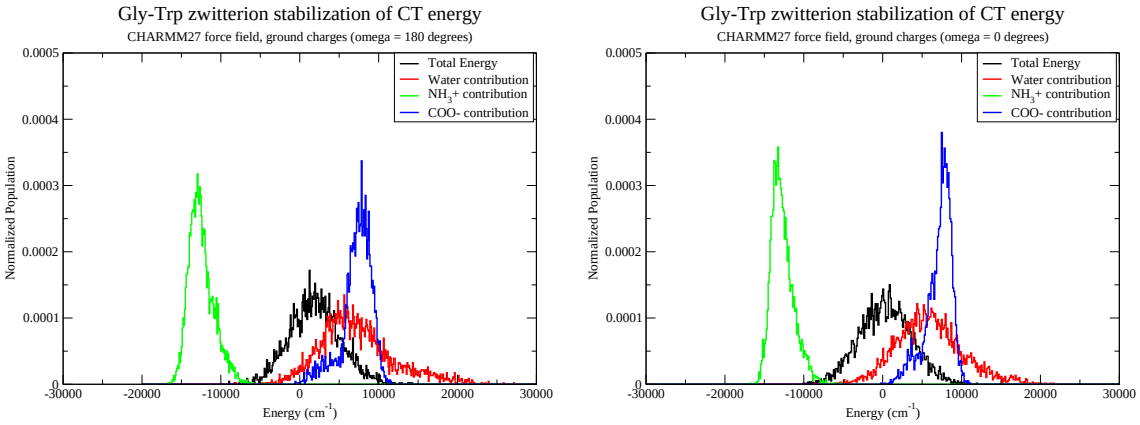

Figure 4.61: The contribution to the (de)stabilization of the CT energy of the Gly-Trp zwitterion in wavenumbers from the -NH_3, -COO, and water solvent molecules and the total wavelength shift. Molecular dynamics conducted with the AMBER99SB force field and L_a state charges on the indole ring. On the left the plot shown is for the peptide with trans peptide bond, on the right the results are shown for the cis peptide bond.

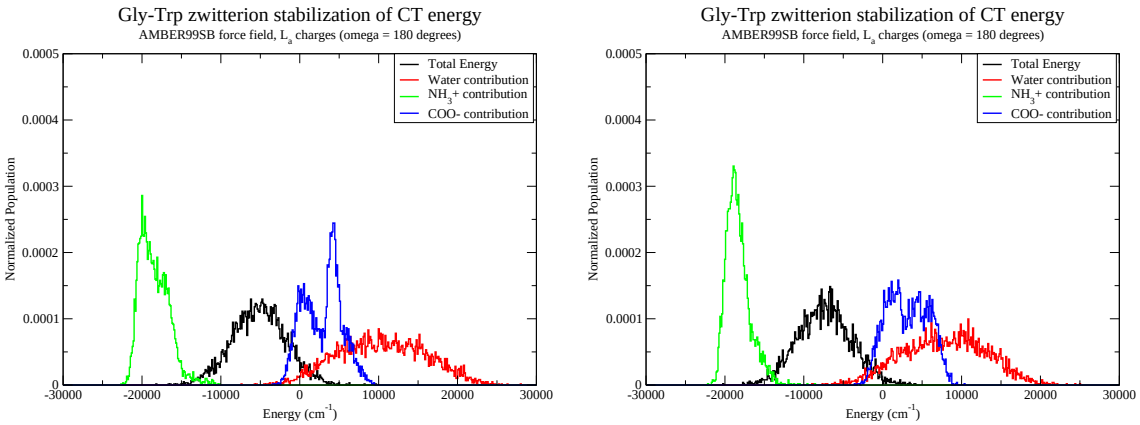

Figure 4.62: The contribution to the (de)stabilization of the CT energy of the Gly-Trp zwitterion in wavenumbers from the -NH_3, -COO, and water solvent molecules and the total wavelength shift. Molecular dynamics conducted with the AMBER99SB force field and ground state charges on the indole ring. On the left the plot shown is for the peptide with trans peptide bond, on the right the results are shown for the cis peptide bond.

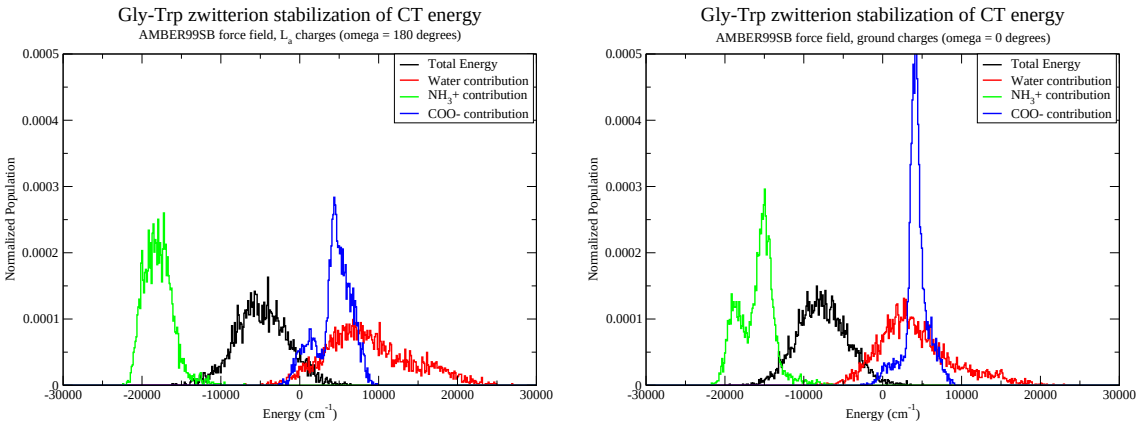

Figures 4.63 - 4.68 display the contributions to the CT energy from major charge groups (ammonium, carboxylate, and water molecules) of the Trp-Gly zwitterion. The results displayed are analogous to the results for Gly-Trp in the previous figures. The distributions have the similar profiles to those in Gly-Trp, with the exception of the strong bimodal behavior of the ammonium group.

Wavelength Prediction Results

Figure 3.15 and table 3.1, in the experimental results section of this report, shows experimental λ_{max} values for 5 Trp-X and 5 X-Trp cases at pH 5 (zwitterion) and pH 10 (anion). These illustrate the phenomenon that is the motivation for the results presented in this section, namely the blue shift in wavelength of the Trp-X zwitterion with respect to all other species.

Figure 4.63: The contribution to the (de)stabilization of the CT energy of the Trp-Gly zwitterion in wavenumbers from the -NH_3, -COO, and water solvent molecules and the total wavelength shift. Molecular dynamics conducted with the OPLS force field and ground state charges on the indole ring. On the left the plot shown is for the peptide with trans peptide bond, on the right the results are shown for the cis peptide bond.

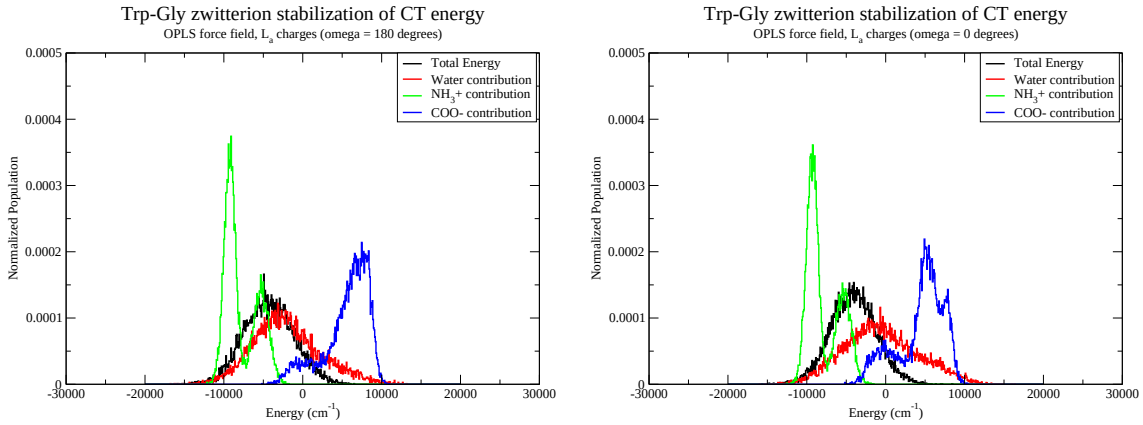

Figure 4.64: The contribution to the (de)stabilization of the CT energy of the Trp-Gly zwitterion in wavenumbers from the -NH_3, -COO, and water solvent molecules and the total wavelength shift. Molecular dynamics conducted with the OPLS force field and ground state charges on the indole ring. On the left the plot shown is for the peptide with trans peptide bond, on the right the results are shown for the cis peptide bond.

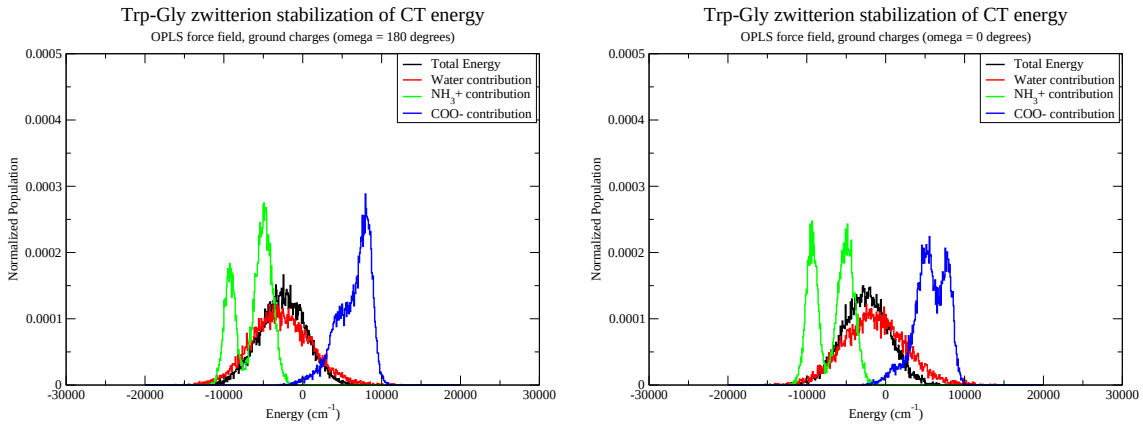

Figure 4.65: The contribution to the (de)stabilization of the CT energy of the Trp-Gly zwitterion in wavenumbers from the -NH_3, -COO, and water solvent molecules and the total wavelength shift. Molecular dynamics conducted with the CHARMM force field and ground state charges on the indole ring. On the left the plot shown is for the peptide with trans peptide bond, on the right the results are shown for the cis peptide bond.

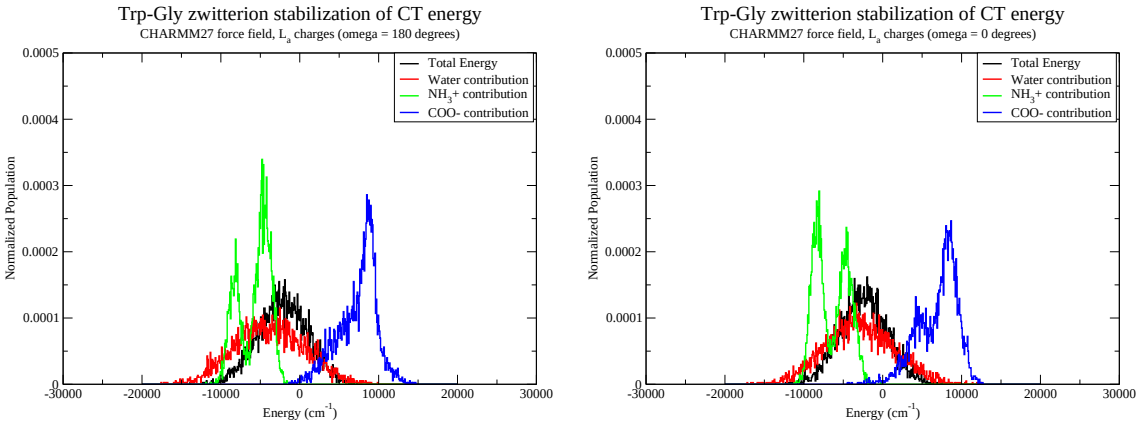

Figure 4.66: The contribution to the (de)stabilization of the CT energy of the Trp-Gly zwitterion in wavenumbers from the -NH_3, -COO, and water solvent molecules and the total wavelength shift. Molecular dynamics conducted with the CHARMM force field and ground state charges on the indole ring. On the left the plot shown is for the peptide with trans peptide bond, on the right the results are shown for the cis peptide bond.

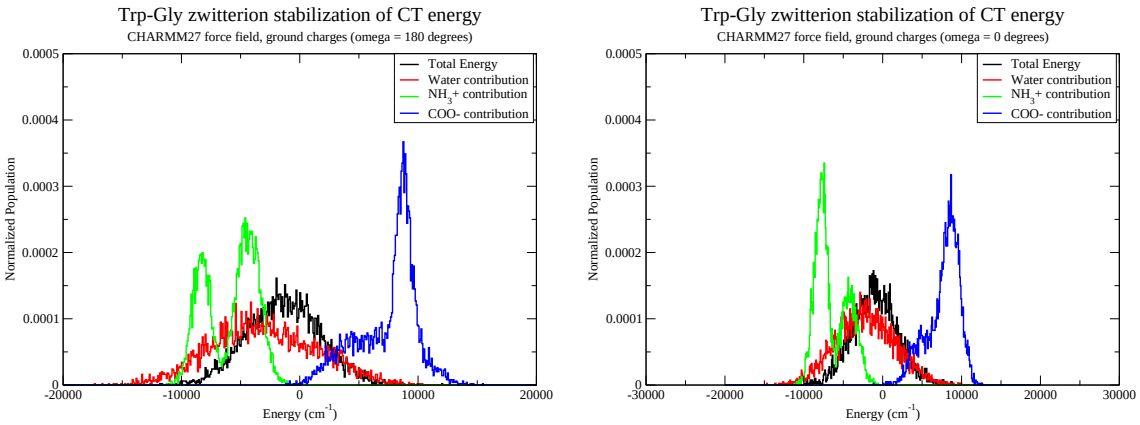

Figure 4.67: The contribution to the (de)stabilization of the CT energy of the Trp-Gly zwitterion in wavenumbers from the -NH_3, -COO, and water solvent molecules and the total wavelength shift. Molecular dynamics conducted with the AMBER99 force field and ground state charges on the indole ring. On the left the plot shown is for the peptide with trans peptide bond, on the right the results are shown for the cis peptide bond.

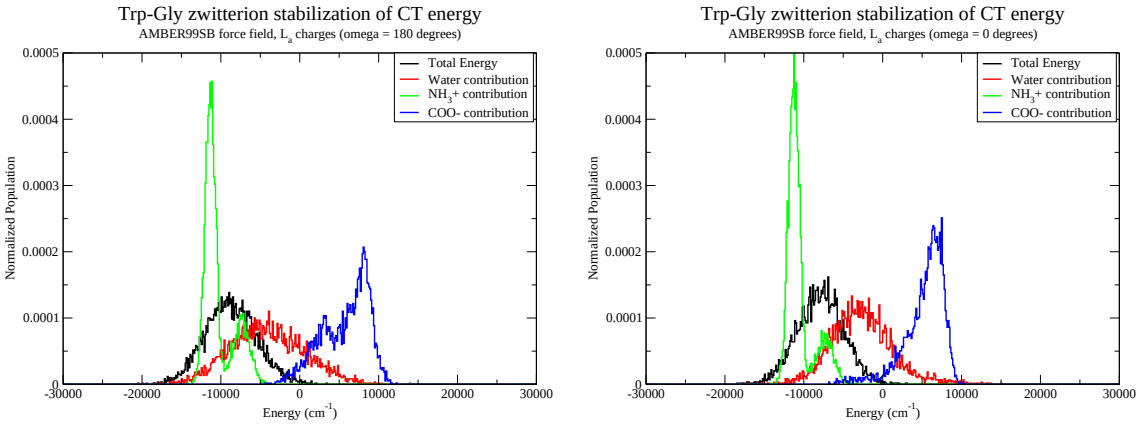

Figure 4.68: The contribution to the (de)stabilization of the CT energy of the Trp-Gly zwitterion in wavenumbers from the -NH_3, -COO, and water solvent molecules and the total wavelength shift. Molecular dynamics conducted with the AMBER99 force field and ground state charges on the indole ring. On the left the plot shown is for the peptide with trans peptide bond, on the right the results are shown for the cis peptide bond.

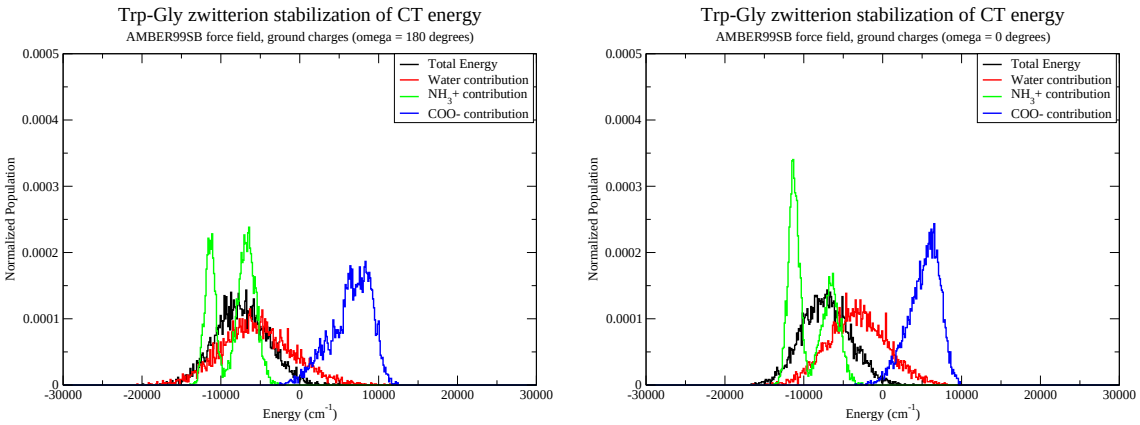

Figures 4.69-4.73 show area normalized distribution functions of how the N- and C-terminal groups, the amide group, and water individually contribute electrostatically to the vertical fluorescence wavelength relative to vacuum for Gly-Trp and Trp-Gly in the zwitterion and anion forms. These are histograms of the instantaneous contributions from each frame of the MD simulation. The charge distribution on the indole ring was that of the 1La (fluorescing) state. The distribution of net effect wavelengths for each case is shown in black. The Trp-Gly zwitterion in figure 4.70 the average computed shift is only 40 nm compared to 50 nm in the other three cases.

Breakdown of Contributions

A number of striking features in Figures 4.69-4.73 are worth mentioning.

1. The contribution from the NH3+ , carboxylate, and amide for the Trp-Gly zwitterion (4.72) are all broad and heterogeneous. There is structure to the distributions that is the result of multiple rotamer contributions. The structure is most evident in the case of the -NH_3^+ and amide distributions. The contributions of amide and carboxylate are centered at zero, contributing relatively little to the wavelength shift. The protonated amine contributes a large blue shift (-30 nm relative to vacuum). Water, in contrast, contributes a very broad, uniformly distributed red shift, of about 50 nm, which apparently more than compensates for the blue shift from the polar groups. The water contribution is larger for Trp-Gly zwitterion than for any of the other peptides. The distributions are largely independent on the configuration of the peptide bond (cis or trans).

2. The red shift with respect to vacuum is dominated by the contribution of the anionic carboxylate group in Gly-Trp zwitterion (4.69). The amide and

protonated amine distributions are both centered at zero. Water again has a very broad distribution of energy contribution, but it is centered about zero. The water distribution is however skewed with a longer tail on the red shift side of the distribution. Only the -NH_3^+ distribution shows any structure based on rotamers. Again no dependence on cis or trans peptide bond is evident.

3. For the anion form of Trp-Gly (figure 4.73), the red shift appears to result mostly from the contributions of water solvent. The contributions from all other groups are centered about zero.

4. Amide and -NH_2 contributions are narrow and close to zero in the case of the Gly-Trp anion (figure 4.71). The water contributions favor a small shift to longer wavelength, but this only contributes a few nanometers. The majority of the wavelength shift is the result of the strong shift to higher wavelength resulting from the negative charge of the carboxylate.

5. The effect of the NH3+ shifts from a distribution centered at approximately zero for Gly-Trp to one near -20 nm for Trp-Gly.

Anticorrelation of Wavelength Contributions

The histograms of wavelength shift contributions for Trp-Gly and Gly-Trp zwitterions appear to show anticorrelation in the protein:water contributions. Figures 4.74 and 4.75 show time series of water and protein contributions. These figures show anticorrelation between the protein and water contributions to the wavelength shift.

Dependence on Rotamer State

This section shows how the shift in fluorescence wavelength depends on rotamer state. Table 4.6 presents the calculated wavelength for the 7 most populated rotamers

Figure 4.69: The contribution to the wavelength shift of the Gly-Trp zwitterion in nm from the -NH_3, -COO, and amide groups of the peptide, water solvent molecules and the total wavelength shift. Molecular dynamics conducted with the OPLS force field and L_a state charges on the indole ring. On the left the plot shown is for the peptide with trans peptide bond, on the right the results are shown for the cis peptide bond. The average total shift for the trans and cis peptides are 48.4 and 44.9 nm respectively.

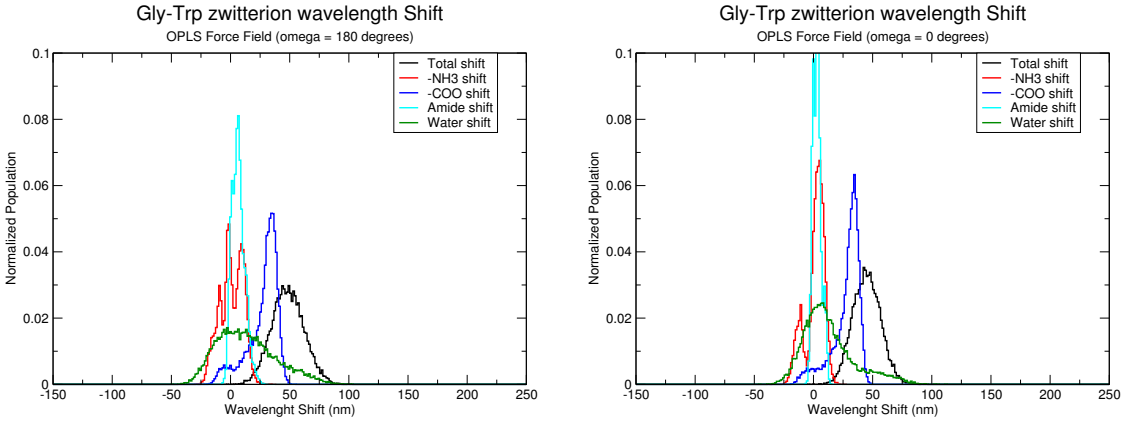

Figure 4.70: The contribution to the wavelength shift of the Trp-Gly zwitterion in nm from the -NH_3, -COO, and amide groups of the peptide, water solvent molecules and the total wavelength shift. Molecular dynamics conducted with the OPLS force field and L_a state charges on the indole ring. On the left the plot shown is for the peptide with trans peptide bond, on the right the results are shown for the cis peptide bond. The average total shift for the trans and cis peptides are 38.2 and 37.2 nm respectively.

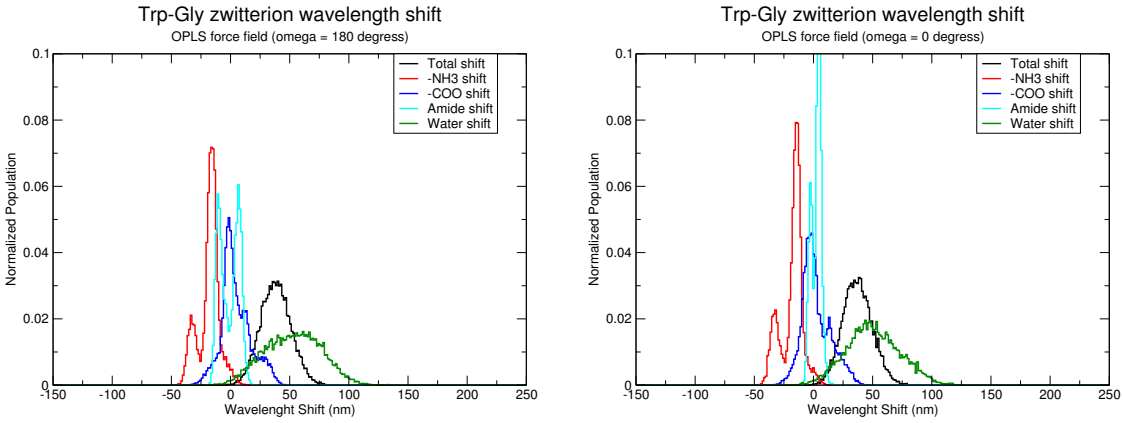

Figure 4.71: Contribution to wavelength shift from peptide groups and water solvent in molecular dynamics simulations of Gly-Trp in the high pH form. These MD simulations were run with the OPLS force field with L_a charges on the indole ring. These are calculated from the electrostatic interaction between the charge differences on the indole ring between the ground and L_a states and the charge of the environment atoms.

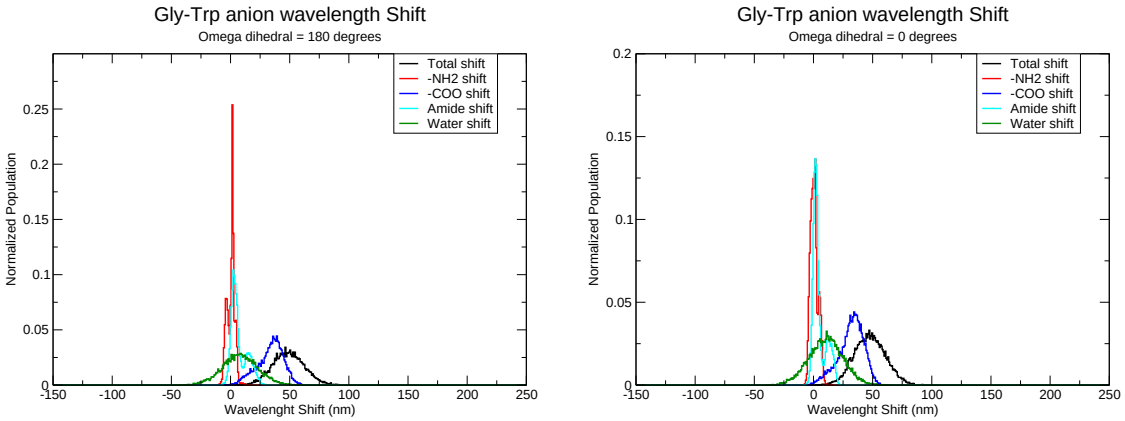

Figure 4.72: Contribution to wavelength shift from peptide groups and water solvent in molecular dynamics simulations of the Gly-Trp dipeptide at high pH. These MD simulations were run with the CHARMM27 force field. These are calculated from the electrostatic interaction between the charge differences on the indole ring between the ground and L_a states and the charge of the environment atoms.

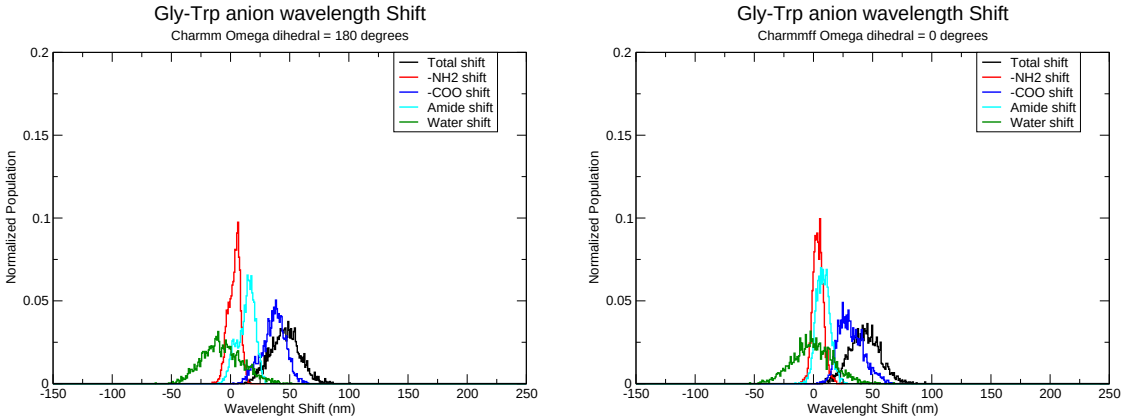

Figure 4.73: Contribution to wavelength shift from peptide groups and water solvent in molecular dynamics simulations of Gly-Trp in the high pH form. These are calculated from the electrostatic interaction between the charge differences on the indole ring between the ground and L_a states and the charge of the environment atoms.

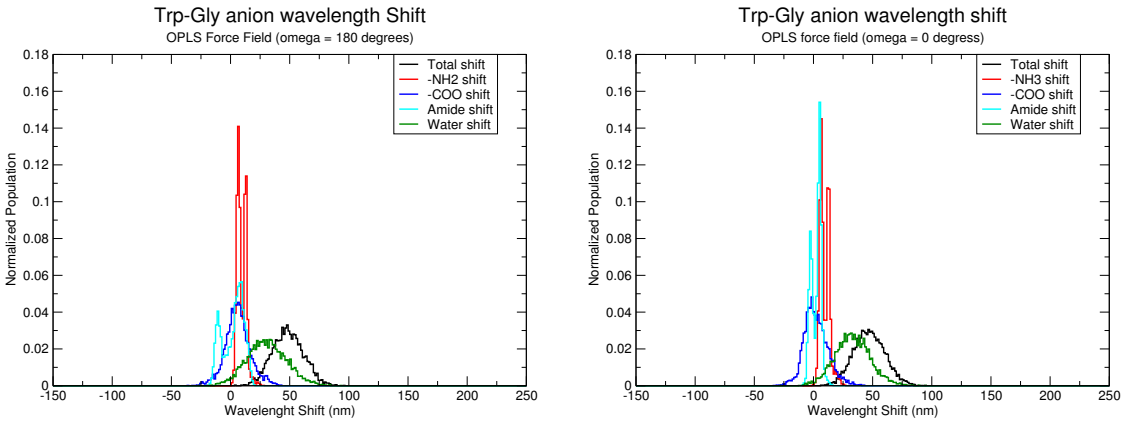

Figure 4.74: These plots show the contributions to the wavelength shift for the Gly-Trp zwitterion from the total protein (sum of nh3, coo, amide) (left graph) and nh3 alone (right graph) plotted together with the contributions of water to the wavelength shift. These plots show substantial anticorrelation between protein and water contributions.

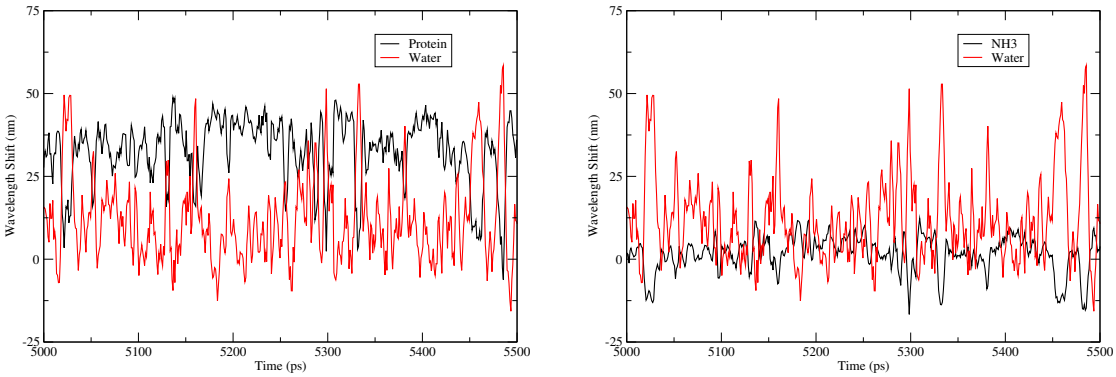

Figure 4.75: These plots show the contributions to the wavelength shift for the Gly-Trp zwitterion from the COO- (left graph) and amide (right graph) plotted together with the contributions of water to the wavelength shift. These plots show substantial anticorrelation between protein and water contributions.

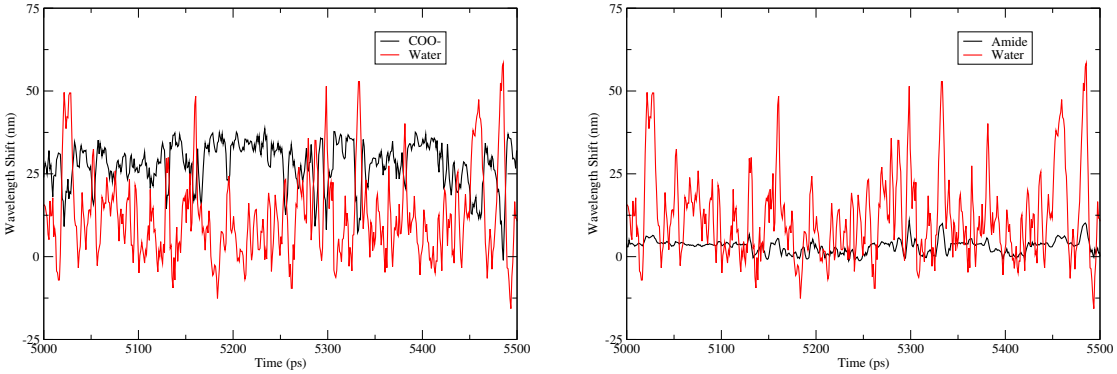

of the Gly-Trp zwitterion. There is a range of approximately 8 nm in the data, showing strong dependence of wavelength on rotamer state.

Many Short Simulations Method

The L_a energies for multiple rotamer calculations, showing the fluorescence wavelength shift in agreement with experimental results, are shown in figure 4.76. This shift is explained in part by the structure in figure 4.77. The wavelength shifts were calculated from 104 initial rotamer conformations produced in CHARMM. These rotamers result from 3 rotamers of chi1 (180, 60, -60), two rotamers of chi2 (90, -90), three rotamers of psi (180, 60, -60), three rotamers of phi (180, 60, -60), and two rotamers of omega (0, 180).

Figure 4.76: Average calculated fluorescence wavelengths for an ensemble of rotamers. This is a histogram of the number of calculations with a given average fluorescence wavelength. Molecular dynamics were performed from 104 starting rotamer structures. These calculations were performed in the CHARMM program prior to the work with GROMACS.

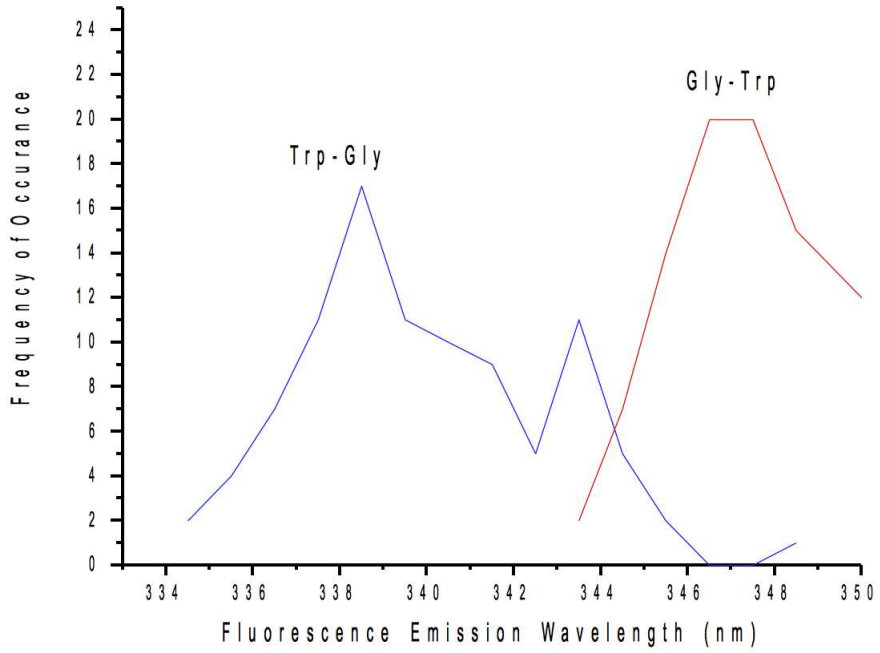

Figure 4.77: Geometry of Trp-Gly zwitterion, showing the direction of the dipole of the L_a state (red arrow) and the dipole created by zwitterion charges (blue arrow), showing that these two are opposing each other leading to higher energy.

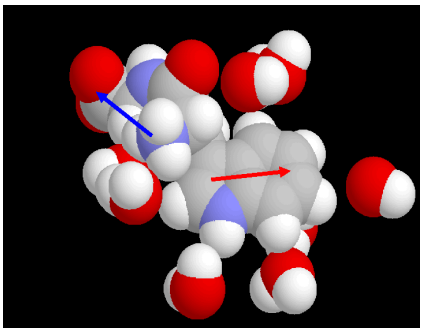

Table 4.1: Populations of each of the possible rotamers for Gly-Trp zwitterion, for ground and La charges, resulting from all combinations of chi1, chi2, psi, phi populations. Rotamer states with less than 0.001 in both ground and La simulations are excluded. Simulations conducted with OPLS force field. Data is sorted by population in the ground state.

Rotamer #	Population (ground)	Population (La)	chi1	chi2	psi	phi
0	0.385	0.453	60	90	180	-150
6	0.209	0.091	60	-90	180	-150
2	0.167	0.203	60	90	180	90
30	0.129	0.278	180	-90	180	-150
8	0.108	0.046	60	-90	180	90
12	0.090	0.026	-60	90	180	-150
24	0.081	0.100	180	90	180	-150
18	0.079	0.028	-60	-90	180	-150
32	0.062	0.137	180	-90	180	90
14	0.050	0.013	-60	90	180	90
26	0.040	0.048	180	90	180	90
20	0.040	0.014	-60	-90	180	90
1	0.004	0.004	60	90	180	-90
7	0.002	0.001	60	-90	180	-90
33	0.002	0.002	180	-90	0	-150
35	0.001	0.001	180	-90	0	90
31	0.001	0.003	180	-90	180	-90
29	0.001	0.000	180	90	0	90
27	0.001	0.001	180	90	0	-150
25	0.001	0.001	180	90	180	-90
19	0.001	0.000	-60	-90	180	-90
15	0.001	0.000	-60	90	0	-150
13	0.001	0.000	-60	90	180	-90

Table 4.2: The lifetime of redistribution of population between rotamer populations predicted from molecular dynamics simulation. N/A indicates that no transitions occurred during the simulation. The results shown are from simulations using the OPLS force field.

Peptide	$\chi 1$ (ns)			$\chi 2$ (ns)
	-60 $\rightleftharpoons$ 60	-60 $\rightleftharpoons$ 180	60 $\rightleftharpoons$ 180	-90 $\rightleftharpoons$ 90
zwitterions				
Gly-Trp cis La	5.05	6.73	3.79	0.43
Gly-Trp cis ground	0.924	1.36	7.38	0.59
Gly-Trp trans La	4.03	3.12	5.35	0.42
Gly-Trp trans ground	1.16	1.75	10.9	0.65
Trp-Gly cis La	9.29	4.50	4.44	0.082
Trp-Gly cis ground	3.79	2.56	7.33	0.14
Trp-Gly trans La	13.6	3.49	3.46	0.083
Trp-Gly trans ground	2.45	3.14	10.4	0.18
anions				
Gly-Trp cis La	3.43	3.51	3.92	0.43
Gly-Trp cis ground	1.08	1.40	5.12	0.57
Gly-Trp trans La	2.62	1.88	7.55	0.40
Gly-Trp trans ground	1.69	1.82	8.94	0.65
Trp-Gly cis La	1.58	1.57	5.72	1.77
Trp-Gly cis ground	19.2	4.17	4.86	2.02
Trp-Gly trans La	1.98	1.40	7.65	0.85
Trp-Gly trans ground	35.2	5.01	9.10	1.23

Table 4.3: The lifetime of redistribution of population between rotamer populations predicted from molecular dynamics simulation. N/A indicates that no transitions occurred during the simulation. The results shown are from simulations using the OPLS force field.

Peptide	ϕ (ns)			ψ (ns)		
	-60 $\rightleftharpoons$ 60	-60 $\rightleftharpoons$ 180	60 $\rightleftharpoons$ 180	-60 $\rightleftharpoons$ 60	-60 $\rightleftharpoons$ 180	60 $\rightleftharpoons$ 180
zwitterions						
Gly-Trp cis La	N/A	0.0977	N/A	129.0	5.11	1.68
Gly-Trp cis ground	N/A	0.306	N/A	N/A	23.4	6.43
Gly-Trp trans La	1020	0.109	145	24.2	0.65	0.91
Gly-Trp trans ground	N/A	0.375	N/A	168.1	3.06	4.25
Trp-Gly cis La	4.06	0.36	0.70	N/A	296	1.12
Trp-Gly cis ground	2.99	0.66	0.32	22.1	18.4	1.14
Trp-Gly trans La	3.66	0.79	0.29	32.6	10.4	0.52
Trp-Gly trans ground	2.99	0.74	0.31	36.4	17.4	0.81
anions						
Gly-Trp cis La	N/A	0.11	N/A	226	1.98	0.97
Gly-Trp cis ground	N/A	0.39	N/A	472	9.85	5.54
Gly-Trp trans La	1130	0.11	125	0.26	0.17	0.17
Gly-Trp trans ground	N/A	0.43	514	2.57	0.50	0.55
Trp-Gly cis La	3.31	0.06	0.28	N/A	N/A	0.17
Trp-Gly cis ground	7.38	0.272	2.13	N/A	N/A	0.72
Trp-Gly trans La	2.29	0.12	0.069	0.10	1.17	0.12
Trp-Gly trans ground	3.15	0.79	0.30	0.87	0.98	0.53

Table 4.4: Table shows the average electronic coupling, average CT-La energy gap and the calculated quantum yield. The energy gap is shifted by the subtraction of 12000 $cm^{-}1$ in the calculation of the quantum yield with the many molecule interpretation. The data in columns 5 and 6 are the quantum yields calculated with offsets of -1000 and -5000 $cm^{-}1$ respectively using the single molecule interpretation.

Peptide	$\langle V_{12}^2 \rangle$	$\langle \Delta E_{CT-La} \rangle$	calc. QY	QY(-1000)	QY(-5000)
zwitterions					
Gly-Trp cis La	121835	17.7	0.096	0.304	0.129
Gly-Trp cis ground	129941	15.4	0.044	0.143	0.005
Gly-Trp trans La	129039	17.59	0.086	0.293	0.067
Gly-Trp trans ground	127150	15.69	0.039	0.043	0.003
Trp-Gly cis La	158845	15.1	0.028	0.165	0.005
Trp-Gly cis ground	219339	13.02	0.0073	0.053	0.001
Trp-Gly trans La	194407	15.02	0.024	0.252	0.012
Trp-Gly trans ground	256565	13.28	0.0088	0.028	0.0006
anions					
Gly-Trp cis La	155752	17.5	0.0957	0.303	0.282
Gly-Trp cis ground	158748	15.8	0.0464	0.302	0.258
Gly-Trp trans La	141587	17.5	0.08877	0.302	0.275
Gly-Trp trans ground	118745	15.8	0.0427	0.304	0.260
Trp-Gly cis La	184555	12.84	0.0115	0.260	0.146
Trp-Gly cis ground	137501	14.01	0.01336	0.296	0.195
Trp-Gly trans La	196362	12.14	0.00974	0.240	0.131
Trp-Gly trans ground	197375	13.38	0.010	0.279	0.168

Table 4.5: This table presents electron transfer rates and wavelength shifts from 3MI in vacuum for the most populated rotamers of Gly-Trp zwitterion. Results are from simulations using La state charges. These results are used to support the concept of pseudo-TDFSS in Gly-Trp. $\langle k_{et} \rangle$ is the average of instantaneous electron transfer rates calculated with an offset of -10000 wavenumbers.

Rotamer #	Population	$\langle k_{et} \rangle$ (ns^{-}1)	$\langle \lambda \; shift \rangle$ (nm)	chi1	chi2	psi	phi
0	0.452	61.27	44.69	60	90	180	-150
30	0.262	8.263	48.71	180	-90	180	-150
2	0.207	18.86	45.41	60	90	180	90
32	0.131	49.77	48.33	180	-90	180	90
6	0.094	9.866	56.80	60	-90	180	-150
24	0.084	2.178	52.92	180	90	180	-150
8	0.044	2.903	56.09	60	-90	180	90
26	0.041	0.4459	53.72	180	90	180	90
12	0.033	50.32	55.06	-60	90	180	-150
18	0.030	567.7	48.23	-60	-90	180	-150

Table 4.6: Table shows the average calculated wavelength for the most populated rotamers of Gly-Trp zwitterion. The rotamer numbers are the same as those in table 4.1. The fraction population change from the ground to La state is shown in column 3.

Rotamer #	$\langle \lambda \rangle$	Δ Population	$\Delta \; \lambda$
0	44.69	0.068	3.04
6	56.80	-0.118	-6.70
2	45.41	0.036	1.63
30	48.71	0.149	7.26
8	56.09	-0.062	-3.48
24	52.92	0.019	1.01
32	49.77	0.075	3.73
total			6.49
average			0.927

DISCUSSION

Steady State Absorbance and Fluorescence

Absorbance Spectra

The absorbance spectra of both the Trp and 5FTrp dipeptides are shifted to shorter wavelength in the configuration of Trp-X(5FTrp-X) compared to the X-Trp(X-5FTrp) form. These results agree with the work of Chen et al. [18] [98] for the Trp dipeptides and indicate that the effect is similar in magnitude for 5FTrp dipeptides. This effect also seems largely unaffected by the charge or hydrophobicity of the X residue.

Fluorescence Excitation Spectra

The difference in fluorescence excitation spectra between Trp-X and X-Trp points to a difference in the absorbance spectra of these species. The significant difference in fluorescence emission spectra between Trp-Gly and Gly-Trp at pH 5 (and the lack thereof between 5FTrp-Gly and Gly-5FTrp) further supports the observation in Figure 3.1. These indicate that the excited states in ground state solvent field are more similar in the case of 5FTrp. In the case of X=Leu the shift in absorbance is similar in both the Trp and 5FTrp variants as indicated by both the absorbance difference spectra and fluorescence excitation. Shifts are also similar for X=Asp or Met in the absorbance difference (fluorescence excitation spectra were not collected for these dipeptides).

Fluorescence Emission Spectra

In agreement with the work of Chen, et al. the peak steady state fluorescence spectra of Trp-X dipeptides are shifted to shorter wavelengths by approximately

10 nm with respect to X-Trp dipeptides in the zwitterion form. This includes the peptides new to this study (arginine (Arg), aspartic acid (Asp), methionine (Met)), that include charged X residues, that do not alter this trend. The 5FTrp-X dipeptides are also shifted in the same way compared to the X-5FTrp, but is smaller in some cases, as in Gly-5FTrp or Leu-5FTrp.

The shift to lower energy in the fluorescence of 5FTrp dipeptides compared to their corresponding Trp dipeptide is consistent with results for 5FNATA [53], and appears to be unaffected by pH or side chain substitution. A red shift in the fluorescence of the 5FTrp peptides vs Trp peptides is seen in all cases and tends to be larger at high pH. This shift is particularly small in the case of Gly-Trp:Gly-5FTrp at pH 5. All cases of X=Leu dipeptides show small shift in fluorescence between Trp and 5FTrp, regardless of configuration or protonation state. When comparing the fluorescence emission spectra of X-Trp and X-5FTrp dipeptide anions it is observed that the X-5FTrp is consistently shifted to longer wavelength. Leu-5FTrp at pH 10 is the only exception, showing a shift that is significantly smaller than the other X-5FTrp dipeptides.

In the case of 5FTrp dipeptides with Gly as the additional residue, it is found that while the fluorescence emission spectra of Gly-5FTrp and 5FTrp-Gly are consistent with the results of the other X-5FTrp and 5FTrp-X dipeptides, the absorbance spectra difference of Gly-5FTrp and 5FTrp-Gly is significantly less than that of any other X-5FTrp:5FTrp-X pair. This suggests that the local environment of the chromophore is more similar in the ground state than in the excited state, therefore there is likely a large conformational change (in dihedral angles) upon excitation for these dipeptides. The fluorescence excitation spectra also show that the shift for Gly-5FTrp:5FTrp-Gly is lower than that of Leu-5FTrp:5FTrp-Leu.

The charge of the non-Trp residue (X residue) leads to a shift of the fluorescence wavelength in addition to that caused by conformation (X-Trp, Trp-X) or by pH (zwitterion, anion), as seen in the case of Asp-5FTrp at both pH 5 and 10 shifted by 4-5 nm with respect to other X-5FTrp residues. 5FTrp-Asp is also shifted to longer wavelengths with respect to other 5FTrp-X.

The peak wavelength of X-5FTrp dipeptide anions appear to be more susceptible to the identity of the X residue than that of X-Trp dipeptides at high pH. The standard deviation in peak fluorescence wavelength is 1.1 nm and 2.0 nm for 5FTrp-X and X-5FTrp anions respectively, with spread of 3 nm for both. In the case of Trp-X and X-Trp dipeptides the standard deviations are 0.4 nm and 0.7 nm respectively, with spread of 1 nm and 2 nm. The zwitterions have more similar variation with change in X residue. Standard deviations are 1.2, 2.0, 0.9 and 1.1 nm for 5FTrp-X, X-5FTrp, Trp-X and X-Trp respectively.

Time Resolved Fluorescence

In this section results of time resolved fluorescence emission spectroscopy will be discussed as they pertain to the proportion of TDFSS and pseudo-TDFSS.

Time Resolved Emission Spectra

A large portion of the time-resolved emission spectra display a time dependent fluorescence emission Stokes shift. These shifts are caused by either relaxation (TDFSS), ET-heterogeneity (pseudo-TDFSS), or a combination of the two. The sections discussing decay associated spectra and computational results present a rationale for assigning a proportion of each mechanism to each of dipeptides.

Decay Associated Spectra

The DAS presented show characteristics of relaxation (equal positive and negative amplitudes) or ET-heterogeneity (all positive amplitudes) or a combination of both (unequal positive and negative amplitudes). DAS that are a combination are considered to be the result of the data fitting algorithm's inability to distinguish between two components of similar amplitude and lifetime.

Free Tryptophan and 5-fluorotryptophan. The decay associated spectra of Trp and 5FTrp zwitterions both display a short lifetime component with positive amplitudes at short wavelength larger than negative amplitudes at longer wavelengths. This is likely the result of two unresolvable components, one ET-heterogeneity and one relaxation. The negative amplitudes in the short component of Trp and 5FTrp zwitterions indicate that this component at least partially originates from relaxation. The proportion of the negative amplitude is enhanced in D_2O for both Trp and 5FTrp zwitterions, suggesting that the relaxation mechanism is enhanced or the quenching mechanism is suppressed to some extent. The large increase in lifetime of the longer lifetime component, which has the higher amplitude, when changing solvent from water to D_2O suggest that the major population rotamer is proton transfer quenched. This result also suggests that there is either only one proton transfer quenched rotamer or that any proton transfer quenched rotamer decays with approximately the same lifetime. Observing that the lifetime of the short lifetime components are largely unaffected by change from water to D_2O solvent, shows that these are not the result of proton transfer quenching.

These results are in agreement with the work of Willis, et al., [95] in which the DAS of Trp zwitterion was obtained by TCSPC, providing significant evidence for the reliability of the direct waveform recording method used in this study. The DAS

of Trp and 5FTrp anions also have nearly identical behavior. The negative amplitude is of greater relative magnitude for 5FTrp compared to Trp. This could result from the greater change in dipole moment in 5FTrp [53] leading to a greater reaction field for reorganization of dihedral angle rotations.

The relaxation of solvent around the excited state of tryptophan has been extensively studied and found to occur on the picosecond time scale. Due to the time resolution of the direct waveform recording instrument (200 ps data spacing, 1-2 ns IRF), the negative amplitudes seen in the DAS shown here are almost certainly not due to solvent relaxation. The hypothesis for the origin of these components is the change of rotational conformation in the dihedral angles defining the orientation of indole ring with respect to the peptide backbone (rotamer change).

Trp and 5FTrp pH 11 will have no quenching; there is no amide to produce electron transfer quenching and no $-NH_3$ to affect proton transfer. This is supported by the DAS shown in figures 3.20 - 3.21. The minor component of these DAS is very low amplitude and characteristic of a relaxation component. Therefore, Trp and 5FTrp anions can be described as having single exponential decay. The fact that the anion forms of Trp and 5FTrp display single exponential decay with unquenched lifetimes allows for the use of these decay rates as the sum of radiative and non-radiative rates of the base chromophore (3MI or 5F3MI) in the determination of the quenching rates. The lifetime of the 3MI chromophore is increased when the solvent is D_2O. The decay rate of 5FTrp anion suggests that this effect is of much lower magnitude for 5F3MI. The increase in lifetime may provide more time for spectral shift before the fluorescence signal is too low to be detected, enhancing the negative amplitude component.

The interpretation of DAS as independent species is supported by results obtained for tryptophan and 5-fluoro-tryptophan at high pH or pD. At pH(D) 10 two

DAS are observed, one long lifetime and one of similar lifetime to the long component of the zwitterion. Upon measurement at pH(D) 11 the we find that the shorter DAS is decreased by approximately a factor of 10. This observation supports our conclusion that this DAS is that of zwitterion still in solution. The pKa of the Trp and 5FTrp zwitterions are higher than the dipeptides, therefore while the dipeptides are purely in the anion form at pH 10, tryptophan and 5FTrp contain a significant portion of zwitterion at pH(D) 10.

The data presented show that while the Trp anion displays a large deuterium isotope effect, no isotope effect is seen for the 5FTrp anion, suggesting that the internal conversion and/or the intersystem crossing rates of 5FTrp are unaffected by the replacement of H at ring position 1 with D.

The decay kinetics of both tryptophan and 5FTrp zwitterions have significant isotope effects. These are likely result from the strong isotope effect, of about 2, for proton transfer quenching.

Dipeptide DAS. The decay associated spectra of Gly-Trp at pH 5 is shown in figure 3.22. These are characterized as heterogeneous decay with no evidence for relaxation, given the lack of negative amplitudes a longer wavelengths and no indication that amplitude will become negative at longer wavelength. These DAS also show an example of the common observation that the shorter component peaks at a shorter fluorescence wavelength compared to the longer component. This leads to a pseudo-TDFSS as the reduction in the population of the short wavelength rotamer results in a longer average wavelength. Analysis of data collected in D_2O at pD 5, leads to components that have a very small increase in lifetime. This suggests that proton transfer does not play a significant role in the quenching of Gly-Trp. However the relative amplitudes of these two components has been shifted to more

equal amplitudes of the two components. This leads to the lack of KIE in the average quenching rate for the Gly-Trp zwitterion.

In contrast to Gly-Trp, the DAS of Gly-5FTrp at pH 5 shows significant evidence for relaxation by the negative amplitudes at long wavelength. The larger amplitudes at shorter wavelength may suggest that quenching rate heterogeneity, leading to similar lifetime, is being mixed with the effect of relaxation by the global analysis of the time resolved fluorescence data. The large overall isotope effect for the quenching rate of Gly-5FTrp zwitterion suggests that the majority of the quenching is the result of proton transfer. The lifetime of the shorter component is affected to a lesser degree by solvent isotope, which is expected for relaxation or electron transfer. This suggest that a small amount of electron transfer quenching may persist even after 5FTrp substitution.

The zwitterions of the X-Trp configuration have small time dependent Stokes shifts that are the result of ET-heterogeneity, whereas the 5FTrp counterparts have slightly larger shifts that are the result of relaxation.

The DAS of Gly-Trp anion are also examples of a fluorescence shift that are the result of pseudo-TDFSS. Again the shorter lifetime component is peaked at shorter wavelength than the longer lifetime component. Due to the lack of proton transfer quenching in the anion, this is unambiguously the result of ET-heterogeneity. The small change in lifetime and amplitude of these components in D_2O is further evidence for a lack of proton transfer, or proton coupled electron transfer. The major component of Gly-5FTrp anion has an unquenched lifetime. The shorter component in water only contains positive amplitude and is blue shifted compared to the major component leading to pseudo-TDFSS. This is the only case of an X-5FTrp dipeptide that does not show evidence for a relaxation component. In D_2O the population minor component was substantially reduced and becomes negative at 400 nm. This

and Leu-5FTrp are the only cases that show a reduction in amplitude and a decrease in lifetime between water and D_2O results. Asp-5FTrp and Met-5FTrp anions (shown in Appendix) display longer lifetimes and similar amplitudes in D_2O than water. The fact that this effect is most prevalent in Gly, and to a lesser extent Leu (which has sightly less steric bulk than Met) suggests the possibility of a mechanism like PCET that is dependent on a conformation that is sterically hindered.

In D_2O Trp-Gly has a similar DAS to that in water with longer lifetimes for both the long and short components. The 5FTrp analog displays a reversal of the amplitudes. The short lifetime component has greater amplitude than the longer lifetime.

A notable feature of the DAS of 5FTrp substituted dipeptides is the appearance of negative amplitudes before 400 nm. Our initial hypothesis to explain this result was a reduction in ET-heterogeneity and enhancement of excited state spectral shift. A negative amplitude component in the fluorescence kinetics of tryptophan is easily explained in terms of changes of dihedral angle conformation during the excited state lifetime. In agreement with results for cyclic hexapeptides [2], the short component DAS is nearly universally peaked at lower wavelength than the long component.

The 5-fluorotryptophan dipeptides used in this study contained 5-fluorotryptophan as a mixture of D and L enantiomers. This leads to a question as to whether this would affect the fluorescence properties of these peptides when the X residue is not glycine. The lack of a stereocenter in glycine leads to dipeptides that are enantiomers with the same physical properties. In other dipeptides the stereocenter of the X residue combined with the D,L mixture of 5-fluorotryptophan leads to four diastereomers which could have different physical properties. Based on the interpretation of decay associated spectra as the fluorescence of individual species in solution and our observation of a single positive amplitude component in the

analysis of 5-fluorotryptophan dipeptide anions, we conclude that the mixture does not significantly effect the results presented here.

The changes in the signatures of the DAS for Trp vs 5FTrp dipeptides are analogous to those observed in Trp-Monellin vs 5FTrp-Monellin by Callis and co-workers. [97] The results for Monellin in the literature and dipeptides in this thesis work reinforce the conclusions that 5FTrp suppresses pseudo-TDFSS and allows observation of TDFSS resulting from relaxation. The two time scales of relaxation introduced by 5FTrp substitution in dipeptide and Monellin, approximately 0.5 ns and 20 ps respectively, indicate two mechanisms of relaxation. The faster mechanism in Monellin is presumably constrained water relaxation. The computational results support rotamer transitions as being the relaxation mechanism in dipeptides.

Quality of Fit for Direct Waveform Recording. Data obtained via the direct waveform recording method do not follow Possion statistics; therefore the quality of fits were determined via visual analysis of residuals and autocorrelation of residuals rather than the χ^2 or reduced χ^2 typically used in the case of TCSPC. [28] The Durbin-Watson values listed in Appendix C provide a measure of the overall autocorrelation in the residuals (a value of 2 would indicate no autocorrelation). These values show that the greatest reduction in residual structure is from the one component fit to the two component fit. There is universally reduction in autocorrelation of residuals between the two and three component fits, however it is universal that additional fitting parameters will improve the ability of the model to match the data. These Durbin-Watson values show that the two component fit is almost universally the best quality fit and that a single component fit is highly deficient in describing the fluorescence decay.

Discussion of Average Rates Results

In this section the results of experimental average quenching rates are discussed.

The fluorescence decay rates of Trp and 5FTrp anions in water and D_2O were used rather than those of 3-methylindole (3MI) or 5-fluoro-3-methylindole (5F3MI) for two reasons: 5F3MI was not easily obtained and while the decay rate in water is reported in literature, the value in D_2O was not; the solvation of the indole ring is greater in the case of 3MI or 5F3MI than it is for the amino acids or dipeptides leading to longer wavelengths of emission and higher radiative rates than the peptides. The non-radiative rate of internal conversion is strongly influenced by solvation in D_2O. The N-H at position 1 of the indole ring is converted to N-D in D_2O, leading to changes in the vibrational frequencies of the indole ring.

Whereas the quenching rates of Trp-X anions are found to be negligible, there remains significant quenching of the anion form of X-Trp dipeptides. As an example the X=Gly anion DAS are shown in figures 3.23 and 3.24. Two components of significantly quenched lifetimes (3 ns and 1 ns) both with relatively similar amplitudes are observed in the case of Gly-Trp. In the case of Trp-Gly, however, a component of nearly unquenched lifetime (8 ns) is observed. The short lifetime component has similar lifetime to the short component of Gly-Trp, but in Trp-Gly this component has a relative amplitude of approximately 10 percent. The Gly-Trp dipeptide in D_2O displays two components of similar shape and relative amplitude as those in for data collected in water with only a KIE of the base indole ring, leading to no KIE in the quenching rate.

As expected the ratios at high pH are all approximately 1 except for Gly-5FTrp and Leu-5FTrp, where both of have very small quenching rates in both water and D_2O, therefore this deviation from 1 is unlikely relevant. The isotope effects of approximately 2 in the cases of tryptophan and 5-fluorotryptophan at low pH are

consistent with the understanding that these species are only quenched by proton transfer quenching.

The fluorescence decay kinetics of Gly-5FTrp zwitterion displays two components, one of which displays significant negative amplitudes at long wavelength. These negative amplitudes indicate spectral shift during the excited state lifetime. Components of this type would have equal positive and negative amplitudes. The larger positive amplitudes in this component indicate that in addition to the relaxation component, there is a heterogeneous decay component with a lifetime too similar to be resolved separately. The decay of Leu-5FTrp at pH 5 shown in Appendix A displays a case in which the short component arises solely from excited state spectral shift. In D_2O, the decay of Gly-5FTrp at pD 5 displays two components with the same shape and relative amplitude as those for measurements in water. The long lifetime component lifetimes have a significant KIE. This is in significant contrast to the case of Leu-5FTrp at pD 5, where there is very little KIE show in this case. This provides evidence that the lack of steric bulk and increased flexibility associated with the Gly residue allows for interaction between the 5-Fluoro-3-methylindole chromophore and the protonated amine group. There is also evidence for ET-heterogeneity in the case of the Gly-5FTrp anion form as evidenced by two substantial positive amplitude components. The Leu-5FTrp dipeptide fluorescence measured at pH 10 displays biexponential decay where the short component appears to be spectral shift. The positive amplitude may be slightly higher than the negative, but this possible ET-heterogeneity would be less than 5 percent of the long lifetime component amplitude.

The decay kinetics of the Trp-Gly zwitterion, as shown in figure 3.25, display biexponential decay (2 and 0.7 ns) with all positive amplitudes; these components are similar to those found in the case of Gly-Trp aside from a shift to shorter wavelengths. In D_2O the DAS components have the same shape and relative amplitudes with

lifetimes of 2.8 and 1.2; this shows a KIE that is stronger in the short comp. At pH 10 the decay kinetics of Trp-Gly are shown in figure 3.27. The decay kinetics of 5FTrp-X and Trp-X at high pH are all characterized by very similar DAS (examples other than Trp-Gly are shown in the appendix). In the case of 5FTrp, the short component is of spectral shift type with a lifetime of approximately 1 ns. The DAS components in Trp-X anions are very similar with slightly more positive amplitude in the short comp, but only on the order of 10 percent the amplitude of the longer lifetime component. The decay kinetics of Trp-X and 5FTrp-X anions all have very similarly characterized decay associated spectra, characterized by a long lifetime decay component (4.8 - 5.6 ns for 5FTrp and 7.5 - 8.4 for trp) and a short spectral shift comp of about 1 ns lifetime. Only the 5FTrp-Gly anion has a short component significantly shorter than 1 ns, of about 0.5 ns. In D_2O the 5FTrp-X anions have DAS of near identical shape, with very similar lifetimes. In contrast the decay kinetics of the Trp-X anions display significant isotope effects in both the long and short lifetime components (around 20% increase in lifetime of all long components and as much as 44% increase in lifetime of short component).

We have provided evidence that the quenching mechanism for the tryptophan and 5-fluorotryptophan zwitterions is proton transfer only. The quenching rates for these are nearly identical and display a large kinetic isotope effect of about 2. If there were electron transfer quenching, the rate would have been reduced in the case of 5-fluorotryptophan. Therefore, our use of the decay rate of the tryptophan or 5-fluorotryptophan anions in water or D_2O as the base chromophore decay rate in the conversion of of average decay rate to quenching rate is justified.

Predicted Rotamer Populations and Interconversion Rates

Relating to goal # 1 of the computational prediction overview, the implications of rotamer populations and interconversion rates on the TDFSS and pseudo-TDFSS are discussed. The conformational populations and dynamics were studied by molecular dynamics simulation with force fields of 3 different types: OPLS, CHARMM, and AMBER. Results of these simulations provide strong evidence for both TDFSS and pseudo-TDFSS. Multiple rotamers are significantly populated in ground state simulations, suggesting et-heterogeneity based pseudo-TDFSS. There are also significant differences between the rotamer populations in the ground and La state simulations, providing driving force for relaxation derived from rotamer transitions.

Rotamer Populations

This work presents a highly comprehensive analysis of the conformational landscape of the Trp-Gly and Gly-Trp dipeptides. The conformational population distribution is strongly dependent on the chosen force field. The chi1 dihedral angle is the highly sensitive to changes in the force field parameters. Distributions of chi2 angles are similar in population when comparing the three force field types. The widths of the two rotamer populations vary with force field.

There is strong dependence on the force field for the distribution of the psi angle in the Trp-Gly zwitterion. OPLS force field yields only a single population at approximately 150 degrees. If CHARMM or AMBER force fields are employed, a populations at -60 and 90 degrees become apparent. This dihedral is of particular importance to the electron transfer rates of zwitterionic dipeptides, as it affects the distance between the positive charge of the $-NH_3$ group and the carbonyl of the

amide. The -NH_3 group likely also strongly influences the orientation of nearby water molecules, affecting how effectively water H-bonds to the amide carbonyl.

Molecular dynamics simulations suggest that ground state heterogeneity is prevalent in the chi1 and chi2 angles of all dipeptides. The OPLS force field favors very narrowly distributed backbone (phi, psi) angles. If this configuration of the backbone does not dominate the ground state population, this force field is not properly sampling the configurational space. AMBER and CHARMM type force fields widen the distribution of individual rotamers and lead to more rotamers being populated. This suggests a way of evaluating OPLS vs AMBER and CHARMM force fields.

Rotamer Transition Rates

Canonical rotamer transitions in the chi1 and chi2 tend to occur on the order of the fluorescence lifetime. The lack of conformational transitions in the Psi angle for the OPLS force field of all zwitterions suggests a strong electrostatic interaction between the positive charge of the NH_3 group and the partial negative charge of the carbonyl of the amide group.

The exchange rate between rotamers has a strong effect on the observed lifetimes and the level of non exponential decay. If the exchange rate were much faster than the fluorescence lifetime, then the observed decay rate would be the average of the lifetimes of the inter-converting species and would be single exponential. The slow exchange limit, where the transition rates are much slower than the rate of fluorescence decay, then the fluorescence decay kinetics will display two exponential components with the individual lifetimes of the species. This is the case where DAS are most appropriate as a means of analysis. The interpretation of DAS as the spectra of individual species is complicated by the interconversion between rotamers. In the

case of interconversion rates that are on the order of the fluorescence decay rate, the observed fluorescence decay lifetimes and amplitudes are dependent on the decay rate of the species and the interconversion rate [88]. If this is indeed the case then, the lifetimes of the decay associated spectra measured would not be the lifetimes of individual conformers. Interconversion rates found in molecular dynamics simulations suggest that this is the case Trp-Gly and Gly-Trp dipeptides.

Computational Evidence for Pseudo-TDFSS

The conformations of Gly-Trp zwitterion with La state charges are distributed into several well populated rotamers with widely varying average electron transfer rates and fluorescence wavelength shifts. Generally the rotamers with higher electron transfer rates are those with lower wavelength shifts. This result is supported by findings in the literature by Callis and co-workers. [67] While the correlation for Gly-Trp zwitterion is not exact, there is significant correlation in the most populated rotamers of a faster decaying population with a shorter wavelength of about 4 nm. This combination gives rise to a time dependent shift to longer wavelength resulting from electron transfer rate heterogeneity. The DAS of Gly-Trp at low pH, shown in figure 3.22, represents a case of time dependent shift interpreted only as pseudo-TDFSS; if only positive components are observed in a DAS, there is no evidence of a relaxation component. The 5 nm shift between the long and short lifetime components in experiment, shown in table 3.5, is in good agreement with simulation results, shown in table 4.5.

Computational Evidence for TDFSS

The comparison of dihedral angle populations between simulations performed with ground state or La state charges on the indole ring of the tryptophan provide evidence for relaxation components in multiexponential decay. Two effects are

observed when changing the MD charges from ground to L_a state charges, shift in the equilibrium angle of a given canonical rotamer and a redistribution of the population within rotamer conformations. The rate of rotamer state transitions in MD simulations indicate that the rotamer population will respond to the change from ground to L_a charges on the order of the fluorescence lifetime.

In order for a rotamer state change to lead to a shift in wavelength, the different rotamer states must have different calculated fluorescence wavelength maxima. Table 4.6 shows that several well populated rotamers of Gly-Trp zwitterion have significantly different average wavelengths. This table also shows that the populations of these rotamers change considerably between ground and La states. These results lead to the possibility of a TDFSS based on change in rotamer population.

Tables 4.2 and 4.3 in the computational results section presents the inverse equilibration rates (relaxation lifetimes) between populations of canonical rotamers. In order for these to be relevant to the explanation of multiexponential decay based on conformational change during the excited state lifetime, lifetimes must be less than or on the order of the inverse of the sum of the radiative and non-radiative rates (7.8 ns). The level of redistribution appears relatively consistent among all dipeptides and protonation in simulation, while not all samples show significant relaxation characterized components (e.g. no negative amplitudes in the decay associated spectra of gly-trp pH 5 in this study).

The top two rotamers by population of the Gly-Trp zwitterion are differentiated only by their chi2 angle (table 4.1). The change from ground to La state charges leads one of these to decrease in population and the other to increase. The redistribution lifetime between chi2 populations is approximately 0.5 ns. Lifetimes on this scale agree with the lifetimes of the experimental DAS that contain negative amplitudes.

Electron Transfer Rates

Relating to goal # 2 of the computational prediction overview, the results of electron transfer rate calculations are discussed in terms of the relative quantum yield of the relative quantum yield of Gly-Trp and Trp-Gly, the occurrence of QSSQ in dipeptides, and the initial brightness defect suggesting lifetimes of less than 300 fs. The methods employed here were unable to accurately reproduce the relative quantum yields of Gly-Trp and Trp-Gly. Possible explanations for this deficiency in the method are discussed.

Instantaneous Rates

The results of QM/MM calculations give instantaneous electron transfer rate constants that are sufficient to explain fluorescence lifetime components of 10-30 ps that are associated with QSSQ. [18] [98] There are not however electron transfer rate constants that explain the initial brightness defect. [98] Explanation of this would require a rate constant sufficient to produce a lifetime of less than 300 fs.

Stabilization of Charge Transfer State by Subgroups

The stabilization of the CT state in the Gly-Trp zwitterion is dominated by the single positively charged -NH_3 group, acting as the primary driving force in electron transfer quenching. This is countered by the contributions of the negative COO and water solvent. The protein contributions are more balanced in the Trp-Gly zwitterion (stabilizing NH_3 and destabilizing COO). In this case the water plays a more substantial role in lowering the energy of the CT state.

The majority of molecular dynamics frames during simulation of Gly-Trp zwitterion contain a configuration of water molecules that increase the energy of the charge transfer state compared to gas phase. This is highly unusual as the high

dielectric constant of water and hydrogen-bonding to the carbonyl oxygen of the amide both lead to lowering of CT energies in typical highly solvated Trp. For example NATA quantum yield is highly dependent on the solvent. Muiño and Callis measured the relative fluorescence intensity of NATA in dioxane, 1-octanol, and water. [62] The fluorescence intensity of NATA in water was the lower than that in the other two solvents.

It has been experimentally observed that single mutations of charged residues near the single Trp140 of Staphylococcal nuclease (STNase), lead to no change in the steady state fluorescence maximum [71]. A QM/MM study, by Scott and Callis, of tryptophan fluorescence wavelength in STNase including in-silico mutations of nearby amino acid residues displayed the same low sensitivity to the charge states of nearby residues. [77] This study showed that there was strong anticorrelation between the contributions of the protein and water to the fluorescence wavelength shift. A similar anticorrelation between water and protein appears to manifest itself in the CT energy contributions in Trp dipeptides.

The lack of sharp structure in the total energy contributions from subgroups suggests that the effect of one group can be compensated for by another group. Most likely water molecules moderate some of the influence of zwitterionic charges.

To further explain the effects of the zwitterion charges and the water solvation in detail, for gly-trp in the zwitterion form, figures 5.1 - 5.3 show the structures of the peptides and the structure of the nearest waters. Figure 5.1 shows this for molecular dynamics frames in which the water molecules act to increase the energy of the CT state. The energy contributions to the CT state from water, NH3, and COO are 12536.4, -12302.4, and 1919.2 respectively for the structure on the left and 25561.6, -14561.4, 1614.7 for the structure on the right. This figure shows frames with similar energy contributions arising from configurations with largely different

chi1 dihedral angles. The two canonical rotamers in chi2 approximate mirror images in a plane parallel to the peptide backbone. Therefore changes in chi2 rotamer have the same effect with regard to the relative orientations of the amide, NH3, COO groups to the indole ring as a change in chi1. This provides an explanation for the relatively narrowly distributed energy contributions see in the histograms in figures 4.57 - 4.68. While the gross effect is insensitive to rotamer state, a multi modal detailed structure to the histograms shows a smaller effect of rotamer state in some, but not all, simulations.

Figure 5.1: Structures of the Gly-Trp zwitterion at time points 1415 ns and 1075 ns. In both of these frames, the NH_3 group lowers the energy of the CT state and the carboxylate increases the energy. It can be seen in these figures that a vector approximating the CT transition (red arrow) and the vector from indole to NH_3 and indole to COO are in the same direction. The images in this figure demonstrate that two largely different chi1 angles lead to similar effects of zwitterion charges on the CT state.

Gly-Trp vs Trp-Gly Quantum Yield

Investigation of the potentials created by the charges of water molecules (surroundings) at each atom of the dipeptides (QM molecule) reveal that these potentials are producing the lower quantum yield for Trp-Gly than Gly-Trp. This

Figure 5.2: Structure of water molecules around Gly-Trp dipeptide during molecular dynamics simulation with ground state charges on the indole ring. The ten waters that most stabilize the CT state are shown in blue. The ten that most destabilize the CT state are show in red. On the left a frame is shown in which the water contribution to the CT energy is an increase of 12536 $cm^{-}1$. The water contribution to the CT energy is an increase of 25561 $cm^{-}1$ for the frame on the right. In both of these frames the electrostatic contribution of the water solvent leads to an overall destabilization of the charge transfer state. The water molecule leading to the greatest increase in energy of the CT state is shown in a spacefilling model. For the frame at 1415 ns a water molecule with a hydrogen interacting with the pi system of the ring. In the case of the frame a 1075 ns, the positive charge of the NH_3 group is organizing the water such that the oxygen is oriented toward the amide carbon.

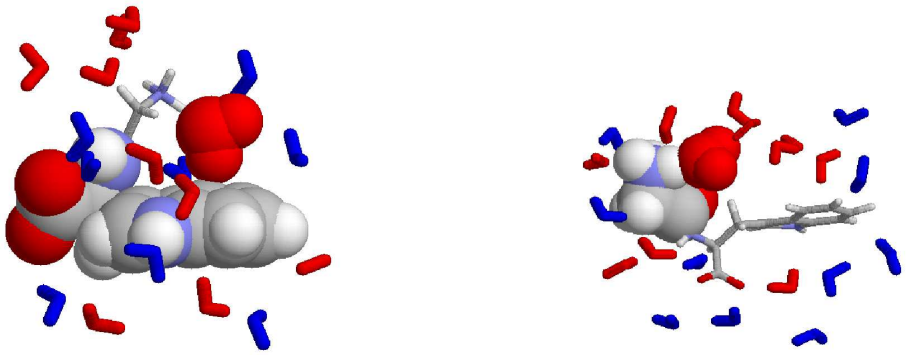

Figure 5.3: This figure shows a frame in which the water solvent provides an overall stabilization of the CT state at 1444 ns. The most (de)stabilizing waters are shown in spacefilling models. The most stabilizing water is hydrogen bonded to the carbonyl oxygen of the amide. This is typical of water solvated tryptophans.

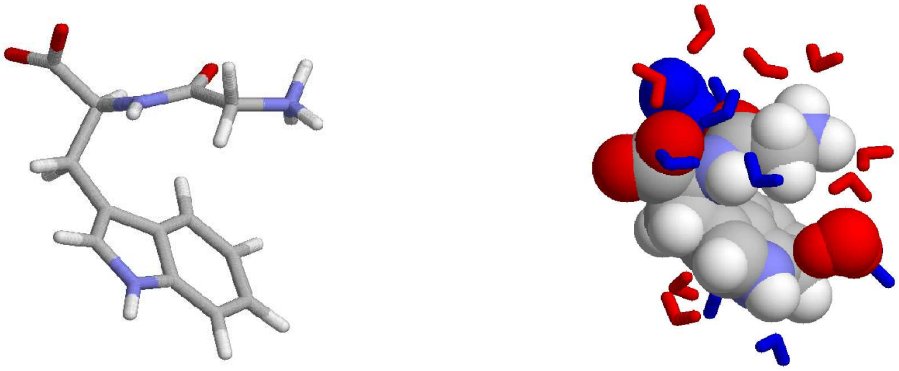

suggests that the water model used in simulations (TIP3P) is insufficient in capturing the local structure of explicit waters around the strong electrostatic environment of the zwitterions.

Contributions to Wavelength Shift

The shift to lower wavelength of approximately 10 nm for Trp-X compared to X-Trp as well as zwitterion as opposed to anion indicated that the fluorescence wavelength is dependent on the local charges. This is at odds with certain results for tryptophan fluorescence in proteins showing minimal dependence of fluorescence wavelength on charged residues adjacent to the tryptophan residue [71] [77]. The results presented here show a case in which the water does not fully compensate for the protein contribution. We observe similar anticorrelation in the contributions of protein vs water to the wavelength shifts.

The contributions of subgroups to the wavelength shift generally do not form a normal Gaussian distribution. Most display multimodal structure or skew in the distribution. However, the overall wavelength shifts are distributed in a Gaussian.

Explanation of Very Fast ET Rates

The instantaneous electron transfer rates presented here show some evidence for conformations that have extraordinarily high electron transfer rates. These high rates provide an explanation for the quasi static self quenching seen in previous experiments [18] [99]. The vast majority of electron transfer rates are very low. This leads to the conclusion that most of the fluorescence quenching happens at a very high rate, but only at very sporadic intervals. This phenomenon has been observed in simulations of NATA as well. [10] [11]

Table 4.1 shows the La-CT energies and electronic coupling for the highest electron transfer rate frames from MD simulation. This is intended to show if the

Table 5.1: Table of La energies, CT-La energy gap, and electronic coupling values for the 3 MD frames with the highest calculated electron transfer rates for the Gly-Trp zwitterion. Average and standard deviation of values over the course of the MD simulation are shown in bold.

peptide	ps	L_a	CT-La	V^2
gly-trp trans la		**34.33 (0.99)**	**17.6 (3.0)**	**129039 (161204)**
	1136000	34.024	9.489	263304.5962
	762000	36.037	10.554	418917.535
	1176000	34.507	8.398	141067.4498
gly-trp trans ground		**36.59 (0.77)**	**15.69 (2.84)**	**127150 (158837)**
	1238000	36.930	5.071	352761.7724
	1328000	36.260	4.166	170398.8789
	1444000	36.687	6.268	176631.1468
gly-trp cis la		**34.39 (0.97)**	**17.68 (2.96)**	**121835 (192401)**
	1432000	35.545	10.285	622737.2848
	1196000	34.631	12.04	828603.7159
	1080000	34.365	12.094	617656.8686
gly-trp cis ground		**36.52 (0.77)**	**15.37 (3.19)**	**129941 (160086)**
	1074000	36.893	6.824	461243.6554
	818000	36.587	8.23	638254.6983
	344000	36.022	9.141	434852.0615

high electron transfer rates are the result of extraordinarily small La-CT gap, large coupling, or the combination of both in a given frame. The specific CT-La gaps are further from the mean of the deviation in terms of standard deviations than the La energies are from theirs. This indicates that the small gaps are due to lower CT energies rather than high La energies.

Table 5.2: Table of La energies, CT-La energy gap, and electronic coupling values for the 3 MD frames with the highest calculated electron transfer rates for the Trp-Gly zwitterion. Average and standard deviation of values over the course of the MD simulation are shown in bold.

peptide	ps	L_a	CT-La	V^2
trp-gly trans la		**34.30 (0.97)**	**15.02 (2.87)**	**194407 (219925)**
	376000	35.603	9.231	710325.4669
	226000	34.949	9.808	752577.7909
	1274000	34.401	7.365	279253.735
trp-gly trans ground		**36.31 (0.82)**	**13.28 (3.15)**	**256565 (252695)**
	474000	36.954	6.012	543967.1436
	564000	36.903	6.996	423012.3101
	428000	37.523	5.513	347174.3547
trp-gly cis ground		**36.41 (0.81)**	**13.02 (3.01)**	**219339 (228668)**
	156000	36.923	7.367	934944.9599
	598000	36.337	7.17	529249.8706
	64000	36.729	7.111	522238.3149
trp-gly cis la		**34.44 (0.96)**	**15.09 (2.95)**	**158845 (188419)**
	388000	35.653	6.711	374469.0346
	488000	35.402	9.211	753217.4783
	734000	35.858	9.153	616884.8748

SUMMARY AND CONCLUSIONS

Scope

The work presented in this thesis represents the first systematic study of Trp-containing peptides with 5FTrp substitution, both experimentally and computationally. The time resolved fluorescence, with a time resolution of approximately 0.5 ns, for dipeptides was measured in the X-Trp and Trp-X configurations(where X=Gly, Leu, Asp, Arg, or Met), with 5FTrp substitution, at pH 5 and pH 10, and in water and D_2O solvent. These combinations produced 84 distinct species, with distinct levels of electron transfer and proton transfer quenching. The substitution of 5FTrp reduced the electron transfer rates; measurements in pH 10 buffer removed the effect of proton transfer quenching; and D_2O buffers introduced an isotope effect, reducing the rate of proton transfer quenching mechanism. Using these permutations of quenching rates, an exhaustive study was performed to differentiate between time dependent spectral shifts resulting from quenching rate heterogeneity (pseudo-shifting or pseudo-TDFSS) and those resulting from time dependent relaxation (TDFSS).

To complement the novel experimental work presented here, the first microsecond time scale molecular dynamics simulations comparing ground and excited state using multiple force fields were performed. Equilibrium molecular dynamics simulations were performed for Gly-Trp and Trp-Gly dipeptides in both zwitterion and anion states with a simulation time of 1.5 - 1.7 microseconds. This simulation time sufficiently sampled the configurational space. Three different force fields were employed and compared in these simulations. Both ground state and L_a state charges on the indole ring were used in MD simulations. At spaced time points during these simulations, the geometries of the peptide and water solvent were extracted. The

fluorescence wavelength, electronic coupling; and CT and L_a state energies at each of these points were calculated. Electron transfer rates were calculated from the electronic coupling and CT-L_a state energy difference. A detailed analysis of the contributions of each subgroup(carboxylate, amine, amide, and water solvent) to the calculated fluorescence wavelength maxima and CT-L_a energy gap was conducted.

Results

The large scope of this study reinforces the evidence for suppression of electron transfer rates by 5FTrp, while presenting a more detailed understanding of the susceptibility of 5FTrp to proton transfer quenching. The effects of pseudo-TDFSS were reduced or eliminated by 5FTrp. Quenching rates were reduced by 5FTrp substitution in all cases. The proportion of the short lifetime component in the DAS was reduced by the substitution of 5FTrp in all 84 cases. Therefore, these short lifetime components are most likely the result of subpopulations with higher electron transfer rates than the majority population.

The absorbance spectral shift between Trp-X and X-Trp, reported by Chen, et al., was also observed for X residues new to this study, including charged residues, and for 5FTrp substitution. The 10 nm shorter fluorescence wavelength maxima of Trp-X zwitterion was also not strongly affected by X residue identity or 5FTrp substitution.

Experimentally three types of multiexponential decay were observed: quenching rate heterogeneity with no relaxation, relaxation only, and combinations thereof. The global analysis of time resolved fluorescence data produced DAS for most cases that consisted of two components, both of which had only positive amplitudes. DAS of this type indicate quenching rate heterogeneity. All non-5FTrp dipeptide zwitterions show this type of DAS. In all 84 cases, the shorter lifetime component was shifted to shorter wavelength in comparison to the longer lifetime component.

This leads to a time dependent shift in fluorescence wavelength that is the result of heterogeneity in quenching rate. As the populations decay the relative effect of the shorter wavelength component on the observed wavelength reduces. The short component of the decay associated spectra of Trp-X, 5FTrp-X, and X-5FTrp anions consisted of equal magnitude positive amplitudes at short wavelength and negative amplitudes at longer wavelength. This indicates only relaxation in their short lifetime component with no evidence for quenching rate heterogeneity. This type of DAS is consistent with the observation that these are unquenched species. The observation of pure relaxation components in these well studied dipeptides provide the first strong evidence for relaxation due to rotamer redistribution.

In the zwitterionic form, results suggest both forms of quenching for most dipeptides. All of the Trp dipeptides zwitterions are quenched to a significant level and show a high degree of electron and/or proton transfer quenching heterogeneity. The only anions that show significant quenching rates are X-Trp dipeptides; and this quenching is almost completely eliminated by 5FTrp substitution.

Results of molecular dynamics simulations indicate that there are several rotamers populated in the ground state of both dipeptides. These populations are significantly altered when L_a state charges are used in the simulation. This difference in population provides a driving force of population redistribution. There are also substantial differences in rotamer populations when different force fields are employed in MD simulations. It is also observed that the interconversion rates between conformations occur on the order of the fluorescence lifetime. These results provide strong evidence for the relaxation mechanism of multiexponential fluorescence decay, with similar time constants to the relaxation type DAS seen in this study, on the order of 0.5 ns. Different rotamers have distinct calculated electron transfer rates

and fluorescence wavelengths. This result support the mechanism of pseudo-TDFSS that is displayed in experimental results.

Calculated fluorescence wavelengths agree well with experiment. These calculations also provided significant insight into the cause of the 10 nm difference in fluorescence wavelength between X-Trp and Trp-X. The effect of the zwitterion charges is extraordinary. With respect to 3MI in vacuum, the carboxylate of Gly-Trp contributes a 30 nm shift to longer wavelength—whereas the -NH_3 contribution is near zero. The NH_3 of Trp-Gly contributes either 20 or 30 nm to shorter wavelength, dependent on rotamer state and the COO contributes near zero. The protein effects alone would represent a 50 nm difference in the fluorescence wavelengths between Gly-Trp and Trp-Gly. The observed wavelength difference of only 10 nm is the result of compensation by the water contribution. Furthermore, these contributions of protein and water appear to be anti-correlated both in frequency of occurrence (histograms) and in the time course of the simulation.

Quantum yields calculated from the electron transfer rates predicted a lower value for Trp-Gly than Gly-Trp—opposite of the experimental finding. For both Trp-Gly and Gly-Trp zwitterions the electron transfer rate is increased by the positive -NH_3 and decreased by the negative COO. The contribution of the water solvent to the electron transfer rate varies greatly between Trp-Gly and Gly-Trp. The calculated instantaneous electron transfer rates range over several orders of magnitude, with occasional extraordinarily high rates, up to 100 ns^{-1}. This result supports the 10-30 ps lifetimes associated with QSSQ. There were no instances of instantaneous rates that would indicate the presence of the initial brightness defect.

Conclusions

This work has shown 5FTrp substitution to be an extremely effective tool in distinguishing between electron and proton transfer quenching mechanisms. Any DAS component that is strongly suppressed by the substitution of 5FTrp for Trp is the result of electron transfer quenching. The short lifetime component of Trp zwitterion is not suppressed to a large extent by the substitution of 5FTrp, suggesting that it is the result of relaxation, proton transfer quenching heterogeneity, or a combination thereof.

The contribution of the charged groups of the zwitterion or anion to the wavelength maxima or CT state energy are extraordinary. These large effects are tempered by a large compensating contribution of water solvent. This indicates a critical role of explicitly defined water in simulations predicting the fluorescence wavelength and electron transfer rates. This suggests that caution should be taken when comparing to the results of continuum solvent models. In addition to the comparison of multiple force field parameterizations of the protein component, different solvent models should also be evaluated.

The sensitivity of computed results to chosen force field suggests that it is important to evaluate the results of multiple force fields. Agreement of results from multiple force fields may suggest a correct result. An example of agreement of different force field results in this work is the calculation of wavelength. The large discrepancies in results between different force fields suggest that a great deal of work is required in terms of force field parametrization before molecular dynamics can reliably describe the reality of complex chemical systems. Future work could include completing electron transfer and wavelength calculations for the CHARMM and AMBER force fields to complete our comparison with the OPLS force field.

Rotamer state reorganization—supported by molecular dynamics simulation—presents the only plausible mechanism for relaxation components on the time scale observed for dipeptide fluorescence. Because of the relatively rapid interconversion rate between rotamers the DAS cannot be strictly interpreted as representing populations in proportion to the amplitudes in the DAS. Therefore, these DAS are not equivalent to species associated spectra. Future work will include the development of a kinetic model to account for the contribution of rotamer interconversion rate on the DAS.

Electron transfer rate calculations failed to reproduce the remarkable difference in quantum yield between Gly-Trp and Trp-Gly. This may result from incorrect potentials from explicit water solvent for a Trp-ring to amide charge transfer, as in electron transfer rate calculations, but correct potentials for an intra-Trp ring charge transfer, as in wavelength calculations. This suggests inaccuracy in the protein and/or solvent parameters of the molecular dynamics force fields.

While Fermi rule methods were successful in predicting rates fast enough to explain QSSQ, they failed to do so for the initial brightness defect. An initial brightness defect indicates quenching rates on the same order as water reorganization (about 100 fs). The MD simulations performed with ground state charges provide potentials from water for this time before reorganization. While ground state simulations have higher electron transfer rates than L_a state simulations, electron transfer rates calculated with Fermi rule methods do not approach the 10000 ns^{-1} rates required to produce an initial brightness defect. This result does not preclude fast electron transfer quenching that is not captured by the Fermi procedure. Other methods that are the subject of ongoing work are adiabatic potential energy surfaces, in the case of high interaction, and conical intersections, for the zero interaction limit.

REFERENCES CITED

[1] Abbyad, P.; Shi, X.; Childs, W.; McAnaney, T. B.; Cohen, B. E.; Boxer, S. G. *Journal of Physical Chemistry B* **2007**. *111*, 8269.

[2] Adams, P. D.; Chen, Y.; Ma, K.; Zagorski, M. G.; Sonnichsen, F. D.; McLaughlin, M. L.; Barkley, M. D. *Journal of the American Chemical Society* **2002**. *124*, 9278.

[3] Andersson, K.; Barysz, M.; Bernhardsson, A.; Blomberg, M.; Cooper, D.; Flscher, M.; de Graaf, C.; Hess, B.; Karlstrm, G.; Lindh, R.; Malmqvist, P.-.; Nakajima, T.; Neogrdy, P.; Olsen, J.; Roos, B.; Schimmelpfennig, B.; Schtz, M.; Seijo, L.; Serrano-Andrs, L.; Siegbahn, P.; Stlring, J.; Thorsteinsson, T.; Veryazov, V.; ; Widmark, P.-O. *Lund University.Sweden* **2002**.

[4] Andersson, K.; Malmqvist, P.; Roos, B. *Journal of Chemical Physics* **1992**. *96*, 1218.

[5] Berendsen, H. J. C.; van der Spoel, D.; van Drunen, R. *Computer Physics Communications* **1995**. *91*, 43.

[6] Besler, B. H.; Jr., K. M. M.; Kollman, P. A. *Journal of Computational Chemistry* **1990**. *11*, 431.

[7] Blancafort, L.; González, D.; Olivucci, M.; Robb, M. A. *Journal of the American Chemical Society* **2002**. *124*, 6398.

[8] Broos, J.; Maddalena, F.; Hesp, B. H. *Journal of the American Chemical Society* **2004**. *126*, 22.

[9] Callis, P. R. *P. callis collection.* personal communication, **2012**.

[10] Callis, P. R. *Journal of Molecular Structure* **2014**. *1077*, 14.

[11] Callis, P. R. *Journal of Molecular Structure* **2014**. *1077*, 22.

[12] Callis, P. R.; Burgess, B. K. *The Journal of Physical Chemistry B* **1997**. *101*, 9429.

[13] Callis, P. R.; Liu, T. Q. *Journal of Physical Chemistry B* **2004**. *108*, 4248.

[14] Callis, P. R.; Petrenko, A.; Muino, P. L.; Tusell, J. R. *The Journal of Physical Chemistry B* **2007**. *111*, 10335.

[15] Callis, P. R.; Vivian, J. T. *Chemical Physics Letters* **2003**. *369*, 409.

[16] Carraway, E. R.; B. L. Hauenstein, J.; Demas, J. N.; DeGraff, B. A. *Analyical Chemistry* **1985**. *57*, 2304.

[17] Cave, R. J.; Newton, M. D. *Chemical Physics Letters* **1996**. *249*, 15.

[18] Chen, R. F.; Knutson, J. R.; Ziffer, H.; Porter, D. *Biochemistry* **1991**. *30*, 5184.

[19] Chen, Y.; Barkley, M. D. *Biochemistry* **1998**. *37*, 9976.

[20] Chen, Y.; Liu, B.; Yu, H.-T.; Barkley, M. D. *Journal of the American Chemical Society* **1996**. *118*, 9271.

[21] Cory, M. G.; Zerner, M. C.; Xu, X. C.; Schulten, K. *Journal of Physical Chemistry B* **1998**. *102*, 7640.

[22] Cowgill, R. W. *Biochimica et Biophysica Acta* **1970**. *200*, 18.

[23] donder Lardeux, C.; Jouvet, C.; Perun, S.; Sobolewski, A. L. *Physical Chemistry Chemical Physics* **2003**. *5*, 5118.

[24] Eftink, M. R.; Jia, Y.; Hu, D.; Ghiron, C. A. *Journal of Physical Chemistry* **1995**. *99*, 5713.

[25] Essmann, U.; Perera, L.; Berkowitz, M. L.; Darden, T.; Lee, H.; Pedersen, L. G. *Journal of Chemical Physics* **1995**. *103*, 8577.

[26] Frisch, M. J.; Trucks, G. W.; Schlegel, H. B.; Scuseria, G. E.; Robb, M. A.; Cheeseman, J. R.; Montgomery, J. A.; Jr.; Vreven, T.; Kudin, K. N.; Burant, J. C.; Millam, J. M.; Iyengar, S. S.; Tomasi, J.; Barone, V.; Mennucci, B.; Cossi, M.; Scalmani, G.; Rega, N.; Petersson, G. A.; Nakatsuji, H.; Hada, M.; Ehara, M.; Toyota, K.; Fukuda, R.; Hasegawa, J.; Ishida, M.; Nakajima, T.; Honda, Y.; Kitao, O.; Nakai, H.; Klene, M.; Li, X.; Knox, J. E.; Hratchian, H. P.; Cross, J. B.; Bakken, V.; Adamo, C.; Jaramillo, J.; Gomperts, R.; Stratmann, R. E.; Yazyev, O.; Austin, A. J.; Cammi, R.; Pomelli, C.; Ochterski, J. W.; Ayala, P. Y.; Morokuma, K.; Voth, G. A.; Salvador, P.; Dannenberg, J. J.; Zakrzewski, V. G.; Dapprich, S.; Daniels, A. D.; Strain, M. C.; Farkas, O.; Malick, D. K.; Rabuck, A. D.; Raghavachari, K.; Foresman, J. B.; Ortiz, J. V.; Cui, Q.; Baboul, A. G.; Clifford, S.; Cioslowski, J.; Stefanov, B. B.; Liu, G.; Liashenko, A.; Piskorz, P.; Komaromi, I.; Martin, R. L.; Fox, D. J.; Keith, T.; Al-Laham, M. A.; Peng, C. Y.; Nanayakkara, A.; Challacombe, M.; Gill, P. M. W.; Johnson, B.; Chen, W.; Wong, M. W.; Gonzalez, C.; ; Pople, J. A. *Gaussian 03, revision d.01*, **2004**.

[27] Gauduchon, P.; Wahl, P. *Biophysical Chemistry* **1978**. *8*, 87.

[28] Gillispie, G. D. *Discussions with gregory d. gillispie, fluorescence innovations.* personal communication, **2010**.

[29] Glasoe, P. K.; Long, F. A. *Journal of Physical Chemistry* **1960**. *64*, 188.

[30] Grdadolnika, J.; Mohacek-Grosevb, V.; Baldwinc, R. L.; Avbelj, F. *Proceedings of the National Academy of Sciences of the United States of America* **2010**. *108*, 1794.

[31] Grimme, S. *Journal of Computational Chemistry* **2004**. *25*, 1463.

[32] Grimme, S. *Journal of Computational Chemistry* **2006**. *27*, 1787.

[33] Grimme, S.; Antony, J.; Schwabe, T.; Muck-Lichtenfeld, C. *Organic and Biomolecular Chemistry* **2007**. *5*, 741.

[34] Hermans, J. *Proceedings of the National Academy of Sciences of the United States of America* **2011**. *108*, 3095.

[35] Hess, B. *Journal of Chemical Theory and Computation* **2008**. *4*, 116.

[36] Hess, B.; Kutzner, C.; van der Spoel, D.; Lindahl, E. *Journal of Chemical Theory and Computation* **2008**. *4*, 435.

[37] Ishikawa, H.; Kwak, K.; Chung, J. K.; Kim, S.; Fayer, M. D. *Proceedings of the National Academy of Sciences of the United States of America* **2008**. *105*, 8619.

[38] Jacyno, G.; Kawski, A. *Bulletin de L Academie Polonaise Des Sciences-Serie Des Sciences Mathematiques Astronomiques et Physiques* **1974**. *22*, 339.

[39] Jennings, W.; McCarthy, N.; Kelly, P.; Malone, J. *Organic and Biomolecular Chemistry* **2009**. *7*, 5156.

[40] Jorgensen, W. L.; McDonald, N. A. *Theochem-Journal of Molecular Structure* **1998**. *424*, 145.

[41] Kaminski, G. A.; Friesner, R. A.; Tirado-Rives, J.; Jorgensen, W. L. *Journal of Physical Chemistry B* **2001**. *105*, 6474.

[42] Kawski, A.; Sepiol, J. *Bulletin de L Academie Polonaise Des Sciences-Serie Des Sciences Mathematiques Astronomiques et Physiques* **1972**. *20*, 707.

[43] King, H. F.; Stanton, R. E.; Kim, H.; Wyatt, R. E.; Parr, R. G. *The Journal of Chemical Physics* **1967**. *47*, 1936.

[44] Knutson, J.; Walbridge, D.; Brand, L. *Biochemistry* **1982**. *21*, 4671.

[45] Kubelka, J.; Chiu, T. K.; Davies, D. R.; Eaton, W. A.; Hofrichter, J. *Journal of Molecular Biology* **2006**. *359*, 546.

[46] Kubelka, J.; Eaton, W. A.; Hofrichter, J. *Journal of Molecular Biology* **2003**. *329*, 625.

[47] Kwon, O.-H.; Yoo, T. H.; Othon, C. M.; Deventer, J. A. V.; Tirrell, D. A.; Zewail, A. H. *Proceedings of the National Academy of Sciences of the United States of America* **2010**. *107*, 17101.

[48] Lakowicz, J. R. *Principles of Fluorescence Spectroscopy*. **2006**.

[49] Lehrer, S. S. *Journal of the American Chemical Society* **1970**. *92*, 3459.

[50] Li, J.; Williams, B.; Cramer, C. J.; Truhlar, D. G. *Journal of Physical Chemistry* **1999**. *110*, 724.

[51] Lill, S. O. N. *Journal of Molecular Graphics and Modeling* **2010**. *29*, 178.

[52] Lindahl, E.; Hess, B.; van der Spoel, D. *Journal of Molecular Modeling* **2001**. *7*, 306.

[53] Liu, T.; Callis, P. R.; Hesp, B. H.; de Groot, M.; Buma, W. J.; Broos, J. *Journal of the American Chemical Society* **2005**. *127*, 4104.

[54] Liu, Z.; Ensing, B.; Moore, P. B. *Journal of Chemical Theory and Computation* **2011**. *7*, 402419.

[55] Lofroth, J.-E. *Journal of Physical Chemistry* **1986**. *90*, 1160.

[56] Lu, W. Y.; Kim, J.; Qiu, W. H.; Zhong, D. P. *Chemical Physics Letters* **2004**. *388*, 120.

[57] Martin, F.; Zipse, H. *Journal of Computational Chemistry* **2005**. *26*, 97.

[58] Mataga, N.; Torihashi, Y.; Ezumi, K. *Theoretica Chimica Acta* **1964**. *2*, 158.

[59] McDonald, N. A.; Jorgensen, W. L. *Journal of Physical Chemistry B* **1998**. *102*, 8049.

[60] McMillan, A. W.; Kier, B. L.; Shu, I.; Byrne, A.; Andersen, N. H.; Parson, W. W. *Journal of Physical Chemistry B* **2013**. *117*, 1790.

[61] Meech, S. R.; Phillips, D.; Lee, A. G. *Chemical Physics* **1983**. *80*, 317.

[62] Muino, P. L.; Callis, P. R. *The Journal of Physical Chemistry B* **2009**. *113*, 2572.

[63] Nakanishi, M.; Kobayashi, M.; Tsuboi, M.; Takasaki, C.; Tamiya, N. *Biochemistry* **1980**. *19*, 3204.

[64] Nilsson, L.; Halle, B. *Proceedings of the National Academy of Sciences of the United States of America* **2005**. *102*, 13867.

[65] Osysko, A. P.; Muino, P. L. *Journal of Biophysical Chemistry* **2011**. *2*, 316.

[66] Pan, C.-P.; Callis, P. R.; Barkley, M. D. *Journal of Physical Chemistry B* **2011**. *115*, 32453253.

[67] Pan, C.-P.; Muino, P. L.; Barkley, M. D.; Callis, P. R. *Journal of Physical Chemistry B* **2011**. *115*, 32453253.

[68] Peon, J.; Pal, S. K.; Zewail, A. H. *Proceedings of the National Academy of Sciences of the United States of America* **2002**. *99*, 10964.

[69] Petrich, J. W.; Chang, M. C.; McDonald, D. B.; Fleming, G. R. *Journal of the American Chemical Society* **1983**. *105*, 3824.

[70] Price, M. L. P.; Ostrovsky, D.; Jorgensen, W. L. *Journal of Computational Chemistry* **2001**. *22*, 1340.

[71] Qiu, W.; Kao, Y.-T.; Zhang, L.; Yang, Y.; Wang, L.; Stites, W. E.; Zhong, D.; Zewail, A. H. *Proceedings of the National Academy of Sciences of the United States of America* **2006**. *103*, 13979.

[72] Ridley, J.; Zerner, M. *Theoretica Chimica Acta (Berlin)* **1973**. *32*, 111.

[73] Saito, I.; Muramatsu, S.; Sugiyama, H.; Yamamoto, A.; Matsuura, T. *Tetrahedron Letters* **1985**. *26*, 5891.

[74] Saito, I.; Sugiyama, H.; Yamamoto, A.; Muramatsu, S.; Matsuura, T. *Journal of the American Chemical Society* **1984**. *106*, 4286.

[75] Sarkar, S. S.; Udgaonkar, J. B.; Krishnamoorthy, G. *The Journal of Physical Chemistry B* **2011**. *115*, 7479.

[76] Schlick, K. H.; Lange, C. K.; Gillispie, G. D.; Cloninger, M. J. *Journal of the American Chemical Society* **2009**. *131*, 16608.

[77] Scott, J. N.; Callis, P. R. *Journal of Physical Chemistry B* **2013**. *117*, 9598.

[78] Shizuka, H.; Serizawa, M.; Kobayashi, H.; Kameta, K.; Sugiyama, H.; Matsuura, T.; Saito, I. *Journal of the American Chemical Society* **1988**. *110*, 1726.

[79] Shizuka, H.; Serizawa, M.; Shimo, T.; Saito, I.; Matsuura, T. *Journal of the American Chemical Society* **1988**. *110*, 1930.

[80] Singh, U. C.; Kollman, P. A. *Journal of Computational Chemistry* **1984**. *5*, 129.

[81] Suzuki, S.; Fujii, T.; Irnal, A.; Akatiori, H. *Journal of Physical Chemistry* **1977**. *81*, 1592.

[82] Teale, F. W. J.; Weber, G. *Biochemical Journal* **1957**. *65*, 476.

[83] Thompson, M. A.; Zerner, M. C. *Journal of the American Chemical Society* **1991**. *113*, 8210.

[84] Tomasi, J.; Mennucci, B.; Cammi, R. *Chemical Reviews* **2005**. *105*, 2999.

[85] Toptygin, D.; Brand, L. personal communication, **2012**.

[86] Toptygin, D.; Brand, L. *Biophysical Journal* **2012**. *102*, 217a.

[87] Tsong, T. Y. *The Journal of Biological Chemistry* **1974**. *249*, 1988.

[88] Tusell, J. R. *Computation of tryptophan fluorescence quenching by amide and histidine*. Ph.D. thesis, Montana State University, **2011**.

[89] van der Spoel, D.; Lindahl, E.; Hess, B.; Groenhof, G.; Mark, A. E.; Berendsen, H. J. C. *Journal of Computational Chemistry* **2005**. *26*, 1701.

[90] Visser, N.; Westphal, A.; Nabuurs, S.; van Hoek, A.; van Mierlo, C.; Visser, A.; Broos, J.; van Amerongen, H. *FEBS Letters* **2009**. *583*, 2785.

[91] Vivian, J. T.; Callis, P. R. *Biophysical Journal* **2001**. *80*, 2093.

[92] Vos, E. P. P.; Bokhove, M.; Hesp, B. H.; Broos, J. *Biochemistry* **2009**. *48*, 5284.

[93] Watkins, E. K.; Jorgensen, W. L. *Journal of Physical Chemistry A* **2001**. *105*, 4118.

[94] Weinryb, I.; Steiner, R. F. *Biochemistry* **1968**. *7*, 2488.

[95] Willis, K. J.; Szabo, A. G.; Kracjarski, D. T. *Chemical Physics Letters* **1991**. *182*, 614.

[96] Winkler, G. R.; Harkins, S. B.; Lee, J. C.; Gray, H. B. *The Journal of Physical Chemistry B* **2006**. *110*, 7058.

[97] Xu, J.; Chen, B.; Callis, P.; Muino, P. L.; Rozeboom, H.; Broos, J.; Toptygin, D.; Brand, L.; Knutson, J. R. *Journal of Physical Chemistry B* **2015**. *119*, 4230.

[98] Xu, J.; Knutson, J. R. *Journal of Physical Chemistry B* **2009**. *113*, 12084.

[99] Xu, J.; Toptygin, D.; Graver, K. J.; Albertini, R. A.; Savtchenko, R. S.; Meadow, N. D.; Roseman, S.; Callis, P. R.; Brand, L.; Knutson, J. R. *Journal of the American Chemical Society* **2006**. *128*, 1214.

[100] Yu, H.-T.; Colucci, W. J.; McLaughlin, M. L.; Barkley, M. D. *Journal of the American Chemical Society* **1992**. *114*, 8449.

[101] Zhang, L. Y.; Wang, L. J.; Kao, Y. T.; Qiu, W. H.; Yang, Y.; Okobiah, O.; Zhong, D. P. *Proceedings of the National Academy of Sciences of the United States of America* **2007**. *104*, 18461.

[102] Zhao, Y.; Truhlar, D. *Theoretical Chemistry Accounts* **2008**. *120*, 215.

APPENDICES

APPENDIX A

EXTRA DAS

This chapter contains the decay associated spectra for peptides with X residues Leu, Met, Arg, Asp.

Figure A.1: Average Decay Associated Spectra of Trp-Arg at pH(D) 5. Error bars are +/- one standard deviation.

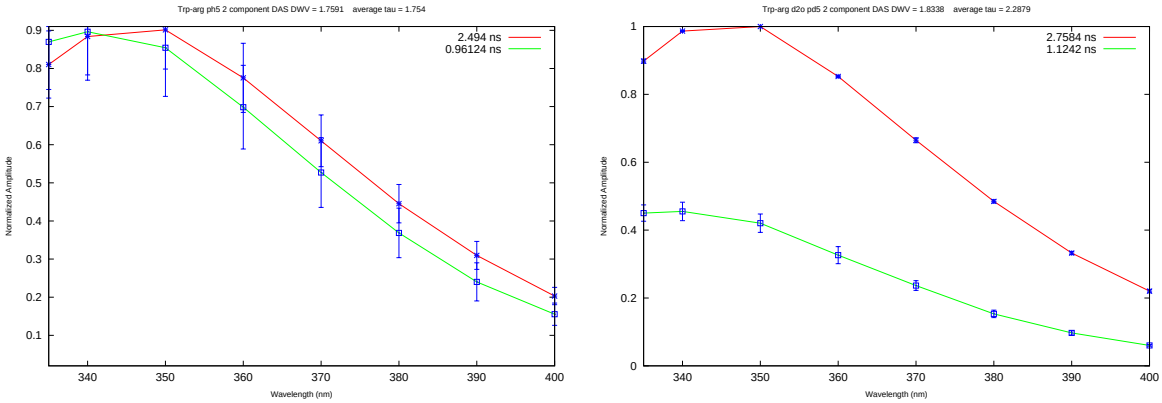

(a) Trp-Arg pH 5 DAS

(b) Trp-Arg pD 5 DAS

Figure A.2: Average Decay Associated Spectra of 5FTrp-Arg at pH(D) 5. Error bars are +/- one standard deviation.

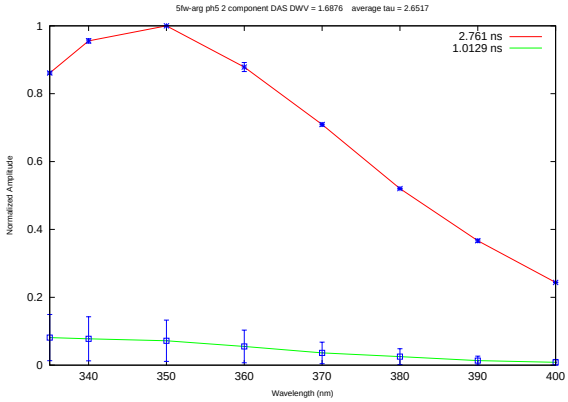

(a) 5FTrp-Arg pH 5 DAS

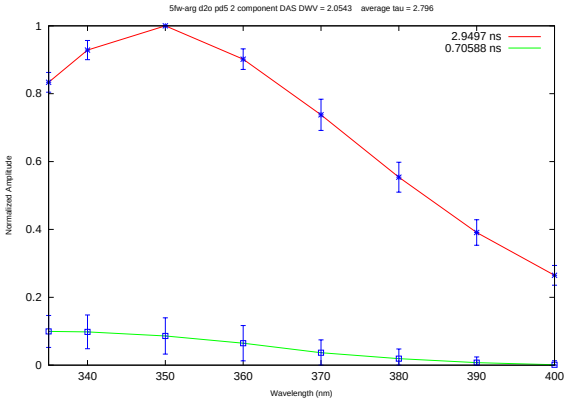

(b) 5FTrp-Arg pD 5 DAS

Figure A.3: Average Decay Associated Spectra of Arg-Trp at pH(D) 5. Error bars are +/- one standard deviation.

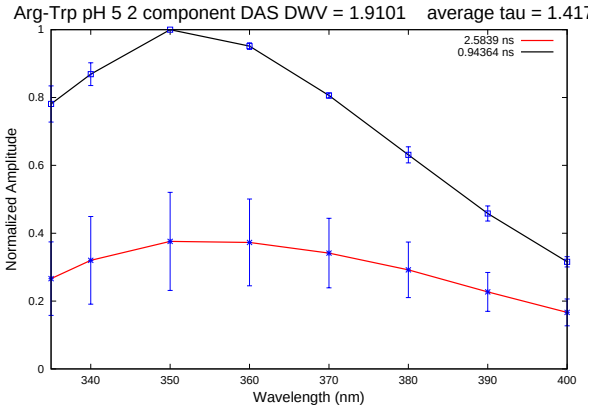

(a) Arg-Trp pH 5 DAS

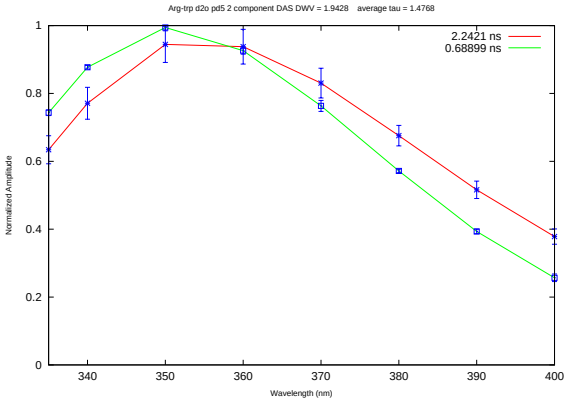

(b) Arg-Trp pD 5 DAS

Figure A.4: Average Decay Associated Spectra of Trp-Asp at pH(D) 5. Error bars are +/- one standard deviation.

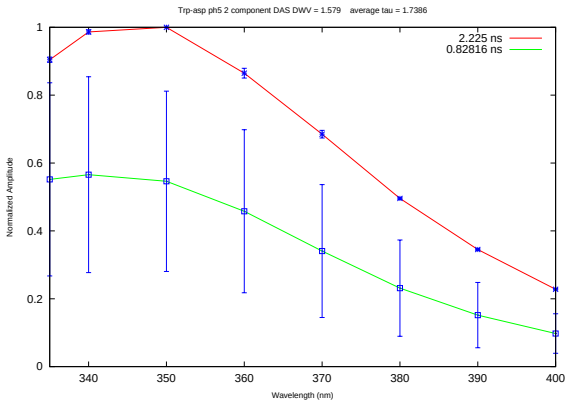

(a) Trp-Asp pH 5 DAS

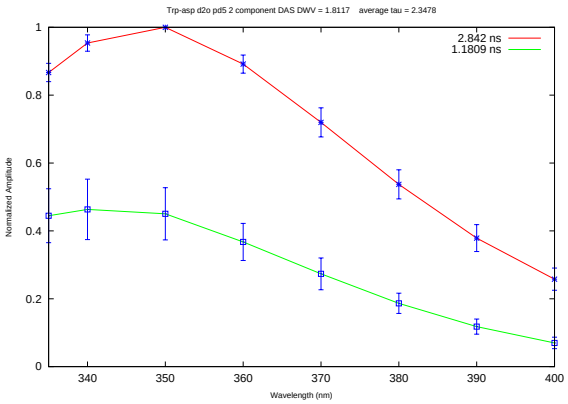

(b) Trp-Asp pD 5 DAS

Figure A.5: Average Decay Associated Spectra of 5FTrp-Asp at pH(D) 5. Error bars are +/- one standard deviation.

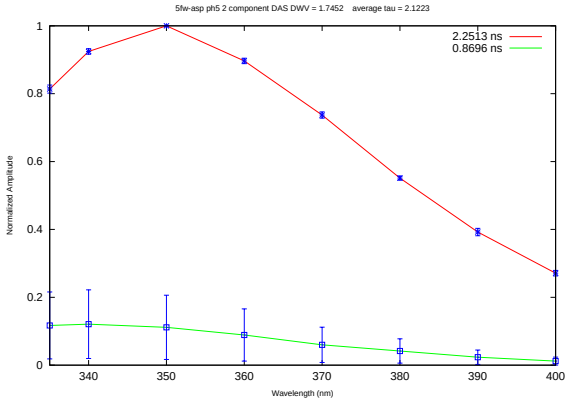

(a) 5FTrp-Asp pH 5 DAS

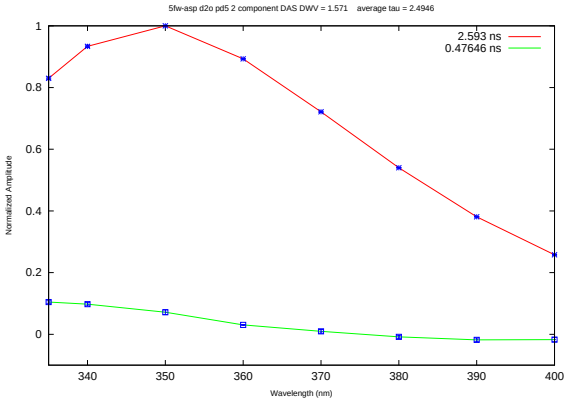

(b) 5FTrp-Asp pD 5 DAS

Figure A.6: Average Decay Associated Spectra of Asp-Trp at pH(D) 5. Error bars are +/- one standard deviation.

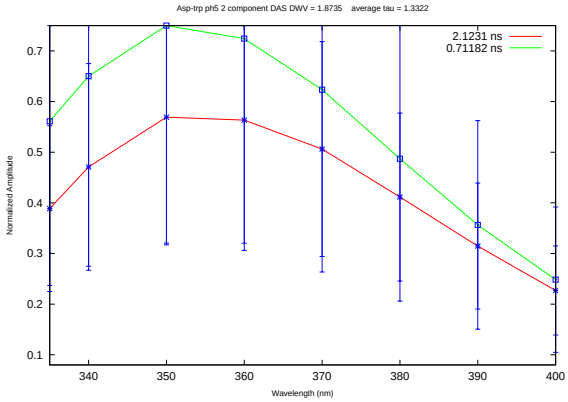

(a) Asp-Trp pH 5 DAS

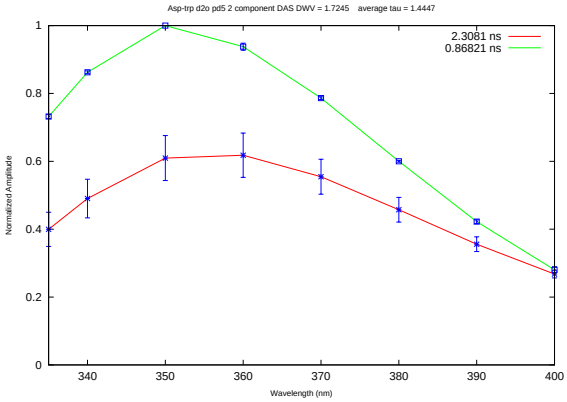

(b) Asp-Trp pD 5 DAS

Figure A.7: Average Decay Associated Spectra of Asp-5FTrp at pH(D) 5. Error bars are +/- one standard deviation.

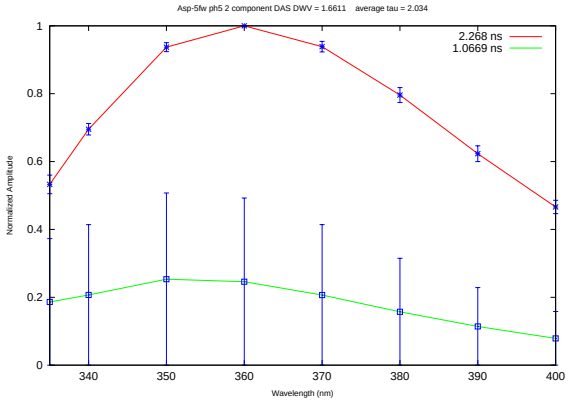

(a) Asp-5FTrp pH 5 DAS

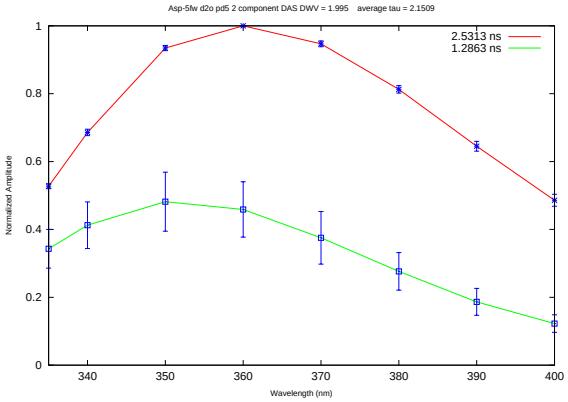

(b) Asp-5FTrp pD 5 DAS

Figure A.8: Average Decay Associated Spectra of Trp-Leu at pH(D) 5. Error bars are +/- one standard deviation.

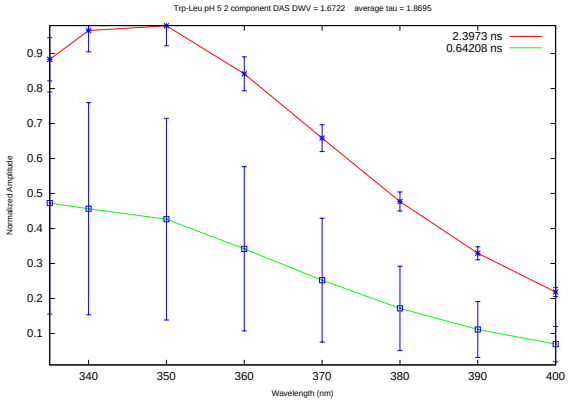

(a) Trp-Leu pH 5 DAS

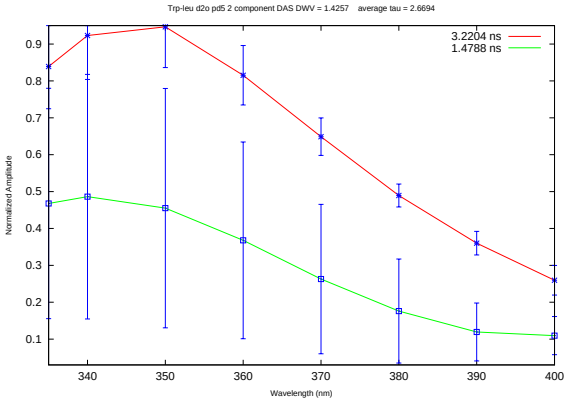

(b) Trp-Leu pD 5 DAS

Figure A.9: Average Decay Associated Spectra of 5FTrp-Leu at pH(D) 5. Error bars are +/- one standard deviation.

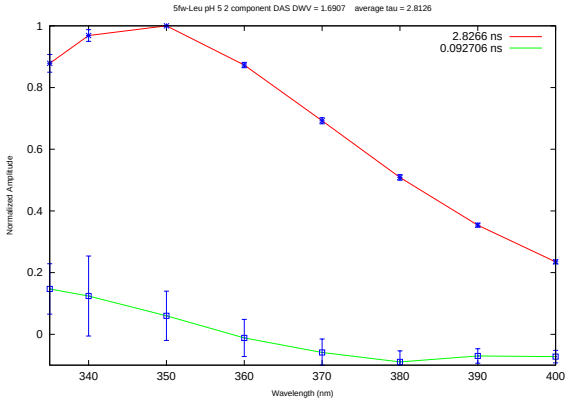

(a) 5FTrp-Leu pH 5 DAS

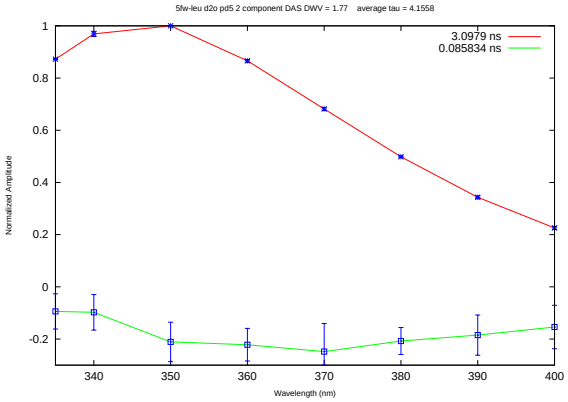

(b) 5FTrp-Leu pD 5 DAS

Figure A.10: Average Decay Associated Spectra of Leu-Trp at pH(D) 5. Error bars are +/- one standard deviation.

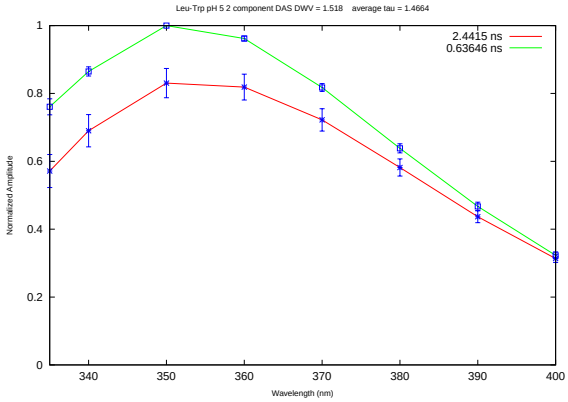

(a) Leu-Trp pH 5 DAS

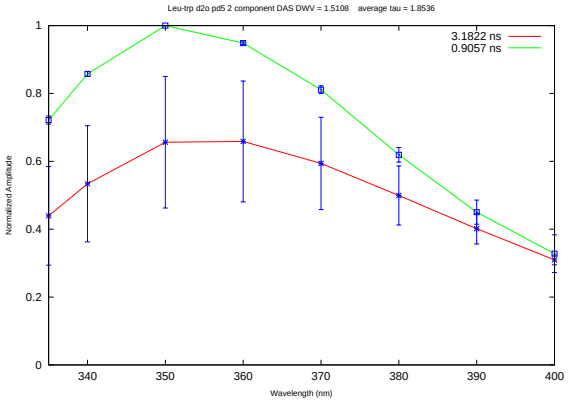

(b) Leu-Trp pD 5 DAS

Figure A.11: Average Decay Associated Spectra of Leu-5FTrp at pH(D) 5. Error bars are +/- one standard deviation.

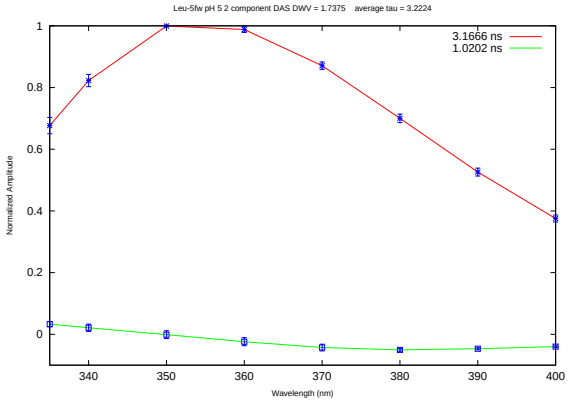

(a) Leu-5FTrp pH 5 DAS

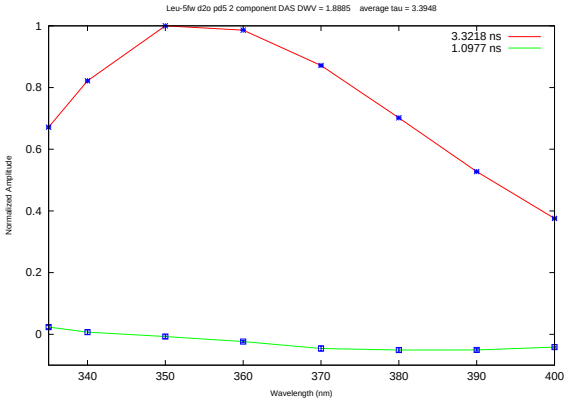

(b) Leu-5FTrp pD 5 DAS

Figure A.12: Average Decay Associated Spectra of Trp-Met at pH(D) 5. Error bars are +/- one standard deviation.

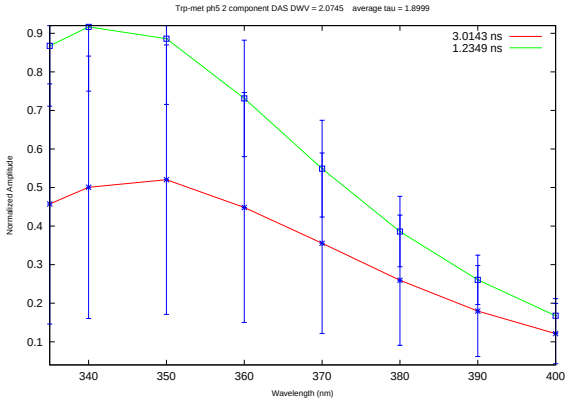

(a) Trp-Met pH 5 DAS

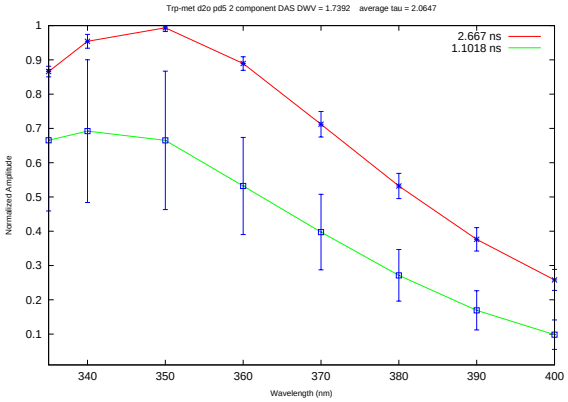

(b) Trp-Met pD 5 DAS

Figure A.13: Average Decay Associated Spectra of 5FTrp-Met at pH(D) 5. Error bars are +/- one standard deviation.

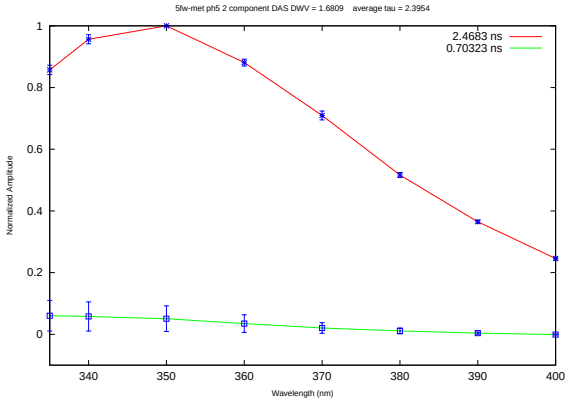

(a) 5FTrp-Met pH 5 DAS

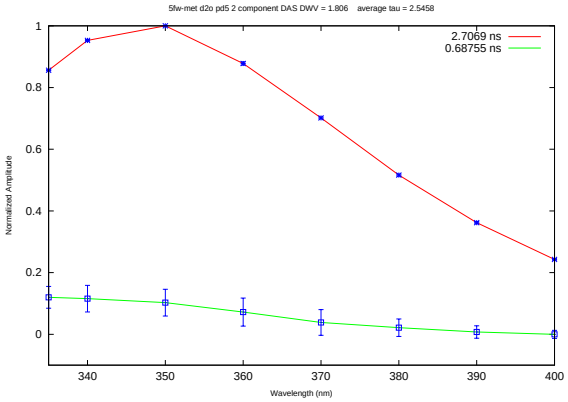

(b) 5FTrp-Met pD 5 DAS

Figure A.14: Average Decay Associated Spectra of Met-Trp at pH(D) 5. Error bars are +/- one standard deviation.

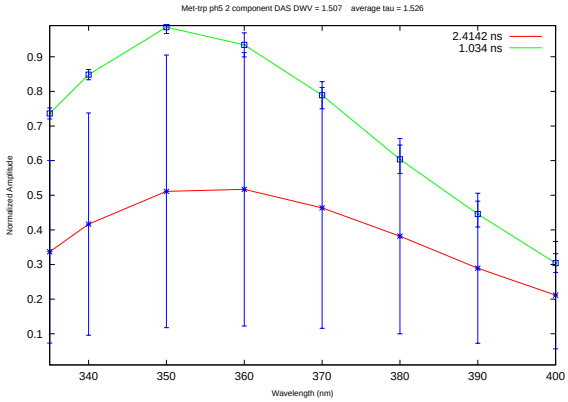

(a) Met-Trp pH 5 DAS

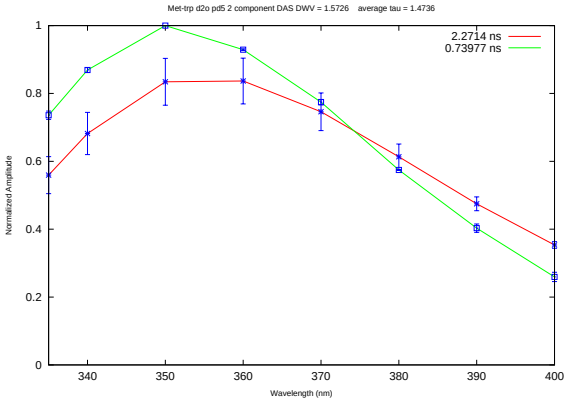

(b) Met-Trp pD 5 DAS

Figure A.15: Average Decay Associated Spectra of Met-5FTrp at pH(D) 5. Error bars are +/- one standard deviation.

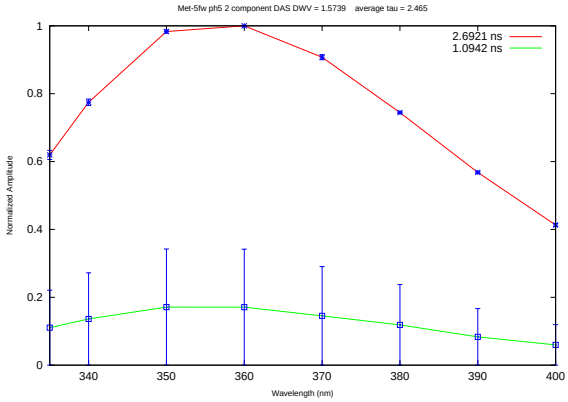

(a) Met-5FTrp pH 5 DAS

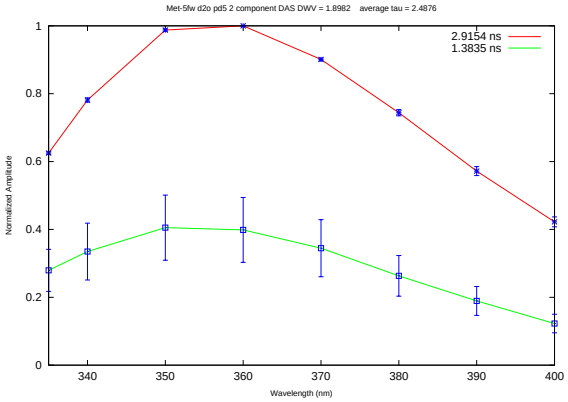

(b) Met-5FTrp pD 5 DAS

Figure A.16: Average Decay Associated Spectra of Trp-Arg at pH(D) 10. Error bars are +/- one standard deviation.

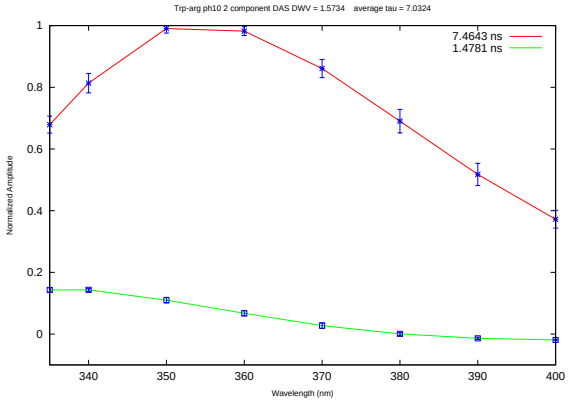

(a) Trp-Arg pH 10 DAS

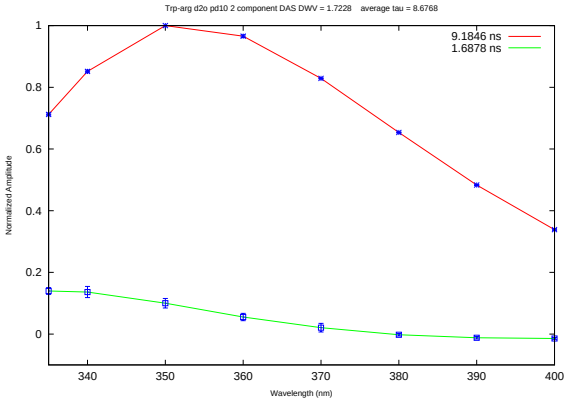

(b) Trp-Arg pD 10 DAS

Figure A.17: Average Decay Associated Spectra of 5FTrp-Arg at pH(D) 10. Error bars are +/- one standard deviation.

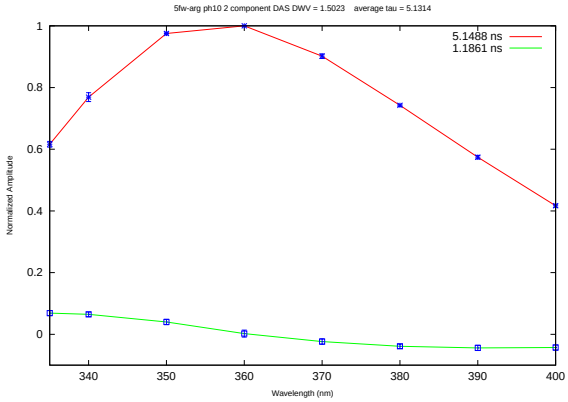

(a) 5FTrp-Arg pH 10 DAS

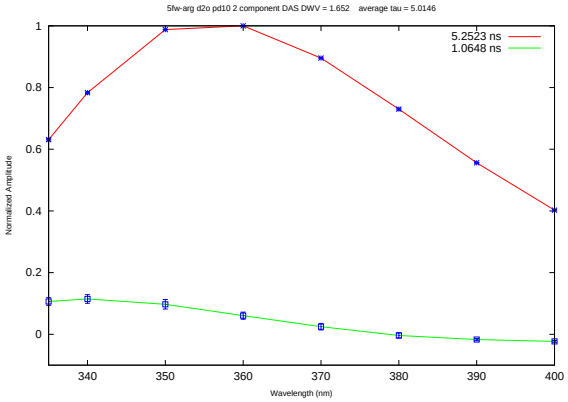

(b) 5FTrp-Arg pD 10 DAS

Figure A.18: Average Decay Associated Spectra of Arg-Trp at pH(D) 10. Error bars are +/- one standard deviation.

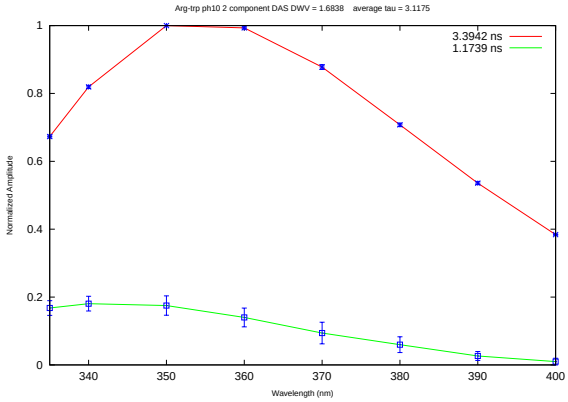

(a) Arg-Trp pH 10 DAS

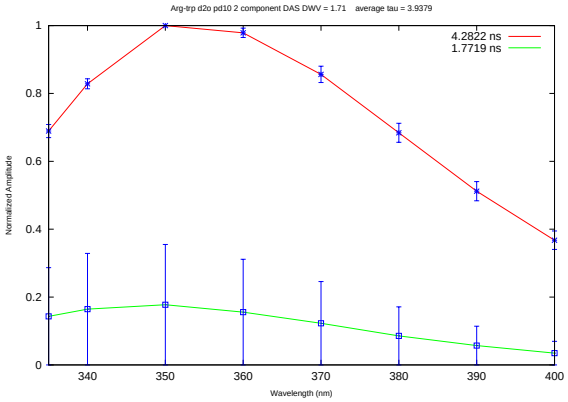

(b) Arg-Trp pD 10 DAS

Figure A.19: Average Decay Associated Spectra of Trp-Asp at pH(D) 10. Error bars are +/- one standard deviation.

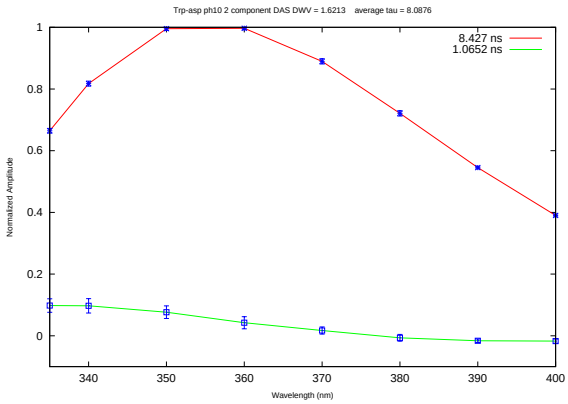

(a) Trp-Asp pH 10 DAS

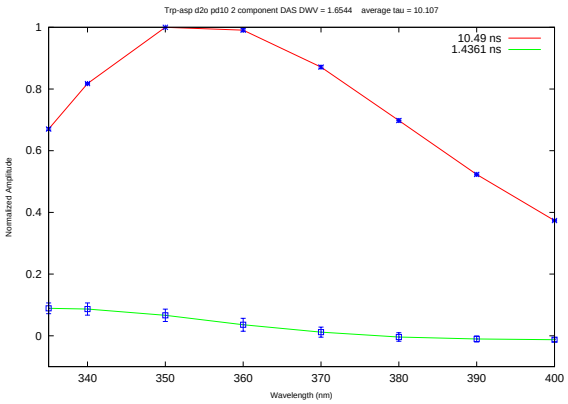

(b) Trp-Asp pD 10 DAS

Figure A.20: Average Decay Associated Spectra of 5FTrp-Asp at pH(D) 10. Error bars are +/- one standard deviation.

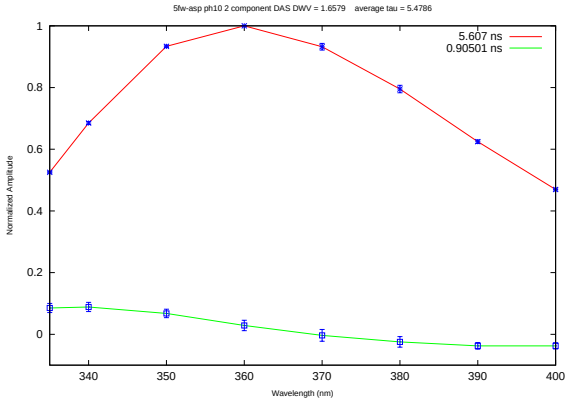

(a) 5FTrp-Asp pH 10 DAS

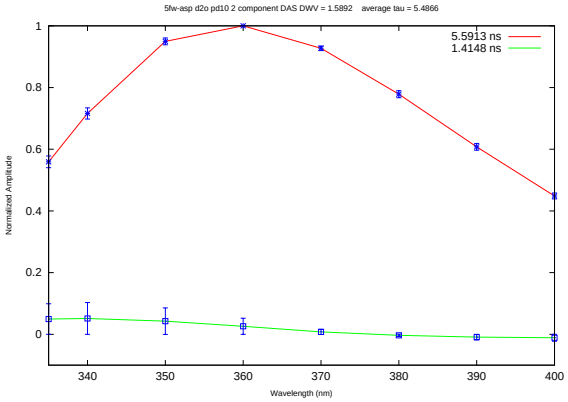

(b) 5FTrp-Asp pD 10 DAS

Figure A.21: Average Decay Associated Spectra of Asp-Trp at pH(D) 10. Error bars are +/- one standard deviation.

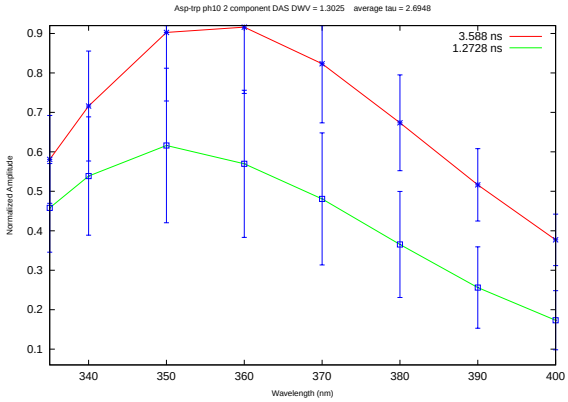

(a) Asp-Trp pH 10 DAS

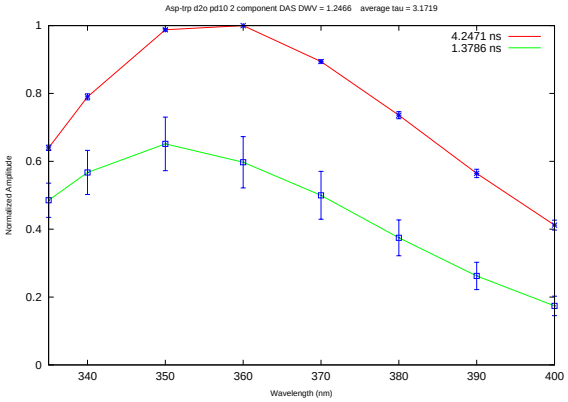

(b) Asp-Trp pD 10 DAS

Figure A.22: Average Decay Associated Spectra of Asp-5FTrp at pH(D) 10. Error bars are +/- one standard deviation.

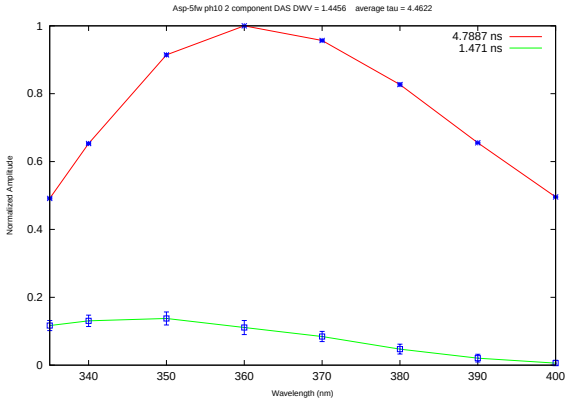

(a) Asp-5FTrp pH 10 DAS

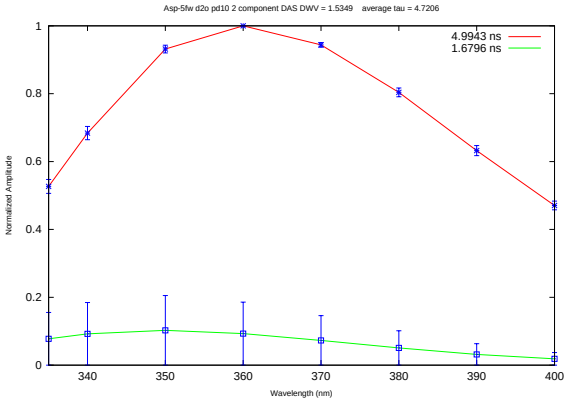

(b) Asp-5FTrp pD 10 DAS

Figure A.23: Average Decay Associated Spectra of Trp-Leu at pH(D) 10. Error bars are +/- one standard deviation.

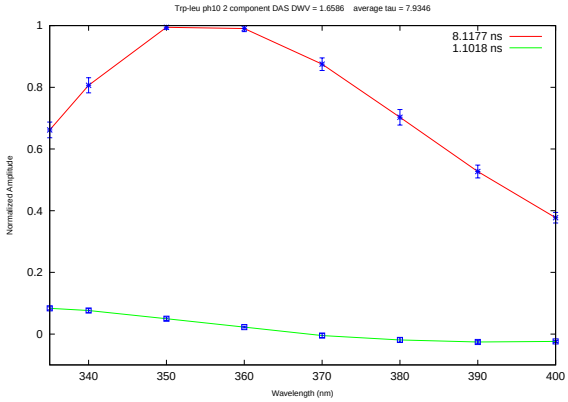

(a) Trp-Leu pH 10 DAS

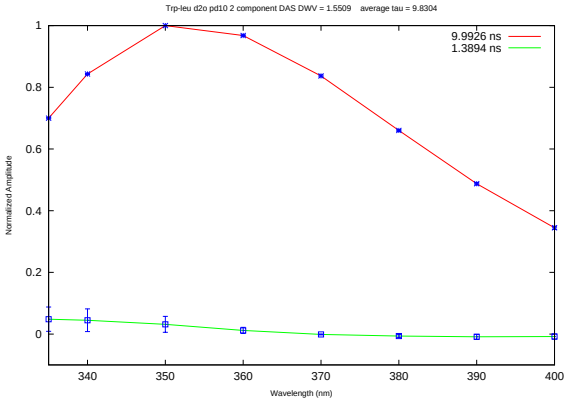

(b) Trp-Leu pD 10 DAS

Figure A.24: Average Decay Associated Spectra of 5FTrp-Leu at pH(D) 10. Error bars are +/- one standard deviation.

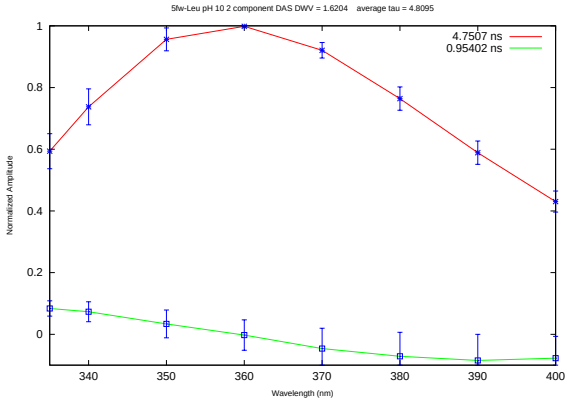

(a) 5FTrp-Leu pH 10 DAS

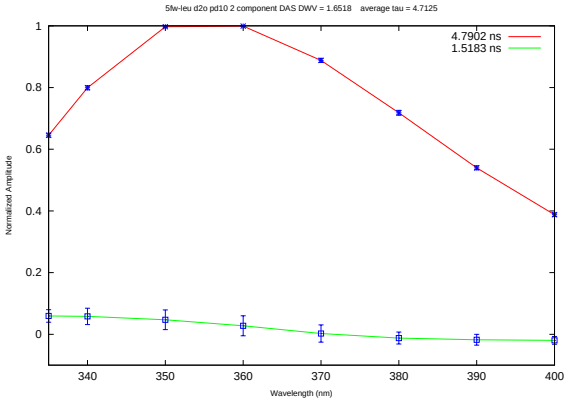

(b) 5FTrp-Leu pD 10 DAS

Figure A.25: Average Decay Associated Spectra of Leu-Trp at pH(D) 10. Error bars are +/- one standard deviation.

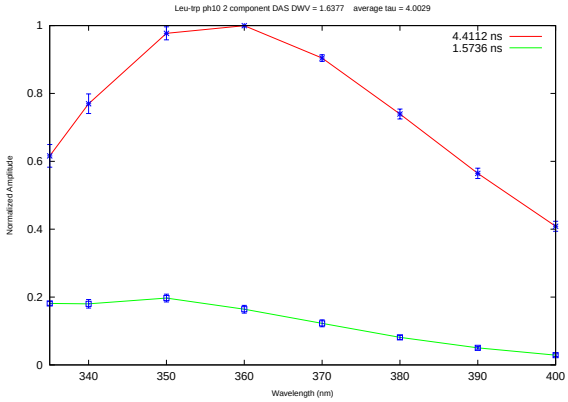

(a) Leu-Trp pH 10 DAS

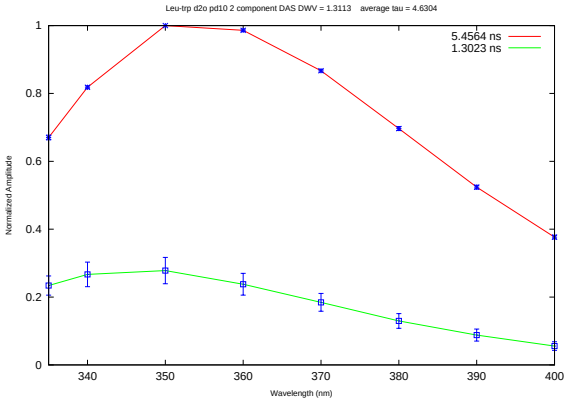

(b) Leu-Trp pD 10 DAS

Figure A.26: Average Decay Associated Spectra of Leu-5FTrp at pH(D) 10. Error bars are +/- one standard deviation.

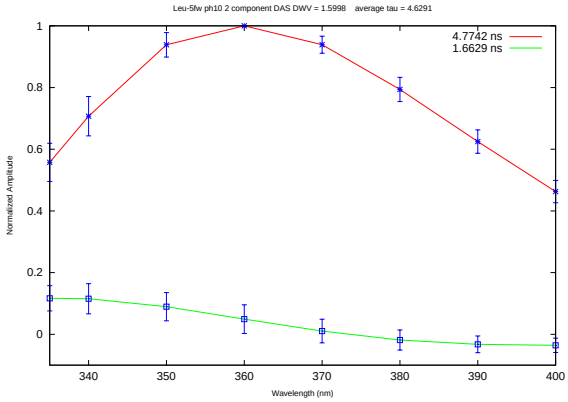

(a) Leu-5FTrp pH 10 DAS

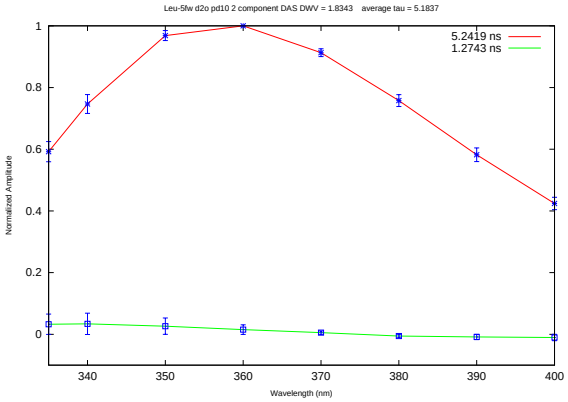

(b) Leu-5FTrp pD 10 DAS

Figure A.27: Average Decay Associated Spectra of Trp-Met at pH(D) 10. Error bars are +/- one standard deviation.

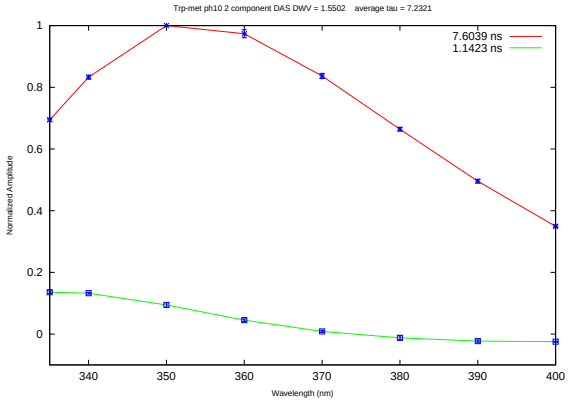

(a) Trp-Met pH 10 DAS

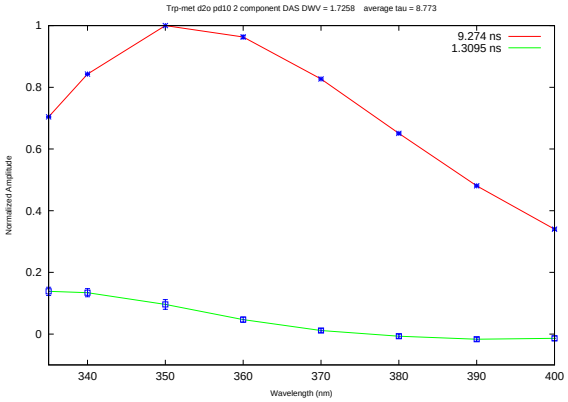

(b) Trp-Met pD 10 DAS

Figure A.28: Average Decay Associated Spectra of 5FTrp-Met at pH(D) 10. Error bars are +/- one standard deviation.

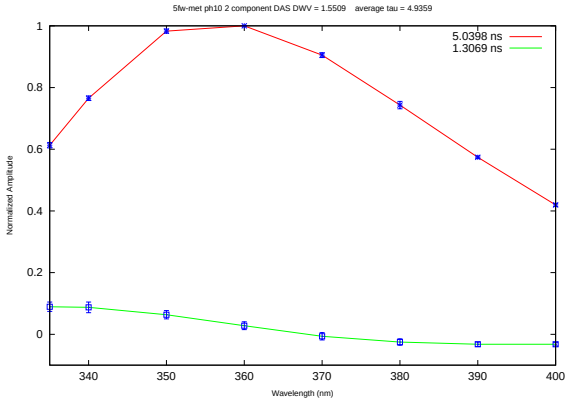

(a) 5FTrp-Met pH 10 DAS

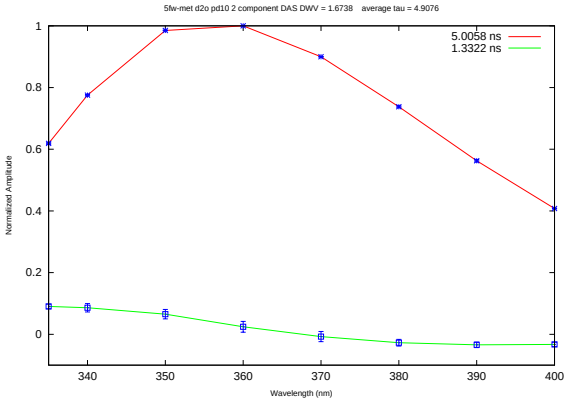

(b) 5FTrp-Met pD 10 DAS

Figure A.29: Average Decay Associated Spectra of Met-Trp at pH(D) 10. Error bars are +/- one standard deviation.

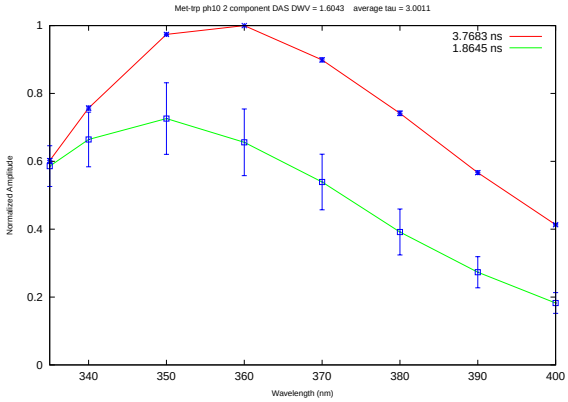

(a) Met-Trp pH 10 DAS

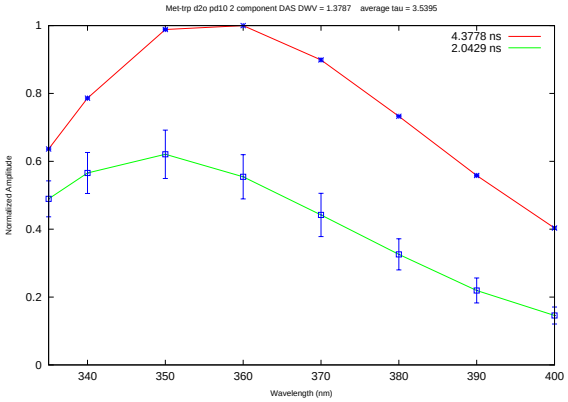

(b) Met-Trp pD 10 DAS

Figure A.30: Average Decay Associated Spectra of Met-5FTrp at pH(D) 10. Error bars are +/- one standard deviation.

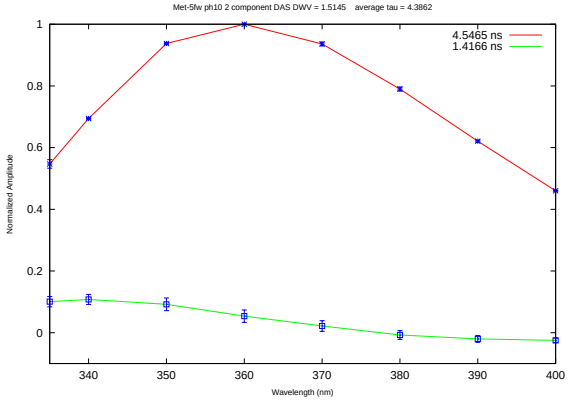

(a) Met-5FTrp pH 10 DAS

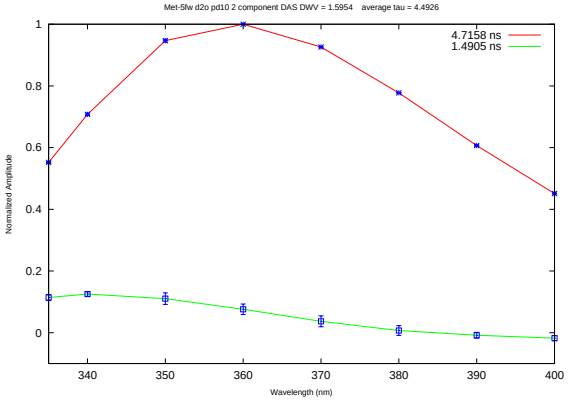

(b) Met-5FTrp pD 10 DAS

APPENDIX B

EXTRA FRACTIONAL FLUORESCENCE PLOTS

This chapter compares the integrated fluorescence to the fractional fluorescence of the 2 exponential fits used in this study. The fact that there is very little difference between these further confirms the completeness of the fits used in this thesis work.

Figure B.1: Fractional fluorescence plot of 2 exponential fit and integrated waveforms as a function of wavelength for Trp-Arg at pH(D) 5.

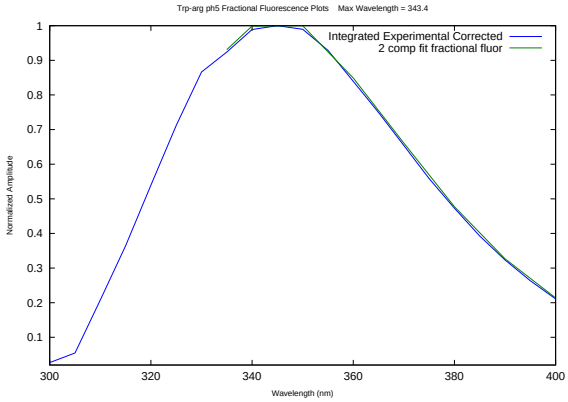

(a) Trp-Arg pH 5 DAS

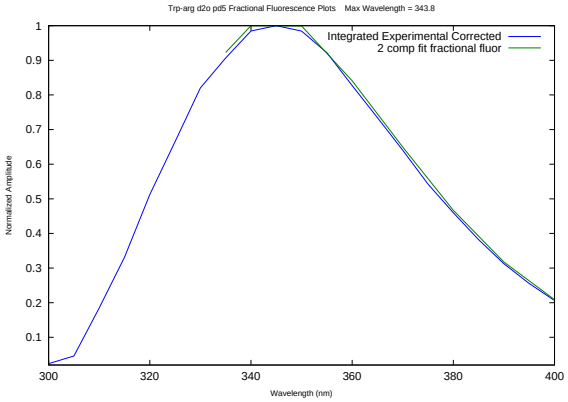

(b) Trp-Arg pD 5 DAS

Figure B.2: Fractional fluorescence plot of 2 exponential fit and integrated waveforms as a function of wavelength for 5FTrp-Arg at pH(D) 5.

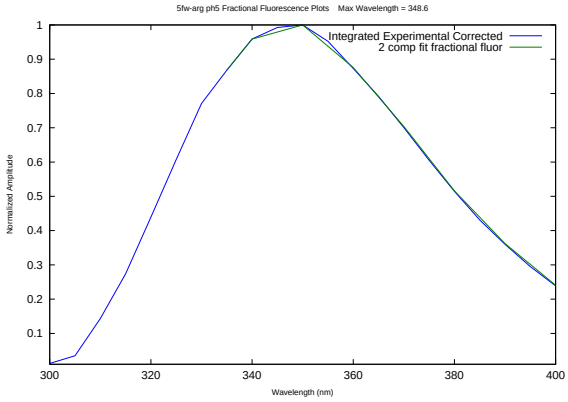

(a) 5FTrp-Arg pH 5 DAS

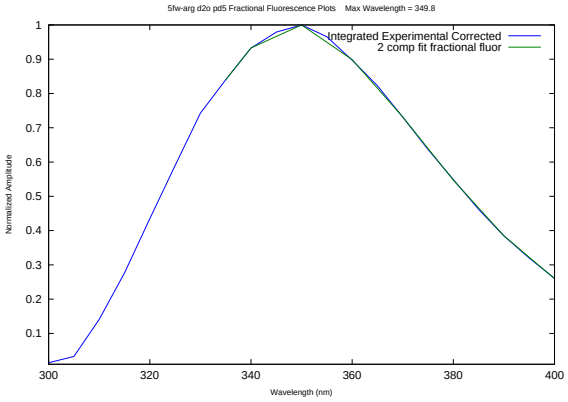

(b) 5FTrp-Arg pD 5 DAS

Figure B.3: Fractional fluorescence plot of 2 exponential fit and integrated waveforms as a function of wavelength for Arg-Trp at pH(D) 5.

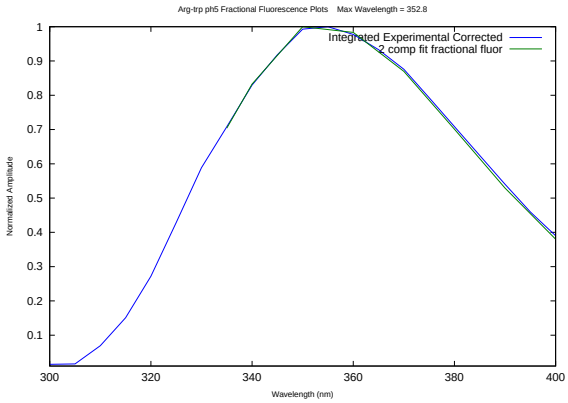

(a) Arg-Trp pH 5 DAS

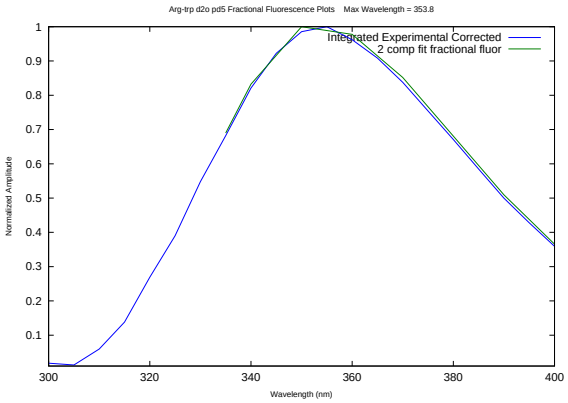

(b) Arg-Trp pD 5 DAS

Figure B.4: Fractional fluorescence plot of 2 exponential fit and integrated waveforms as a function of wavelength for Trp-Asp at pH(D) 5.

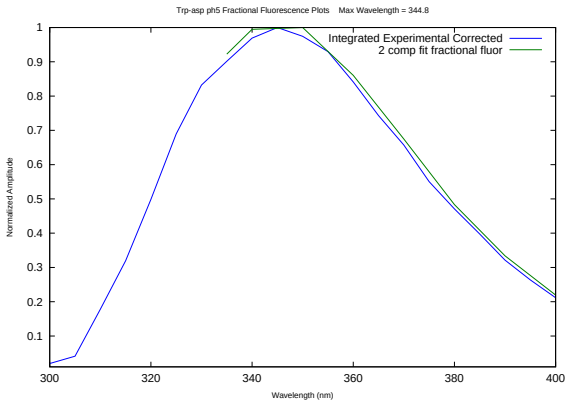

(a) Trp-Asp pH 5 DAS

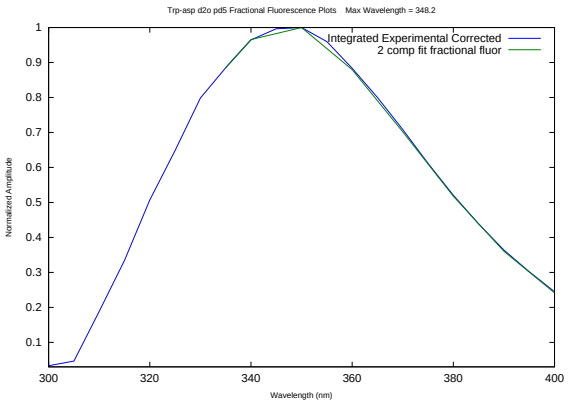

(b) Trp-Asp pD 5 DAS

Figure B.5: Fractional fluorescence plot of 2 exponential fit and integrated waveforms as a function of wavelength for 5FTrp-Asp at pH(D) 5.

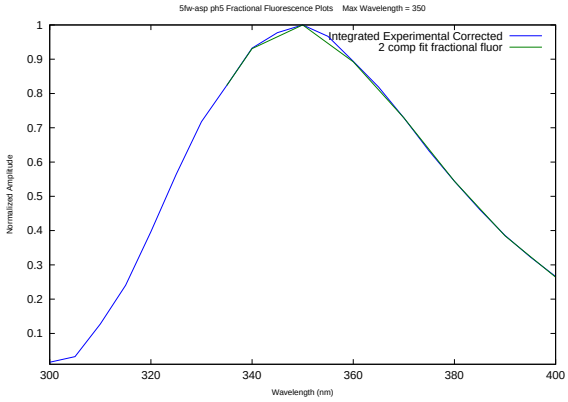

(a) 5FTrp-Asp pH 5 DAS

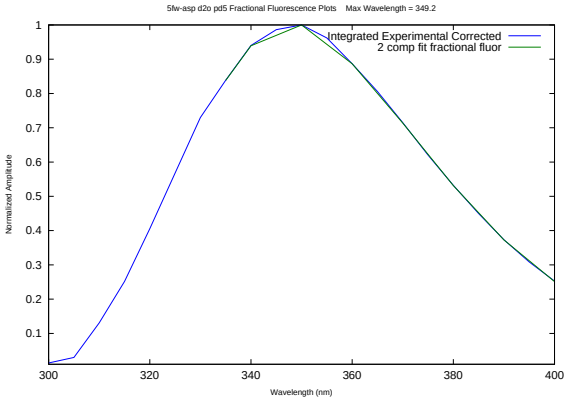

(b) 5FTrp-Asp pD 5 DAS

Figure B.6: Fractional fluorescence plot of 2 exponential fit and integrated waveforms as a function of wavelength for Asp-Trp at pH(D) 5.

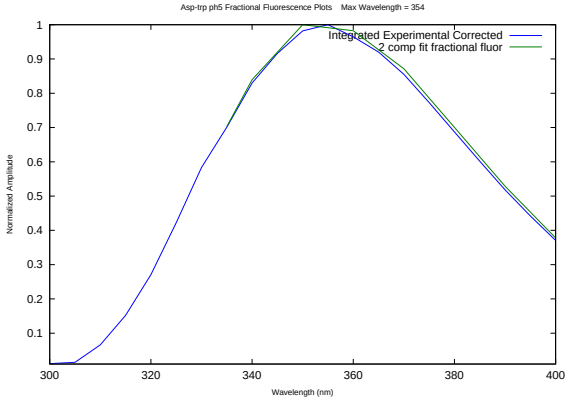

(a) Asp-Trp pH 5 DAS

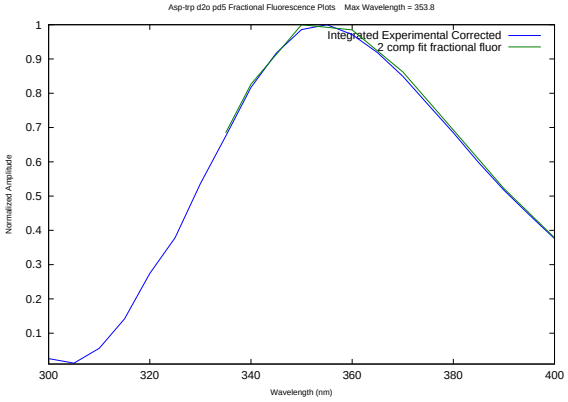

(b) Asp-Trp pD 5 DAS

Figure B.7: Fractional fluorescence plot of 2 exponential fit and integrated waveforms as a function of wavelength for Asp-5FTrp at pH(D) 5.

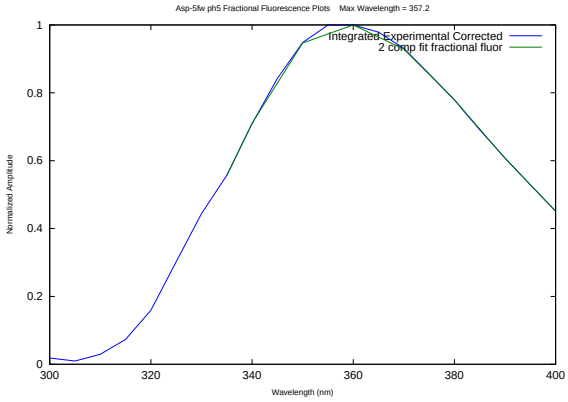

(a) Asp-5FTrp pH 5 DAS

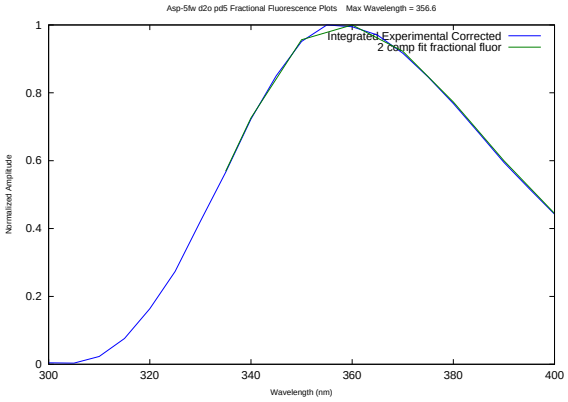

(b) Asp-5FTrp pD 5 DAS

Figure B.8: Fractional fluorescence plot of 2 exponential fit and integrated waveforms as a function of wavelength for Trp-Leu at pH(D) 5.

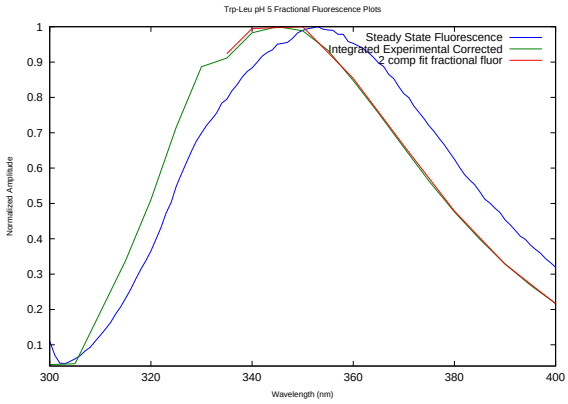

(a) Trp-Leu pH 5 DAS

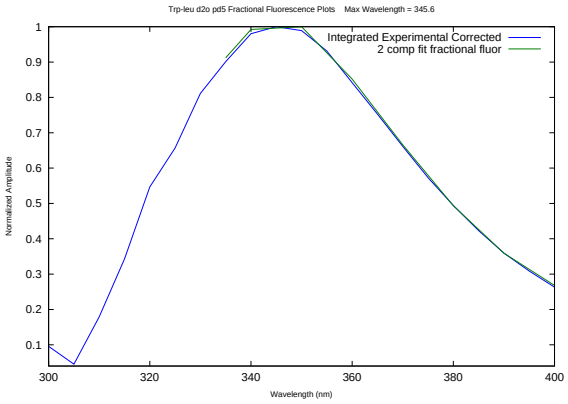

(b) Trp-Leu pD 5 DAS

Figure B.9: Fractional fluorescence plot of 2 exponential fit and integrated waveforms as a function of wavelength for 5FTrp-Leu at pH(D) 5.

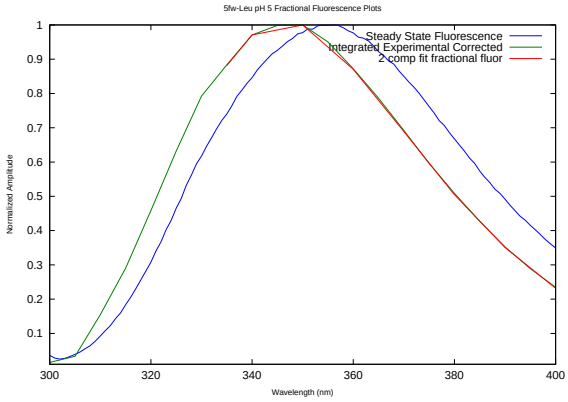

(a) 5FTrp-Leu pH 5 DAS

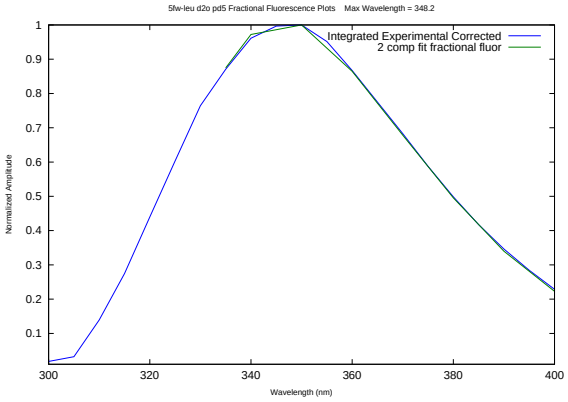

(b) 5FTrp-Leu pD 5 DAS

Figure B.10: Fractional fluorescence plot of 2 exponential fit and integrated waveforms as a function of wavelength for Leu-Trp at pH(D) 5.

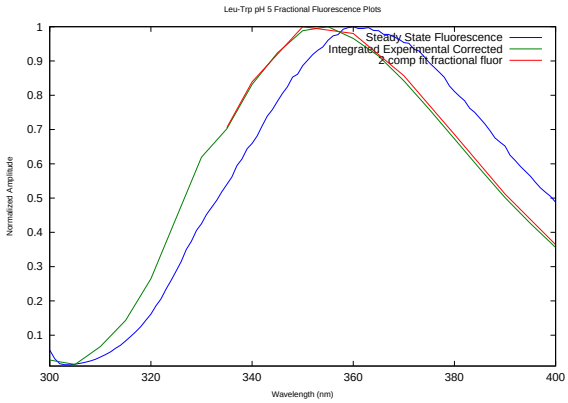

(a) Leu-Trp pH 5 DAS

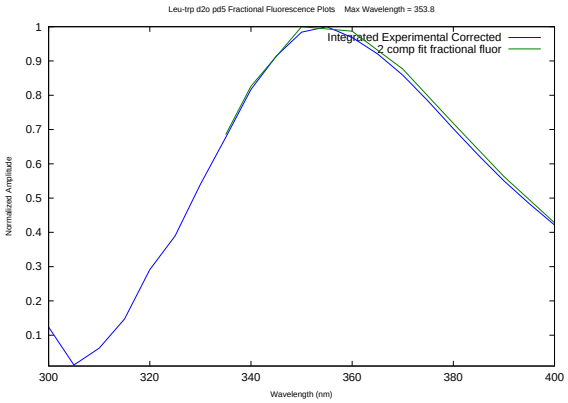

(b) Leu-Trp pD 5 DAS

Figure B.11: Fractional fluorescence plot of 2 exponential fit and integrated waveforms as a function of wavelength for Leu-5FTrp at pH(D) 5.

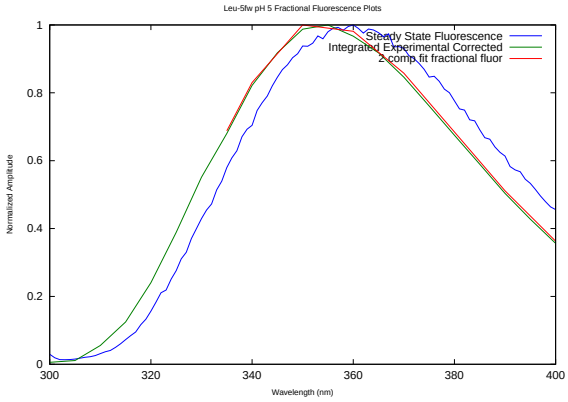

(a) Leu-5FTrp pH 5 DAS

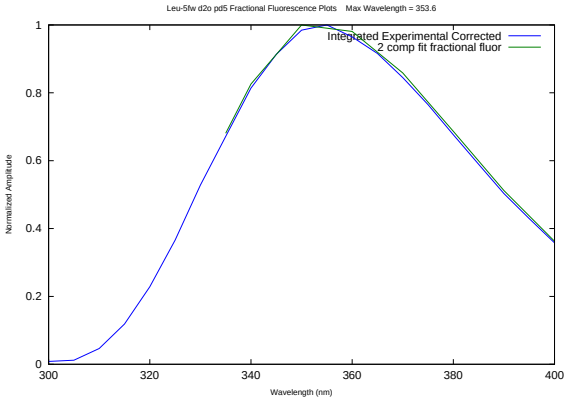

(b) Leu-5FTrp pD 5 DAS

Figure B.12: Fractional fluorescence plot of 2 exponential fit and integrated waveforms as a function of wavelength for Trp-Met at pH(D) 5.

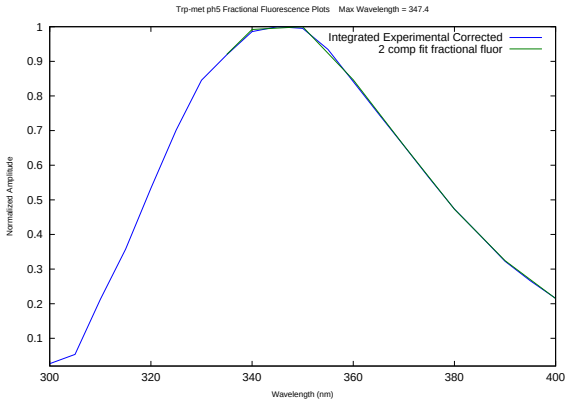

(a) Trp-Met pH 5 DAS

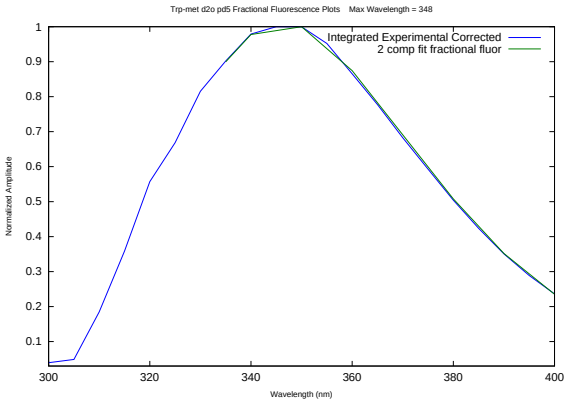

(b) Trp-Met pD 5 DAS

Figure B.13: Fractional fluorescence plot of 2 exponential fit and integrated waveforms as a function of wavelength for 5FTrp-Met at pH(D) 5.

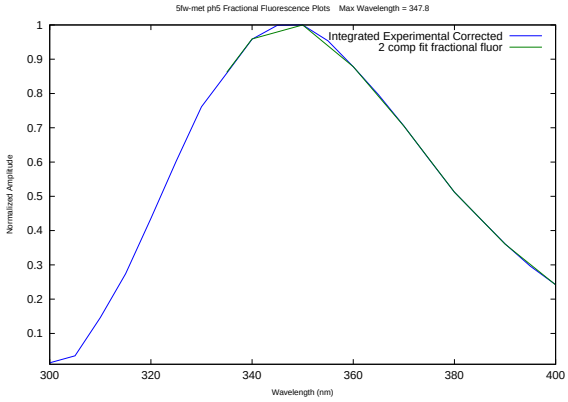

(a) 5FTrp-Met pH 5 DAS

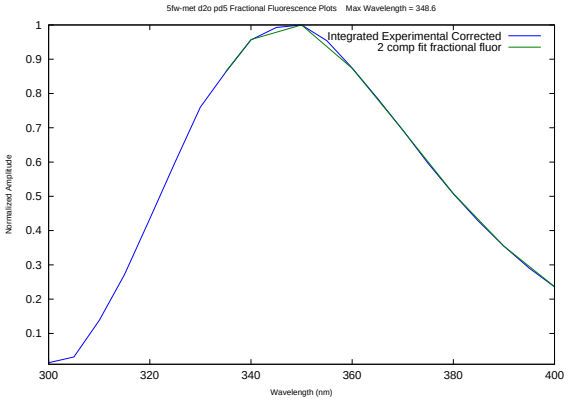

(b) 5FTrp-Met pD 5 DAS

Figure B.14: Fractional fluorescence plot of 2 exponential fit and integrated waveforms as a function of wavelength for Met-Trp at pH(D) 5.

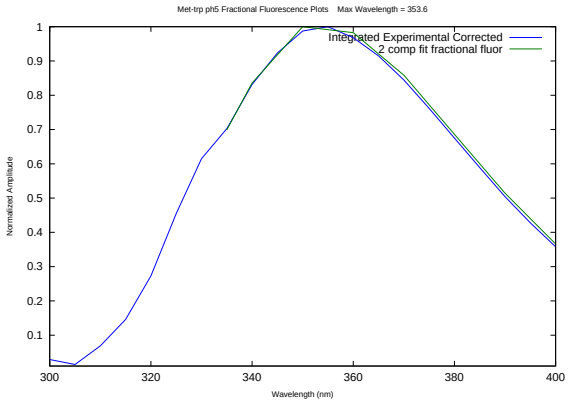

(a) Met-Trp pH 5 DAS

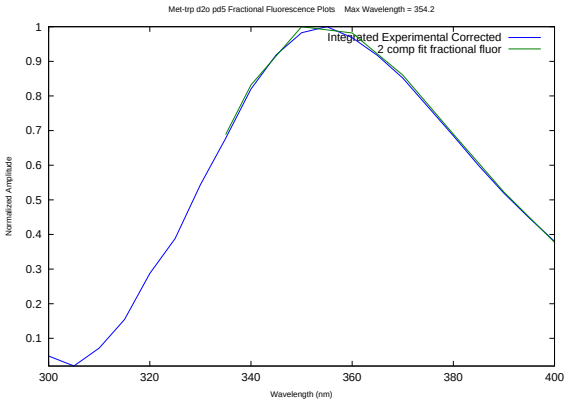

(b) Met-Trp pD 5 DAS

Figure B.15: Fractional fluorescence plot of 2 exponential fit and integrated waveforms as a function of wavelength for Met-5FTrp at pH(D) 5.

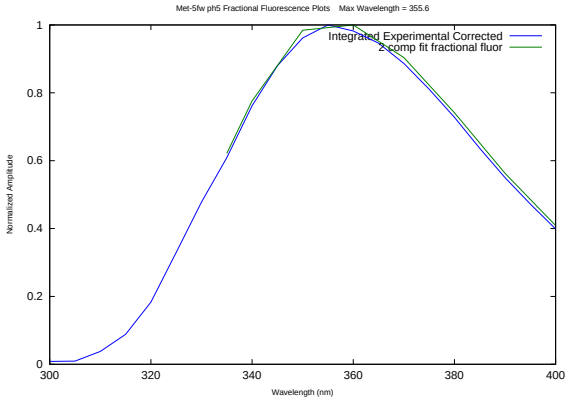

(a) Met-5FTrp pH 5 DAS

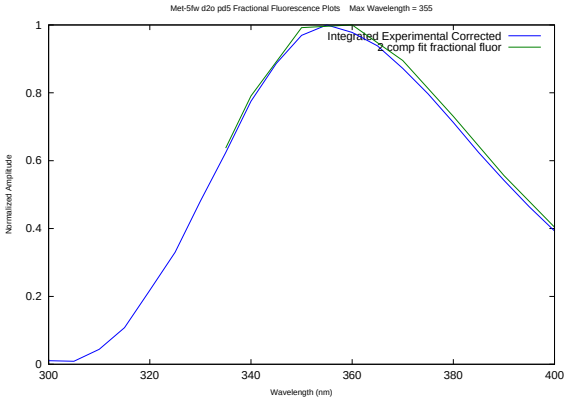

(b) Met-5FTrp pD 5 DAS

Figure B.16: Fractional fluorescence plot of 2 exponential fit and integrated waveforms as a function of wavelength for Trp-Arg at pH(D) 10.

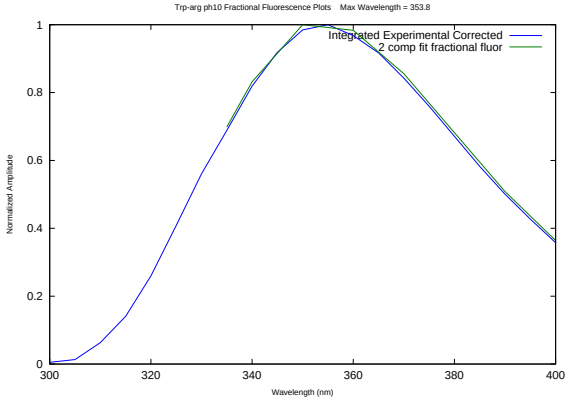

(a) Trp-Arg pH 10 DAS

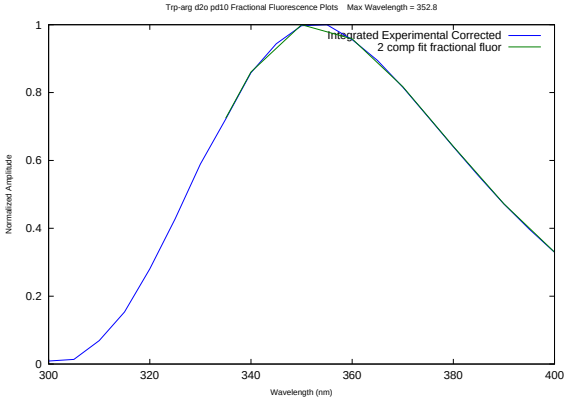

(b) Trp-Arg pD 10 DAS

Figure B.17: Fractional fluorescence plot of 2 exponential fit and integrated waveforms as a function of wavelength for 5FTrp-Arg at pH(D) 10.

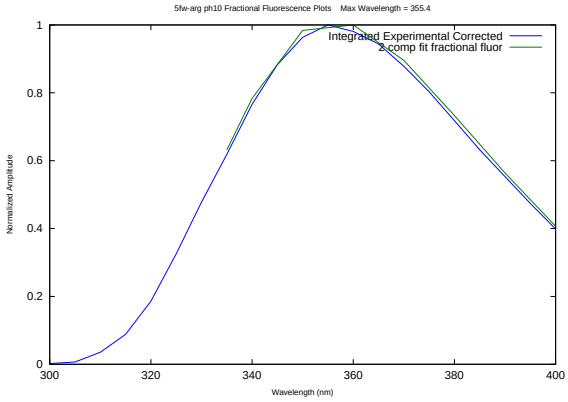

(a) 5FTrp-Arg pH 10 DAS

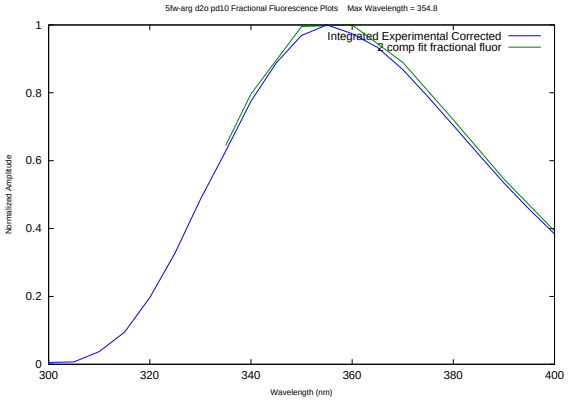

(b) 5FTrp-Arg pD 10 DAS

Figure B.18: Fractional fluorescence plot of 2 exponential fit and integrated waveforms as a function of wavelength for Arg-Trp at pH(D) 10.

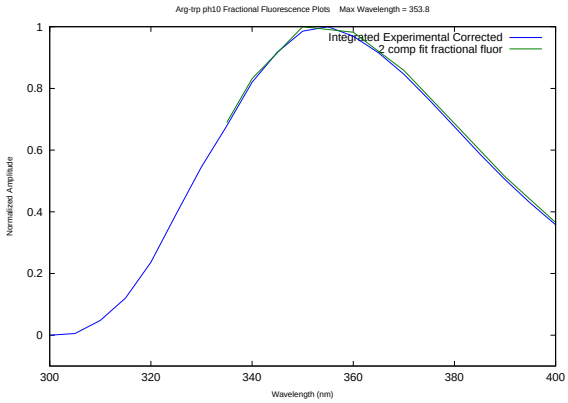

(a) Arg-Trp pH 10 DAS

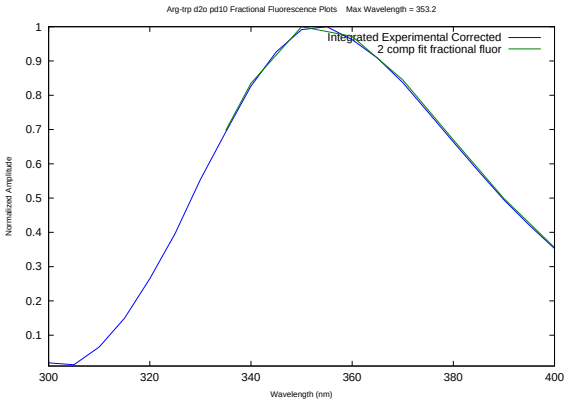

(b) Arg-Trp pD 10 DAS

Figure B.19: Fractional fluorescence plot of 2 exponential fit and integrated waveforms as a function of wavelength for Trp-Asp at pH(D) 10.

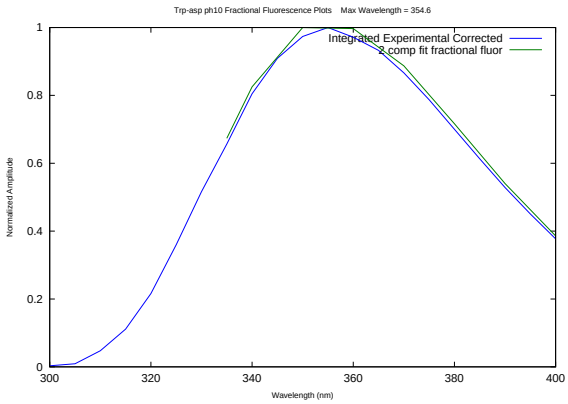

(a) Trp-Asp pH 10 DAS

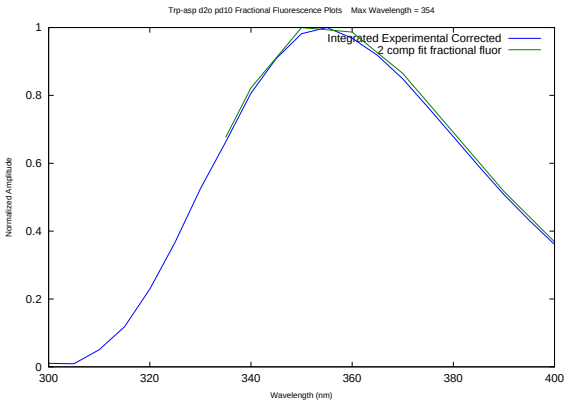

(b) Trp-Asp pD 10 DAS

Figure B.20: Fractional fluorescence plot of 2 exponential fit and integrated waveforms as a function of wavelength for 5FTrp-Asp at pH(D) 10.

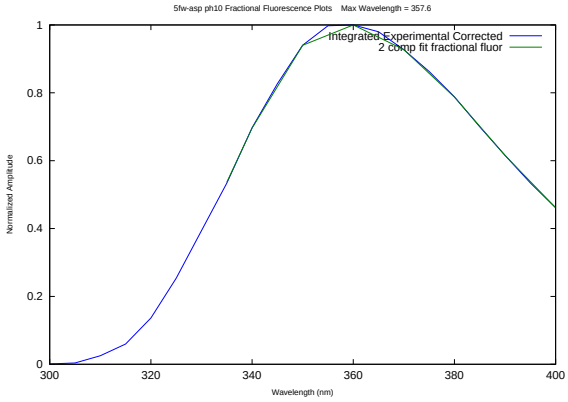

(a) 5FTrp-Asp pH 10 DAS

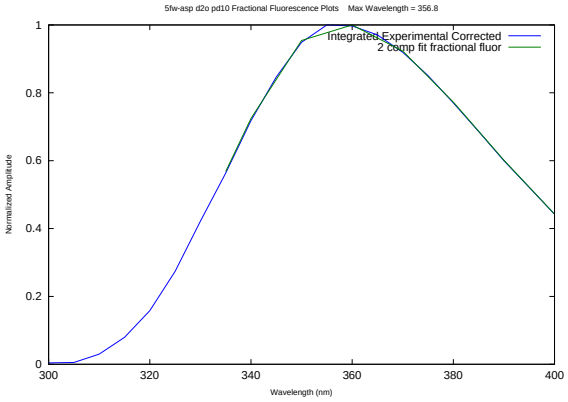

(b) 5FTrp-Asp pD 10 DAS

Figure B.21: Fractional fluorescence plot of 2 exponential fit and integrated waveforms as a function of wavelength for Asp-Trp at pH(D) 10.

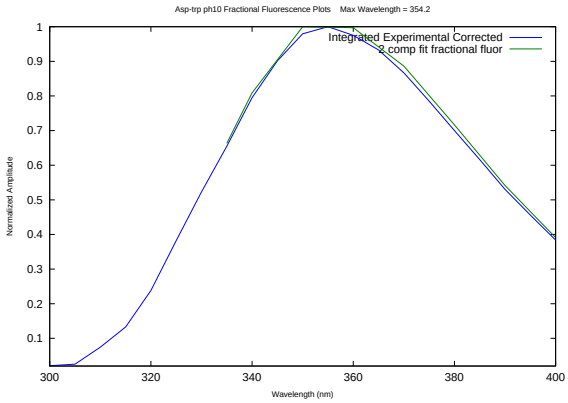

(a) Asp-Trp pH 10 DAS

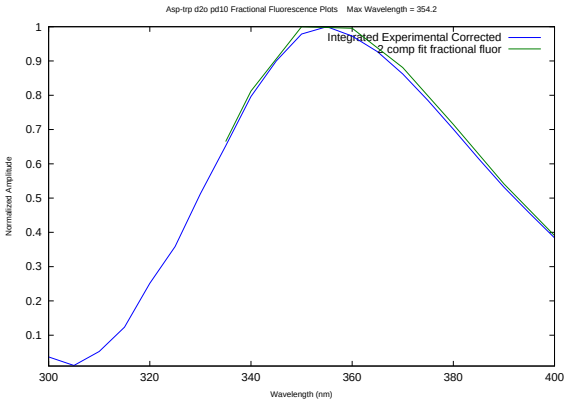

(b) Asp-Trp pD 10 DAS

Figure B.22: Fractional fluorescence plot of 2 exponential fit and integrated waveforms as a function of wavelength for Asp-5FTrp at pH(D) 10.

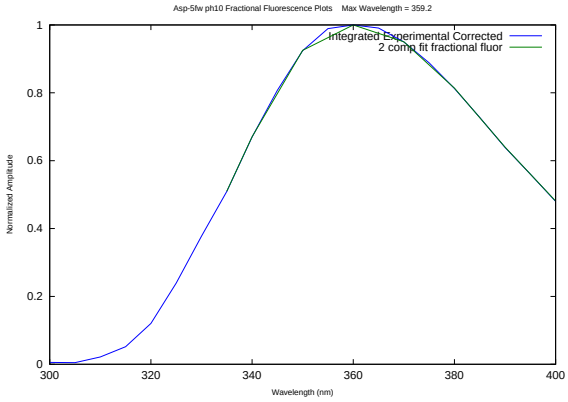

(a) Asp-5FTrp pH 10 DAS

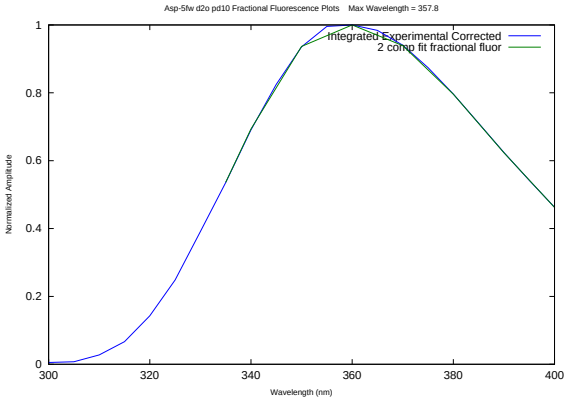

(b) Asp-5FTrp pD 10 DAS

Figure B.23: Fractional fluorescence plot of 2 exponential fit and integrated waveforms as a function of wavelength for Trp-Leu at pH(D) 10.

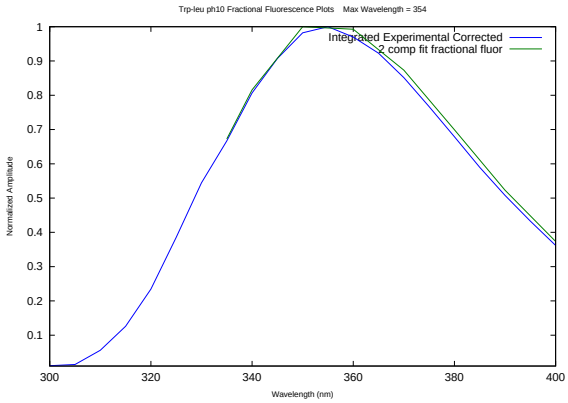

(a) Trp-Leu pH 10 DAS

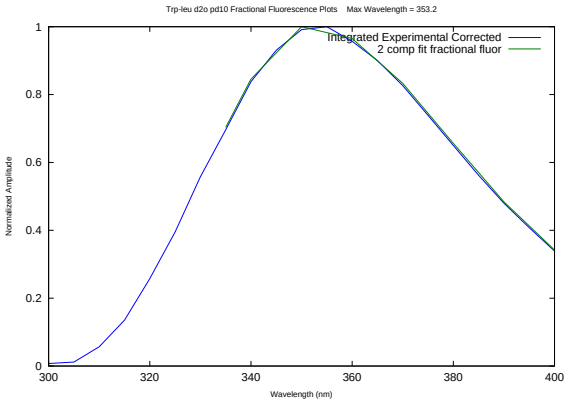

(b) Trp-Leu pD 10 DAS

Figure B.24: Fractional fluorescence plot of 2 exponential fit and integrated waveforms as a function of wavelength for 5FTrp-Leu at pH(D) 10.

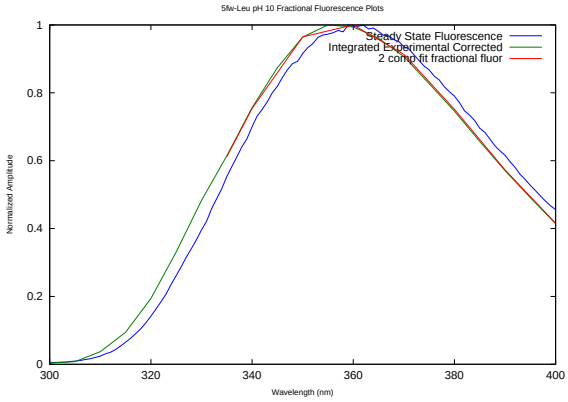

(a) 5FTrp-Leu pH 10 DAS

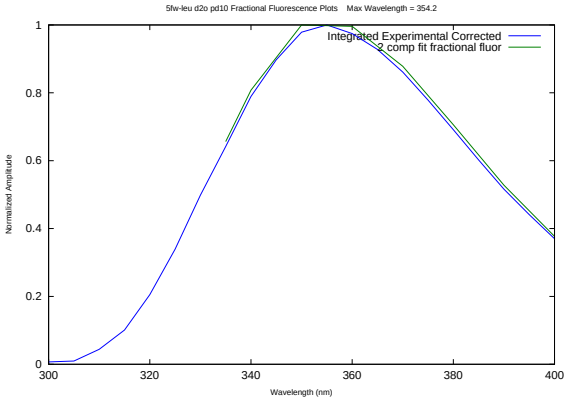

(b) 5FTrp-Leu pD 10 DAS

Figure B.25: Fractional fluorescence plot of 2 exponential fit and integrated waveforms as a function of wavelength for Leu-Trp at pH(D) 10.

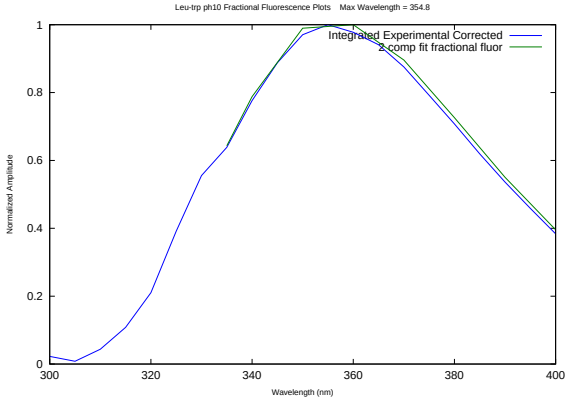

(a) Leu-Trp pH 10 DAS

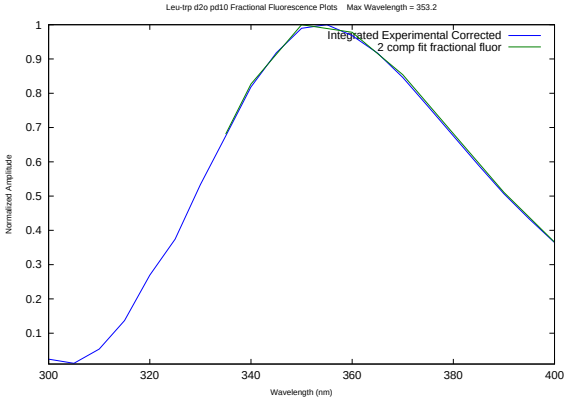

(b) Leu-Trp pD 10 DAS

Figure B.26: Fractional fluorescence plot of 2 exponential fit and integrated waveforms as a function of wavelength for Leu-5FTrp at pH(D) 10.

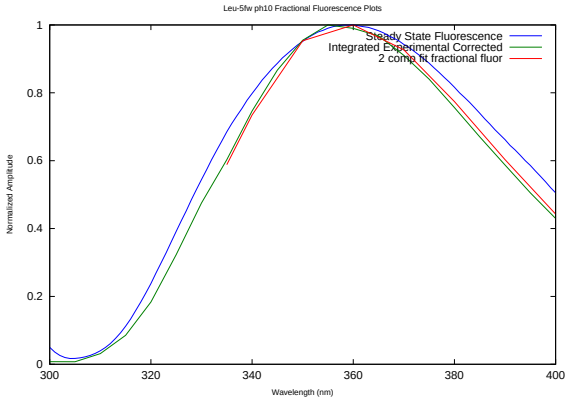

(a) Leu-5FTrp pH 10 DAS

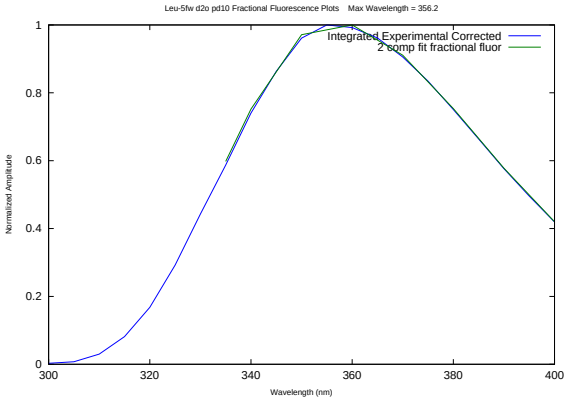

(b) Leu-5FTrp pD 10 DAS

Figure B.27: Fractional fluorescence plot of 2 exponential fit and integrated waveforms as a function of wavelength for Trp-Met at pH(D) 10.

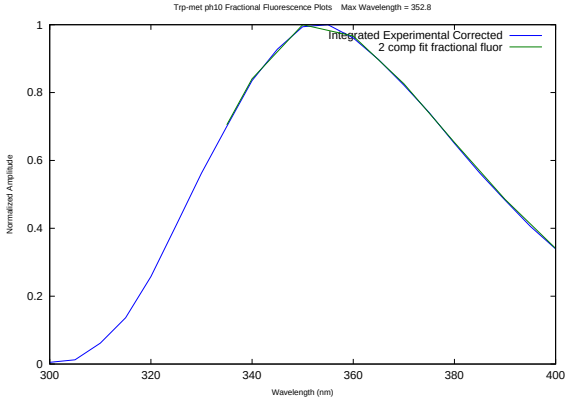

(a) Trp-Met pH 10 DAS

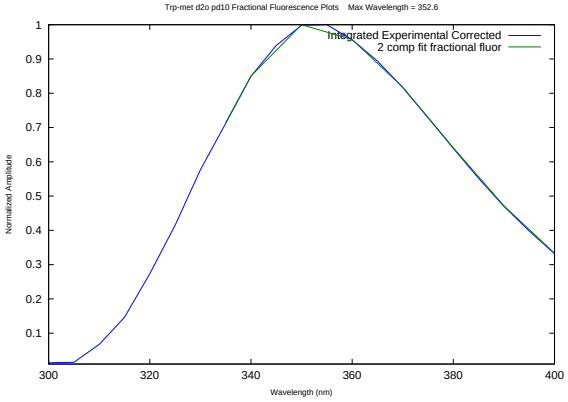

(b) Trp-Met pD 10 DAS

Figure B.28: Fractional fluorescence plot of 2 exponential fit and integrated waveforms as a function of wavelength for 5FTrp-Met at pH(D) 10.

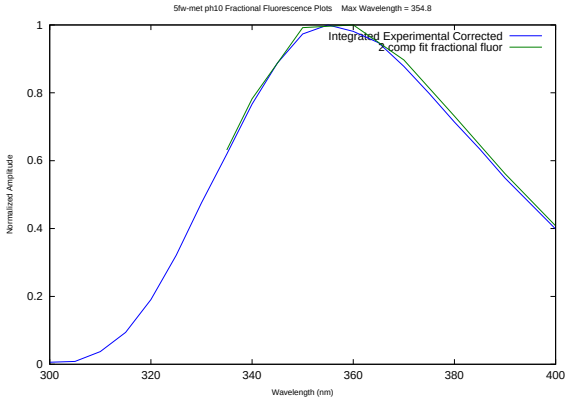

(a) 5FTrp-Met pH 10 DAS

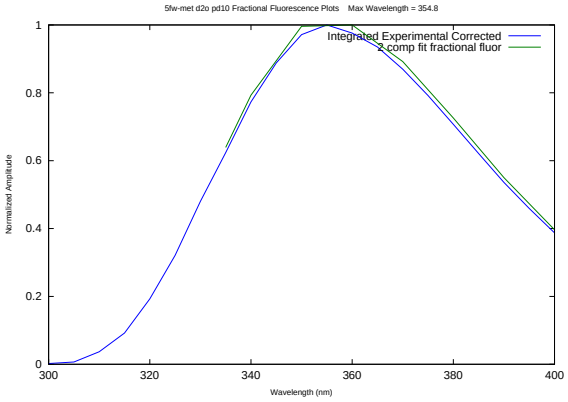

(b) 5FTrp-Met pD 10 DAS

Figure B.29: Fractional fluorescence plot of 2 exponential fit and integrated waveforms as a function of wavelength for Met-Trp at pH(D) 10.

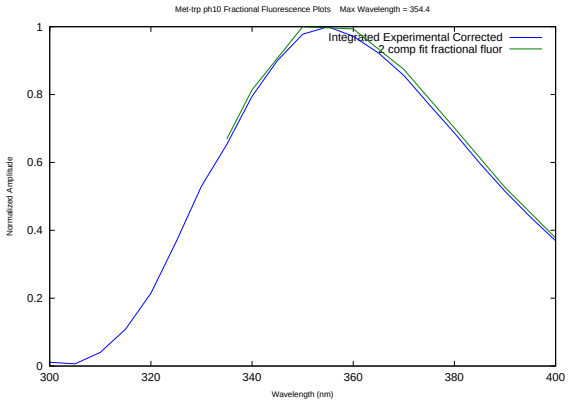

(a) Met-Trp pH 10 DAS

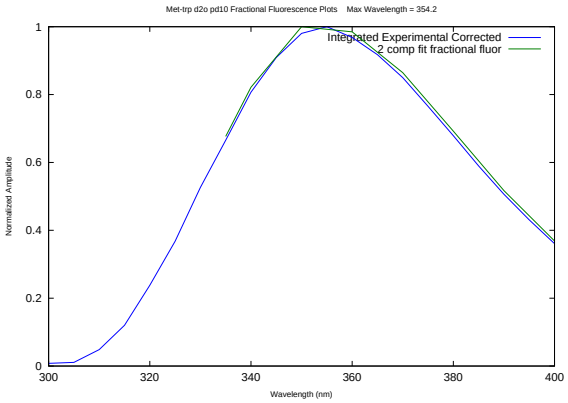

(b) Met-Trp pD 10 DAS

Figure B.30: Fractional fluorescence plot of 2 exponential fit and integrated waveforms as a function of wavelength for Met-5FTrp at pH(D) 10.

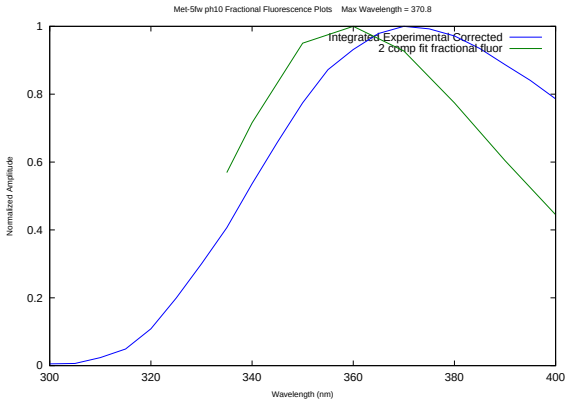

(a) Met-5FTrp pH 10 DAS

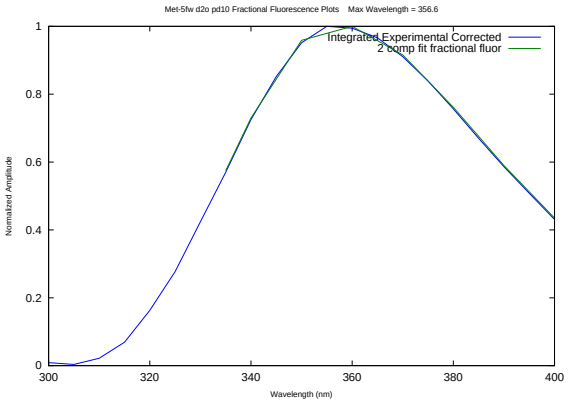

(b) Met-5FTrp pD 10 DAS

APPENDIX C

DURBIN-WATSON VALUES

This chapter contains tables of Durbin-Watson values that were used to evaluate the quality of fits to experimental data. These values were used rather than χ^2 due to the fact that direct waveform recording does not fallow Poison statistics. A value of 2 for this value indicates no autocorrelation in the residuals of the fit.

Table C.1: Durbin-Watson Values from Global analysis for 1, 2 and 3 exponential component fits of time resolved fluorescence for tryptophan dipeptides (Reported value is average value over 8 analyzed wavelengths and number of samples collected)

Sample	1 comp. DWV	2 comp. DWV	3 comp. DWV	# of samples
Trp pH 5	0.451	1.92	1.95	
Trp pD 5	0.283	1.75	1.83	
Trp pH 10	0.136	1.61	1.96	
Trp pD 10				2
Trp pH 11	0.492	1.1.36	1.48	
Trp pD 11				2
Gly-Trp pH 5	0.642	1.87	1.63	4
Gly-Trp pD 5	0.371	1.78	1.97	2
Gly-Trp pH 10	0.305	1.81	1.86	3
Gly-Trp pD 10	0.0982	1.31	1.71	2
Trp-Gly pH 5	0.607	1.78	1.90	3
Trp-Gly pD 5	0.554	1.38	1.58	2
Trp-Gly pH 10	1.0364	1.8985	1.9812	3
Trp-Gly pD 10	0.50182	1.4884	1.6974	3
Leu-Trp pH 5	0.11315	1.518	1.7954	4
Leu-Trp pD 5	0.095878	1.5108	1.931	2
Leu-Trp pH 10	0.54184	1.6377	1.9231	3
Leu-Trp pD 10	0.24694	1.3113	1.7484	3
Trp-Leu pH 5	0.34355	1.7088	1.8047	3
Trp-Leu pD 5	0.57183	1.3423	1.6854	2
Trp-Leu pH 10	0.83182	1.6586	1.7133	3
Trp-Leu pD 10	0.52651	1.5509	1.7086	3

Table C.2: Durbin-Watson Values from Global analysis for 1, 2 and 3 exponential component fits of time resolved fluorescence for tryptophan dipeptides (Reported value is average value over 8 analyzed wavelengths and number of samples collected)

Sample	1 comp. DWV	2 comp. DWV	3 comp. DWV	# of samples
Asp-Trp pH 5	0.24281	1.8735	2.0527	2
Asp-Trp pD 5	0.1966	1.7245	1.939	2
Asp-Trp pH 10	0.18557	1.3025	1.5041	2
Asp-Trp pD 10	0.14204	1.2466	1.7885	2
Trp-Asp pH 5	0.58255	1.579	1.6343	2
Trp-Asp pD 5	0.51442	1.8117	1.8948	2
Trp-Asp pH 10	0.51086	1.6213	1.7356	2
Trp-Asp pD 10	0.5797	1.6544	1.7865	2
Arg-Trp pH 5	0.4055	2.0585	1.9682	2
Arg-Trp pD 5	0.20367	1.9428	2.1264	2
Arg-Trp pH 10	0.62181	1.6838	1.6616	2
Arg-Trp pD 10	0.55884	1.71	1.8896	2
Trp-Arg pH 5	0.29251	1.7591	2.0831	2
Trp-Arg pD 5	0.35016	1.8338	1.847	2
Trp-Arg pH 10	0.26393	1.596	1.7214	2
Trp-Arg pD 10	0.245	1.7228	1.8469	2
Met-Trp pH 5	0.43134	1.507	1.8509	2
Met-Trp pD 5	0.20092	1.5726	1.7959	2
Met-Trp pH 10	0.25824	1.6043	2.0268	2
Met-Trp pD 10	0.18339	1.3787	1.8494	2
Trp-Met pH 5	0.65358	2.0745	2.2337	2
Trp-Met pD 5	0.52424	1.7392	1.8867	2
Trp-Met pH 10	0.35055	1.5502	1.6081	2
Trp-Met pD 10	0.36709	1.7258	1.779	2

Table C.3: Durbin-Watson Values from Global analysis for 1, 2 and 3 exponential component fits of time resolved fluorescence decays for 5FW dipeptides. (Reported value is average value over 8 analyzed wavelengths and number of samples collected)

Sample	1 comp. DWV	2 comp. DWV	3 comp. DWV	# of samples
5FW pH 5				
5FW pD 5				
5FW pH 10				
5FW pD 10				
5FW pH 11				
5FW pD 11				
Gly-5FW pH 5	0.3196	1.6272	1.9586	2
Gly-5FW pD 5	0.26164	1.6236	1.6031	2
Gly-5FW pH 10	0.23697	1.7091	2.0436	2
Gly-5FW pD 10	0.20323	1.4298	1.8911	2
5FW-Gly pH 5	1.2042	1.8112	1.7947	2
5FW-Gly pD 5	1.5329	1.9747	1.9335	2
5FW-Gly pH 10	1.1931	1.8445	1.8401	3
5FW-Gly pD 10	0.75664	1.6565	1.712	3
Leu-5FW pH 5	0.99385	1.7375	1.7958	2
Leu-5FW pD 5	1.1771	1.8885	1.8549	2
Leu-5FW pH 10	0.74117	1.5536	1.6775	2
Leu-5FW pD 10	0.80959	1.7501	1.8754	2
5FW-Leu pH 5	1.5067	1.6907	1.7017	2
5FW-Leu pD 5	1.5268	1.77	1.7462	2
5FW-Leu pH 10	1.0016	1.6814	1.8274	3
5FW-Leu pD 10	0.98427	1.6518	1.7674	2

Table C.4: Durbin-Watson Values from Global analysis for 1, 2 and 3 exponential component fits of time resolved fluorescence decays for 5FW dipeptides. (Reported value is average value over 8 analyzed wavelengths and number of samples collected)

Sample	1 comp. DWV	2 comp. DWV	3 comp. DWV	# of samples
Asp-5FW pH 5	0.55836	1.6611	1.7599	2
Asp-5FW pD 5	0.61049	1.995	2.0126	2
Asp-5FW pH 10	0.36107	1.4456	1.6651	2
Asp-5FW pD 10	0.41644	1.5349	1.7622	2
5FW-Asp pH 5	0.9367	1.7452	1.8074	2
5FW-Asp pD 5	0.9805	1.571	1.7517	2
5FW-Asp pH 10	0.60056	1.6579	1.746	2
5FW-Asp pD 10	0.56854	1.5892	1.7171	2
5FW-Arg pH 5	0.48702	1.5023	1.6507	2
5FW-Arg pD 5	1.3076	2.0543	1.8566	2
5FW-Arg pH 10	1.0996	1.6876	1.7683	2
5FW-Arg pD 10	0.46767	1.652	1.8085	2
Met-5FW pH 5	0.54538	1.5739	1.6749	2
Met-5FW pD 5	0.68844	1.8982	1.9789	2
Met-5FW pH 10	0.37569	1.5145	1.7432	2
Met-5FW pD 10	0.48984	1.5954	1.7201	2
5FW-Met pH 5	1.3182	1.6809	1.7266	2
5FW-Met pD 5	1.1375	1.806	1.9614	2
5FW-Met pH 10	0.43759	1.5509	1.6882	2
5FW-Met pD 10	0.58641	1.6738	1.7706	2